

ABSTRACT

Name: Katrina Emilee Vaitkunas

Department: Chemistry and
Biochemistry

Title: Using Ion-Molecule Reactions to Probe the Structure and Reactivity of
Metal Ion Complexes with Amino Acids in the Gas Phase

Major: Chemistry

Degree: Doctor of Philosophy

Approved by:

Date:

Victor Ryher

Dissertation Director

02-21-2007

NORTHERN ILLINOIS UNIVERSITY

ABSTRACT

Understanding the structure and reactivity of amino acids is necessary for the investigation of functionality and reactivity of proteins and peptides in biological systems. It has been determined that amino acids tend to be zwitterions at neutral pH. Previous electrospray ionization mass spectrometry (ESI-MS) studies have shown that gas-phase analysis of these amino acids can provide a means to determine the structure preference of a residue (i.e., charge solvation vs. zwitterion form).

Computational investigations using the computer program Gaussian 03 were set up to theoretically model these ion-molecule interactions. Structural optimization and energetic information were obtained for both the [amino acid- M^+] and [amino acid- M^+ -neutral] complexes. These data can be compared to the experimental ESI-MS data to corroborate findings.

A series of ion-molecule reactions were used with ESI-MS to gather pertinent information. This analysis can be performed by introducing a volatile neutral species into the quadrupole ion trap of the mass spectrometer and allowing a reaction to occur between the neutral and an [amino acid- M^+] complex. Rates determined from these kinetic experiments can then be used to correlate the structure and reactivity of the gas-phase [amino acid- M^+] complex. Structural

studies have confirmed that Pro is zwitterionic in the gas phase. Ala, Arg, and Lys are also likely to be zwitterions in the gas phase. Both Gly and His are found to be charge-solvated in the gas phase.

It is also possible to analyze the reactivity of aromatic amino acids in a similar manner. Using pseudo-first-order kinetics, the equilibrium constant, K_{eq} , for these reactions was determined. From this value, the bond energy (ΔH) of the reaction was calculated. Aromatic amino acid reactivity studies have shown that there is a linear correlation between the theoretical stabilization energy (bond) energy of $[A.A.-H+Ca^{2+}]$ with benzene and the proton affinity of the amino acids. Furthermore, experimental and theoretical experiments have shown that there is a direct correlation between the observed reaction efficiency and the theoretical stabilization energy of $[A.A.+Cu^{+}+toluene]$ complexes. Observed bonding energies for the $[A.A.+Cu^{+}+toluene]$ complexes were calculated to be between approximately 96 and 107 kJ mol⁻¹.

NORTHERN ILLINOIS UNIVERSITY

USING ION-MOLECULE REACTIONS TO PROBE THE
STRUCTURE AND REACTIVITY OF METAL ION
COMPLEXES WITH AMINO ACIDS
IN THE GAS PHASE

A DISSERTATION SUBMITTED TO THE GRADUATE SCHOOL
IN PARTIAL FULFILLMENT OF THE REQUIREMENTS
FOR THE DEGREE
DOCTOR OF PHILOSOPHY

DEPARTMENT OF CHEMISTRY AND BIOCHEMISTRY

BY

KATRINA EMILEE VAITKUNAS

© 2007 Katrina Emilee Vaitkunas

DEKALB, ILLINOIS

MAY 2007

UMI Number: 3272170

INFORMATION TO USERS

The quality of this reproduction is dependent upon the quality of the copy submitted. Broken or indistinct print, colored or poor quality illustrations and photographs, print bleed-through, substandard margins, and improper alignment can adversely affect reproduction.

In the unlikely event that the author did not send a complete manuscript and there are missing pages, these will be noted. Also, if unauthorized copyright material had to be removed, a note will indicate the deletion.

UMI[®]

UMI Microform 3272170

Copyright 2007 by ProQuest Information and Learning Company.

All rights reserved. This microform edition is protected against unauthorized copying under Title 17, United States Code.

ProQuest Information and Learning Company
300 North Zeeb Road
P.O. Box 1346
Ann Arbor, MI 48106-1346

Certification:

In accordance with departmental and
Graduate School policies, this dissertation
is accepted in partial fulfillment of degree
requirements.

Victor Ryzhov

Dissertation Director

02 - 21 - 2007

Date
ANY USE OF MATERIAL CONTAINED
HEREIN MUST BE DULY ACKNOWLEDGED.
THE AUTHOR'S PERMISSION MUST BE OBTAINED
IF ANY PORTION IS TO BE PUBLISHED OR
INCLUDED IN A PUBLICATION.

ACKNOWLEDGEMENTS

The author wishes to express appreciation to:

- Dr. Victor Ryzhov
- Dr. Dave Ballantine, Dr. Lee Sunderlin, and Dr. Robert Sobel
- Dr. Tom Gilbert
- Dr. Marianny Combariza
- Dr. Manorama Tummala and Emily Jellen-McCullough
- Erin Goken, Carrie Underwood, and Sara Koepke
- FONA, Int.
- Dan Edwards, Larry Metcalf, Larry Gregerson, and Andy Small
- PRF Grant #39429-66
- NIU Department of Chemistry and Biochemistry

DEDICATION

To Mom and Dad, with love and gratitude

TABLE OF CONTENTS

	Page
LIST OF TABLES	x
LIST OF FIGURES	xiii
LIST OF APPENDICES	xx
Chapter	
1. INTRODUCTION	1
Biomolecules	1
The Amino Acids	1
Peptides and Proteins	5
The Biological Elements	10
Biomolecules and Metals	14
The Hard and Soft Acid-Base Principle	15
Bioinorganic Compounds in Medicine	21
Analysis Methods	22
Mass Spectrometry	24
MS Analysis of Noncovalent Complexes	27
Ion-Molecule Reaction Analysis via ESI-QIT-MS	35
Zwitterions	36
Aromatic Amino Acids	39

Chapter	Page
2. EXPERIMENTAL DESIGN AND METHODOLOGY	47
Ion-Molecule Reactions	47
Neutrals	47
Reaction Mechanism and Kinetics	49
Ion-Molecule Reaction Methodology	51
Theoretical Calculations	52
Zwitterions Revisited	56
Metal Ion Effects	58
Aromatic Amino Acids Revisited	61
Ion-Molecule Reactions	62
Methodology for Zwitterion Analysis.....	62
Amino Acid Standards	63
Neutral Species Selection	65
Methodology for Aromatic Amino Acid Analysis	73
Experimental Details	73
Mass Spectrometry	73
Determination of Neutral Pressure	80
Theoretical Calculations	81

Chapter	Page
3. THE INVESTIGATION OF AMINO ACID – ALKALI METAL ION COMPLEXES: STRUCTURAL ANALYSIS THROUGH ION – MOLECULE REACTIONS	85
Observed Trends	86
Kinetics Data	93
Gas-Phase Zwitterions	93
Gas-Phase Nonzwitterions	95
The Analysis of Selected Amino Acids and Their Corresponding Methyl Esters	99
Alanine	99
Arginine	103
Glycine	108
Histidine	112
Lysine	116
Proline	120
Summary	123
Other Amino Acids	123
Lithiated Amino Acids	126
Sodiated Amino Acids	126
Potassiated Amino Acids	129
Conclusion	130

Chapter	Page
4. USING ION-MOLECULE REACTIONS TO SIMULATE AROMATIC AMINO ACID INTERACTIONS WITH AMINO ACID – METAL ION COMPLEXES	133
The Relevance of Cation- π Interactions	134
Protein Structure	135
Protein Regulation	135
Studying Aromatic Interactions with Metal Cations	137
Model Neutrals	146
Theoretical Studies with Benzene	149
Phenylalanine Modeling	155
Method	156
Experimental Findings	157
Silver Studies	157
Calcium Studies	162
Cobalt Studies	166
Copper Studies	170
Iron Studies	175
Nickel Studies	180
Zinc Studies	183
Summary	186

Chapter	Page
Tyrosine Modeling	188
Ion-Molecule Reactions	189
Silver Studies	189
Copper Studies	194
Summary	197
Results and Discussion	198
Conclusions	203
5. FUTURE DIRECTIONS	205
Structural Analysis	206
Reactivity of the Amino Acids	208
Real-Time Analysis	211
Conclusion	213
REFERENCES	214

LIST OF TABLES

Table	Page
1. Examples of Some Less Commonly Occurring Amino Acids ...	4
2. Examples of Biological Functions of Fibrous and Globular Proteins	8
3. Classes of Proteins and Specific Biological Examples	10
4. Specific Metals, the Biological Roles They Play, and Dietary Sources	14
5. Metal Ions and Their Preferred Ligand Binding Groups	16
6. HSAB Identifications for Relevant Species	17
7. Common Metal-Protein Species	18
8. Medical Disorders Related to Metal-Protein Malfunction	21
9. Analysis Methods	23
10. Mass Spectrometers Available for Bioinorganic Investigation ..	25
11. Common Ionization Methods Available for Mass Spectrometers	26
12. Amino-Aromatic Interactions in 33 Proteins	44
13. Boiling Points and Vapor Pressures of Various Neutral Species .	48
14. Colors of the Atoms as Used by Gaussian	84
15. Kinetic and Thermodynamic Data for Selected Sodiated Amino Acids and Model Compounds Reacting with Acetone	125
16. Experimental Results for Lithiated Amino Acids Reacting with Acetone	127

Table	Page
17. Experimental Results for Sodiated Amino Acids Reacting with Acetone	128
18. Experimental Results for Potassiated Amino Acids Reacting with Acetone	131
19. Theoretical Data for Benzene Reactions	152
20. Reaction Data for Amino Acids Complexed to Silver Cations Reacting with Toluene	159
21. Calculated Kinetic and Thermodynamic Values for Silver Reactions with Toluene	161
22. Data for Amino Acids Complexed to Calcium Reacting with Toluene	164
23. Thermodynamic and Kinetic Data for $[A.A.-H+Ca^{2+}]^+$ Species Reacting with Toluene	166
24. Data Obtained for Amino Acids Complexed to Cobalt Reacting with Toluene	168
25. Calculated Thermodynamic and Kinetic Results for Cobalt Complexes Reacting with Toluene	170
26. Experimental and Theoretical Results for Reactions of Amino Acids Complexed to Copper Reacting with Toluene	173
27. Kinetic and Thermochemical Data for Copper Complexes Reacting with Toluene	175
28. Experimental Results for Amino Acids Complexed with Iron Reacting with Toluene	177
29. Kinetic and Thermodynamic Data for Iron Complex Reactions with Toluene	179

Table	Page
30. Experimental Results for Amino Acids Complexed with Nickel Reacting with Toluene	181
31. Calculated Kinetic and Thermodynamic Values for [A.A.-H+Ni ²⁺] ⁺ Complexes Reacting with Toluene	183
32. Reaction Data for Amino Acid Complexes with Zinc Reacting with Toluene	185
33. Thermodynamic and Kinetic Data for Reactions with Zinc and Toluene	186
34. Reaction Data for Amino Acid Complexes with Silver Reacting with Methylanisole	191
35. Thermodynamic and Kinetic Data for Reactions with Silver and Methylanisole	194
36. Reaction Data for Amino Acid Complexes with Copper and Methylanisole	196
37. Kinetic and Thermodynamic Data for Reactions with Copper and Methylanisole	197

LIST OF FIGURES

Figure	Page
1. The general amino acid structure	2
2. The condensation reaction of amino acids	5
3. Iron uptake and conservation	13
4. The zinc finger motif	20
5. The fragmentation pathways for the ACTH decapeptide as observed under low-energy and high-energy CID	29
6. Determination of kinetic constants from BIRD data	31
7. The two possible gas-phase amino acid structures	38
8. The model used to calculate the theoretical location of lysine-phenylalanine interacting pairs	45
9. The amino acid serine in both charge-solvated and zwitterion structures	56
10. Gaussian modeling results of glycine complexed to Ca^{2+}	59
11. The structures of the zwitterionic amino acid and betaine complexing a metal ion	63
12. A comparison of a charge-solvated amino acid complex and the charge-solvated complex of glycine methyl ester	64
13. The slow reaction of sodiated amino acids and butylamine (But) .	66
14. Proton transfer to the neutral species triethylamine (TEA)	67

Figure	Page
15. The reaction of sodiated amino acids with triethylamine over a 1000 ms scan delay period	68
16. Protonation of TEA over a 1000 ms time frame	68
17. A demonstration of the slow kinetics of the oxygen base tetrahydrofuran	70
18. The slow reaction kinetics of the oxygen base ethyl acetate (EA) ..	70
19. An example of the reaction kinetics of the neutral acetone	71
20. The reaction of four representative sodiated amino acids with acetone after a scan delay period of 1000 ms	72
21. Ion isolation	75
22. The neutral introduction scheme	76
23. An example of the increase in product formation as the scan delay time is increased	78
24. The typical kinetics trend observed for these reactions	79
25. The use of Gaussian optimization	83
26. The structure of acetone	85
27. Representative reaction trends for alkali metals complexed to amino acids	87
28. Amino acids and cesium	89
29. Kinetics variations with respect to various lithiated amino acids reacting with acetone	90

Figure	Page
30. Representative kinetics plots for sodiated amino acids reacting with acetone	91
31. Reaction kinetics for various potassiated amino acids reacting with acetone	92
32. Proline and betaine zwitterions	94
33. A comparison of the reaction rates of Pro and Bet with acetone in the gas phase	95
34. A comparison of the zwitterionic and charge-solvated lysine species to the permanently charge-solvated lysine methyl ester ...	96
35. Lithiated methyl ester kinetics with acetone	97
36. Sodiated methyl ester kinetics with acetone	98
37. Potassiated methyl ester kinetics with acetone	99
38. Alanine kinetics compared to the amino acid standards in their lithiated forms for reactions with acetone	101
39. Sodiated alanine kinetics for reactions with acetone	102
40. The reaction trend of potassiated alanine with acetone	103
41. Arginine kinetics for reactions with acetone	104
42. Zwitterionic and charge-solvated [Arg+Na ⁺]	106
43. The kinetic trends of potassiated arginine species reacting with acetone	107
44. Lithiated glycine kinetics for reactions with acetone	109
45. Sodiated glycine kinetics for reactions with acetone	110

Figure	Page
46. A comparison of the structures and energies of Gly, GlyME, and Bet	111
47. Lithiated histidine kinetics for reactions with acetone	113
48. Sodiated histidine kinetics for reactions with acetone	113
49. Reaction kinetics of potassiated histidine for reactions with acetone	114
50. Theoretical calculations involving sodiated histidine	115
51. Lysine kinetics for reactions with acetone	116
52. The rate kinetics of potassiated lysine for reactions with acetone .	117
53. Computational results for sodiated Lys and LysME reacting with acetone	119
54. The reaction trends of the lithiated amino acids Pro, ProME, and Bet with acetone	121
55. Sodiated proline kinetics for species reacting with acetone	121
56. The kinetic trends of the $[\text{Pro}+\text{M}^+]$ species reacting with acetone .	122
57. Computational results for sodiated Pro, ProME, and Bet reacting with acetone	124
58. A visualization of the cation- π interaction	134
59. Cation- π interactions in proteins	136
60. The nicotinic acetylcholine receptor	138
61. Aromatic interactions with metal cations	140
62. The substituted structures of the benzene molecule	141

Figure	Page
63. The indole side chain of tryptophan	142
64. Modeling cation- π interactions	145
65. The aromatic amino acids and their corresponding model neutrals used in this study.....	148
66. An identical match for the side chain of Tyr	149
67. Benzene	150
68. An example of the benzene-metal interaction	151
69. The side chain coordination of calcium by Arg and Lys	153
70. A comparison of the calculated stabilization energies and the proton affinities of the amino acids	155
71. Toluene	156
72. The reaction of $[\text{Ala}+\text{Ag}^+]$ with toluene with a 5000 ms scan delay	158
73. The reaction of $[\text{Leu}+\text{Ag}^+]$ with toluene	158
74. A structural comparison of Leu, Ile, and Val	160
75. The reaction of $[\text{Asp-H}+\text{Ca}^{2+}]^+$ with toluene over a scan delay of 1000 ms	163
76. Reaction kinetics for $[\text{Asp-H}+\text{Ca}^{2+}]^+$ with toluene	163
77. The structures of Asp and Glu	165
78. A sample spectrum of $[\text{Asn-H}+\text{Co}^{2+}]^+$ reacting with toluene over a 5000 ms scan delay	167
79. The kinetics plot of $[\text{Asn-H}+\text{Co}^{2+}]^+$ reacting with toluene	168

Figure	Page
80. A comparison of Thr, Ser, and Ile	169
81. The reaction of [Ala+Cu ⁺] with toluene over a 1000 ms scan delay	172
82. The kinetics of [Ala+Cu ⁺] reacting with toluene	172
83. The linear correlation between stabilization energy and reaction efficiency	174
84. [Met-H+Fe ²⁺] ⁺ reacting with toluene over a 5000 ms scan delay ..	176
85. A kinetics plot for [Met-H+Fe ²⁺] ⁺ reacting with toluene	176
86. A comparison of Thr, Ser, and Pro	178
87. A comparison of Ile, Ala, and Val	179
88. A spectrum of [Leu-H+Ni ²⁺] ⁺ reacting with toluene over a scan delay period of 5000 ms	180
89. The kinetics of [Leu-H+Ni ²⁺] ⁺ reacting with toluene	181
90. [Asn-H+Zn ²⁺] ⁺ reacting with toluene over a scan delay period of 1000 ms	184
91. The kinetics of [Asn-H+Zn ²⁺] ⁺ reacting with toluene	184
92. The reaction efficiencies of the amino acids	187
93. Methylanisole	188
94. The reaction of [Ala+Ag ⁺] with methylanisole over a scan delay period of 1000 ms	190
95. The reaction kinetics of [Ala+Ag ⁺] with methylanisole	191
96. The structures of Asn, Gln, Glu, and Asp	193

Figure	Page
97. The reaction of [Ala+Cu ⁺] with methylanisole after a 1000 ms scan delay	195
98. The reaction kinetics of [Ala+Cu ⁺] with methylanisole	195
99. The reaction efficiencies of methylanisole reactions	198
100. A comparison of reaction efficiencies for [A.A.+Ag ⁺] complexes with toluene and methylanisole	200
101. A comparison of reaction efficiencies for [A.A.+Cu ⁺] complexes with toluene and methylanisole	201
102. Cyclic amino acids and potential neutral models	210
103. Neutral models for sulfur-containing amino acids	212

LIST OF APPENDICES

Appendix	Page
A. THE AMINO ACIDS	239
B. STRUCTURES OF THE STANDARD CHARGE-SOLVATED SPECIES	245
C. THEORETICAL MODELING RESULTS FOR AMINO ACID--METAL ION COMPLEXES WITH BENZENE	247
D. THEORETICAL MODELING OF PHENYLALANINE INTERACTIONS USING TOLUENE	252
E. ABBREVIATIONS	255

CHAPTER 1

INTRODUCTION

The study of biomolecules is a rich and growing field due to interest in a variety of areas: life science, medicine, pharmaceuticals, and polymer technology are just a few examples. The broad interest surrounding biomolecules makes it essential to develop a better understanding of the interactions, reactivity, and structures of peptides. This information can further be applied to proteins, which are much more complex biomolecules. Often, these peptide and protein interactions can be quite complex. The study of amino acids is essential in order to gain insight into their function in larger peptides and proteins.

Biomolecules

The Amino Acids

There are twenty common α -amino acids that compose peptides and proteins. Peptides are low molecular weight organic polymers of amino acids (less than 50 amino acids long), many of which are functionally important to biological processes.^{1,2} For instance, the peptide insulin is responsible for the

regulation of sugar levels in blood.¹ Proteins are composed of larger amino acid chains (up to hundreds of thousands of Daltons). Each α -amino acid consists of a chiral carbon atom to which a basic amino ($-\text{NH}_2$) group, an acidic carboxyl ($-\text{COOH}$) group, an R-group side chain, and a hydrogen atom are attached (Fig.1). The different R-group side chains of the amino acids provide variation in the chemical properties of the molecules, allowing for differences in binding energies, charge solvation, activity, and structure.

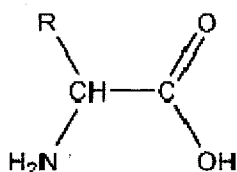


Figure 1. The general amino acid structure. The amino group is attached to the α -carbon. R represents the individual side-chain group that each amino acid contains. The twenty natural amino acids are found in the L-configuration.

Appendix A shows the general structures of the twenty natural α -amino acids. Glycine (Gly) is the simplest amino acid, where the R-group is hydrogen. However, these R-groups can be more complex, including hydroxyl groups (e.g., serine³, threonine⁴), sulfur groups (e.g., cysteine [Cys], methionine [Met]), and aromatic rings (e.g., phenylalanine [Phe], tyrosine [Tyr], tryptophan [Trp]). There are four main categories that the amino acids can be broken into at physiological

pH: nonpolar hydrophobic, polar neutral, acidic, and basic. The size and composition of these side chains can affect the coordination capabilities, structure, and activities of these amino acids and the biomolecules in which they are contained.⁵

The nonpolar amino acids are the common amino acids with alkyl-chain R-groups (alanine, isoleucine, leucine, and valine), proline (which technically is an α -imido acid), and the aromatics phenylalanine and tryptophan. These nonpolar amino acids are often found inside the protein, where they are less likely to interact with the aqueous cellular environment.⁶

Polar, neutral amino acids often form hydrogen bonds with water through their R-groups. The polar, uncharged amino acids include asparagine, cysteine, glutamine, glycine, threonine, tyrosine, and serine. The hydrogen-bonding interactions with water generally make these amino acids more soluble in water than nonpolar amino acids. A few exceptions do apply: glycine does not contain an R-group that can hydrogen-bond to water, and tyrosine has the lowest solubility in water of all the twenty amino acids.⁶

Acidic amino acids have R-groups which contain a carboxyl group. The two amino acids that fall into this category are aspartic acid and glutamic acid. At pH 7, these amino acids have a net negative charge. Many proteins that bind metal ions for structural purposes often contain one or more aspartic acid or glutamic acid side chains.⁶

Finally, the basic amino acids have side chains that are positively charged at pH 7. These include arginine, histidine, and lysine. Often, arginine and lysine participate in electrostatic interactions in proteins, while histidine participates as a proton donor or acceptor in enzyme reactions.⁶

Besides the twenty common amino acids, there are other amino acids that occur rarely in proteins or are derivatives of amino acids used for other biological functions. For example, the amino acids hydroxylysine and hydroxyproline are less common components of proteins but can be found in connective tissues in collagen and gelatins. The amino acid histamine is derived from the decarboxylation of histidine. Histamine is released by mast cells (cells found in loose connective tissue) during allergic reactions.⁶ Additionally, these rarely occurring amino acids can be found in other biological organisms, such as plants and bacteria. Table 1 provides some examples of a few of these amino acids.

Table 1

Examples of Some Less Commonly Occurring Amino Acids.⁷

Amino Acid	Biological Function
Carnitine	Transports fatty acids to the mitochondria
Citrulline	Detoxifies and eliminates ammonia in the liver
Cystine	An oxidation product of cysteine; found in hair keratin, insulin, and digestive enzymes
Ornithine	Functional in the urea cycle and a precursor to other amino acids
Taurine	Functions as a neuroinhibitory transmitter and bile acid metabolism

Peptides and Proteins

Peptides and proteins are formed by the condensation reaction of amino acids, where the loss of water occurs as a peptide bond is formed (Fig. 2). The beginning of the chain is considered to be the N-terminus, where the free amino group is found. The end of the chain is the C-terminus, where the last amino acid contains a free carboxyl group. The peptide bond forms the rigid backbone of the protein, which provides the primary structure of the protein. The backbone has a repeating sequence of amide bonds (-NH-CO-). Proteins contain secondary and tertiary structures, and proteins with multiple peptide chains also contain a quaternary structure.⁵

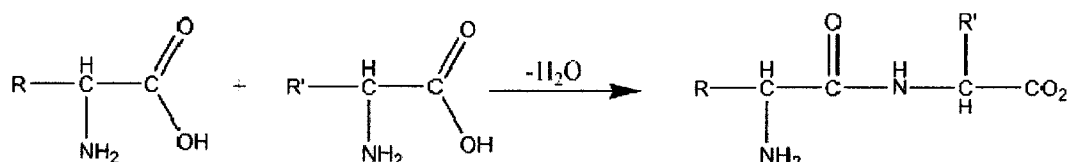


Figure 2. The condensation reaction of amino acids. A peptide bond is formed between the amino group of one amino acid and the carboxyl group of another. The loss of a water molecule occurs as the bond is formed.

Hydrogen bonding, both inter- and intramolecular, is the basis for the secondary structure of the protein. Intermolecular hydrogen bonds occur between carbonyl and NH groups in the form $\text{C}=\text{O} \cdots \text{H}-\text{N}$.¹ Intramolecular hydrogen

bonding occurs when the carbonyl group of an amino acid of one peptide hydrogen bonds to a NH group of an amino acid of another peptide. The bond strength of one such bond is approximately 5 kcal/mol. Compared to a typical covalent bond, this is rather weak. However, peptides and proteins are capable of forming numerous interchain hydrogen bonds, making the occurrence of these bonds significant.¹

The secondary structure of the protein consists of the α -helix and the β -sheet. The α -helix forms when an intramolecular hydrogen bond forms between the carboxyl-group oxygen of one amino acid and the amine hydrogen of the amino acid four positions away. Each amino acid in the helix participates in hydrogen bonding, which helps to strengthen the structure. The R-groups of the amino acids are positioned outwardly to prevent contortion of the helical core.^{1, 5}

The β -sheet forms when intermolecular hydrogen bonding occurs between the carboxyl-group oxygen of one amino acid and hydrogen on another peptide chain. In the β -sheet structure, the amino acids are bound in the same plane, with their R-groups alternating above and below the plane of the sheet.^{1, 5} Any unstructured parts of the secondary structure are referred to as either loops or random coils.⁵

The tertiary structures of proteins arise from various interactions between the R-groups of the peptide chain: ionic bonds, van der Waals forces, hydrophobic bonds, hydrogen bonds, and cation- π interactions. Hydrophobic amino acids typically orient themselves towards the interior of the protein to minimize

interaction with water, whereas hydrophilic amino acids are more likely to be oriented on the surface of the protein.⁵ There are two main classes of tertiary structures for proteins: fibrous and globular.¹

Fibrous proteins are contained in the structural materials of bio-organisms. These are the proteins contained in keratins (skin, hair, nails), collagens (cartilage, blood vessels, tendons), and silks (webs, cocoons). It has been found that keratins and collagens are mainly helical in nature, whereas the silks are composed largely of β -sheets. Amino acids with nonpolar R-groups and disulfide cross-link capabilities are the main components of fibrous proteins. These features provide fibrous proteins with a rigid, insoluble structure.¹

Globular proteins are typically spherical. They function as enzymes, hormones, transport proteins, or storage proteins. Although the globular proteins are mostly helical in nature, the large amount of amino acids with polar or ionic side chains allows for a water-soluble, spherical structure.¹ Table 2 summarizes common biologically relevant fibrous and globular proteins.

Quaternary protein structure occurs when multiple subunits aggregate to form high molecular weight proteins. Aggregation of the subunits can prevent nonpolar amino acids from interacting from the aqueous cellular environment, and it can also act as a biological control mechanism. For instance, a protein may only be active in an aggregated form. Hemoglobin is an example of a quaternary protein. It consists of four subunits that participate in oxygen transport in red blood cells.¹

Table 2

Examples of Biological Functions of Fibrous and Globular Proteins.^{1, 2}

Fibrous proteins	Function
Collagens	Tendons, animal hide, cartilage
Elastins	Blood vessels, ligaments
Fibrinogen	Blood clotting
Keratins	Skin, feathers, wool, hooves, silk, nails
Myosins	Muscle tissue
Silks	Webs, cocoons
Globular proteins	Function
Hemoglobin	Oxygen transport in blood cells
Myoglobin	Oxygen transport in muscle
Immunoglobins	Immune response
Insulin	Hormone used to control glucose metabolism
Ribonuclease	Enzyme used to control RNA synthesis

Proteins are biological workhorses. Almost all cellular activity is reliant on the function of proteins. The largest class of proteins is enzymes. Enzymes function as catalysts in biological reactions and are often named for the specific biological reaction that they operate on. Regulatory proteins are used to mediate the function of other active proteins. Certain proteins are required to move a specific species from one area to another. These proteins are called transport proteins and can be responsible for activities such as moving oxygen in the lungs to muscle tissue or transferring essential nutrients into the cell. Storage proteins provide “holding tanks” for essential nutrients.⁶

Not all proteins are stationary. Contractile and motile proteins have the ability to move. They function in cell division, muscle contraction, and cell motility processes. On the other hand, some proteins are more stationary. Structural proteins maintain biological structures by strengthening and protecting cells and tissues.⁶

Proteins can also interact with each other for activation and functionality. Scaffold proteins (also known as adaptor proteins) have segments which are able to recognize and bind structural elements of compatible proteins. These protein-protein interactions can be used to assemble multiprotein complexes which are often used in coordinating and communicating various cellular signaling mechanisms.⁶

Protective and exploitive proteins take an active role in cell defense. Mostly these proteins are antibodies or immunoglobins which are specifically designed to recognize foreign molecules. Also included in this category are blood-clotting proteins (fibrinogen), neurotoxic proteins (bee venom, ricin), and bacterial toxins (diphtheria, cholera). Specific examples for all the classes of proteins are give in Table 3.⁶

To summarize proteins, amino acids are joined together through a condensation reaction. These peptide chains continue to grow, forming proteins. The secondary structure of the protein develops as hydrogen bonding occurs between the amino acids in the chain. Further interactions between the amino acids of the protein cause a tertiary structure to arise. Finally, the tertiary peptide

units can aggregate to form a larger quaternary structure. The size and composition of these proteins greatly affect all of the structural aspects previously mentioned, as well as functional characteristics, which can complicate the fundamental understanding of these species. This is why it is important to study individual amino acids so that the fundamental understanding of these can be applied to larger species.

Table 3

Classes of Proteins and Specific Biological Examples.⁶

Protein Class	Representative Examples
Enzymes	Ribonuclease; trypsin; catalase; alcohol dehydrogenase.
Regulatory	Insulin; somatotropin; thyrotropin.
Transport	Hemoglobin; serum albumin; glucose transporter.
Storage	Ovalbumin; casein; ferritin; phaseolin; zein.
Contractile/motile	Actin; myosin; tubulin; dynein; kinesin.
Structural	Collagen; α -keratin; elastin; fibroin; proteoglycans.
Scaffold	Grb 2; crk; shc; stat; IRS-1.
Protective/exploitive	Immunoglobins; thrombin; fibrinogen; diphtheria toxin.

The Biological Elements

There are four major categories of elements available to living organisms: bulk elements, macrominerals and ions, trace elements, and ultratrace elements. As can be discerned from their names, they are found in various concentrations in nature. The bulk elements consist of the components of the amino acids

themselves: H, C, N, O, P, and S. These bulk elements are readily available to bio-organisms. The bulk elements O, N, C, and H are responsible for 96% of the weight of a human body. The remaining 4% of the human body weight is provided by the essential and nonessential elements.⁸

The essential and nonessential elements are composed of the macrominerals, trace elements, ultratrace elements and ions. The macrominerals are the species Na, K, Mg, Ca, and Cl and the ions are PO_4^{3-} and SO_4^{2-} .⁵ These macrominerals are contained in the body at 100 mg to 1 g levels.⁸ Trace elements are the metals Fe, Zn, and Cu.⁵ These are found in both microgram and milligram levels.⁸ The ultratrace elements require sensitive detection techniques and can be both metals and nonmetals; the metals can include the elements Mn, Mo, Co, Cr, V, Ni, Cd, Sn, Pb, and Li and the nonmetal elements F, I, Se, Si, As, and B.⁵ Many of these species are obtained through diet.

There are minimum daily intake requirements of these elements required to maintain appropriate elemental levels in the body. The macrominerals are typically required at higher than 100 mg per day. Trace elements require much lower levels, at approximately one milligram per day. The ultratrace elements are required in such small quantities that there are no general guidelines for their dietary intakes.⁸ Although there are recommended daily intake requirements, the human body is capable of maximizing the use of the elemental species.

The uptake of iron by the human body occurs in the stomach. As iron is acquired, it is often conserved and recycled by the body in a closed system. This

is because the uptake of iron is relatively inefficient. Iron levels in the body must be carefully optimized to ensure continued biological function. The major loss of iron by the body is blood loss. Figure 3 depicts the closed system of iron in the body.⁹

Metals can play many roles in biological processes. The Group I and Group II metals affect the protein structure, molecular charge, and osmotic balance of the system. Transition metals with single oxidation states can also affect the protein structure while also functioning as protein activators. Multiple oxidation- state transition metals serve as electron carriers, oxygen transport mediators, and activators at catalysis sites in enzymes. Thus, there is a wide variety of roles that metals attain in these interactions.⁵ Table 4 identifies some of these metals alongside their respective biological roles within humans.

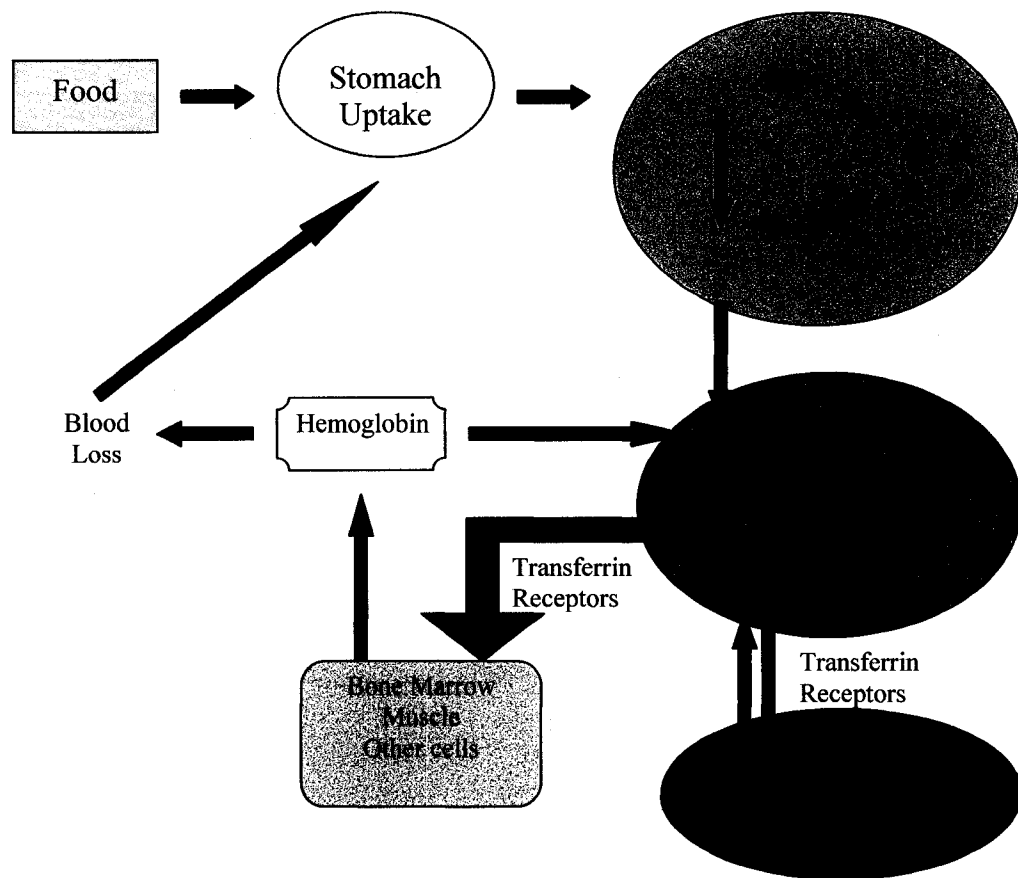


Figure 3. Iron uptake and conservation (adapted from Berdanier).⁹ Most of the iron is recycled through the system, while the uptake of iron is mainly triggered through blood loss.

Table 4

Specific Metals, the Biological Roles They Play, and Dietary Sources^{8, 10-13}

Element	Composition in a 70 kg Human	Role	Sources
Calcium	1 kg	Bone and tooth structure; trigger; charge carrier; blood clotting; hormone control.	Milk, cheese, broccoli, salmon, shellfish, kale, beans.
Cobalt	~3 mg	Oxidase; alkyl group transfer; vitamin B ₁₂ .	Liver, shellfish
Copper	72 mg	Oxidase; dioxygen transport; electron transfer.	Liver, lobster, cherries, almonds, raisins, meat.
Iron	4.2 g	Oxidase; dioxygen transport and storage; electron transfer.	Liver, meat, clams, figs, dates, spinach, egg yolks.
Lithium	7 mg	--	--
Magnesium	19 g	Structure; hydrolase; isomerase; enzyme activation.	Chocolate, nuts, bran, instant coffee, beans, peas
Manganese	12 mg	Carbohydrate and lipid metabolism.	Nuts, blueberries
Nickel	15 mg	(Suggested) Arginase activator; membrane conformation; DNA and RNA structure.	Cereal, vegetables
Potassium	140 g	Charge carrier; essential for osmotic balance.	Fruits, nuts, fish, instant coffee, bran
Silver	2 mg	--	--
Sodium	100 g	Charge carrier; essential for osmotic balance; glucose regulation.	Table salt, preserved foods, MSG.
Zinc	2.3 g	Enzyme function; hormone component; wound healing.	Oysters, crab, meat, nuts, poultry, eggs, cereal.

Biomolecules and Metals

Metals can be coordinated by amino acids and are expected to form inclusion complexes within proteins. Approximately 40% of known proteins and enzymes contain complexed metal ions.¹⁴ These proteins can be divided into two distinct classes: metalloproteins and metal-binding proteins. Metalloproteins have

relatively high-affinity binding interactions between the metal ion and the protein. These interactions are strong enough to resist breaking during sample isolation and dilution. Metal-binding proteins have weaker affinity interactions, so the metal ion is easily removed from the species. In general, monovalent ions (Na^+ and K^+) are weakly coordinated to proteins. Species such as Ca^{2+} and Mg^{2+} are more stably bound than the alkali metal ions; however, transition metals are found to have the strongest organometallic interactions.¹⁴ Often, amino acid side chains are the ligating atoms of the biomolecule.¹¹ Table 5 identifies some preferred ligands for metal ion binding.

For example, the zinc finger protein coordinates Zn^{2+} using four ligands: two histidine and two cysteine residues.¹¹ It is important to note that there is binding specificity for the Zn^{2+} ion; that is, there is a preference for the protein to bind a Zn^{2+} ion over a Ca^{2+} ion. A possible explanation for this observation is that metal binding and interaction with biomolecules are largely governed by ligand basicity (i.e., hard/soft acid-base properties).

The Hard and Soft Acid-Base Principle

A theory, called the hard and soft acid-base (HSAB) principle, was developed by Pearson in the early 1960's to rationalize the interactions that are observed between different chemical species.¹⁵ The principle states that "hard acids prefer to coordinate to hard bases and soft acids to soft bases."¹⁶ That is, a

hard ligand is most likely to interact with a hard metal cation while a soft ligand is more likely to interact with a soft metal cation.⁵

Table 5

Metal Ions and Their Preferred Ligand Binding Groups.⁹

Metal Ion	Ligand Groups
K^+	Singly charged nitrogen donors; neutral oxygen ligands
Mg^{2+}	Carboxylate; phosphate; nitrogen donors
Ca^{2+}	Similar to Mg^{2+} , but less binding affinity
Fe^{2+}	-SH; NH_2 ; carboxylates (less affinity than NH_2)
Fe^{3+}	Carboxylate; tyrosine; $-NH_2$; porphyrin
Co^{3+}	Similar to Fe^{3+}
Cu^+	-SH groups of cysteine
Cu^{2+}	Amines >> carboxylates

Due to their high charge and/or small electronic radii, hard metal cations are unable to share much electron density with ligands. Hard ligands are also unable to share their electron density, causing a stabilized interaction with hard cations due to electrostatic effects. Conversely, soft metal cations are more likely to share electron density, participating in covalent bonds with soft ligands. It is important to note that it is also possible to have intermediate ions and ligands that can conditionally act as either soft or hard acids or bases (Table 6).^{11, 15}

Amino acids can be identified as either hard, soft, or intermediate as follows: the hard amino acids are glutamic acid, aspartic acid, tyrosine, serine, and threonine; the intermediate amino acid is histidine; and the soft amino acids

are cysteine and methionine.¹¹ To clarify, since the amino acid tyrosine is a hard ligand, it would be likely to interact more favorably with K^+ , according to HSAB theory. This is because both species are less prone to share their electron density and will participate in a strong electrostatic interaction. However, the interaction of metals and biomolecules can also be affected by the concentration, ion size, and charge of the metal species.⁵

Table 6

HSAB Identifications for Relevant Species.

Hard	Soft	Intermediate
H^+ , Li^+ , Na^+ , K^+ Mg^{2+} , Ca^{2+} , Mn^{2+} Fe^{3+} Glutamic Acid Aspartic Acid Tyrosine Serine Threonine	Cu^+ , Ag^+ Cysteine Methionine	Co^{2+} , Ni^{2+} , Cu^{2+} , Zn^{2+} Fe^{2+} Histidine

There is some concern as to the feasibility of the HSAB theory in gas-phase situations. Previous *in silico* (i.e., computational) studies have shown a significant number of instances when the HSAB theory fails in the gas phase;¹⁷ specifically, for the species HF , H^+ , Li^+ , Na^+ , and Ag^+ .¹⁷⁻¹⁹ Shoeib et al. have suggested that the interactions of ions and neutrals in the gas phase are predominantly directed by electrostatics.¹⁷ Only when the ion is sufficiently solvated in the gas phase is the HSAB theory found to apply.¹⁷ To better

understand the importance and complexity of these metal-protein species, it is prudent to identify some representative examples (Table 7).

Table 7

Common Metal-Protein Species.^{6, 8, 9}

Metal	Protein
Calcium	Calbindin, calmodulin, parvalbumin, troponin C, casein, osteocalcin.
Copper	Cytochrome oxidase, tyrosinase, metallothionein.
Iron	Ferritin, cytochrome oxidase, nitrogenase, hemoglobin, cytochrome C, peroxidase, catalase.
Magnesium	Hexokinase, glucose-6-phosphatase.
Potassium	Aldosterone synthetase; pyruvate kinase.
Nickel	Urease.
Sodium	Endothelin I.
Zinc	Carbonic anhydrase, alcohol dehydrogenase, metallothionein, DNA polymerase.

The zinc finger is a protein segment containing a zinc cation bound by four amino acids (Fig. 4). Zinc fingers are often found to participate in transcription regulation, where the role of zinc is structural. The tetrahedral binding of the zinc cation is responsible for the protein folding appropriately. A complete loss of binding is observed when a coordinating cysteine or histidine is replaced by a different amino acid residue. A review of the literature suggests that zinc has been chosen for these protein motifs not only because of its availability, but also due to its lack of redox activity. This lack of redox activity protects DNA

from potential damage (as would be likely to occur with species such as Fe(II)/Fe(III) or Cu(I)/Cu(II)).⁵

Although the zinc finger provides an example of a metal cation in a structural role, it is also possible to find examples of metals which have a more active role. For instance, many copper-containing compounds are responsible for electron transfer (azurin, plastocyanin) reactions, oxygenation reactions (tyrosinase), and oxygen transport (hemocyanin). Often, these proteins and others like them require the metal cation to be coordinated for functional activation. A tight regulation of cations is required to moderate the activity of these types of proteins.⁵

Serious medical conditions can result from a lack of control over metal-protein interactions (Table 8). Not only can the structure of the protein be disrupted, but the activity of the protein can also be inefficiently controlled. Many of these conditions can prove to be fatal. For those that are not fatal, some of the symptoms surrounding problematic metal-protein interactions can be alleviated by medicinal treatments.

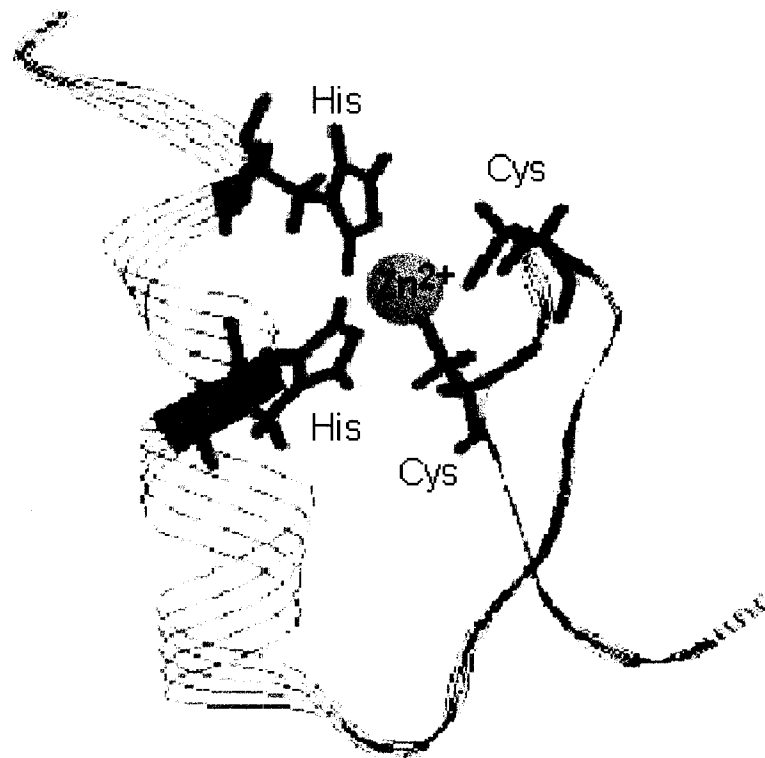


Figure 4. The zinc finger motif (image from the [Molecular Biology Web Book](#)²⁰). The Protein Data Bank (PDB) ID for this motif is 1SP1. Note that the cation is coordinated by two His and two Cys residues.

Table 8

Medical Disorders Related to Metal-Protein Malfunction.⁹

Metal ion	Medical disorder
Calcium	Osteoporosis (deficiency) Rickets (deficiency) Hypertension (deficiency)
Copper	Wilson's disease (excess) Menke's disease (deficiency)
Cobalt	B ₁₂ deficiency (deficiency)
Iron	Anemia (deficiency) Hemochromatosis (excess)
Zinc	Dwarfism (deficiency) Retinitis pigmentosa (rhodopsin binding deficiency)

Bioinorganic Compounds in Medicine

There are two main types of metallic compounds used in medicine: chemical elements necessary for life and nonessential (sometimes toxic) elements used for specific medicinal treatments. The elements essential for life are obtained through diet. Nonessential elements are introduced for diagnostic or therapeutic purposes. For example, cis-platin (a platinum-containing drug) is used as an anticancer agent, calamine (a zinc-containing ointment) is used to treat skin conditions, and auranofin (a gold-containing therapeutic) is used as an antiarthritic.⁵ The large scope of metal-protein interactions – really, metal-amino acid interactions on a smaller scale – makes the analysis of these systems integral to the advancement of the fundamental understanding of biological processes.

This has further potential to impact the pharmaceutical and medical research arenas.

Understanding the entire scope of biomolecule--metal ion interactions is complicated due to the large number of amino acids contained in biocompounds and the degrees of freedom of metal ions available for coordination. There are many combinations of amino acids and subsequent interactions possible. As the size of the peptide chain increases, so does the number of interactions. For instance, a peptide that is composed of eight individual amino acids can be arranged in 40,320 different ways.¹ It is sensible to investigate the interactions that occur with single amino acids; specifically, the interactions that occur between the amino acids and biologically relevant metal ions.

Analysis Methods

There are multiple methods available to analyze the metal--amino acid interactions. These include optical spectroscopy, resonance, radiation, electrochemical, and spectrometry techniques (Table 9).¹¹ It is also possible to perform computational analysis of these interactions using computer modeling systems available through such programs as Gaussian or Spartan.⁵

Table 9

Analysis Methods.

Method	Techniques
Optical	Electronic absorption Circular dichroism Raman spectroscopy Luminescence spectroscopy
Resonance	Nuclear magnetic resonance (NMR) Electron paramagnetic resonance (EPR)
Radiation	Extended X-ray adsorption fine structure Mossbauer spectroscopy
Electrochemical	Cyclic voltammetry Differential pulse polarography
Spectrometry	Mass spectrometry Flow tube Ion mobility

Many of these techniques provide important information about these bioinorganics. Nuclear magnetic resonance (NMR) can provide structural information about these species. NMR is often used to determine the carbon-hydrogen interactions of organic molecules.² While operating under optimized conditions, NMR can be quite sensitive. However, these instruments are expensive and require specially equipped rooms for operation. In addition, the sample being analyzed must be pure in order to obtain clean NMR spectra. This requirement is often inconvenient for biological analysis, where the structure of the species may change due to environmental factors.

As with NMR analysis, many of these techniques require that the species are treated so that they are no longer in their native or near-native state. An example of this is the need for a crystallized sample for X-ray structure analysis.

The crystallization process removes the sample from its native environment. This can alter the overall structure of the species, even causing proteins and peptides to denature. Although information about the composition of the amino acids in proteins and peptides can still be found, most of the structural information of the species is no longer available. Analysis techniques like mass spectrometry (MS) and *in silico* theoretical calculations provide a relatively inexpensive solution to the aforementioned problems.

Mass Spectrometry

There are a wide variety of commercially available mass spectrometers and ionization sources available for biomolecule analysis. The different combinations of instruments and sources provide a wide range of applications to researchers: exact mass calculations, fragmentation patterns, structures, binding affinity, thermodynamics, kinetics, and protein/peptide modifications are just some of the possible topics that can be studied. Additionally, MS techniques have a wide range of “real-world” applications including explosives detection at airport security, semiconductor analysis, determination of steroid use in athletes, food purity analysis, etc. It is important to note that each instrument and source must be carefully selected to optimize data quality, cost, and acquisition time factors. Table 10 summarizes the various MS instruments and Table 11 summarizes ionization sources commercially available for these instruments.²¹

Table 10

Mass Spectrometers Available for Bioinorganic Investigation.²¹

Mass Analyzer	Mass Range (Da)	Resolution	Dynamic Range	Cost
Magnetic sector	15,000	200,000	****	****
Quadrupole	4,000	Unit	***	*
Quadrupole ion trap (QIT)	100,000	30,000	***	*
Time-of-flight (TOF)	Unlimited ^a	15,000	***	**
Fourier transform--ion cyclotron resonance (FT-ICR)	>10 ⁶	>10 ⁶	**	****

a. The mass range of a TOF is theoretically unlimited; however, limitations in software and hardware prevent this in actuality.

* Represents relative amounts.

Table 11

Common Ionization Methods Available for Mass Spectrometers.²¹

Ionization Method	Ion Type	Sample Type	Mass Analyzer	Pros	Cons
Electron ionization (EI)	M^+ fragments	Nonpolar compounds Some polar organics	Quadrupole QIT Sector	Can be coupled to GC Good for small molecules	Fragmentation can be extensive
Chemical ionization (CI)	$[M+H]^+$ $[M-H]^-$ M^-	Nonpolar compounds Some polar organics	Quadrupole QIT Sector	Can be coupled to GC More stable ions than with EI	Cannot ionize nonvolatiles
Thermospray	$[M+H]^+$ $[M-H]^-$ $[M+NH_4]^+$	Polar compounds	QIT	Can be coupled to LC Soft ionization technique Good for small nonvolatiles	Limited sensitivity
Fast atom bombardment (FAB)	$[M+H]^+$ $[M-H]^-$	Peptides, proteins, lipids, carbohydrates, nucleotides, oligonucleotides, etc.	Sector	Can be coupled to LC, CE Soft ionization technique	Requires a liquid matrix
Atmospheric pressure chemical ionization (APCI)	$[M+H]^+$ $[M-H]^-$	Polar compounds Drugs	Quadrupole QIT Sector	Can be coupled to LC Good for low mass compounds	Water and solvent molecule clusters can form
Electrospray ionization (ESI)	$[M+nH]^{n+}$ $[M-nH]^{n-}$	Peptides, proteins, lipids, carbohydrates, oligosaccharides, oligonucleotides	Quadrupole QIT Sector TOF FT-ICR	Can be coupled to LC, CE Continuous flow operation Good for high and low masses	The liquid matrix can greatly affect ionization
Matrix-assisted laser desorption/ionization (MALDI)	$[M+H]^+$ $[M-H]^-$	Peptides, proteins, lipids, carbohydrates, oligosaccharides, oligonucleotides	TOF, sector, QIT, FT-ICR	Can be coupled to LC, CE Soft ionization technique	Requires a matrix Large matrix background

GC: Gas chromatography

LC: Liquid chromatography

CE: Capillary electrophoresis

MS Analysis of Noncovalent Complexes

The analysis of noncovalent complexes (biomolecule--metal ion interactions) is essential to protein chemistry. There are many mass spectrometry techniques available to analyze these noncovalently bound species: collision-induced dissociation (CID), blackbody infrared dissociation (BIRD), ligand exchange experiments (both in solution and in the gas phase), ion mobility mass spectrometry, and gas-phase ion-molecule reactions are just a few examples.

CID, also known as collisionally activated dissociation (CAD), is a method which can be used to determine the dissociation or ion fragmentation energies of noncovalent complexes in the gas phase. In CID experiments, the intact precursor ions are collisionally activated and subsequent unimolecular dissociation occurs. Atoms of an inert gas, such as helium or argon, are used to collide with the precursor ions, exciting them to higher energy states. These fragments of the precursor ions are then analyzed by a detector.²¹⁻²³

There are two main types of CID: low-energy collisions and high-energy collisions. Low-energy CID is typically performed in triple quadrupole and ion-trapping instruments, where the collision energy is in the 1-100 eV range. High-energy CID experiments are run in sector and TOF/TOF instruments and involve collision energies in the keV range. Mid-range collision energies on the order of 10-1000 eV are not commonly used for CID experiments.²³

Due to the energy differences employed during low-energy and high-energy CID experiments, different fragmentation patterns of precursor ions can be observed. This can be seen in Fig. 5. The m/z ratio of the fragments obtained using CID can be used to determine the initial structure of the precursor ion. For peptide and protein analysis, high-energy CID experiments usually show more side-chain fragmentation than is displayed with low-energy CID.²³

Quadrupole ion trap mass spectrometers have been used with CID in a variety of studies to analyze dissociation mechanisms of mononucleotides,²⁴ ion-ligand bond energies and ion fragmentation energies,²⁵⁻²⁹ ion solvation effects,³⁰ molecular recognition of amino acids,³¹ and structures of amino acid-metal ion species in the gas phase.³² It is also common to use a quadrupole ion trap with CID experiments to analyze noncovalent complexes^{33,34} and peptide fragmentation.³⁵ Guided ion beam mass spectrometers have been used for threshold CID experiments to investigate cation- π interactions,³⁶⁻⁴¹ structure and binding energies of copper and acetone,⁴² noncovalent interactions of various species with alkali metals,^{43,44} metal-ion interactions with biological systems,⁴⁵ and binding affinities of alkali metal ions to neutrals.^{46,47} An advantage of using CID experiments to analyze various species is that many commercially available mass spectrometers are capable of performing this type of analysis; triple quadrupoles, quadrupole ion traps, and FT-ICR analyzers are examples.

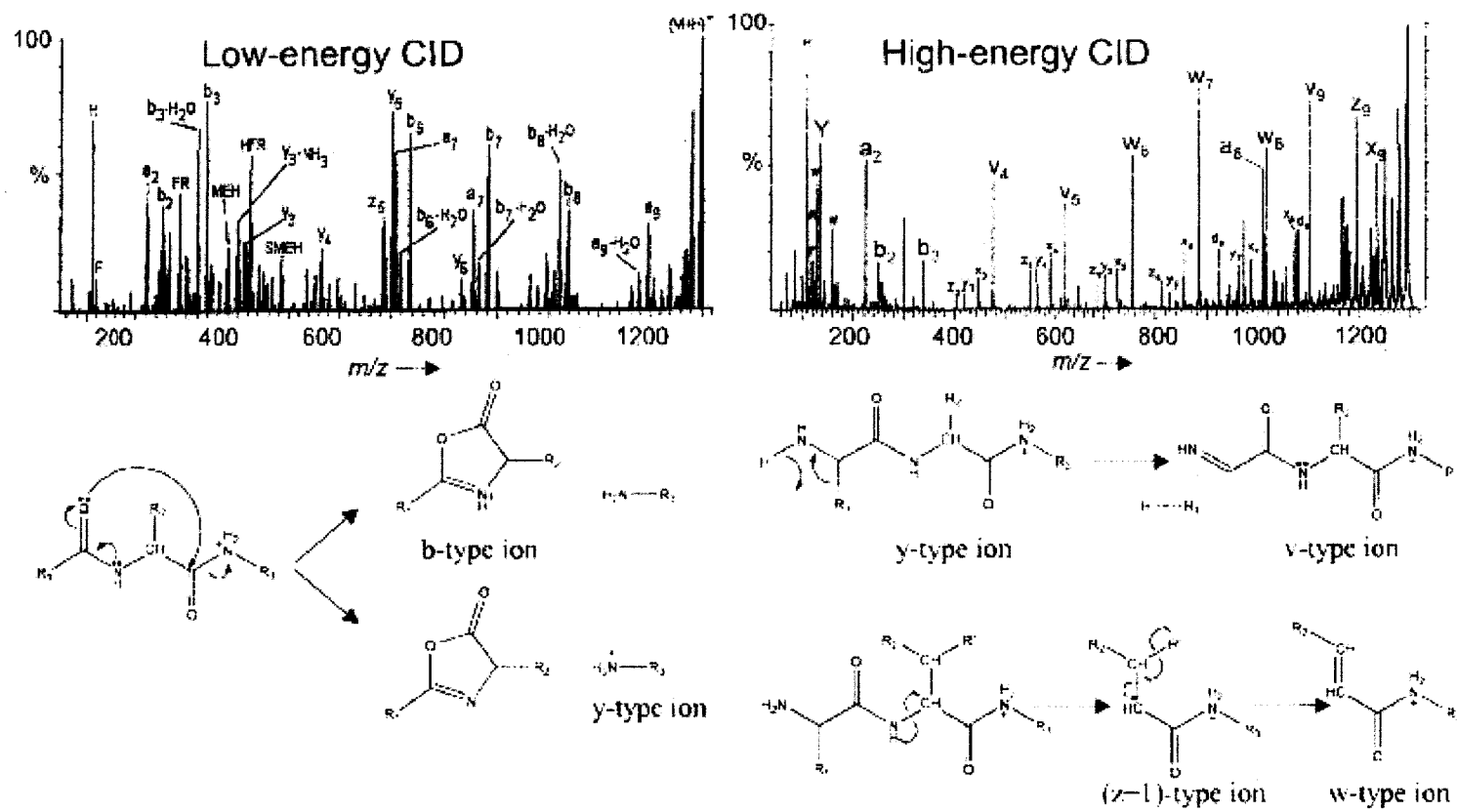


Figure 5. The fragmentation pathways for the ACTH decapeptide as observed under low-energy and high-energy CID (from Sleno and Volmer²³). Low-energy CID produces mostly *b* and *y* ions, whereas high-energy CID results in mostly *v* and *w* ions.

In addition to structural information, CID experiments can be used to determine binding energies of noncovalent complexes in the gas phase.

Dissociation cross sections of noncovalent complexes are obtained as a function of collision energy. The minimum energy required to dissociate the species is called the threshold energy. The threshold energy is directly related to the binding energies of the noncovalent complexes.^{36-38, 40, 41, 46}

Variable-energy CID is also used to compare the binding energies of species with similar sizes and structures.^{33, 48} These experiments are performed by increasing the applied CID voltage until complete dissociation of the complex is achieved. The determination of the $E_{1/2}$ energy (the applied voltage required to observe equal intensities of [precursor+M⁺+neutral] and [precursor+M⁺]) for various complexes allows for binding energy comparisons between precursor species.³³

Blackbody infrared radiative dissociation (BIRD) occurs when infrared blackbody photons are emitted from the heated walls of the vacuum chamber of a mass spectrometer. Ions isolated in the mass spectrometer at pressures less than 10^{-8} Torr absorb the photons and subsequently dissociate. BIRD is a collision-independent method of analysis; rates of dissociation can be calculated due to the temperature dependence of the dissociation.⁴⁹⁻⁵¹

The activation energy of BIRD can be calculated by performing this experiment at various temperatures. Fourier transform mass spectrometers are

used for these BIRD experiments. The Arrhenius equation is used to determine the threshold energy for dissociation as follows (Eq. 1.1):

$$k = Ae^{-E_a/RT} \quad (1.1)$$

where k is the rate constant, A is the pre-exponential rate factor, E_a is the activation energy, R is the gas constant, and T is the temperature in the ICR cell. When large molecules are analyzed this way, the E_a can be considered to be equal to the threshold dissociation energy, E_0 . The dissociation rate constants (k_{diss}) for the unimolecular dissociation can be derived from the BIRD data. These parameters are found as shown in Fig. 6.²³

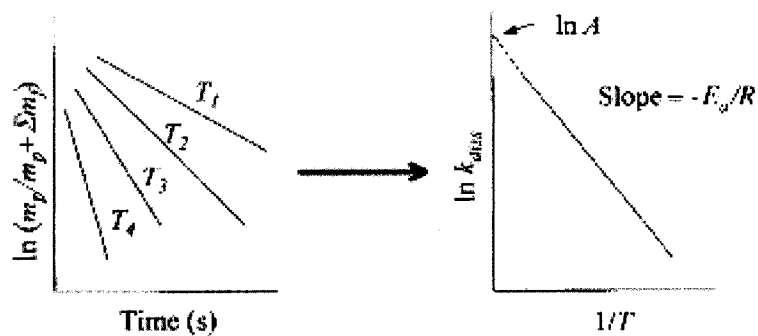


Figure 6. Determination of kinetic constants from BIRD data (from Sleno and Volmer²³). First-order dissociation rate constants can be obtained from the slope of a plot with respect to the complex fragmentation over time. The dissociation rate constants can then be plotted vs. $1/T$ to determine the activation of the energy of the system for the BIRD experiment.

BIRD-FT-ICR experiments have been used to determine the structures of lithiated lysine and similar molecules in the gas phase.⁵² BIRD is also useful for determining isomeric purity, as shown by Schnier and Williams.⁵³ BIRD-FT-ICR can also be used to determine binding energies,⁵⁴ fragmentation pathways of proteins,⁴⁹ solvation effects on metal-ligand complexes,⁵⁵ amino acid structures,⁵⁶⁻⁵⁸ and gas-phase basicities of organic zwitterions.⁵⁹

BIRD-FT-ICR methods provide accurate thermochemical data due to the high mass range and resolution provided by the FT-ICR analyzer. However, these instruments are expensive. Alone, the FT-ICR mass spectrometer is one of the most expensive systems on the market. There is currently no commercially available BIRD-FT-ICR, so these instruments must be custom designed and built for this analysis.

Similar to BIRD experiments, tunable infrared lasers can be used to excite gas-phase ions. Spectroscopic analysis of these excited ions can help to measure N-H and O-H stretches, which are sensitive to hydrogen bonding. Information about the bond stretches can be used to determine structural information about the species of interest.^{34, 60-62} As with BIRD-FT-ICR, these instruments are not commercially available.

Infrared multiphoton dissociation (IRMPD) is a photodissociation technique in which lasers operating at various wavelengths provide sufficient energy for molecular fragmentation. Gaseous molecules trapped in an FT-ICR cell absorb IR radiation, which is redistributed from IR active modes to other

vibrational modes of the ion. The energy provided by photon absorption promotes ion fragmentation. This technique has been applied to the analysis of proteins, oligosaccharides, oligonucleotides, and pharmaceuticals.²³

In radiative association kinetics (RAK) experiments, the complexation of an ion and neutral species in the gas phase can be stabilized by the emission of an infrared photon.⁶³ RAK can be used to analyze metal ion--ligand association reactions, typically in an FT-ICR mass spectrometer.⁶⁴ These RAK experiments can provide details on binding energies and reaction rates.^{63, 65-67} Although no alteration to the mass analyzer is required, a drawback to this method is the expense of the analyzer itself.

Additionally, structural and reactivity information can be obtained through ion mobility experiments. Ion mobility spectrometry separates ions as a function of mobility, as opposed to m/z ratio, as is typical with mass spectrometry. Ions in a tube that contains a buffer gas are allowed to move freely under an applied electric field. As the ions travel through the tube, they are separated according to their size to charge ratio.²¹ Noncovalent interactions and structures of peptides,⁶⁸⁻⁷¹ protein structure,⁷² molecular structure,⁷³⁻⁷⁸ nucleotide structure and interactions,⁷⁷⁻⁷⁹ amino acid cluster formation,⁸⁰ and amino acid structure⁸¹ have all been studied by ion mobility experiments.

The kinetic method can be used to probe the relative binding energies to molecules such as amino acids. Developed by Cooks et al.,⁸² the kinetic method is an "approximate method for the determination of thermochemical properties

based on the rates of competitive dissociation of mass-selected cluster ions.⁸³

The kinetic method has been used to investigate alkali metal-ion binding with DNA and RNA nucleobases,⁸⁴ to analyze sodium cation binding to dipeptides,⁸⁵ to provide structural information on [alkali metal+amino acids] in the gas phase,⁸⁶ and to probe copper (I) ion affinities to amino acids.⁸⁷

Last, ion-molecule reactions can be used to study the structures and reactivities of a variety of molecules and complexes. Ion-molecule reactions occur when an ion of interest interacts with a neutral ambient molecule in the mass spectrometer. These interactions are often fast and efficient and can be analyzed in a variety of mass spectrometers.⁸⁸ For instance, quadrupole ion traps (QIT),^{33, 88-96} sectors and double-sector instruments,⁸⁸ triple quadrupoles,^{28, 88} and double sector⁸⁸ and FT-ICR spectrometers^{88, 93, 97} have all been used to analyze ion-molecule reactions.

Ion-molecule reactions via ligand-exchange equilibrium experiments take advantage of thermochemical observations to analyze gas-phase cation- π interactions. FT-ICR mass spectrometers are used to determine equilibrium thermochemistry, as described for sodiated amino acids by Gapeev and Dunbar.^{98, 99} These experiments measure the transfer of metal ions to amino acids in the gas phase. Ligand-exchange experiments have also been performed using a guided ion beam instrument with a quadrupole mass filter as an analyzer. Amicangelo and Armentrout used this experimental setup to determine dissociation energies and entropies of sodium complexes.¹⁰⁰ For ligand-exchange experiments utilizing

FT-ICR mass analyzers, the cost of the mass spectrometer is largely a problem. That prevents this technique from being more widely used.

All of these presented methods are sufficient for analyzing noncovalent species and to experimentally determine structure and reactivity. Some of these techniques are more time and cost effective than others. Additionally, some of the instrumentation is not commercially available. A viable alternative for many of these methods is the more cost-effective ion-molecule reaction method.

Ion-Molecule Reaction Analysis via ESI-QIT-MS

Electrospray ionization (ESI) is a common and commercially available ionization source. ESI-MS is well suited for the analysis of biomolecules, specifically for the analysis of noncovalent interactions which occur between the amino acids and metal ions. This is because the sample can be analyzed in a near-native state, while the ionization technique is soft, preventing fragmentation of the species of interest; the noncovalent complex survives the ionization process.¹⁰¹ Since the sample analysis is performed in the gas phase, solvent is removed from the species of interest. This helps to eliminate problems that “bulk sample” analysis can present. Additionally, simple and fairly inexpensive modifications can be implemented on a commercially available ESI-QIT-MS in order to attain a setup capable of providing structural and kinetic data via ion-molecule reactions.

The structure of amino acid--alkali metal ion species and the binding affinities of the aromatic amino acids to amino acid--metal ion species are the focal points of this study. A modified commercial ESI-MS instrument can be used to analyze ion-molecule reactions of these species. Data from these experiments can then be used to determine the structure and reactivity of amino acids in the gas phase.

Zwitterions

In solution at neutral pH, amino acids tend to have a protonated N-terminus and a deprotonated C-terminus, causing the molecule to be zwitterionic. The term "zwitterion" stems from the German word *zwitter*, meaning "hybrid." This term describes the dipolar (charge-separated) nature of the amino acid due to the acidic and basic groups it contains.²

In the gas phase, molecules do not interact with the bulk solution that causes this zwitterion stabilization to occur.¹⁰² Previous electrospray ionization mass spectrometry (ESI-MS) studies have shown that amino acids in the gas phase tend to exist as charge-solvated (nonzwitterionic) structures. However, some are observed to be zwitterionic.¹⁰¹⁻¹⁰⁴

There are currently a handful of general systems being used to probe the gas-phase structure of amino acids. Each involves exploiting the stabilization of amino acid structures by various means. One method focuses on the analysis of hydrated amino acids.¹⁰⁵⁻¹⁰⁷ Another method uses protonated amino acids to analyze gas-phase structure.^{58, 81} Julian et al. used neutral arginine clusters to

analyze the structure of arginine in the gas phase.^{96, 108}

It is also possible to stabilize zwitterionic amino acids using localized charge density by alkali metal ions,^{62, 81, 86, 103, 109-111} alkaline earth metals,¹⁰⁴ and transition metals.¹¹² Amino acids can be complexed to a metal ion before introduction to the mass spectrometer. The stabilized amino acid--metal ion ($[A.A.+M^+]$) complex will exhibit either the nonzwitterionic (charge-solvated) or zwitterionic (salt-bridge) structure in the gas phase.¹⁰²

Charge-solvated amino acids typically display NO-coordination with the metal ion. The amine nitrogen and the carbonyl oxygen will interact with the metal. Sometimes a third electron-rich site will also interact, but the overall structure of the amino acid remains neutral.¹¹¹ Salt-bridge amino acid--metal complexes display OO-coordination of the metal ion. In this case, both oxygens of the carboxyl terminal interact with the metal. The amino terminal is protonated (and positively charged), so the deprotonated oxygen on the carboxyl terminal carries the negative charge.⁸⁶ The salt-bridge structure has a spread of charge density which can be visualized as $NH_3^+ \dots COO^- \dots M^{n+}$ (Fig. 7).

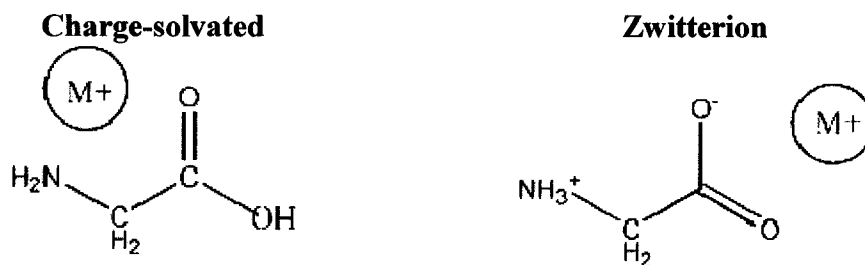


Figure 7. The two possible gas-phase amino acid structures. The charge-solvated structure of the amino acid remains neutral while the zwitterionic structure has a spatial separation of charges.

The structural preference of the amino acid can be influenced by many factors, including the charge associated with the metal ion, the size of the metal ion, and the nature of the amino acid side chains. Studies have shown that both glycine and alanine form charge-solvated structures with Cu^+ , but they prefer the salt-bridge structure with Cu^{++} .^{112, 113} The size of the metal ion is another factor in the structural preference of amino acids. For instance, the structure of arginine complexed with alkali metals changes from a charge-solvated to a salt-bridge structure as the size of the metal ion increases. These results were corroborated by theoretical modeling calculations, which supported the observed change in structure.^{57, 104} Furthermore, the chelating ability of the side chain may also affect the resulting gas-phase structure. Glutamic acid, tryptophan, and aspartic acid have the highest relative binding energies to lithium (all have a metal coordinating group in the side chain), whereas glycine and alanine have much weaker relative

binding energies to lithium and also lack a coordinating group on their side chain.¹⁰⁹

An inherent drawback to ESI-MS is the lack of direct structural information. $[A.A.+M^+]$ complexes will display identical mass-to-charge ratios, regardless of which gas-phase structure they exhibit.¹⁰¹ Methods have been developed to include structural information with mass spectrometric analysis, including the use of ion mobility^{78, 114-116} and blackbody infrared radiative dissociation.^{117, 118} However, the analysis of the reactivities of the amino acid--metal ion complexes through ion-molecule reactions provides a means to compare the structures of the species.

Aromatic Amino Acids

Of recent interest are the cation- π interactions of aromatic amino acids and metal ions. Cation- π interactions tend to be mostly electrostatic in nature, where the metal ion interacts with the electrons of the delocalized π -electron cloud of an aromatic ring. The metal cation- π interactions are fairly strong, often greater than the interactions involving other π -systems such as π - π and π -hydrogen bonds.¹¹⁹

These noncovalent interactions are involved in protein structure, receptor-ligand interaction, ligand binding, and other important biological processes.¹¹⁹⁻¹²² The role that cation- π interactions play in molecular recognition is also important from a medicinal standpoint. Mecozzi et al. have suggested that the cation- π

interactions of aromatic amino acid side chains could be exploited as binding sites for cationic ligands.¹²³

A statistical study of the three aromatic amino acids found that proteins contain approximately 3.9% Phe, 3.2% Tyr, and 1.3% Trp. This means that up to 8.4% of amino acids in a protein could participate in cation- π interactions.^{37, 124} Nearly one in twelve amino acids could be involved in these interactions.³⁷

It has been shown that of the aromatic amino acids, Trp is more likely to participate in cation- π interactions than either Phe or Tyr.³⁹ The computer program Cation- π Trends Using Realistic Electrostatics (CAPTURE) was used by Gallivan and Dougherty¹²⁵ to identify proteins that are likely to participate in cation- π interactions. In the comparative study of 593 proteins selected from the crystallized protein structures in the Protein Data Bank (PDB), the authors found that just over 26% of all Trp residues in the studied proteins are involved in cation- π interactions. Conversely, only 10.0% of Phe and 14.3% of Tyr residues participated in these interactions.¹²⁵ In theory, Trp is more likely to participate in cation- π interactions due to the indole substituent on its side chain. Computer calculations have shown that indole is capable of binding cations more strongly than benzene or phenol, the side-chain substituents of Phe and Tyr.³⁹

In silico analysis of cation- π interactions has shown that the size of the cation and the type of π -system involved can influence the strength of the interaction. Using AIM (a wave function analysis of atoms in molecules) and NBO (natural bond orbital) analysis, Mohajeri and Karimi¹¹⁹ studied the

interaction of Li^+ , Na^+ , K^+ , H^+ , and NH_4^+ with C_2H_2 , C_2H_4 , and C_6H_6 . They found as the size of the alkali metal cation increases, the charge transfer between the π -system and the cation decreases. In addition, it was confirmed that the interactions of cations and benzene are highly electrostatic. Finally, the N-H... π interaction between NH_4^+ and benzene was calculated to have a similar bond strength to that of a hydrogen bond.¹¹⁹

Cation- π interactions can also influence the folding of membrane proteins. Two major classes of proteins, transmembrane strand (TMS) and transmembrane helical (TMH) proteins, were analyzed for potential cation- π interactions. Gromiha¹²⁶ observed that TMS proteins are involved in more cation- π interactions than TMH proteins; TMS proteins participate in an average of five cation- π interactions, whereas the TMH proteins contain an average of three cation- π interactions. This indicates that one cation- π interaction is present for every 74 residues of a TMS protein. Cation- π interactions between Arg-Phe, Arg-Tyr, and Lys-Phe have average energy contributions of approximately -6.5 kcal/mole in TMH proteins. For TMS, these interactions provide an average contribution energy of -4.5 kcal/mole.¹²⁶

Recently, aromatic amino acids have been implicated in the binding of a ribosomal protein to rRNA. The *Xenopus* ribosomal protein L5 complexes with 5S rRNA, which facilitates RNA transport to the nucleus for ribosome assembly. A large number of aromatic amino acids are contained in the L5 protein. Several of these conserved aromatic amino acids are found to be essential for the

formation of the L5-5S rRNA complex. At least two aromatic amino acids in L5 are positioned to interact with the 5S rRNA through π -stacking interactions, which is thought to be the recognition event in the formation of the complex.¹²⁷

Protein-DNA complexes are also found to be stabilized by cation- π interactions. The studies by Wintjens et al.¹²⁸ focused on interactions of positively charged amino acids, specifically Arg. Although aromatic amino acids were not the focus of this study, it is quite possible that aromatic amino acids could also be implemented in similar protein-DNA interactions.

Finally, aromatic amino acids are also capable of interaction with metal cations to selectively control cation transport. An example of this is the Trp residue of the *N*-Methyl-D-Aspartate (NMDA) receptor responsible for Mg^{2+} blocking. NMDA receptors are ion channels which are voltage-dependently blocked by Mg^{2+} . A tryptophan residue in the NMDA channel was found to face the channel pore, providing an opportunity for cation- π interaction with a Mg^{2+} cation. Mutagenic analysis revealed that a substitution of Trp by Leu, Asn, or Ala reduced Mg^{2+} blocking. However, mutagenic substitution of the aromatics Tyr or Phe for Trp did not significantly alter Mg^{2+} blocking. This finding indicates that cation- π interactions involving aromatic amino acids play a large role in ion-channel control.¹²⁹

A better characterization of these interactions is essential to understanding the roles that metals play in biological processes. Dunbar et al. used the kinetic method to analyze the affinity of alkali metal ions to the aromatic amino acids

Phe, Tyr, and Trp.¹³⁰ Ion-molecule reactions can also be used to probe the reactivities of the [A.A.+M⁺] complexes to compare the binding preferences of the aromatic amino acids. Studying the interaction of amino acid--metal ion complexes with the aromatic amino acids phenylalanine (Phe), tyrosine (Tyr), and tryptophan (Trp) will help to increase the understanding of these cation- π interactions. Both mass spectrometric techniques and theoretical calculations have provided evidence for the occurrence of these interactions.¹³¹ Data obtained from this study can then be used to predict the interactions of aromatic amino acids in larger biomolecules.

Amino-aromatic interactions have also been found to occur in proteins. It has been suggested that the positively charged side chain of some amino groups interacts favorably with the π -system of aromatic rings. Burley and Petsko¹³² studied interactions between the side chains of lysine, arginine, asparagine, glutamine, and histidine with the aromatic amino acids phenylalanine, tyrosine, and tryptophan. High-resolution (≥ 2 Å) crystal structures of 33 proteins were analyzed for amino-aromatic interactions. It was found that these interactions were most favorable when the amino and aromatic groups were positioned at a distance, r , of $3.4 < r < 6$ Å. Table 12 summarizes the results of the study.¹³²

Table 12

Amino-Aromatic Interactions in 33 Proteins.¹³²

	Amino-aromatic contacts < 6 Å							
	Phe	Tyr	Trp	Lys	Arg	Asn	Gln	His
Total number of residues	171	156	74	170	94	137	88	111
Number and fraction of residues interacting	84(0.49)	86(0.55)	35(0.47)	45(0.26)	44(0.47)	43(0.31)	35(0.40)	44(0.40)
Number of amino-aromatic interactions				49	80	49	44	111
Number of amino-aromatic interactions per residue				1.09	1.82	1.14	1.26	2.52
Number of amino-aromatic interactions per amino group				1.09	0.91	1.14	1.26	1.26

Of the identified amino-aromatic contacts which occurred at less than 6 Å, approximately half of the aromatics interacted with amino groups (Table 12). That is, 49% of Phe residues, 55% of Tyr residues, and 47% of Trp residues were involved. Arg was the most reactive non-aromatic amino acid studied; nearly half of the Arg residues were involved in amino-aromatic interactions. Lys was found to be least involved in these interactions. In situations where amino-aromatic interactions occur, the amino group is positioned at the center of the aromatic ring.¹³²

In their CAPTURE analysis of 593 proteins, Gallivan and Dougherty¹²⁵ found that over 70% of all Arg side chains are located near aromatic side chains. Arg is more likely to be involved in an aromatic interaction than Lys. This is likely due to increased van der Waals interactions available to the larger Arg side chain as well as additional hydrogen atoms available for both donation and bonding.

It is important to determine if folded proteins orient amino acid side chains so that amino-aromatic interactions can occur. Gallivan and Dougherty¹²⁵ set up a geometric modeling analysis to determine if Lys residues are placed in a more electrostatically favorable orientation with respect to the aromatic group of Phe than would occur by random distribution. The model for this analysis is shown in Fig. 8.

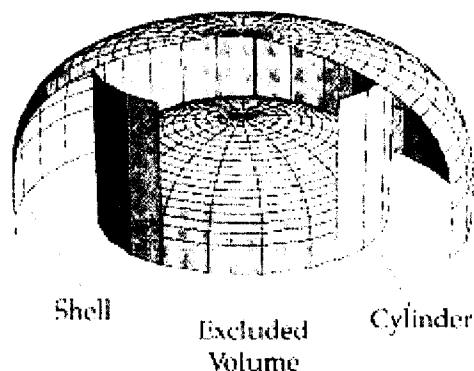


Figure 8. The model used to calculate the theoretical location of lysine-phenylalanine interacting pairs (from Gallivan and Dougherty).¹²⁵

The bisected three-dimensional model in Fig. 8 includes excluded volume, cylinder, and shell regions. The excluded volume region is a sum of the volume of benzene plus the volume for which atoms with a 1.7 Å radius cannot be found. The cylinder region is obtained by summing the radii of benzene and a neighboring carbon atom. The shell is positioned at a radius of 2.8 Å (the diameter of a water molecule) from the excluded volume region.¹²⁵

The cylinder region of Fig. 8 makes up 32% of the total volume of the model. This means that 32% of Lys residues should ideally be found in this volume region. Out of 1,716 Lys residues studied, 48% of the Lys were found to be positioned in the cylinder region. Statistical analysis indicated this to be a nonrandom distribution at a confidence level of greater than 99.999%. Therefore, cation residues are positioned for favorable cation- π interactions in proteins.¹²⁵ A further discussion of cation- π interactions can be found in Chapter 4.

CHAPTER 2

EXPERIMENTAL DESIGN AND METHODOLOGY

Ion-Molecule Reactions

It is possible to probe the preferential gas-phase structure and binding preferences of amino acid--metal ion complexes by studying their relative reactivity when participating in ion-molecule reactions. This analysis can be done by introducing a neutral species into the mass spectrometer's quadrupole ion trap^{94, 133} through the helium line and allowing a reaction to occur with an [A.A.+M⁺] complex. By monitoring the relative amounts of [A.A.+M⁺+neutral] formed over increasing scan delay times, it is possible to determine reaction kinetics. Rates from these kinetic experiments can then be compared and used to compare the structure and reactivity of the gas-phase [A.A.+M⁺] complex.

Neutrals

Neutral species selection is an essential consideration for these particular ion-molecule reactions. The neutral must be volatile so that it can be efficiently

introduced into the helium line. This limits the neutral options to those in the liquid phase at room temperature. Table 13 shows relevant physical data for some potential neutral species. Charge (proton) transfer from the $[A.A.+M^+]$ complex to the neutral can be detrimental to kinetics experiments. However, charge transfer from the complex to the neutral can be exploited for investigating $[A.A.+M^+]$ acidity. To avoid proton transfer in these experiments, it is necessary to use neutral species with similar proton affinities. The rate at which the base associates with the complex is also important. Bases that do not interact within the time frame of the experiment are unable to provide useful kinetics data.

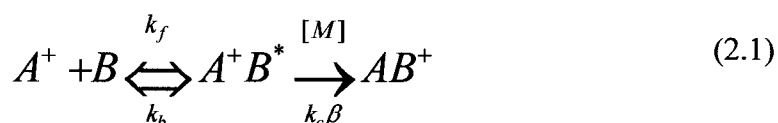
Table 13

Boiling Points and Vapor Pressures of Various Neutral Species.

Neutral	Boiling Point (°C)	Vapor pressure (mmHg at 20°C)
Acetone	56	184
Aniline	184	0.7
Benzene	80	74.6
Boron trifluoride-diethyl etherate	126	4.2
n,o-Bis(trimethylsilyl) acetamide	71-73	--
Butylamine	78	68
Ethyl acetate	76.5-77.5	73
Formic acid	100-101	44.8
4-Methylanisole	174	5.25
1-Methylindole	133	--
Piperidine	106	23
Tetrahydrofuran	65-67	143
Toluene	110-111	22
Trimethyl borate	68-69	--

Reaction Mechanism and Kinetics

These ion-molecule reactions are association reactions; stabilization of the complex occurs via collisions or radiation emission. The mechanism for these reactions is shown in Eq. 2.1,



where k_f is the bimolecular rate constant, k_b is the unimolecular redissociation rate constant, and $k_c\beta$ is the bimolecular rate constant for collisional stabilization by collision with the neutral, M. Here, M is the helium in the ion trap.

Equation 2.2 can be used to obtain the efficiencies of the $[A.A.+M^+]$ complex reactions,

$$\Phi = \frac{k_2}{k_f} \quad (2.2)$$

where k_2 is the overall bimolecular rate constant (the one we observe experimentally) and k_f is the collisional rate constant. The most efficient reaction will occur so that the overall bimolecular rate constant will equal the collisional rate constant. That is, a reaction will occur between the $[A.A.+M^+]$ and the neutral every time there is a collision. Less efficient reactions will occur with a rate constant smaller than the collisional rate constant. The values for the efficiency of the reactions can be compared between the various species to observe which

reactions proceed more efficiently than others.

Since these reactions occur within the ion trap, in the presence of relatively high pressures of helium, it is expected that the stabilization occurs by collisional cooling.^{33, 94} Therefore, it is important to consider the collisional rate constant when calculating the efficiency of the ion-molecule reactions. The calculation of the collisional rate constant is performed as shown by Eq. 2.3:

$$k_f = 2\pi e \sqrt{\frac{\alpha}{\mu}} \chi(\alpha, \mu_D) \quad (2.3)$$

where e is the charge of an electron, α is the polarizability of the neutral, μ is the reduced mass of the $[A.A.+M^+]$ complex and the neutral species, and χ is the dipole correction factor. This dipole correction factor is directly dependent on the polarizability and dipole moment of the neutral species. The collisional rate constant is calculated to determine the rate that collisions occur in the ion trap with respect to the neutral species that is present.

For these experiments, the pressure of the neutral in the ion trap is constant; the reactions occur under pseudo-first-order kinetics. This causes the overall bimolecular rate constant for the reaction to be dependent on the experimental rate constant, k_1 , and the pressure of neutral species in the quadrupole ion trap, according to the relation (Eq. 2.4):

$$k_2 = \frac{k_1}{P_{(acetone)} (\text{molecules} / \text{cm}^3)} \quad (2.4)$$

The bimolecular rate constant describes the selected reaction of the neutral species

to the $[A.A.+M^+]$. The value for the rate constant k_1 is determined from an exponential fitting of a plot of the decay of the $[A.A.+M^+]$ species over the time period of the experiment.

To calculate the efficiency of the reaction, the pressure of the neutral in the system must first be determined. Since the actual pressure of the neutral cannot be determined experimentally, the pressure must be calculated mathematically. To do this, it can be assumed that the standardizing species, discussed in later chapters for specific cases, reacts at the collision rate of the ions in the quadrupole ion trap. This causes the reaction efficiency, Φ , of the fastest reaction to be set to unity ($k_f = k_2$). The pressure of the neutral species in the ion trap can then be calculated as follows (Eq. 2.5):

$$P_{neutral} (\text{molecules} / \text{cm}^3) = \frac{k_{1(AA+M^+)}}{k_{2(AA+M^+)}} \quad (2.5)$$

Ion-Molecule Reaction Methodology

Variable scan delays of ion-molecule reactions were used to determine rate kinetics. The $[A.A.+M^+]$ was isolated in the quadrupole ion trap and was then allowed to react with the neutral species for increasing amounts of time. As the reaction time in the trap increased, the intensity of the $[A.A.+M^+]$ decreased, whereas the intensity of the $[A.A.+M^++\text{neutral}]$ complex increased. The relative intensities of ion products can be calculated and plotted against the time allowed to

pass for the reaction to proceed. Data fitting can then be applied to the kinetics data, and the k_f experimental rate constant can be determined. It is important to note that the uncertainty in the experimental rate can vary $\pm 30\%$. This can occur due to minor fluctuations in the pressure of the neutral species or helium in the ion trap. However, useful comparisons among the amino acids can still be made.

Theoretical Calculations

The experimental data can be compared to data obtained *in silico*, calculated using the computer modeling programs GaussView and Gaussian 03.³ These theoretical modeling calculations were calculated with the program operating under a method employing the density functional theory (DFT) at the B3LYP/6-311G+(d) level. These calculations are performed at the same or higher order levels as currently published results.^{106, 108, 134-140} It is prudent to gain a basic background of the calculation theory and level.

There are three method groups currently employed for model calculations: the semi-empirical, the *ab initio*, and the density functional theory (DFT). Semi-empirical methods rely on experimental observations and data for their calculations. Each semi-empirical method relies on different data parameters, and the quality of the calculations depends on the quality of the data set used. Conversely, *ab initio* methods do not use any experimental parameters for their calculations. They rely solely on the laws of quantum mechanics and on the values of physical constants such as the speed of light, the masses of electrons, etc.¹⁴¹

The determination for using either the semi-empirical or the *ab initio* method often relies on the balance between output accuracy and computational cost. Semi-empirical calculations are relatively inexpensive and are reasonably accurate for calculations in which a quality parameter set exists. On the other hand, *ab initio* methods are able to handle a wide range of systems and are not limited to specific classes or molecules. The inherent drawback to this method is that the calculations are limited by the computational abilities of the workstation. As the system increases in size, so does the time and energy required to perform the calculations.¹⁴¹

The third type of method available for these calculations is the density functional theory (although it is currently under debate as to whether this method is in fact an *ab initio* method). DFT is an improvement on the other methods because the correlation and interaction between electrons is considered in the calculations. It also affords the benefit of accurate calculations at a lesser cost.¹⁴¹

DFT methods use functionals (a function of a function) to compute electron correlations. Electric energies of the system are partitioned into kinetic energy, electron-nuclear interaction, Coulomb repulsion, and exchange-correlation term components. These are calculated separately, and the manners in which the calculations are performed describe the DFT used. It is also possible to use hybrid functionals (linear combinations of various terms), which increase the accuracy of the theoretical calculations. For the calculations presented here, the hybrid functional Becke-style 3-parameter density functional theory employing the Lee-

Yang-Parr correlation functional, or B3LYP, was used.¹⁴¹ The use of B3LYP functional theory is fairly standard for these types of amino acid calculations.

As with methods, there are a variety of basis sets available to the user for performing these calculations. A basis set is defined by Foresman and Frisch as “a mathematical representation of the molecular orbitals within a molecule.”¹⁴¹ Basis sets available through computational programs use linear combinations of Gaussian functions to describe the molecular orbitals. The number and types of functions that each basis set contains is used to characterize the set. As the size of the basis set increases, so does the accuracy of the calculation since the electrons are operating under fewer constraints. However, an increase in basis set size also corresponds to an increase in computational capability.¹⁴¹

The smallest of the basis sets are referred to as minimal basis sets because they have the fewest functions to describe the molecular orbitals. For example, the STO-3G is considered to be a minimal basis set. In the name, STO refers to the “Slater-type orbitals” used to describe the function, whereas 3G represents the three Gaussian component functions that construct the basis function.¹⁴¹

For these calculations, the 6-311G(+)d basis set was used. Here, 6-311G indicates that a triple split valence basis set was used; this means that each orbital description consists of three sizes of linear Gaussian functions. Adding the (+) to the descriptor allows for diffuse functions to be used in the calculation. Diffuse functions are s- and p-type functions which allow the orbitals to occupy more space. These functions are useful for calculations on molecules with lone pair electrons,

anions, and other instances when electrons are farther from the nucleus than would be normally considered. The “d” indicates that d-functions are applied to heavy atoms. What is important here, however, is that the 6-311G(+)*d* basis set is recommended for use on medium-sized molecules containing the elements hydrogen to bromine.¹⁴¹ For amino acid complex modeling, this is a reasonable basis set for these calculations.

The stabilization energies of the [A.A.+M⁺+neutral] complex can be compared to the relative rates of the ion-molecule reactions in order to explain observed kinetics. The charge solvation and zwitterion structures can be modeled to predict which species would likely be more stable in the gas phase. *In silico* calculations can also provide information about the distances between the [A.A.+M⁺] complex and the neutral species for the aromatic amino acid binding experiments. Together with experimental data, these computer-based calculations can provide a great deal of insight to the interactions and structures of amino acids, furthering the fundamental understanding of bioinorganic molecules.

Both ESI-MS ion-molecule reaction techniques and computer-based modeling calculations can be used to analyze and compare the structure of the twenty common amino acids complexed to alkali amino acids. These methods can also be used to probe the reactivities of the aromatic amino acids with respect to the non-aromatic amino acids complexed to alkali earth metals and transition metals.

Zwitterions Revisited

The stability and reactivity of bioinorganics greatly influence biological processes such as signal transduction, reaction control and specificity, molecular structure, and electrostatic interactions. The stability of these species with charged functional groups is related directly to the gas-phase acidities and basicities that they display.⁵⁶ Environmental species, such as water, can provide stabilization for these charges. The addition of metal cations can also stabilize the charges on an amino acid. Figure 9 shows the representative amino acid serine in both zwitterionic and charge-solvated structures when complexed with a sodium cation.



Figure 9. The amino acid serine in both charge-solvated and zwitterion structures. The Gaussian software suite was used to model these molecules. Charge-solvated species complex metal ions through NO-coordination. Zwitterions complex the metal ion through OO-coordination. The atoms are represented as follows: carbon is grey, hydrogen is white, oxygen is red, nitrogen is blue, and sodium is purple.

In neutral solutions (pH of 7), the zwitterion of the amino acid is prevalent, where the carboxyl terminal is deprotonated and the amino terminal is protonated.¹⁴² In the gas phase, the solvent is no longer associated with the amino acid, creating a situation in which the amino acid is more likely to have an overall neutral charge (charge-solvated form).^{34, 143} In a solvent-free environment, it is possible to probe the reactivities of species of interest to better understand the differences between gas- and condensed-phase systems.¹⁴⁴ A greater understanding of the gas-phase properties of these species will provide better information about these species *in vivo*.⁵⁶

The basicity and acidity of the functional groups of the amino acid seem to influence the stability of a zwitterion in the gas phase (i.e., the more acidic the acid is, or the more basic the base is, the more stable the zwitterion will be). It would be expected that arginine would be a likely amino acid to form a zwitterion in the gas phase due to its basic guanidine group.^{103, 139} Julian and Jarrold explain that the formation of the zwitterion in the gas phase depends on Coulombic forces; that is, “the Coulombic energy gained from the interaction of oppositely charged groups must exceed the difference in the basicity between the protonated base and the deprotonated acid.”¹³⁹ For instance, when the side chain of arginine is methylated, the basicity of the amino acid is increased, and zwitterion formation in the gas phase is favored.¹³⁹

Amino acid zwitterions can be formed in the gas phase through stabilization with other species. This can be achieved by hydrating the amino acid¹⁴³ or through

the complexation of the species to a metal ion.^{57, 81, 86, 135, 145} Using BIRD-FT-ICR analysis, Jockusch et al.¹⁴³ have shown that only a few water molecules are necessary to hydrate a $[\text{Val}+\text{M}^+]$ species to prefer the zwitterion structure. They have also shown that in the case of $[\text{Val}+\text{Li}^+(\text{H}_2\text{O})_2]$, the water molecules interact only with the lithium ion, yet the structure remains charge-solvated. With the addition of a third water molecule, the structure of the $[\text{Val}+\text{Li}^+]$ complex appears to change from the charge-solvated structure to that of the zwitterion. This third water molecule, unlike the first two, does not interact with the lithium ion; it interacts with the N-terminal of valine. As the cation size increases, it seems that fewer water molecules are necessary for zwitterion stabilization. For instance, when the $[\text{Val}+\text{K}^+]$ complex is analyzed, two water molecules are sufficient for zwitterion stabilization.¹⁴³

Metal Ion Effects

The charge and size of the metal cation can also affect the stability of gas-phase amino acid zwitterions. For example, the complexation of a singly charged (alkali) metal ion to glycine can increase the zwitterion's stability over 80 kJ/mole relative to the charge solvation form. It is important to note, however, that the charge-solvated form for glycine remains lower in energy. When a doubly charged (alkali earth) metal ion is complexed to glycine, the zwitterion becomes energetically more stable than the charge-solvated form.^{103, 104, 112, 117} Theoretical computations confirm this finding, as shown in Fig. 10.

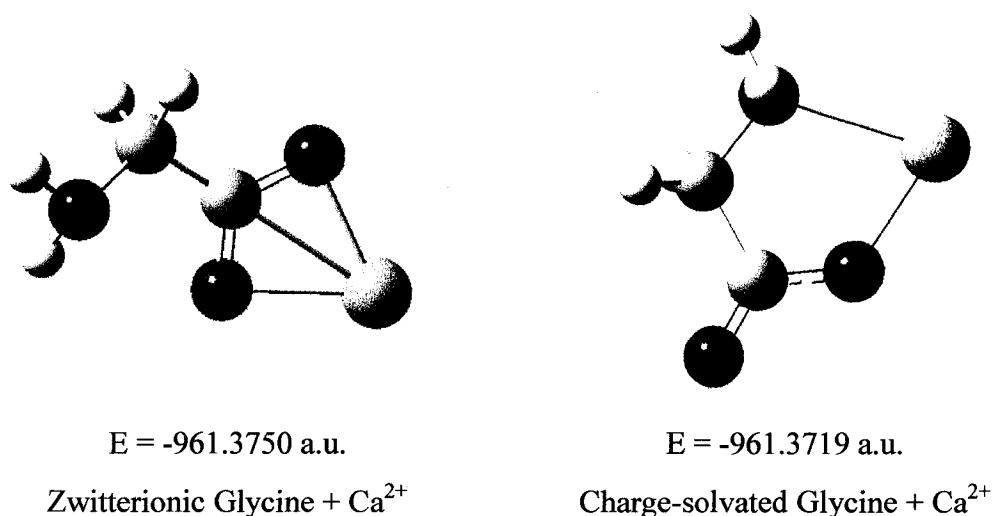


Figure 10. Gaussian modeling results of glycine complexed to Ca²⁺. The energy of the complex was computed under the same conditions as all theoretical computations in this study. The energy is reported in arbitrary units (a.u.). The lowest energy structure is the zwitterion, which is calculated to be ~8 kJ/mole more stable than the charge-solvated structure.

The size of the metal cation also affects the gas-phase stability of the zwitterion. It would be expected that the size of the metal ion would affect the binding affinity of the amino acid as follows: Li⁺>Na⁺>K⁺>Rb⁺>Cs⁺. In general, the smaller the metal ion is, the easier it is for the ligand to complex it. This trend can be altered when the ligating portion of the amino acid is incapable of efficiently binding the ion. That is, when the metal ion is small, it may easily be complexed. When the metal ion is larger, the ligating arm may no longer be able to surround the metal ion. This could, in fact, cause a structural change for a molecule like an amino acid.

Specifically, the smaller alkali metals (i.e., Li^+ , Na^+ , and K^+) complexed to the amino acids alanine, valine, leucine, and isoleucine appear to be charge-solvated in the gas phase; however, when a larger alkali metal (Cs^+) is complexed to the amino acids, the zwitterionic structure is preferred.¹⁴⁶ This finding was determined using the kinetic method. Glycine complexed to alkaline earth metals¹⁰⁴ and arginine complexed to alkali metals have shown similar trends.^{57, 146} The apparent size trend may not hold true, however, as it has been suggested that rubidium ions actually stabilize the charge-solvated structure of the amino acid more than a smaller metal ion (i.e., sodium).¹⁰³

The proton affinity of the amino acid can also affect the stability of the zwitterionic structure in the gas phase.^{102-104, 117} Previous studies have shown that a relatively linear relationship exists between the proton affinity of aliphatic amino acids and the stability of the zwitterionic structures of the complexes.^{103, 117} The addition of a cation to the amino acid reduces the effect of the proton affinity on zwitterion stability, which can complicate the analysis.¹¹⁷

Experimentally identifying the stable structure of amino acids in the gas phase has led to many conflicting results. It is widely accepted that proline complexes are zwitterions in the gas phase: Pro is the only amino acid to lack an amino group, making it capable of only OO coordination. Much debate continues as to the structure of arginine, lysine, and many of the other amino acid complexes.¹⁴² For instance, it has been reported that sodiated glutamine is both zwitterionic¹⁰³ and

charge-solvated¹¹¹ in the gas phase. Consequently, it is relevant to continue to investigate the gas-phase structure of amino acids.

To summarize, both mass spectrometric and *in silico* studies can be used to analyze the gas-phase structure of amino acid complexes. Information gathered from CID studies, the kinetic method, ion-molecule reactions, and other techniques can provide relevant kinetic information. Along with the thermochemical data provided by theoretical computational analysis, this information can be pieced together to determine the structure of amino acid complexes in the gas phase.

Aromatic Amino Acids Revisited

It is widely agreed that cation- π interactions play an important role in the structure of peptides and proteins. In addition to the roles that hydrogen bonds and salt bridges play in biological structure, the noncovalent cation- π interactions can also play a large role.¹²⁵ Pletneva et al. have suggested that cation- π interactions “can be as strong as the familiar salt bridges and hydrogen bonds.”¹⁴⁷

Studies concerning cation- π interactions range from analysis of individual amino acids¹⁴⁸⁻¹⁵⁰ to peptides containing aromatic amino acids^{151, 152} to protein interaction analysis.^{122, 125, 126, 128, 153, 154} Mostly, these studies have greatly relied on the use of theoretical computations and other *in silico* analysis techniques to investigate the role of amino acids in cation- π interactions. Many of these studies investigated [amino acid+M^{X+}] species, where M represents alkali, alkali earth, and

transition metals.^{148, 149, 151, 155, 156} Often, the aromatic amino acids are of interest, although Arg and Lys have also been studied.¹⁵²

Spectroscopic measurements have been used to compare the interaction of Phe and Tyr to silver through surface-enhanced Raman scattering.¹⁵⁷ NMR experiments have been used to study amino acid interactions in coiled-coil protein domains.¹⁵⁴ Cation- π interactions have also been experimentally studied via mass spectrometric techniques. CID has been used to study a variety of metal cation and amino acid complexes.^{36-41, 158}

Ion-Molecule Reactions

Methodology for Zwitterion Analysis

As previously discussed, it is possible to probe the preferential gas-phase structure of amino acid--metal ion complexes by studying their relative reactivity. Neutral bases react with the $[A.A.+M^+]$ by solvating the metal. The rate and amount of reaction with a neutral will differ depending on the $[A.A.+M^+]$. Ion-molecule reactions between the $[A.A.+M^+]$ and the neutral can be performed by introducing the neutral into the quadrupole ion trap¹³³ and allowing a reaction to occur with an $[A.A.+M^+]$ complex, where $M = Li^+, Na^+, K^+, \text{ and } Cs^+$. By varying the scan delay reaction time, it is possible to follow the kinetics of formation of the $[A.A.+M^++neutral]$. Rates from these kinetic experiments can then be used to

surmise the structure and reactivity of the gas-phase $[A.A.+M^+]$ complex by comparison to known zwitterions. The calculations for the kinetics are detailed in Eqs. 2.2-2.5.

Amino Acid Standards

To accurately use the reaction kinetics data, it is necessary to use standards (i.e., molecules with known permanent gas-phase structure) for the kinetics comparisons. Betaine (Sigma Aldrich) was used as a known gas-phase zwitterion. As can be seen in Fig. 11, betaine (Bet) has a permanent zwitterionic structure. The betaine molecule has three methyl groups attached to the amino terminus, preventing NO coordination of the metal ion. The metal must be complexed by the carboxyl oxygens in a zwitterionic manner.

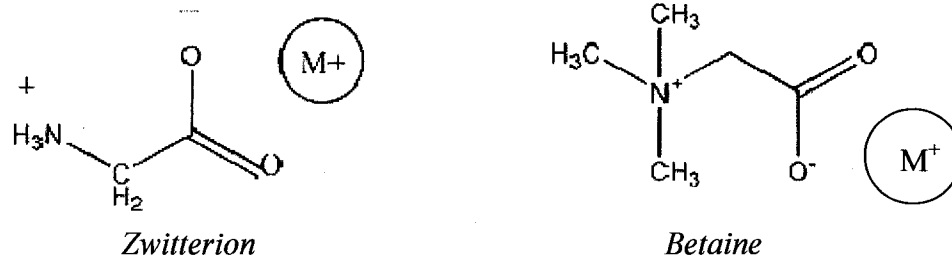


Figure 11. The structures the zwitterionic amino acid (left) and betaine (right) complexing a metal ion. Betaine displays permanent charge separation.

To model permanent charge-solvated structures, the methyl esters of select amino acids were used as known gas-phase nonzwitterions. Methyl esters contain a methyl group on the singly bound oxygen on the carboxyl terminal. This methyl group remains on the carboxyl oxygen, as opposed to the transferable hydrogen of the amino acid, creating a permanent charge-solvated structure. This causes the methyl esters to complex the metal ion through NO coordination. The structures of all of the methyl esters (obtained from Sigma Aldrich) are depicted in Appendix C.

To review, charge-solvated amino acids complex the metal cation through NO coordination. Zwitterions complex the metal cation through OO coordination. Methyl esters of amino acids are only capable of complexation through NO coordination, which makes them permanently charge-solvated, as shown in Fig. 12.

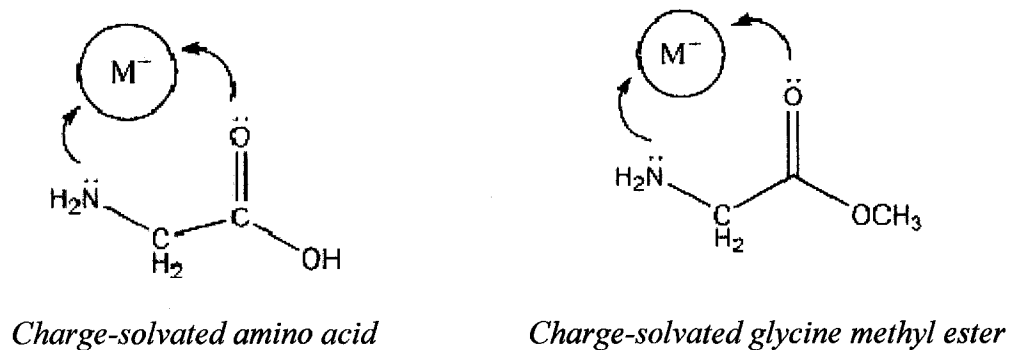


Figure 12. A comparison of a charge-solvated amino acid complex and the charge-solvated complex of glycine methyl ester. Note that the carboxyl group cannot be deprotonated in a methyl ester due to the methyl group on the carboxyl oxygen.

Neutral Species Selection

It was necessary to determine an appropriate neutral species for structural ion-molecule reaction experiments. The neutral species for these reactions must be a volatile liquid with a relatively high vapor pressure. These features guarantee that the neutral species will enter the helium stream to the instrument in the gas phase. Besides these requirements, it is also necessary that the neutral species is reactive towards the $[A.A.+M^+]$. This ensures that kinetic data can be obtained for these experiments. All of the neutrals that were used for these experiments were obtained from Sigma Aldrich.

Both nitrogen bases (e.g., butylamine, di-isopropylamine, triethylamine) and oxygen bases (e.g., ethyl acetate, tetrahydrofuran, acetone) were tested as potential neutral species. In the experiments involving butylamine (But) as the neutral, the association reaction was too slow to be observed within a reasonable time frame for these experiments (Fig. 13). As can be seen in the mass spectrum for sodiated proline reacting with butylamine, only a small amount of $[Pro+Na^++But]$ is formed during a fairly long reaction period of 5000 ms. Since the scan delay limit is 9999 ms, pertinent kinetic data cannot be obtained if the reaction is not observable at approximately half the time limit.

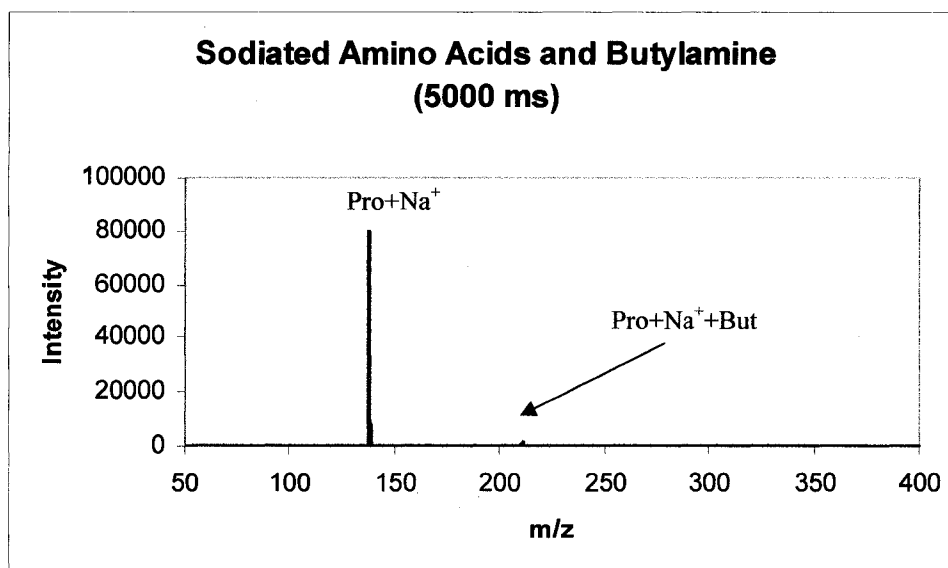


Figure 13. The slow reaction of sodiated amino acids and butylamine (But). An addition of 73 m/z to the [A.A.+Na⁺] is expected for an addition of a butylamine molecule. A small amount of [Pro+Na⁺] is found to complex with butylamine, with an m/z of 211.

Other nitrogen bases reacted with the [A.A.+M⁺] to form the [A.A.+M⁺+neutral] complex, although significant amounts of proton transfer to the neutral species were observed. This is readily apparent for the reaction of [Asn+Li⁺] and triethylamine (TEA) (Fig. 14). In Fig. 14, it can be seen that an ion of 102 m/z is observed after a 1000 ms reaction time. This ion corresponds to the protonation of the neutral TEA, which has a molecular weight of 101. TEA has a high proton affinity (PA) (~235), which is why this transfer occurs.

The ion observed at 157 m/z corresponds to an addition of water to the [Asn+Li⁺] species; the addition of 18 m/z to an ion is indicative of water-complex

formation. Finally, an ion of 140 m/z is also present in the spectrum. This ion corresponds to the addition of TEA (101 m/z) to the $[\text{Asn}+\text{Li}^+]$ species (139 m/z).

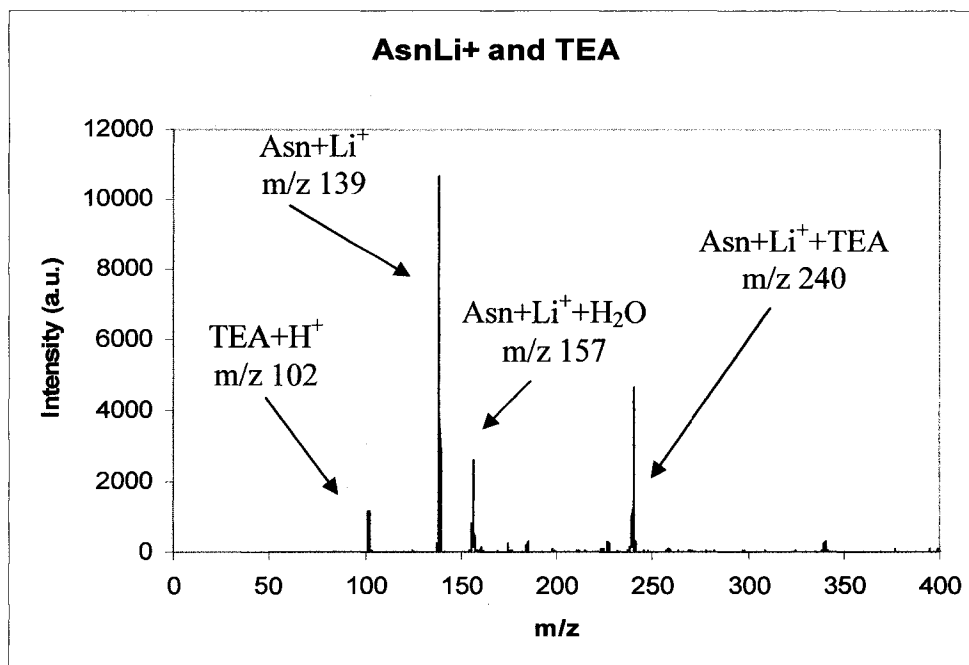


Figure 14. Proton transfer to the neutral species triethylamine (TEA). The reaction was observed over a scan delay of 1000 ms. The molecular mass of TEA is 101. The protonated molecule has an m/z of 102.

Sodiated amino acids do not exhibit as much proton transfer as lithiated amino acids. However, proton transfer is still present (Fig. 15). Figure 16 focuses on the mass range of 102 m/z to better highlight this observation for multiple spectra. Figure 15 also shows that TEA does form complexes with the sodiated amino acids in a reasonable time frame of 1000 ms. TEA is not an optimal neutral for these experiments, though, due to the proton transfer that is observed.

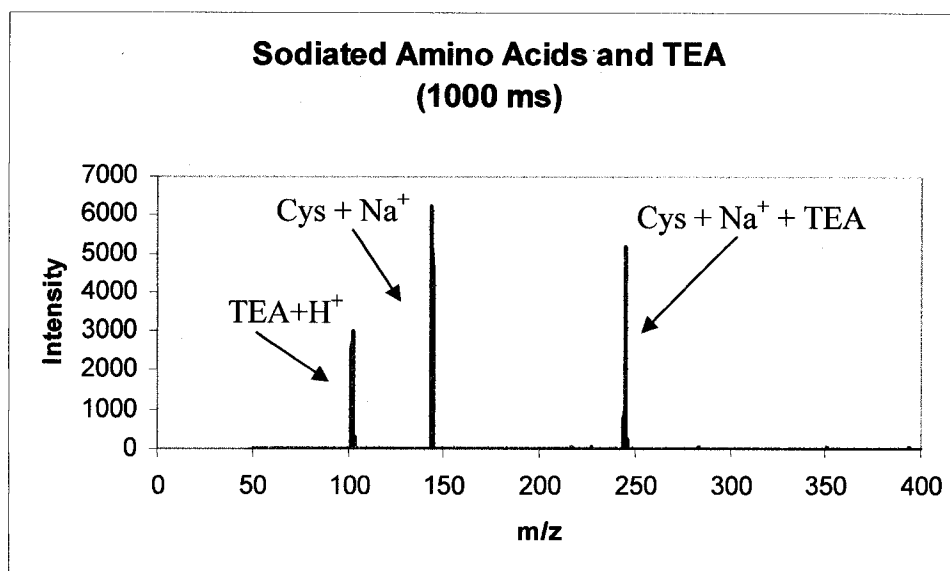


Figure 15. The reaction of sodiated cysteine with triethylamine over a 1000 ms scan delay period. Both proton transfer to TEA (observed at 102 m/z) and addition of TEA to the amino acid complex can be observed at 1000 ms.

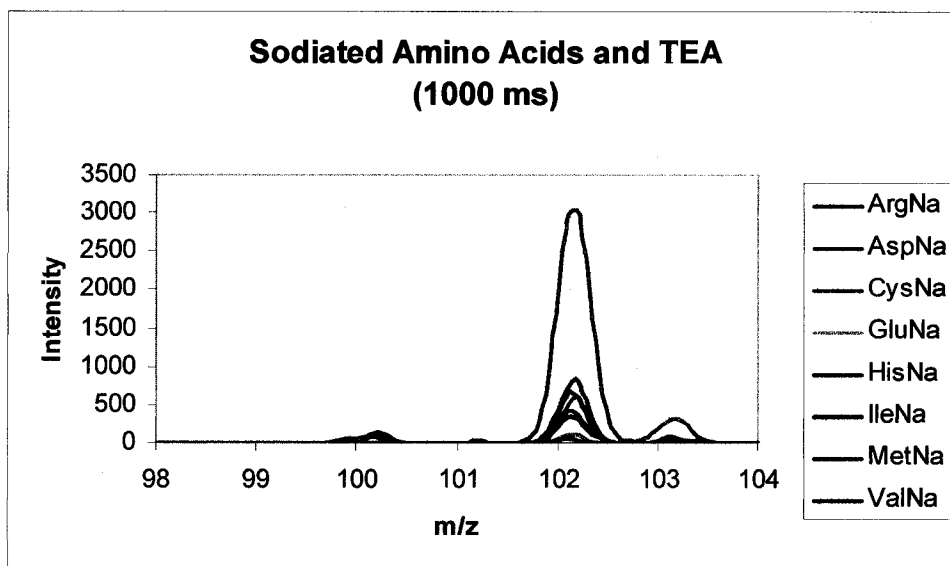


Figure 16. Protonation of TEA over a 1000 ms time frame. Varying amounts of protonation are observed for each of the reactions involving the eight sodiated amino acids shown above. The reaction involving [Arg+K⁺] shows the most proton transfer, whereas the reaction involving [Glu+K⁺] shows the least amount of proton transfer to TEA.

The protonation of the neutral lowers the amount of neutral available to complex with the $[A.A.+M^+]$ species. This competition directly alters the reaction kinetics of the experiment, which complicates the data analysis. Ion-molecule reactions involving neutrals with proton transfer were not used for these experiments. The proton transfer reactions, however, can be used to study the acidity of the $[A.A.+M^+]$ complexes, which can also shed light on their structure.

The oxygen bases tetrahydrofuran (PA~197) and ethyl acetate (PA ~200) exhibited slow reaction kinetics with the $[A.A.+M^+]$, preventing the reactions to proceed within the time limitations of the experiment (9999 ms). This can be seen for tetrahydrofuran (THF) in Fig. 17. After 9000 ms, there is very little addition of THF to the $[Pro+Na^+]$ ion. Since the $[Pro+Na^+]$ species has a 138 m/z, the addition of THF (72 m/z) should result in an ion corresponding to 210 m/z. A low-intensity ion is observed at 210 m/z after a reaction time of 9000 ms. Since this reaction time is near the upper time limit of the experiment, THF is not an optimal neutral to use for these ion-molecule reaction experiments. Similar results were also observed for different sodiated amino acids reacted with ethyl acetate (EA) as shown in Fig. 18.

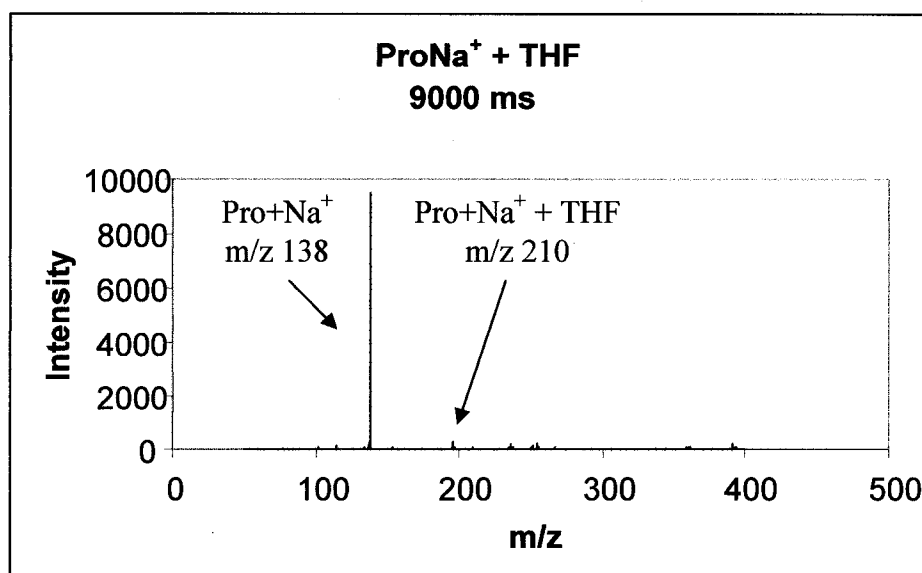


Figure 17. A demonstration of the slow kinetics of the oxygen base tetrahydrofuran. After a reaction time of 9000 ms, there is no noticeable addition of THF to [Pro+Na⁺]. An addition of m/z 72 should be observed for the addition, with an expected [Pro+Na⁺+THF] m/z of 120.

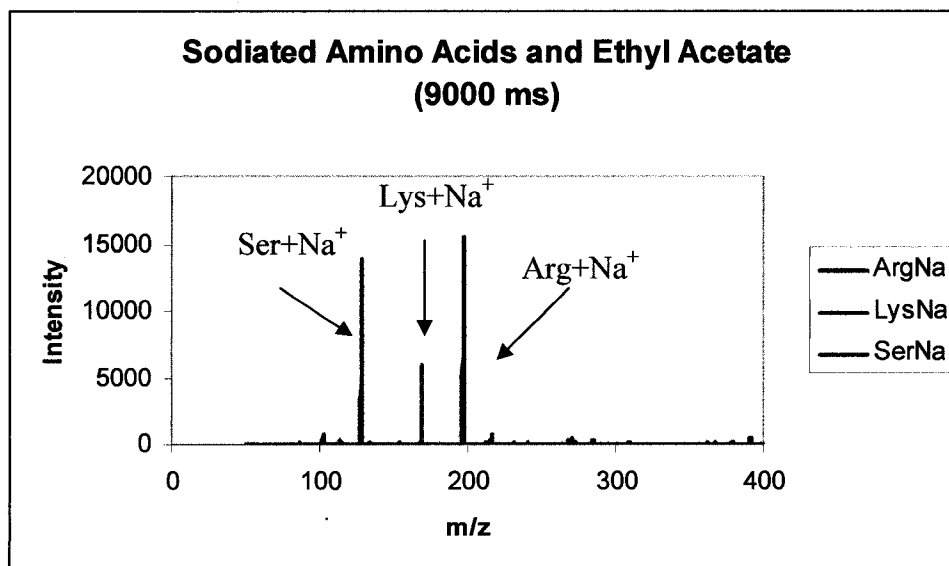


Figure 18. The slow reaction kinetics of the oxygen base ethyl acetate (EA). As observed for reactions with THF, there is no significant addition of EA during the 9000 ms scan delay reaction period.

It was found that acetone, an oxygen base, was the optimal neutral to use for these experiments. Reactions with the $[A.A.+M^+]$ complex and acetone did not demonstrate proton transfer (PA ~ 194) and the reaction kinetics were found to be appropriate for the time frame of the study (Fig. 19). As can be seen from Fig. 19, a significant amount of acetone addition can be observed in the reasonable scan delay time frame of 2000 ms. In this figure, the $[Pro+Na^+]$ species (138 m/z) is shown to react with acetone (molecular weight of 58) to form an ion corresponding to 196 m/z.

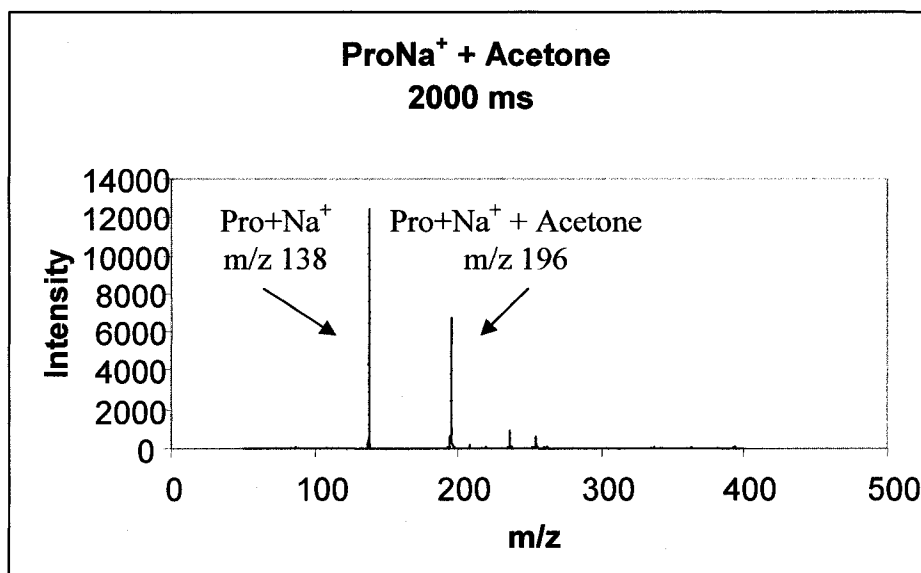


Figure 19. An example of the reaction kinetics of the neutral acetone. The addition of acetone to the same $[A.A.+M^+]$ species occurs at a much faster rate compared to THF and EA. The $[Pro+Na^++Acetone]$ complex has an m/z of 196.

A survey of all twenty common amino acids was performed in order to ensure that the kinetics of these reactions would be appropriate for the time frame of this experiment. Since lithium complexes react fairly quickly, it was necessary to establish that slower reactions would be observable. Therefore, sodiated amino acids were allowed to react with the acetone for 1000 ms at a pressure of 7×10^{-8} Torr to ensure that addition of the neutral (however limited) could be observed. Example spectra are shown for four of the amino acids tested (Fig. 20).

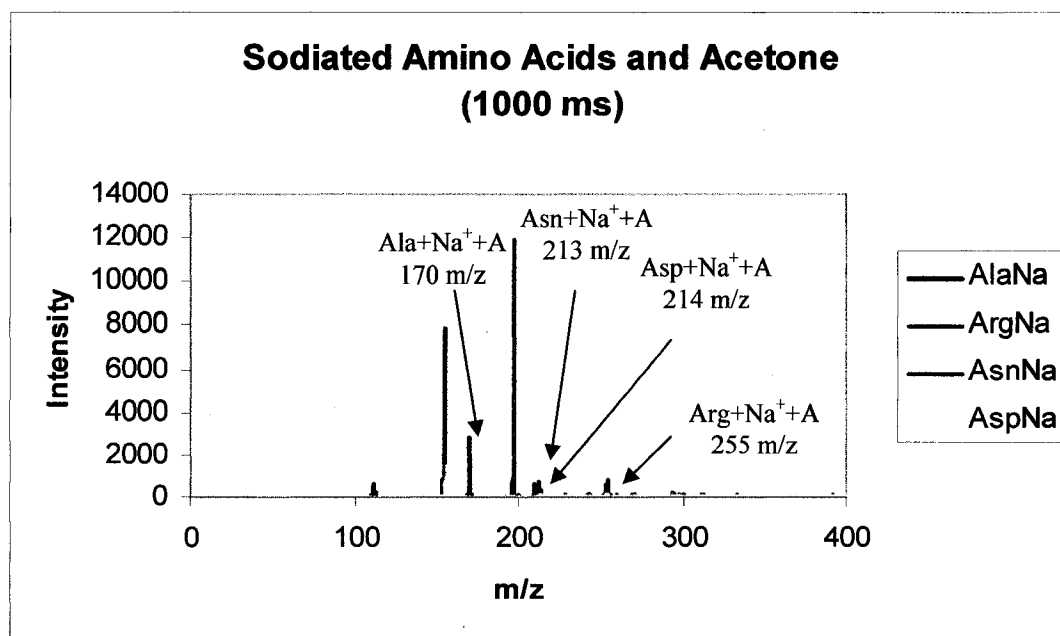


Figure 20. The reaction of four representative sodiated amino acids with acetone after a scan delay period of 1000 ms. An addition of 58 m/z can be observed in all spectra presented here. To minimize confusion, only the [A.A.+Na⁺+acetone] species is identified. Acetone is abbreviated to A for ease of data labeling.

Methodology for Aromatic Amino Acid Analysis

The analysis of aromatic amino acids and their cation- π interactions can be analyzed in a similar manner to the structural analysis experiments described previously. The $[A.A.+M^+]$ complex is formed through ESI, and a reaction is allowed to occur with a neutral contained in the quadrupole ion trap. A variety of alkaline earth metals and transition metals were used in these experiments. The neutral species was selected to model the side chains of the aromatic amino acids Phe and Tyr. A further explanation of the neutral selection is provided in Chapter 4. The scan delay times for the reaction were increased, and an increase of the $[A.A.+M^+ + \text{neutral}]$ was observed. The scan delay time was continually increased until a steady-state equilibrium of $[A.A.+M^+]$ and $[A.A.+M^+ + \text{neutral}]$ was obtained. The data-fitting and rate-kinetics calculations were performed using the KinFit macro in Excel.

Experimental Details

Mass Spectrometry

A commercial Bruker Esquire 3000 quadrupole ion trap mass spectrometer (Bruker Daltonics, Billerica, MA) with an electrospray ionization (ESI) source was used in this study. Metal ion – amino acid complexes were formed by ESI from 10-

50 μM solutions of amino acid – metal acetate mixtures. The solutions were introduced to the mass spectrometer by a syringe pump (Fisher) at a flow rate of 4 $\mu\text{L min}^{-1}$. The ESI source was operated under the following conditions: nebulizer gas at 15 psi, dry gas flowing at a rate of 5 L min^{-1} , and a capillary temperature of 200°C. Source voltages were optimized for maximum ion yield.

Following Gronert's method,^{133, 159} a syringe pump (Fisher) was set up to continuously introduce the neutral (Sigma Aldrich) directly into the helium line at rates of 3 $\mu\text{L hr}^{-1}$ or 30 $\mu\text{L hr}^{-1}$. The neutral species was introduced to the ion trap through the helium line for a sufficient amount of time (at least one hour) before the experiments were performed in order to allow for a stabilization of neutral pressure in the quadrupole ion trap. A gas flow meter (Kurt-Lesker) was used to measure the flow of helium, held at a constant 2.00 L min^{-1} .

The $[\text{A.A.}+\text{M}^+]$ complexes were isolated in the quadrupole ion trap using a peak width isolation set at 0.7 (Fig. 21). The isolation width was optimized to ensure that only the selected ion was trapped. After isolation, the $[\text{A.A.}+\text{M}^+]$ species were then allowed to react with the acetone for different amounts of time. The variable scan delay option was used to monitor reaction kinetics, which occurred within the limits of 0 to 9999 ms. These scan delay limits are imposed by the Bruker Esquire 3000 software and cannot be increased for these experiments.

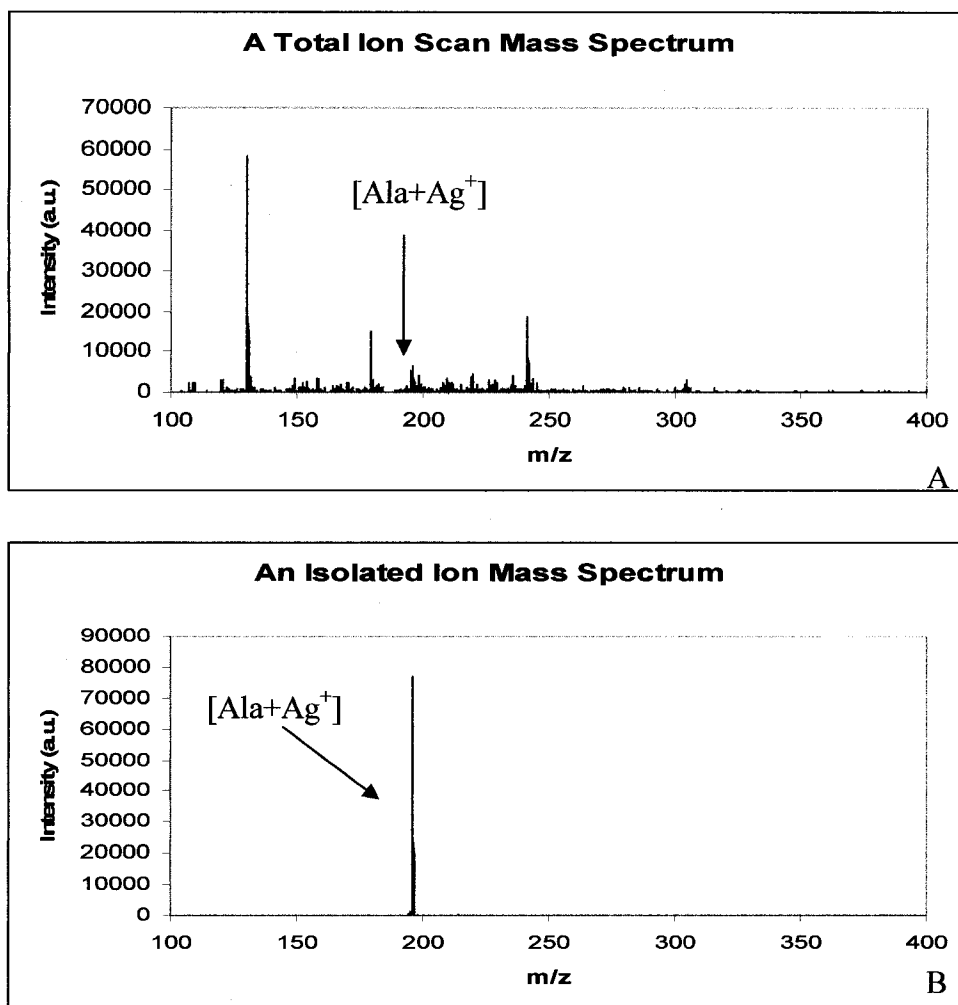


Figure 21. Ion isolation. a) The full scan ion spectra without isolation. This is a sample mixture containing alanine and silver. b) Isolation of the desired ion species, [Ala+Ag⁺]. The m/z of the selected ion is 196.

Figure 22 shows the experimental ESI-MS setup for neutral introduction. As can be seen from the diagram, the mass spectrometer can be operated in either normal or ion-molecule reaction mode. Helium is sent directly to the ion trap for normal operating mode. In ion-molecule reaction mode, the neutral is directly introduced to the helium line. The flow of the neutral is controlled by the syringe pump and can vary between 3 and 120 $\mu\text{L hr}^{-1}$. The estimated neutral pressure in the quadrupole ion trap for these flow rates is on the order of 10^{-8} to 10^{-9} Torr, as calculated by Gronert's method. Higher flow rates can effectively clog the helium line. The helium carrying the neutral is directed to the ion trap at a flow rate of 2.00 L min^{-1} . The excess helium/neutral gas is diverted to waste.

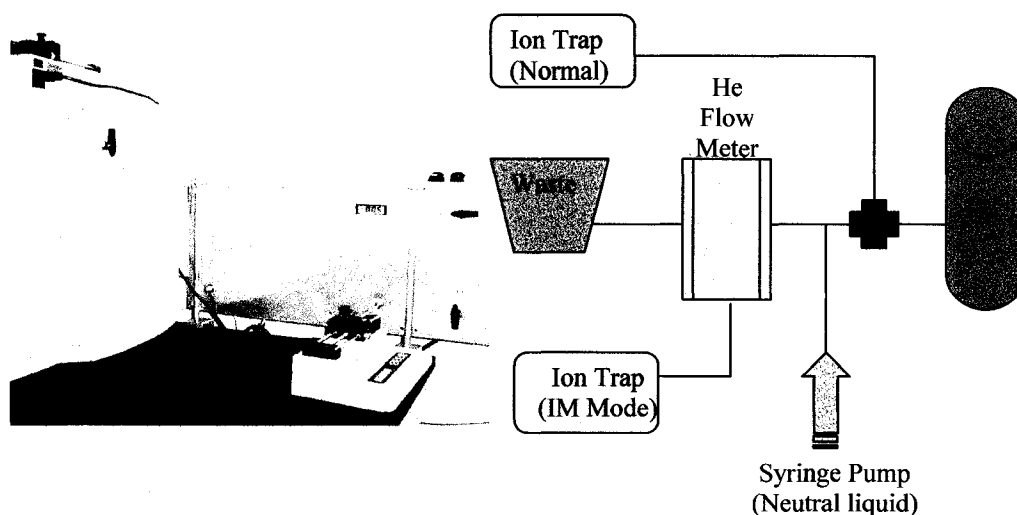


Figure 22. The neutral introduction scheme. When operating in ion-molecule reaction mode, the neutral is introduced into the helium line and directed to the quadrupole ion trap. A digital read-out flow meter regulates the pressure of gas flowing to the trap. Excess He gas is directed to waste.

Initially, the most intense ion present in the quadrupole ion trap under isolation mode is the $[A.A.+M^+]$. Typically, before the reaction takes place, the isolated species has a relatively high intensity. As the reaction (scan delay) time in the ion trap is increased, the intensity of the product $[A.A.+M^++\text{neutral}]$ species also increases. This observation is demonstrated by $[\text{Leu}+\text{Li}^+]$ and acetone experiments in Fig. 23. At 0 ms, the $[\text{Leu}+\text{Li}^+]$ species is the most intense ion peak. It can be seen that for a 400 ms scan delay, the intensity of the $[\text{Leu}+\text{Li}^+]$ species was a bit less than the intensity of the $[\text{Leu}-\text{Li}^+-\text{acetone}]$ species. As the scan delay was increased to 1000 ms, the greatest intensity ion becomes the $[\text{Leu}+\text{Li}^++\text{acetone}]$ species. Note that the addition of water to $[\text{Leu}+\text{Li}^+]$ can also be observed.

The scan delay was incrementally increased over an extended period of time (i.e., increased from 0 to 5000 ms at 200 ms intervals). The data from each time point was then plotted to compare the relative intensities of the parent ion ($[A.A.+M^+]$) and the complex ($[A.A.+M^++\text{neutral}]$) versus the scan delay time (Fig. 24). The relative intensity (RI) of the selected species was obtained by calculating the fraction of the species of interest to the total ions present using the following equation (Eq. 2.6):

$$\text{RI} = \frac{\text{Ion Intensity}_{\text{species}}}{\text{Ion Intensity}_{\text{total}}} \quad (2.6)$$

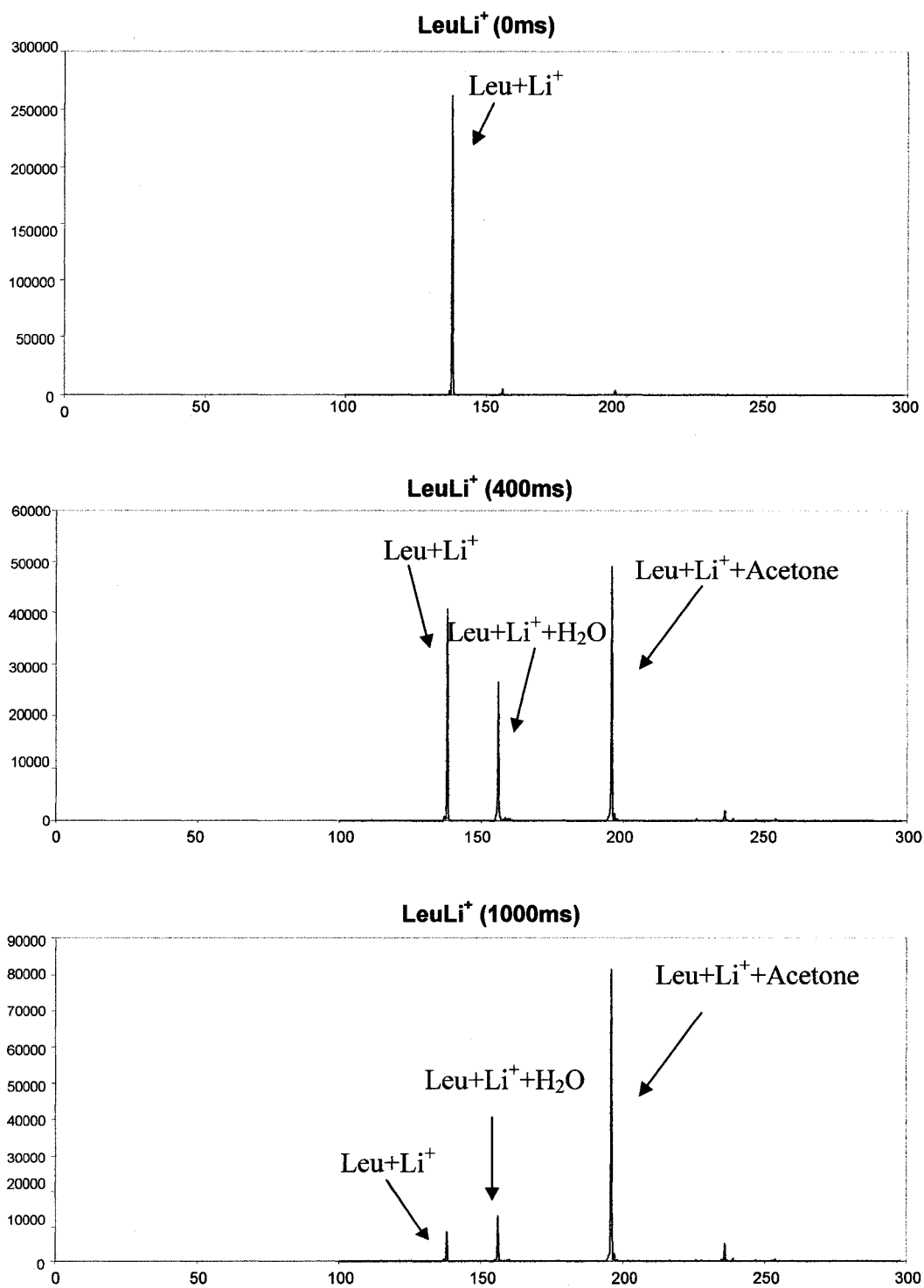


Figure 23. An example of the increase in product formation as the scan delay time is increased.

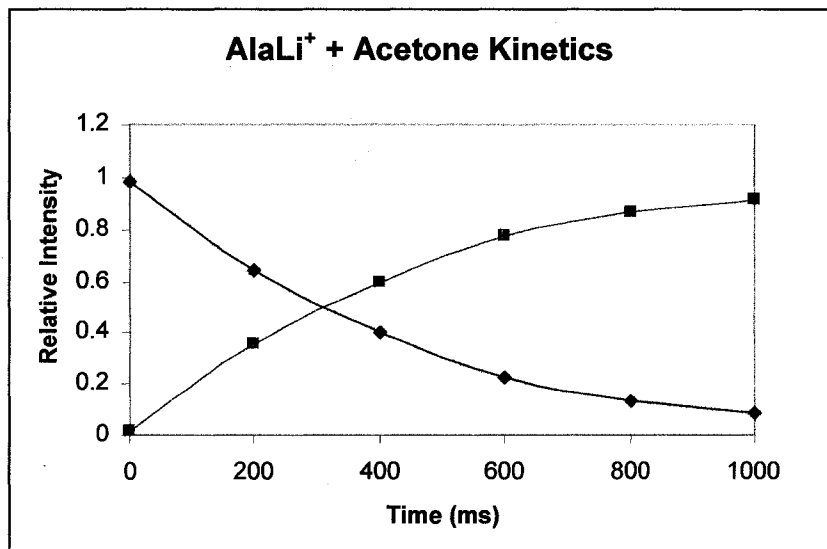


Figure 24. The typical kinetics trend observed for these reactions. The decrease in the $[A.A.+M^+]$ occurs simultaneously with the increase of the $[A.A.+M^++\text{acetone}]$ formation over time.

The relative intensity was calculated for both the $[A.A.+M^+]$ and the $[A.A.+M^++\text{neutral}]$ species. For zwitterion analysis experiments, the data collection concluded when the relative intensity of the $[A.A.+M^+]$ complex no longer decreased or when the scan delay time reached the limit of 9999 ms. In aromatic amino acid studies, the observation of equilibrium signaled the end of data collection.

Pseudo first-order rate constants (k_1) for the exponential decay of the $[A.A.+M^+]$ were obtained by data fitting using Excel. In the structural analysis experiments, exponential line fitting was used to determine decay constants. The KinFit macro for Excel was used to fit data obtained for aromatic amino acid

experiments. The kinetics data were then used to compare the reactions of the [A.A.+M⁺] species.

Determination of Neutral Pressure

It is possible to estimate the pressure of the neutral in the ion trap using Gronert's method as follows:

$$P_{Neutral} (Torr) \approx (1 \times 10^{-3} Torr) \left(\frac{F_R \cdot d_R}{MW_R} \right) \left(\frac{1}{F_{He}} \right) \left(\frac{MW_R}{MW_{He}} \right)^{1/2} \quad (2.7)$$

In this equation, the pressure of the neutral can be estimated by the flow rate of the neutral (F_R) from the syringe pump, the density of the neutral (d_R), the flow rate of helium into the ion trap (F_{He}), and the molecular weights of the neutral (MW_R) and helium (MW_{He}). For example, the estimated pressure of acetone ($d = 0.0872 \text{ g mL}^{-1}$) flowing at a rate of $3 \text{ } \mu\text{L Hr}^{-1}$ into the helium line would be estimated by:

$$P_{Acetone} (Torr) \approx (1 \times 10^{-3}) \left(\frac{3 \mu\text{L Hr}^{-1} \cdot 0.791 \text{ gmL}^{-1}}{58 \text{ gmol}^{-1}} \right) \left(\frac{1}{2.00 \text{ L min}^{-1}} \right) \left(\frac{58 \text{ gmol}^{-1}}{4.003 \text{ gmol}^{-1}} \right)^{1/2} \quad (2.8)$$

The result of Eq. 2.8 estimates the pressure of acetone in the quadrupole ion trap to be approximately 2.9×10^{-8} Torr.

Although it was possible to estimate the pressure of acetone mathematically, it was necessary to determine the neutral pressure experimentally. To do this, it can be assumed that the fastest reaction occurs at the collisional rate of the species in the trap, as previously described. Here, this calculation is demonstrated for experiments

using acetone as the neutral species. Similar calculations can be performed for neutrals used in the aromatic amino acid modeling experiments to determine the neutral pressure in the ion trap.

The lithiated amino acid species demonstrates the fastest reaction kinetics in these experiments. The fastest reacting [A.A.+Li⁺] species, in this instance [Ala+Li⁺], can be used to determine the pressure of acetone in the quadrupole ion trap as follows:

$$\mu = \frac{m_{\text{Gly+Li}^+} \times m_{\text{acetone}}}{m_{\text{Gly+Li}^+} + m_{\text{acetone}}} = \frac{96 \times 58}{96 + 58} = 36.16 \quad (2.9)$$

$$k_f = 2\pi e \sqrt{\frac{\alpha}{\mu}} = 2\pi(4.8 \times 10^{-10}) \sqrt{\frac{6.33}{36.16 \cdot 1.67}} = 9.765 \times 10^{-10} \frac{\text{cm}^3}{\text{molecule} \cdot \text{s}} \quad (2.10)$$

where μ is the reduced mass of the [Ala+Li⁺] species and acetone, k_f is the collisional rate constant, and α is the polarizability of the neutral. The term “1.67” in the denominator is used to convert the mass of the species to grams. From Eq. 2.10, the pressure of acetone in the quadrupole ion trap was calculated to be approximately 7×10^{-8} Torr for acetone entering the helium line at a flow rate of $3 \mu\text{L hr}^{-1}$. The estimated pressure uncertainty is approximately $\pm 30\%$.

Theoretical Calculations

Theoretical modeling calculations, performed by the Gaussian 03 suite³ operating under the density functional theory (DFT) at the B3LYP/6-311G+(d)

level, as previously described, were performed. These calculation parameters are the published standard for ion-molecule reaction calculations. The preliminary structures of the $[A.A.+M^+]$ complexes were entered into the GaussView³ program, and the structure was neatened by GaussView and then optimized by Gaussian 03 calculations. The energy of the optimized structure was calculated using the same parameters. The neutral species was added to the optimized $[A.A.+M^+]$ complex, and the $[A.A.+M^++neutral]$ complex was subsequently optimized and analyzed in the same fashion (Fig. 25).

For comparison purposes, the stabilization energies of the systems were converted from the hartree units computed by Gaussian to kJ mol^{-1} . The stabilization energy is calculated as the energy difference between the $[A.A.+M^+]$ and $[A.A.+M^++neutral]$ species. For experiments with neutral acetone, the distance between the oxygen atom of the acetone and the complexed metal ion is also reported. This distance is important because it shows how well the metal ion and acetone are complexed to the amino acid species; the closer the metal ion and the oxygen of the acetone are, the greater the stabilization of the system is. This information facilitates the evaluation of the data when comparing the $[A.A.+M^+]$ species to the $[A.A.+M^++acetone]$ species. For future reference, the atomic color system employed by GaussView is as listed in Table 14.

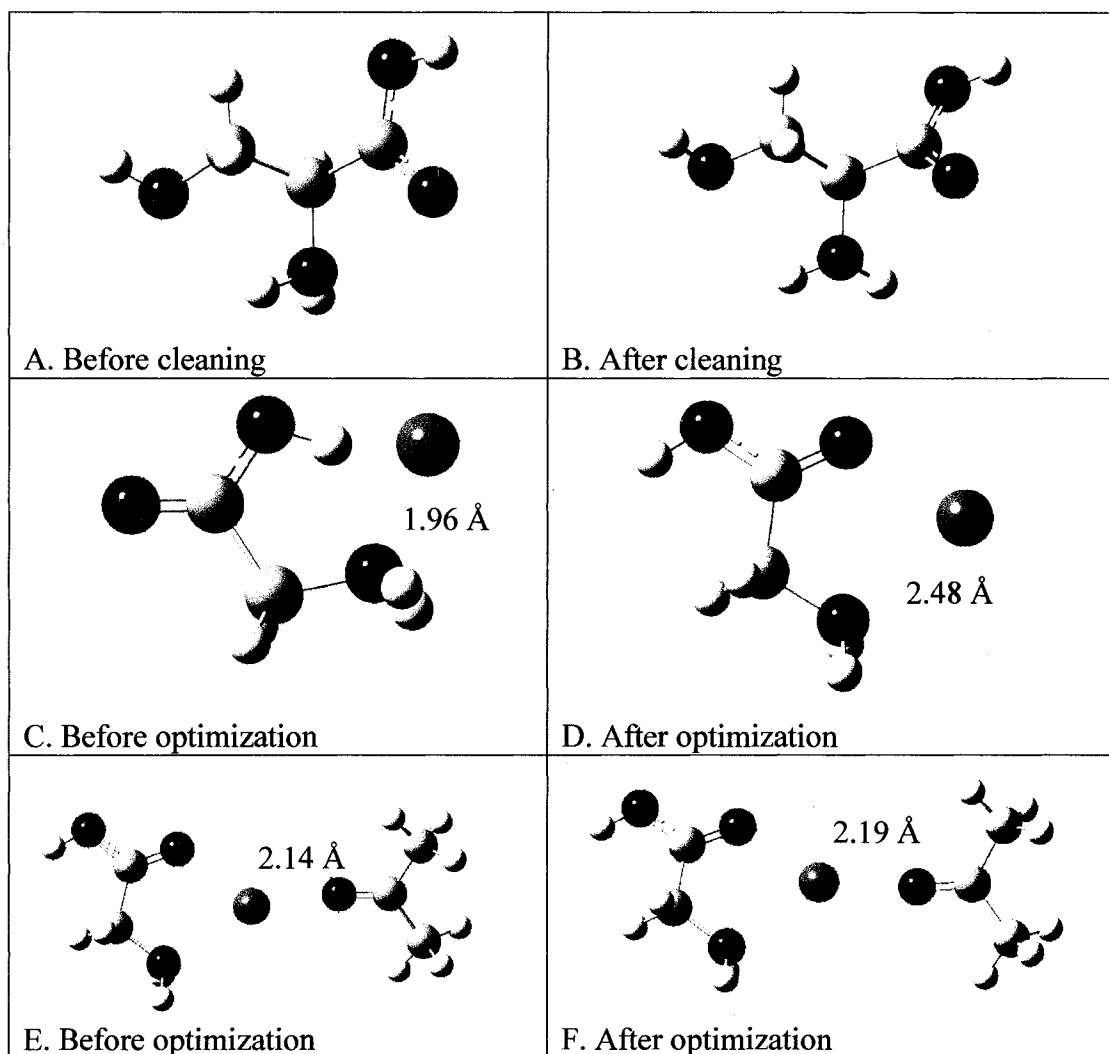


Figure 25. The use of Gaussian optimization. A serine molecule before (A.) and after (B.) cleaning by the Gaussian program. The most visible change is the position of the hydrogens on the nitrogen atom. (C.) The [Gly+Na⁺] complex before optimization and (D.) after optimization. (E.) The [Gly+Na⁺] complex in (D.) with acetone added. (F.) The optimized structure of the [Gly+Na⁺+Acetone].

Table 14

Colors of the Atoms as Used by Gaussian.

Atom	Color
Carbon	Grey
Oxygen	Red
Nitrogen	Blue
Hydrogen	White
Sodium	Purple
Potassium	Dark Purple
Calcium	Olive
Copper	Salmon

CHAPTER 3

THE INVESTIGATION OF
AMINO ACID--ALKALI METAL ION COMPLEXES:
STRUCTURAL ANALYSIS THROUGH
ION-MOLECULE REACTIONS

Ion-molecule reactions were used to probe the structure of amino acids in the gas phase as described in Chapter 2. The structure of neutral species acetone is shown in Fig. 26. Acetone has a boiling point of 56 °C and a vapor pressure of 184 mmHg (at 20°C). The published polarizability for acetone is 6.33 Å³ and was the value used in the calculations.¹⁶⁰ Data obtained using acetone as the neutral species for the zwitterion analysis experiments will be presented here.

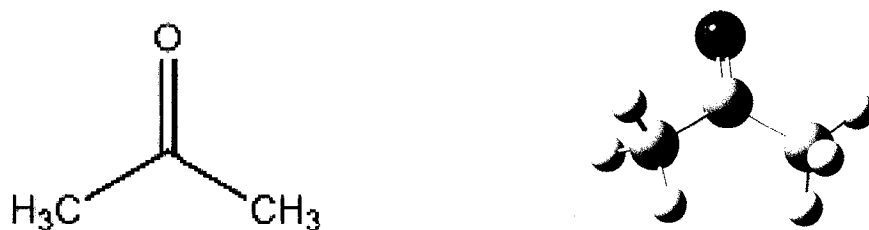


Figure 26. The structure of acetone. On the left, acetone is shown as a simple drawing. The figure on the right is the acetone molecule as optimized by Gaussian 03.

Observed Trends

For the group 1A metals studied, a general reactivity trend of the [A.A.+M⁺] complexes of Li⁺>>Na⁺>K⁺>>Cs⁺ is observed (Fig. 27). It can be seen from the representative kinetics plot in Fig. 27 that the relative intensity of the parent [Ala+Li⁺] complex decreases at a reasonably fast rate when compared to the other alkali metal complexes. In fact, complexes of amino acids with lithium react too fast to be able to draw useful conclusions. Some of the lithium reactions reacted close to or at the collisional rate of the association reaction, preventing acquisition of kinetics data. Since a rate constant could not be obtained for these fast reactions, it is difficult to compare them to other reactions involving lithium.

These lithium complexes can also react with water molecules present in the background pressure as well as the neutral species, which also further complicates data analysis. The peaks corresponding to the addition of water can sometimes be fairly intense even at short reaction times, as can be seen occurring for the [Leu+Li⁺] complex in Fig. 23. The addition of water to the [A.A.+Li⁺] complex was not observed for all of the amino acids studied here.

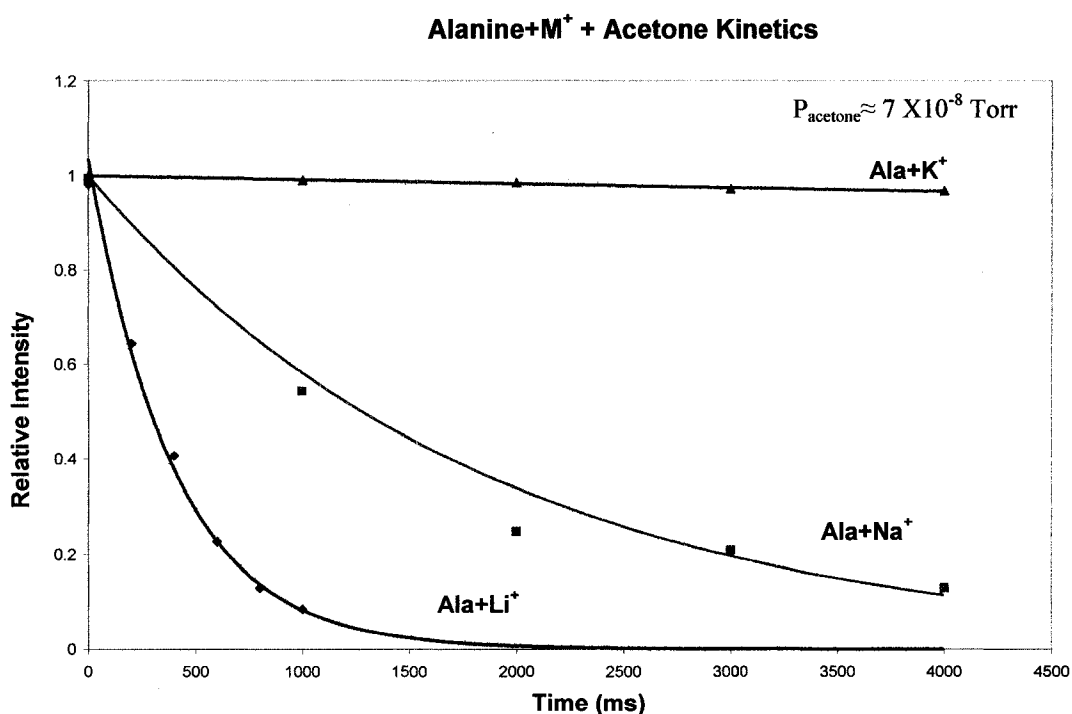


Figure 27. Representative reaction trends for alkali metals complexed to amino acids. It can be seen that the general reaction trend of $\text{Li}^+ \gg \text{Na}^+ > \text{K}^+$ is observed for alanine experiments.

Following the observed reactivity trend, the $[\text{Ala}+\text{Na}^+]$ complex intensity decreased at a slower rate than that of the lithiated complex (Fig. 27). However, unlike lithiated amino acids, sodiated amino acids do not form complexes with water molecules under these experimental conditions. This simplifies the interpretation of kinetics obtained for the $[\text{A.A.}+\text{Na}^+]$ species. Similarly, potassiated species show a slower reaction trend than both lithiated and sodiated species and do not form complexes with water. Again, this provides more simplified kinetics interpretations.

Studying amino acids complexed with cesium was problematic due to their slow reaction kinetics, many of which reacted too slowly to observe under this particular experimental setup. In addition, it was difficult to form a stable complex of an amino acid and the Cs^+ due to the size of the cation and the apparent lack of ability of the side chain to complex the species. Only two amino acids were observed to form a cesium complex. These complexes were isolated but not found to react with acetone in the time frame of this experiment. Both $[\text{Gln}+\text{Cs}^+]$ and $[\text{Leu}+\text{Cs}^+]$ are shown in Fig. 28. Representative kinetic data for Cs^+ complexes are not shown in Fig. 27 because it could not be obtained.

Although the general trend occurs so that the smaller alkali metal ion complexes will react faster than the larger alkali metal ions, the kinetics of each $[\text{A.A.}+\text{M}^+]$ species will vary. Each $[\text{A.A.}+\text{M}^+]$ will react with acetone at a different rate. Figure 29 shows an example of the relative rate kinetics of a variety of amino acids with lithium.

It is important to note that although the lithiated amino acid species will react faster than larger alkali metals complexed to the same amino acid, lithiated amino acids do not react with the same kinetic rate. For instance, it can be seen that out of the five amino acids selected here, $[\text{Gly}+\text{Li}^+]$ and $[\text{Ala}+\text{Li}^+]$ react faster than $[\text{Ile}+\text{Li}^+]$, which, in turn, reacts faster than the $[\text{Gln}+\text{Li}^+]$ and $[\text{Lys}+\text{Li}^+]$ species.

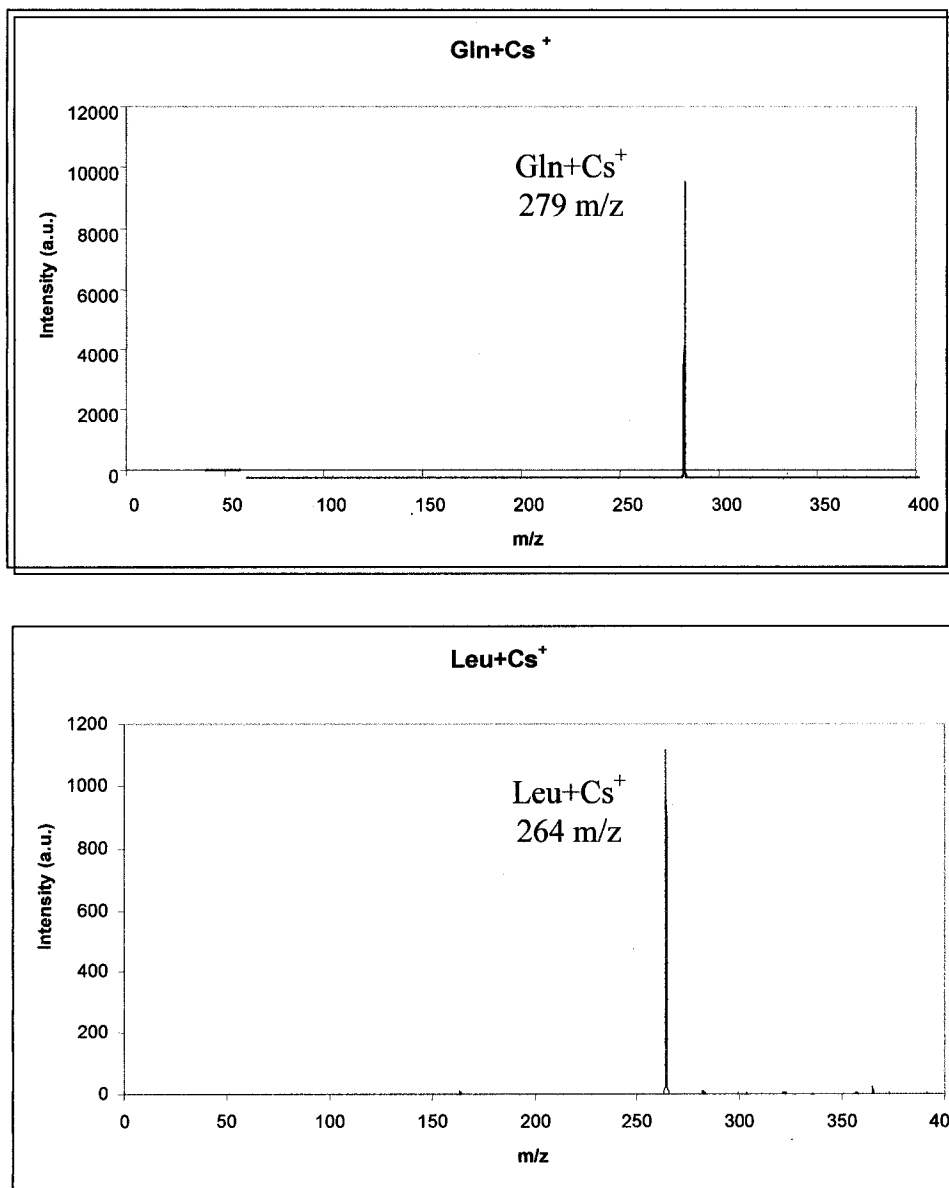


Figure 28. Amino acids and cesium. Both Gln and Leu were found to complex cesium. This was not observed for the other eighteen common amino acids.

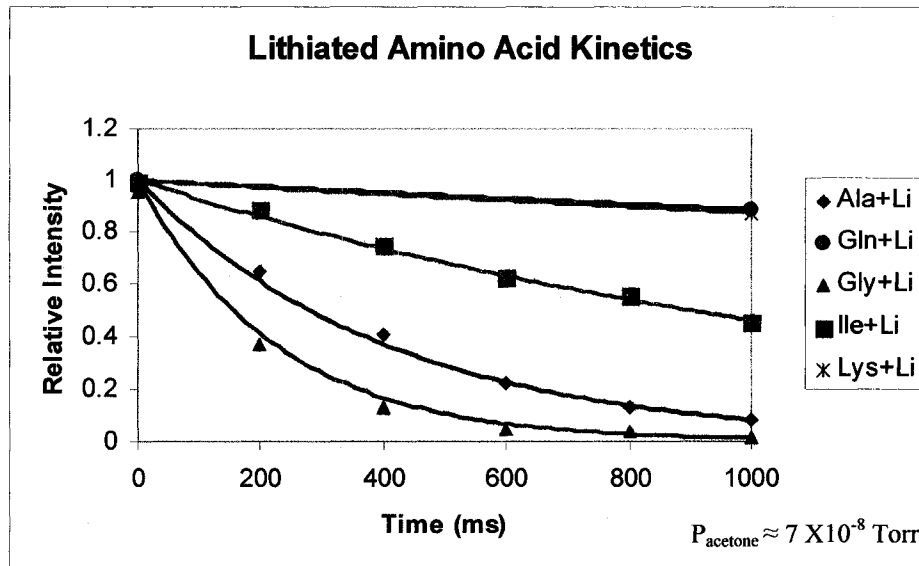


Figure 29. Kinetics variations with respect to various lithiated amino acids reacting with acetone. Significant variations can be seen between the five selected amino acids between 0 and 1000 ms reaction times.

These differences in reaction kinetics can help to establish differences in the structures of the amino acids in the gas phase. Similar structures should tend to react with similar efficiency in the gas phase. Therefore, it is valuable and pertinent to compare data not only between individual amino acids but also among the amino acids and structural models used in this study.

The kinetic variations between the amino acids can also be observed when looking at data for sodiated representative amino acids. The kinetic trends in Fig. 30 show that the variation between amino acids complexed with the same alkali metal ion has a similar trend to that observed with the lithiated species in Fig. 29. That is, each amino acid will react with acetone with a different kinetic rate.

Structural determination can be performed by comparing the kinetic trends of sodiated amino acids to the model compounds presented earlier.

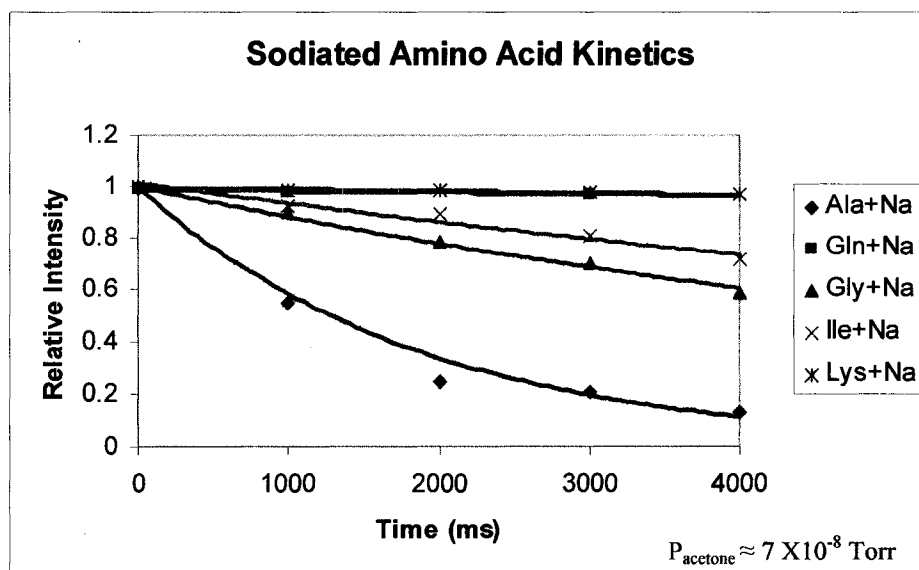


Figure 30. Representative kinetics plots for sodiated amino acids reacting with acetone.

The kinetics plots for amino acids complexed to potassium ions are shown in Fig. 31. Comparing Fig. 29 and Fig. 30, it can be seen that the reaction rate decreases as the size of the metal ion increases. Most of the potassiated amino acids react much more slowly with respect to their lithiated and sodiated counterparts. A key feature of Fig. 31 is the kinetics displayed by the $[\text{Gln}+\text{K}^+]$ species. Both lithiated and sodiated Gln react slowly (Fig. 29 and 30); however, here Gln reacts faster than would be expected. This finding suggests that Gln undergoes a structural change as the size of the cation increases. This could also possibly explain the

finding that Gln is one of the two amino acids capable of forming a stable complex with a cesium cation.

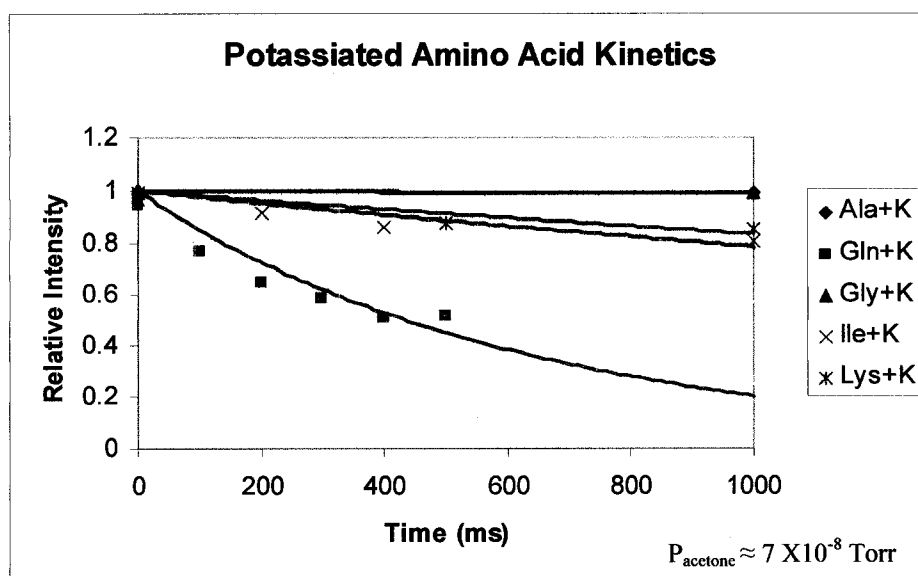


Figure 31. Reaction kinetics for various potassiated amino acids reacting with acetone.

It is difficult to experimentally determine if amino acids with large chelating side chains are charge-solvated or zwitterionic. The problem was predominantly apparent for the amino acids arginine, lysine, and histidine. This is mainly due to the fact that the bulky chelating side chain is likely to “wrap” around the metal ion, preventing the neutral species (i.e., acetone) from interacting with the ionic charge; the amino acid could coordinate the metal ion through OO or NO interaction, but the side chain could affect the expected kinetics that those interactions would display. Molecular modeling calculations can provide theoretical information that

can be used to help clarify the identification of gas-phase zwitterions in these instances.

Kinetics Data

The results presented from here on will focus on data collected for lithiated, sodiated, and potassiated amino acids using an acetone as the neutral species. All rate constants were obtained from kinetic plots of the data, using exponential fitting. These constants were then used to determine the reaction efficiency (Φ) of the amino acid complexes with acetone. The experimental rate can vary $\pm 30\%$. However, the comparison of known and permanent zwitterions and charge-solvated species to the amino acids with unknown structures can still be made.

Gas-Phase Zwitterions

Proline differs from the other common amino acids in that the cyclic portion of the amino acid significantly inhibits the mobility of the molecule. Unlike the other amino acids containing cyclic species as a part of their side chains, the main portion of proline contains the cyclic structure. Thus, proline has more restrained capabilities for binding metal ions.¹⁵⁵

Spectroscopic experiments have identified the sodiated form of proline to be zwitterionic in the gas phase.^{62, 155} Additional theoretical and experimental results

indicate that the $[\text{Pro}+\text{M}^+]$ complex will be zwitterionic. This is because the hydrogen bonds in Pro tend to form without deforming the ring structure, creating a more energetically favorable situation for zwitterion structure.¹⁵⁵ In addition, proline is able to bind alkali metal cations much stronger than any of the other common amino acids, thus giving it noticeably different complex chemistry.¹⁵⁵

Proline and betaine are used here to help identify zwitterions in the gas phase. As previously mentioned, the betaine molecule is organized so that the two carboxyl oxygens are the chelating position for metals. The Gaussian 03-optimized structures of proline and betaine are shown in Fig. 32.

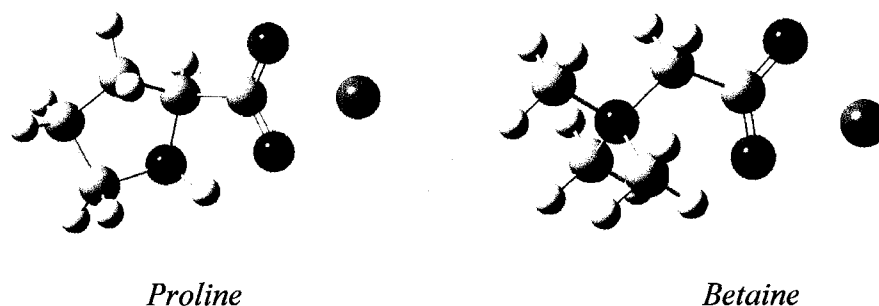


Figure 32. Proline and betaine zwitterions. Proline is a known zwitterion in the gas phase, and betaine is as permanent zwitterion. Both amino acids are shown complexed with a sodium ion. The atom color scheme is as follows: hydrogen is white, carbon is grey, nitrogen is blue, oxygen is red, and sodium is purple.

The kinetics data for the lithiated and sodiated species of Pro and Bet are shown in Fig. 33. As can be seen from the graph, both of the known zwitterions have similar reaction trends. As expected, the lithiated species react much faster

than the sodiated species. Another interesting feature of these kinetics is that the sodiated species of Pro and Bet react similarly and relatively slowly. These data indicate that ions with a salt-bridge gas-phase structure will likely react with similar efficiencies.

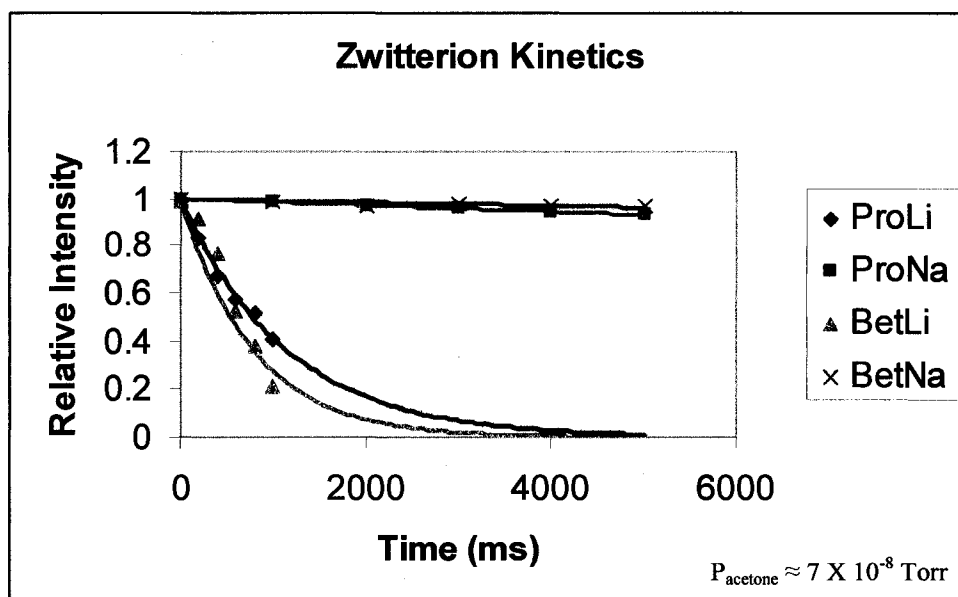


Figure 33. A comparison of the reaction rates of Pro and Bet with acetone in the gas phase.

Gas-Phase Nonzwitterions

As previously mentioned, methyl esters of amino acids are permanent charge-solvated molecules. The methyl ester on the carboxyl terminal prevents the metal ion from being chelated by the two carboxyl oxygens. To better depict this,

Fig. 34 shows the structure of zwitterionic lysine, charge-solvated lysine, and lysine methyl ester. The change in chelating position of the metal ion can easily be seen. In zwitterionic lysine, the sodium ion is complexed through the two carboxyl oxygens. For the charge-solvated species, the sodium is complexed by a carboxyl oxygen and the amino nitrogen. The methyl esters of alanine, arginine, glycine, histidine, lysine, and proline were used for these studies.

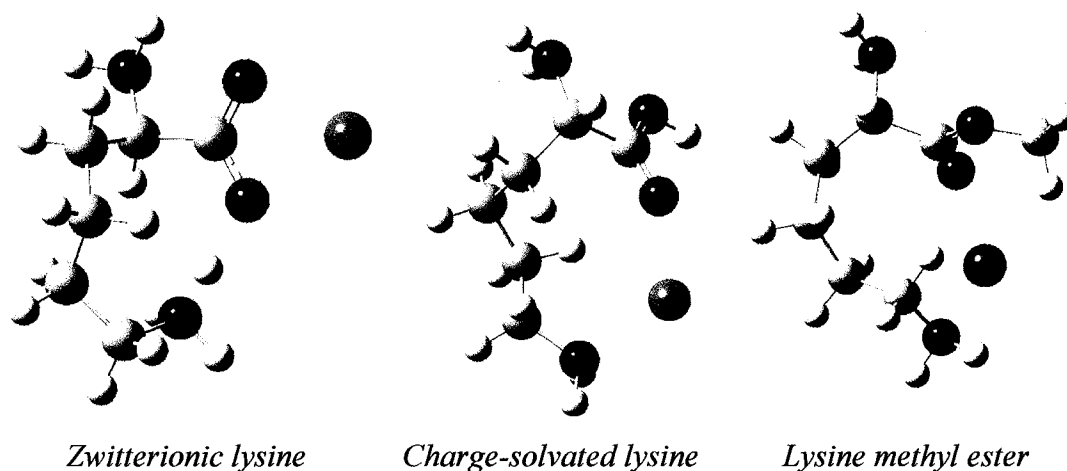


Figure 34. A comparison of the zwitterionic and charge-solvated lysine species to the permanently charge-solvated lysine methyl ester. All species are complexed with a sodium cation. The atom color scheme is as follows: carbon is grey, hydrogen is white, nitrogen is blue, oxygen is red, and sodium is purple.

Kinetics data was obtained for all of the methyl esters previously mentioned. The results for lithiated methyl esters are shown in Fig. 35. As would be expected, there is variation between the reaction kinetics of the amino acids. This can be attributed to the difference in availability of the lithium to the acetone for each of the species. Arginine methyl ester (ArgME), histidine methyl ester (HisME), and

lysine methyl ester (LysME) all have side chains which are capable of surrounding the lithium ion and effectively reducing its ability to interact with acetone. The fastest reacting methyl ester, proline methyl ester (ProME), has little rotational ability, allowing for availability of the complexed lithium ion to acetone. Alanine methyl ester (AlaME) and glycine methyl ester (GlyME) have bulkier side chains than ProME but offer less Li^+ protection than ArgME, HisME, or LysME.

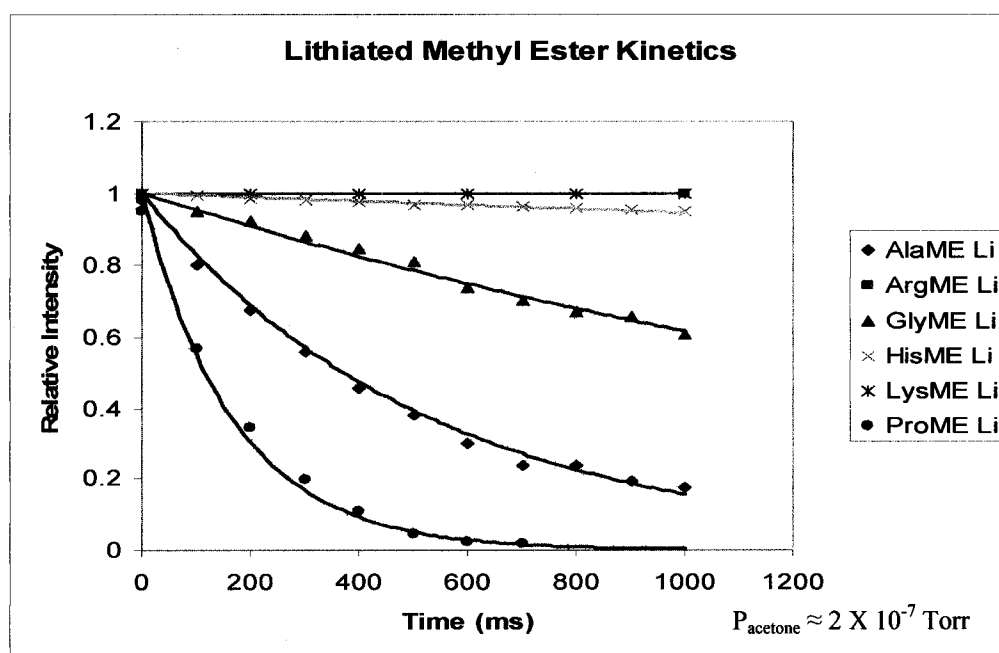


Figure 35. Lithiated methyl ester kinetics with acetone.

When complexed with sodium, the methyl esters displayed kinetics as shown in Fig. 36. Upon comparison with Fig. 35, it is apparent that the rates of the sodiated reactions occur more slowly than the lithiated ones. As before, the fastest

reacting species is the methyl ester with the least chelating ability, ProME. The Na^+ complexed to ProME is readily available to react with the acetone molecule.

AlaME and GlyME do not have side chains capable of chelating a metal. They react slower than ProME but much faster than methyl esters with chelating side chains.

As the size of the chelating group of the methyl ester increases, the reaction rate decreases. This is why HisME displays a slower reaction rate than ProME, AlaME, or GlyME. ArgME and LysME were also analyzed in the sodiated form, yet no reaction with acetone was observed. This can again be attributed to the protection of Na^+ by their larger side chains.

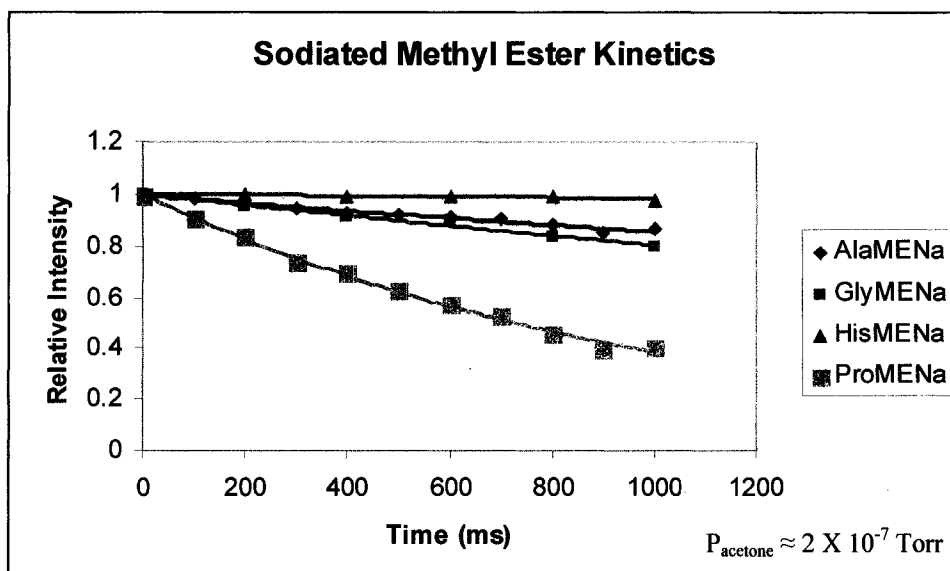


Figure 36. Sodiated methyl ester kinetics with acetone.

The methyl esters were also complexed to potassium ions and are shown in Fig. 37. These potassium species are likely to have reacted slowly due to ion size constraints; the metal ion is likely to be farther away from the amino acid, preventing the formation of a stabilized complex. Where available, kinetics data will be presented for $[A.A.+K^+]$ species that were observed to react within the time frame of this experiment.

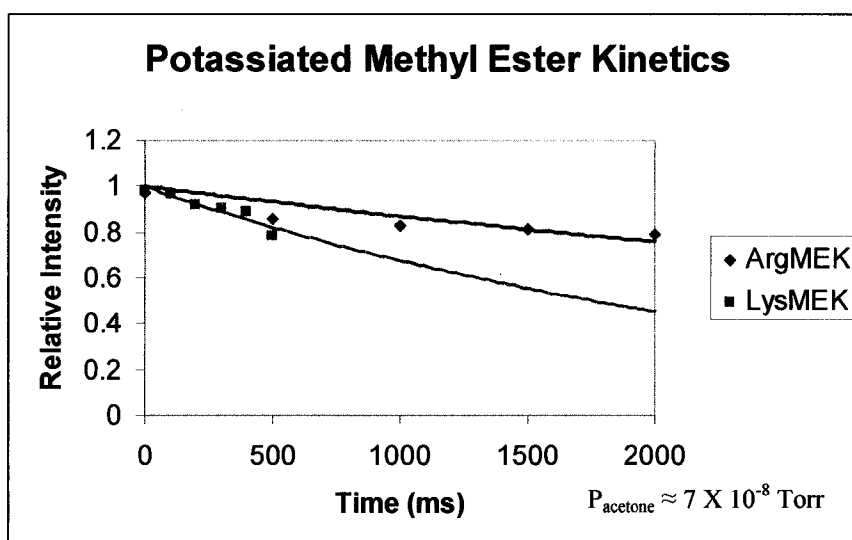


Figure 37. Potassiated methyl ester kinetics with acetone.

The Analysis of Selected Amino Acids and Their Corresponding Methyl Esters

Alanine

Anh et al.¹⁰⁷ focused on a computational look at charge-solvated and zwitterionic alanine. The computational analysis focused on bare alanine, neutral

alanine $-(\text{H}_2\text{O})_n$, and the alanine zwitterion $-(\text{H}_2\text{O})_n$ ($n=1$ and 2) clusters. Similar to the experiments with valine performed by Jockusch et al.,¹⁴³ the calculations on the various alanine species were designed to determine the stability that water molecules can provide zwitterions in the gas phase. Anh et al. found that neutral (charge-solvated) alanine is calculated to be more stable in the gas phase than zwitterionic alanine, whereas the reverse is true for solution-phase alanine. However, the authors also found that the zwitterionic alanine molecule could be stabilized by the binding of at least two water molecules.¹⁰⁷ Alkali metal ion complexation to the alanine molecule should result in a similar stabilization of the zwitterionic structure.

Here, alanine, alanine methyl ester (AlaME), and betaine kinetics are compared to identify the gas-phase structure of alanine. The $[\text{Ala}+\text{Li}^+]$ complex and the corresponding standards were analyzed, and their reaction kinetics are shown in Fig. 38. The exponential decay of $[\text{Ala}+\text{Li}^+]$ and $[\text{Bet}+\text{Li}^+]$ display an almost identical kinetic trend. $[\text{AlaME}+\text{Li}^+]$ reacts more slowly than the other two species. This observation indicates that lithiated alanine is zwitterionic in the gas phase.

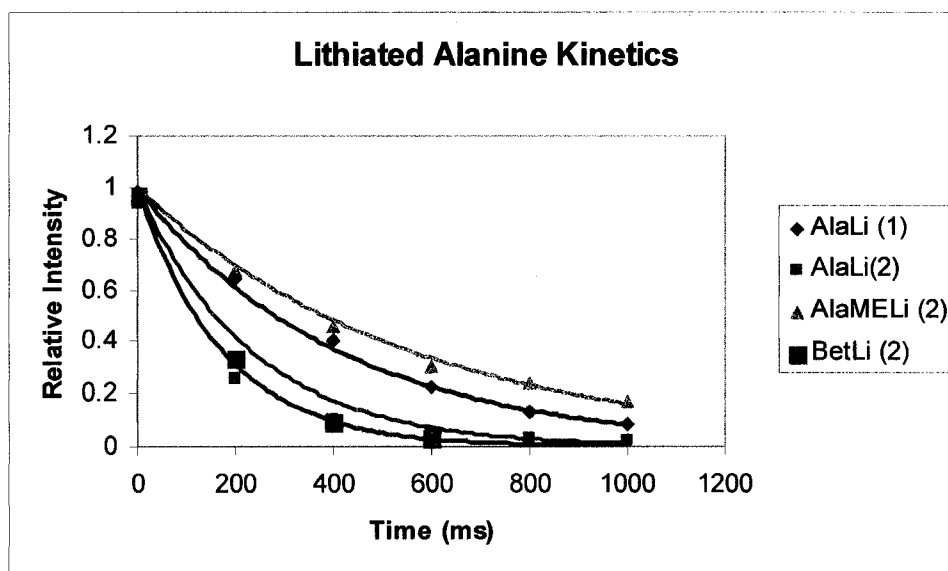


Figure 38. Alanine kinetics compared to the amino acid standards in their lithiated forms for reactions with acetone. The kinetics data were obtained at an estimated acetone pressure of 7×10^{-8} Torr (1) or 2×10^{-7} Torr (2).

When sodiated alanine is compared to $[\text{AlaME}+\text{Na}^+]$ and $[\text{Bet}+\text{Na}^+]$, it becomes more difficult to determine the gas-phase structure of $[\text{Ala}+\text{Na}^+]$. It can be seen that out of the three species, $[\text{Ala}+\text{Na}^+]$ reacts fastest and the $[\text{AlaME}+\text{Na}^+]$ species reacts slowest (Fig. 39). This would indicate that the Na^+ complexed to alanine is readily available for interaction with acetone. Conversely, AlaME likely shields the Na^+ from acetone, which explains the slower reaction kinetics that system displays. Although the sodiated alanine complex reacts faster than the zwitterionic $[\text{Bet}+\text{Na}^+]$ species, the reaction kinetics indicate that $[\text{Ala}+\text{Na}^+]$ is most likely zwitterionic in the gas phase.

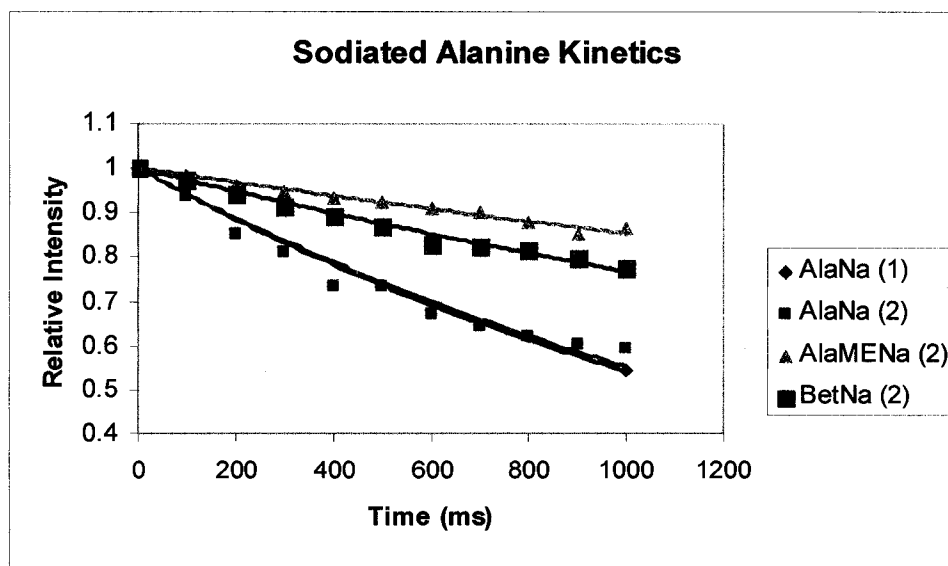


Figure 39. Sodioted alanine kinetics for reactions with acetone. The kinetics of the charge-solvated AlaME and the zwitterion Bet are compared to Ala. Data acquired at estimated acetone pressures of 7×10^{-8} Torr (1) or 2×10^{-7} Torr (2).

When the kinetic trends of potassiated alanine and betaine are compared, it can readily be seen that the two species have similar reactions (Fig. 40). Betaine is a permanent zwitterion in the gas phase. Ala reacts similarly, indicating that $[\text{Ala}+\text{K}^+]$ is a zwitterion in the gas phase. Furthermore, Ala does not react with acetone in a similar manner as AlaME. This concurs with the findings for the lithiated and sodiated amino acids in the gas phase.

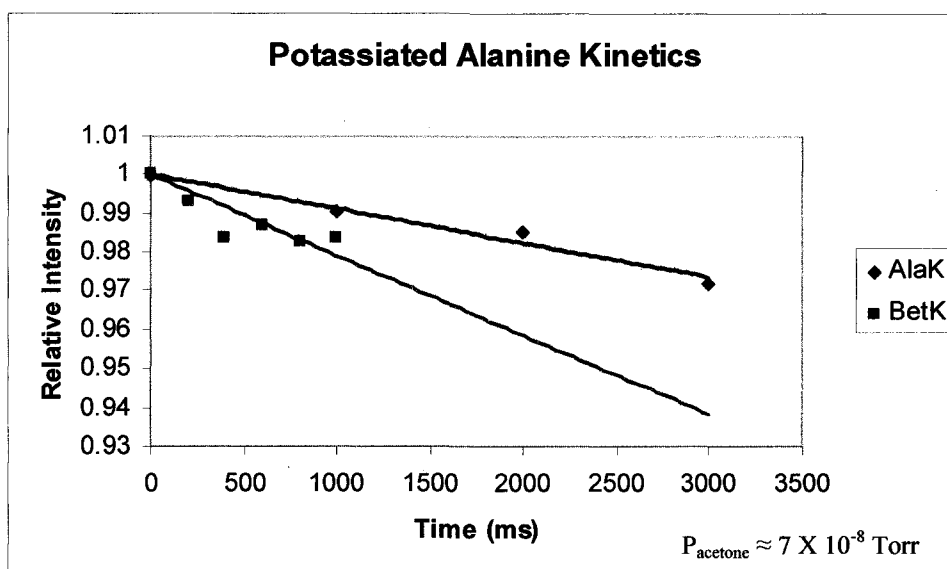


Figure 40. The reaction trend of potassiated alanine with acetone.

Although Gaussian analysis was not performed on alanine species for these experiments, it can be concluded that Ala is a zwitterion in the gas phase. As previously described, Ahn et al. found that two water molecules were needed to bind to alanine to form a stable zwitterion in the gas phase.¹⁰⁷ Instead of using water in these experiments, alkali metal ions are used to stabilize these ions. Therefore, the finding that alanine is zwitterionic in the gas phase is consistent with expectations for this amino acid.

Arginine

Figure 41 shows a comparison of the kinetics of arginine, arginine methyl ester (ArgME), and betaine. From the kinetics data, it can be seen that the Arg and

ArgME species react more similarly than the Bet species. The reactions with Arg and ArgME were considerably slower, both in the lithiated and sodiated forms. Because the lithiated and sodiated arginine displays similar reaction kinetics as the known charge-solvated species ArgME, it is possible that the Arg chelates the metal ions in a charge-solvated manner.

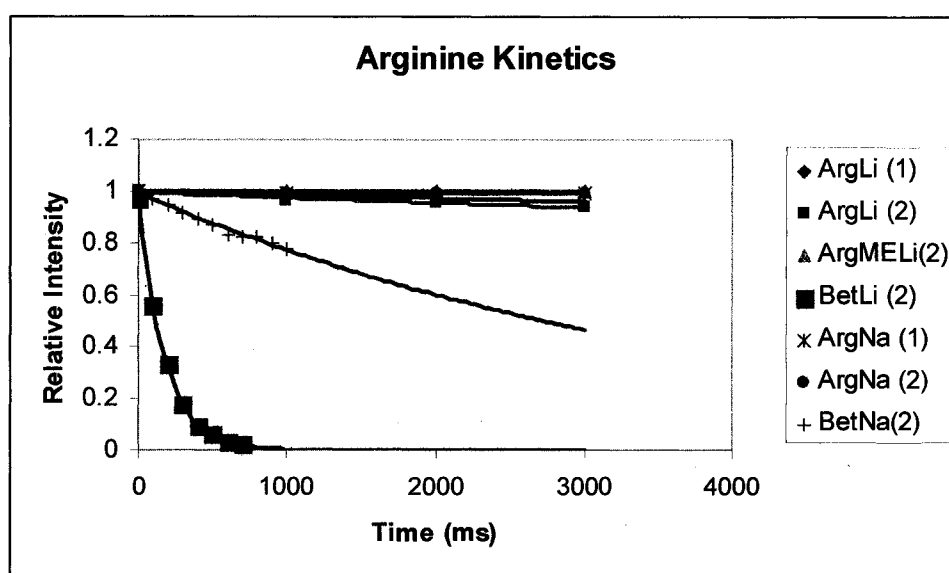


Figure 41. Arginine kinetics for reactions with acetone. The kinetics of both the lithiated and sodiated forms of arginine, arginine methyl ester, and betaine are shown above. Data acquired at estimated acetone pressures of 7×10^{-8} Torr (1) or 2×10^{-7} Torr (2).

Arginine has a large side chain, able to interact with the metal ion in a few ways. The sodiated arginine species were modeled in the Gaussian program to help understand these observations. The optimized structures of zwitterionic and charge-solvated species of $[\text{Arg}+\text{Na}^+]$ and $[\text{Arg}+\text{Na}^++\text{acetone}]$ are shown in Fig. 42. The

distance from the sodium ion and the oxygen of the amino acid are reported. The charge on the sodium cation is also shown. A comparison of the two structures shows that the arginine zwitterion has a lower energy of stabilization than the charge-solvated species. It would be expected that the zwitterion structure of arginine would be favored in the gas phase.

Kinetics data previously discussed demonstrate that this does not appear to be the case. However, there is little difference between the computed energies and distances of the two arginine structures. In the optimized zwitterion structure, the nitrogen atom on the Arg side chain is shown to “share” a hydrogen atom with a carboxyl oxygen. When this occurs, the charge separation usually observed for zwitterions is somewhat mediated. This could cause the zwitterion to react more slowly than the known betaine zwitterion, but faster than the ArgME.

Additionally, the charge-solvated structure of Arg used for these calculations is not the only possible structure.^{57, 86} In Fig. 42, Arg is shown to chelate the sodium ion through NO coordination. However, it is possible for the amino nitrogen to also participate in chelating the sodium ion. This charge-solvated structure would display a higher energy of stabilization.

Kinetics data was also acquired for the potassiated arginine species (Fig. 43). It can be seen from Fig. 43 that $[\text{Arg}+\text{K}^+]$ and $[\text{Bet}+\text{K}^+]$ react similarly and that they both react slowly. It can also be seen that although $[\text{ArgME}+\text{K}^+]$ reacts slowly, it reacts faster than the other potassiated species. This finding is interesting since the lithiated and sodiated forms of Arg seem to be charge-solvated in the gas phase.

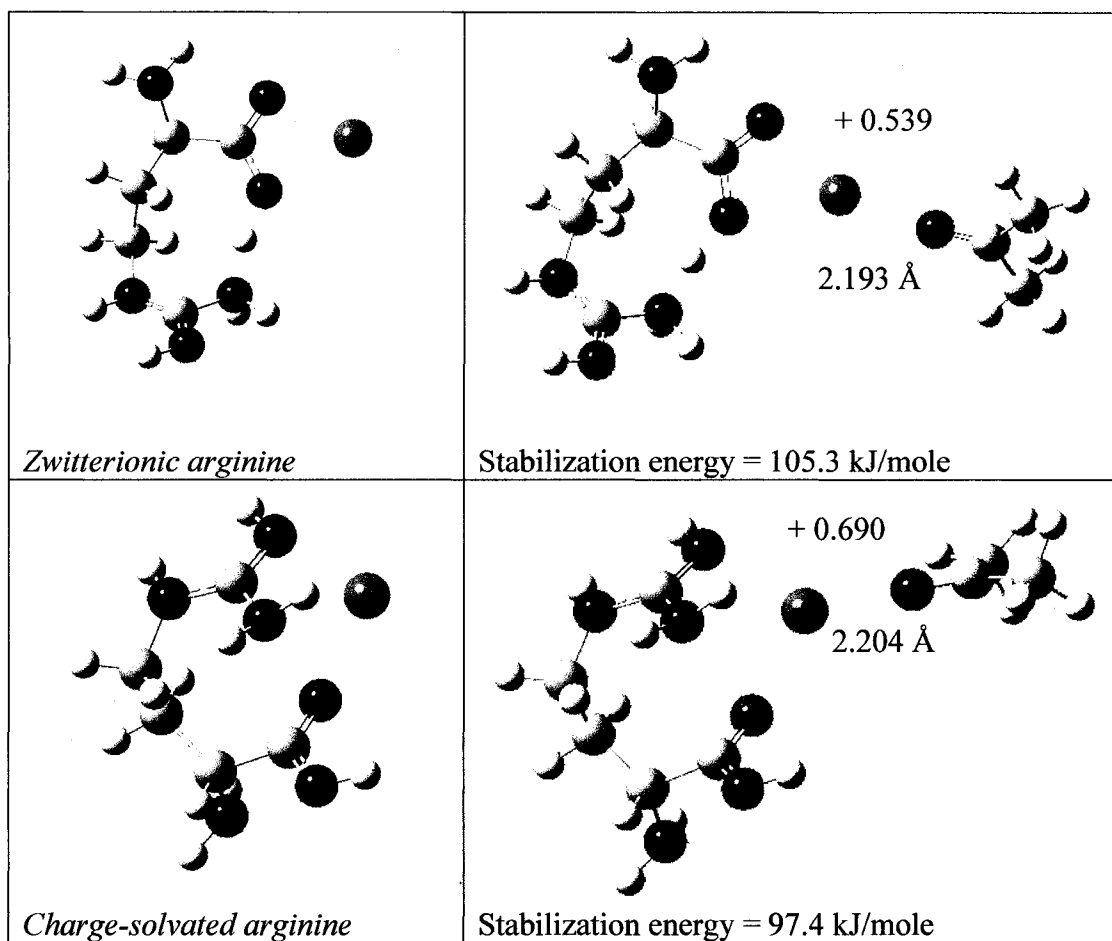


Figure 42. Zwitterionic and charge-solvated $[\text{Arg}+\text{Na}^+]$. Both structures are shown complexed with acetone. The stabilization energy of zwitterionic arginine is calculated to be greater than that of the charge-solvated arginine species.

One possibility is that the complexation of K^+ to Arg is more capable of stabilizing the zwitterionic structure than Li^+ or Na^+ . It has been previously suggested that the size of the metal ion has a significant effect on the stabilized structure; as the size of a metal ion increases, the stabilization of the zwitterion is found to increase. Jockusch et al. have suggested that this finding could be observed for Arg.⁵⁷ Therefore, the finding that Arg becomes a more stable zwitterion as the size of the cation increases is reasonable.

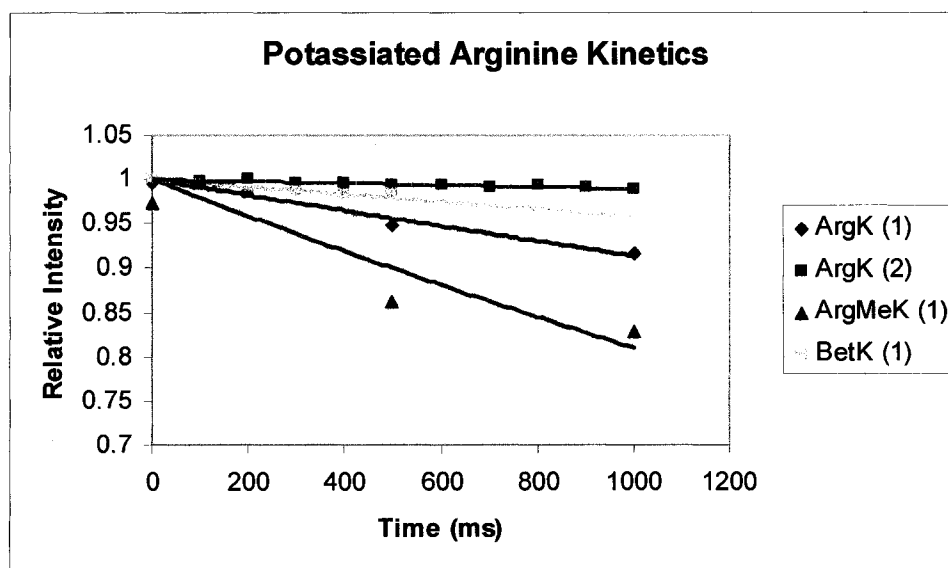


Figure 43. The kinetic trends of potassiated arginine species reacting with acetone. Data acquired at estimated acetone pressures of 7×10^{-8} Torr (1) or 2×10^{-7} Torr (2).

Glycine

Glycine is the simplest amino acid, where its R-group is a hydrogen molecule. Since it does not have a long side chain, it would be expected that the metal ion would be readily available for reaction with acetone in both the zwitterion and charge-solvated structures. It is widely accepted that glycine is charge-solvated in the gas phase. Thus, it would be expected that the experimental reaction kinetics of Gly would display similar reaction trends as glycine methyl ester (GlyME).

Figure 44 shows the kinetic trends for lithiated Gly, GlyME, and Bet. It is apparent from the data that both $[\text{Gly}+\text{Li}^+]$ experiments show similar reactions to $[\text{Bet}+\text{Li}^+]$ and $[\text{GlyME}+\text{Li}^+]$. This observation can be attributed to the availability of the Li^+ to the acetone molecule. In all three amino acid species, the lithium ion is unrestricted from interacting with acetone. The slower reaction rate of $[\text{GlyME}+\text{Li}^+]$ can be explained by the added polarity of the molecule. Since the reaction of acetone with lithiated species is so fast, little structural information can be obtained from this experiment.

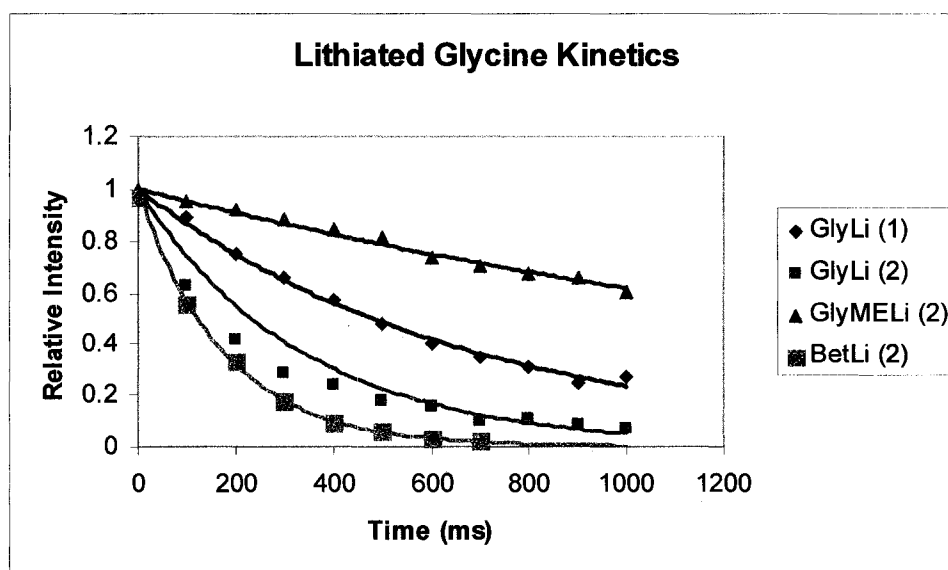


Figure 44. Lithiated glycine kinetics for reactions with acetone. Gly is compared to the charge-solvated GlyME and the zwitterionic Bet. Data acquired at estimated acetone pressures of 7×10^{-8} Torr (1) or 2×10^{-7} Torr (2).

When the data for the sodiated forms of Gly, GlyME, and Bet are compared, an analogous trend appears (Fig. 45). All three species exhibit similar reaction kinetics. Again, this observation can be attributed to the readily available sodium ion. Since glycine is the simplest amino acid, there is no side chain to interfere with the binding of the alkali ion or interaction of the acetone to the $[A.A.+M^+]$ complex.

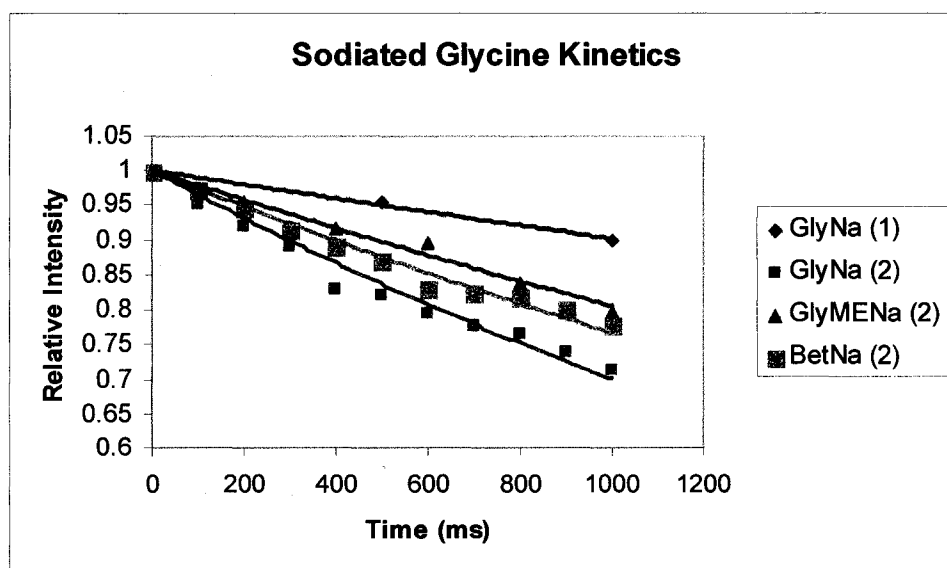


Figure 45. Sodiated glycine kinetics for reactions with acetone. All three species are found to react with similar rates. Data acquired at estimated acetone pressures of 7×10^{-8} Torr (1) or 2×10^{-7} Torr (2).

Theoretical calculations indicate that the observed trends are reasonable. All three systems are calculated to have similar distances between the sodium ion and acetone, as well as similar stabilization energies (Fig. 46). The theoretical data indicate that a similar reaction trend between glycine, glycine methyl ester, and betaine is a predictable observation. Since the calculated thermodynamic observations are similar, it is understandable that the sensitivity of ion-molecule reactions may not be good enough to distinguish these species. Given the $\pm 30\%$ variation in the experimental rate of the kinetics experiments, this conclusion is reasonable. However, it is important to note that Gly is accepted to be charge-solvated in the gas phase and that the theoretical computations predict that charge-solvated Gly will have the greatest stabilization energy.

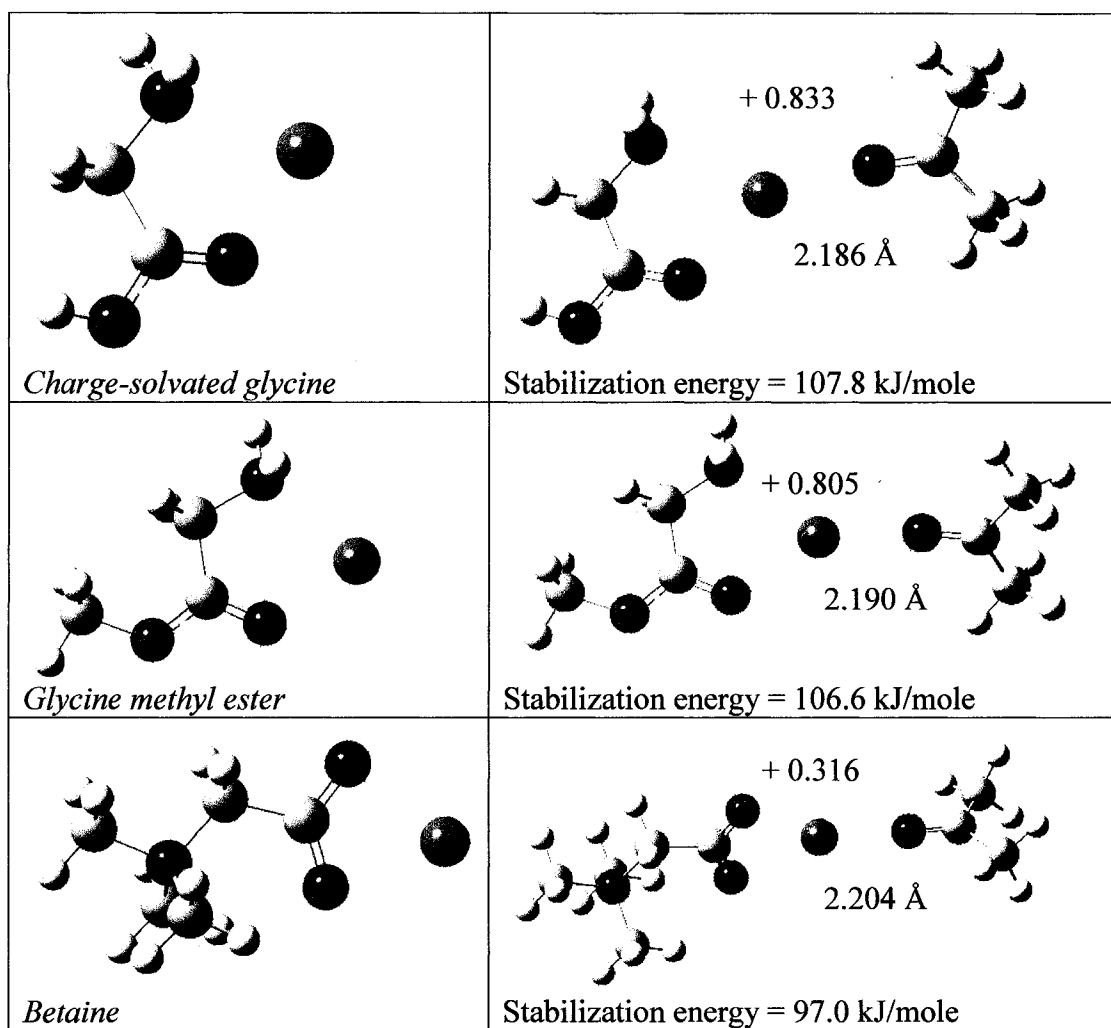


Figure 46. A comparison of the structures and energies of Gly, GlyME, and Bet. All the amino acids are shown complexed with Na^+ on the left and with the subsequent addition of acetone on the right.

Histidine

The analysis of lithiated histidine is fairly straightforward. Both $[\text{His}+\text{Li}^+]$ and $[\text{HisME}+\text{Li}^+]$ display similar reaction kinetics, dissimilar to what is shown by $[\text{Bet}+\text{Li}^+]$ (Fig. 47). When the lithium cation is complexed to betaine, there is little ability for the side chain to protect the ion from acetone. However, histidine has a large aromatic arm that is capable of hindering interaction of the lithium and acetone. It would be expected that if the aromatic ring were to participate in coordination of the metal ion, it would play more of a factor in the charge-solvated structure. This is because the carbon chain can position the aromatic moiety closer to the amino terminus than the carboxyl terminus. The kinetic trend displayed for $[\text{His}+\text{Li}^+]$ indicates that the structure of the amino acid is charge-solvated in the gas phase.

It would be expected that the $[\text{His}+\text{Na}^+]$ and $[\text{His}+\text{K}^+]$ species would have structure and kinetics similar to that of the $[\text{His}+\text{Li}^+]$ species. A kinetics plot of sodiated His, HisME, and Bet confirms this expectation (Fig. 48). Both $[\text{His}+\text{Na}^+]$ and $[\text{HisME}+\text{Na}^+]$ react similarly, indicating that His prefers the charge-solvated structure in the gas phase. As with the experiment with lithium, $[\text{Bet}+\text{Na}^+]$ reacts faster than the charge-solvated species.

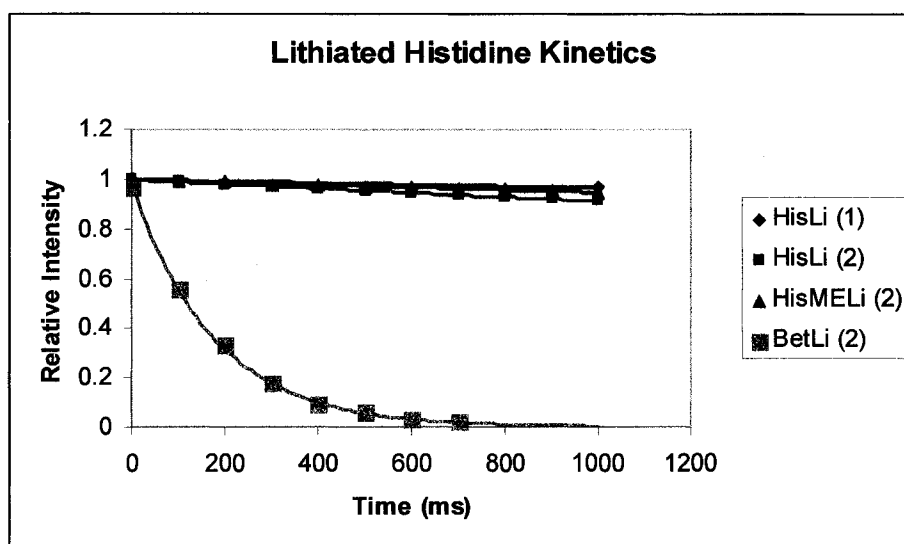


Figure 47. Lithiated histidine kinetics for reactions with acetone. Data acquired at estimated acetone pressures of 7×10^{-8} Torr (1) or 2×10^{-7} Torr (2).

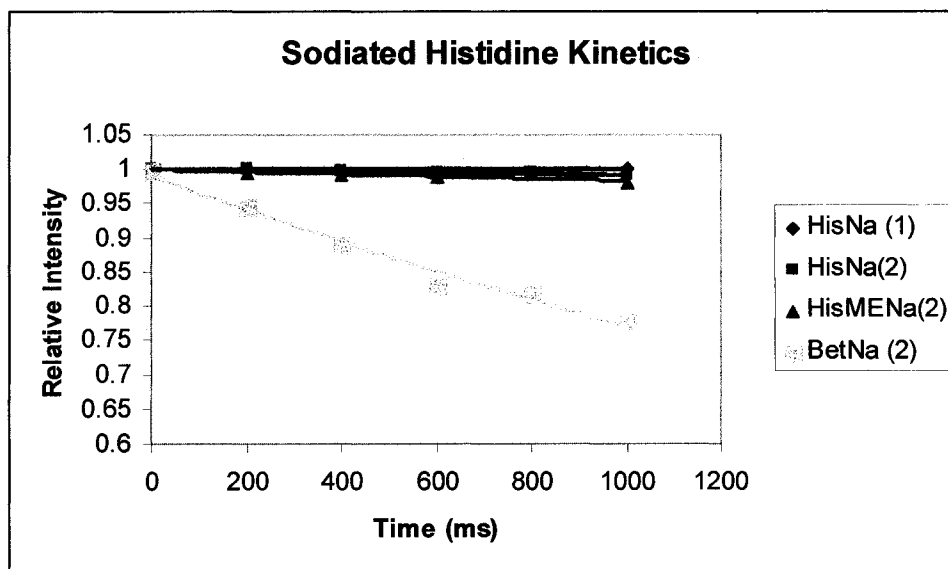


Figure 48. Sodiated histidine kinetics for reactions with acetone. His and HisME react with similar reaction kinetics. Data acquired at estimated acetone pressures of 7×10^{-8} Torr (1) or 2×10^{-7} Torr (2).

When $[\text{His}+\text{K}^+]$ and $[\text{Bet}+\text{K}^+]$ kinetics are compared, it can be seen that the kinetic trend between the two species differs as before (Fig. 49). There is no kinetics data available for $[\text{His}+\text{K}^+]$ reacting with acetone due to the slow reaction kinetics the species exhibited. Since Bet is a zwitterion, this finding confirms that His is likely to be charge-solvated in the gas phase. From these data, it is possible to experimentally determine that histidine prefers the charge-solvated structure in the gas phase.

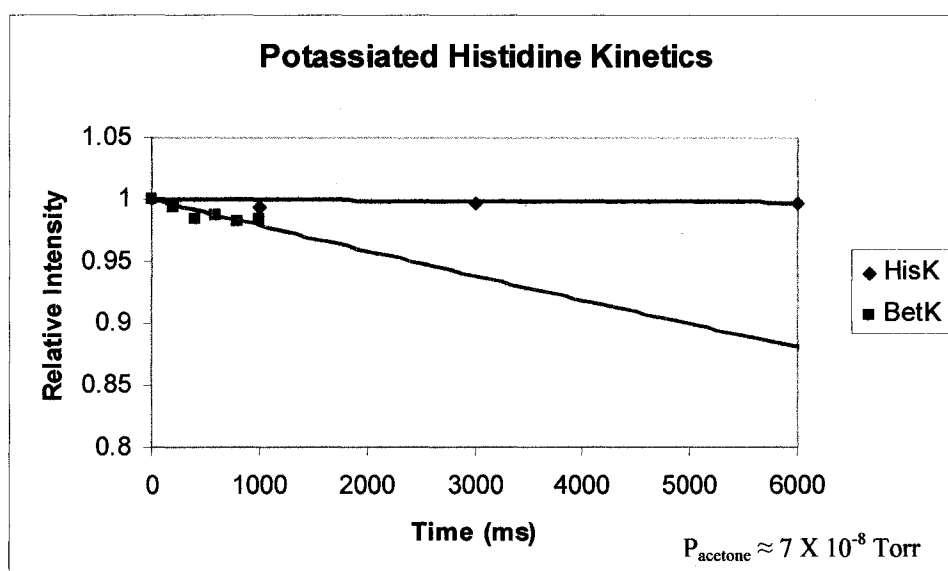


Figure 49. Reaction kinetics of potassiated histidine for reactions with acetone.

Theoretical calculations were performed with sodiated histidine in both the charge-solvated and zwitterionic structure. Figure 50 compares the theoretical results from the analysis. The distances between the metal ion and the acetone are almost identical for both the charge-solvated and zwitterion structures. The charge-solvated histidine structure is calculated to have the greatest stabilization energy.

Since the structure with the greatest energy of stabilization is the most likely structure to be formed, it is likely that charge-solvated histidine is preferred in the gas phase.

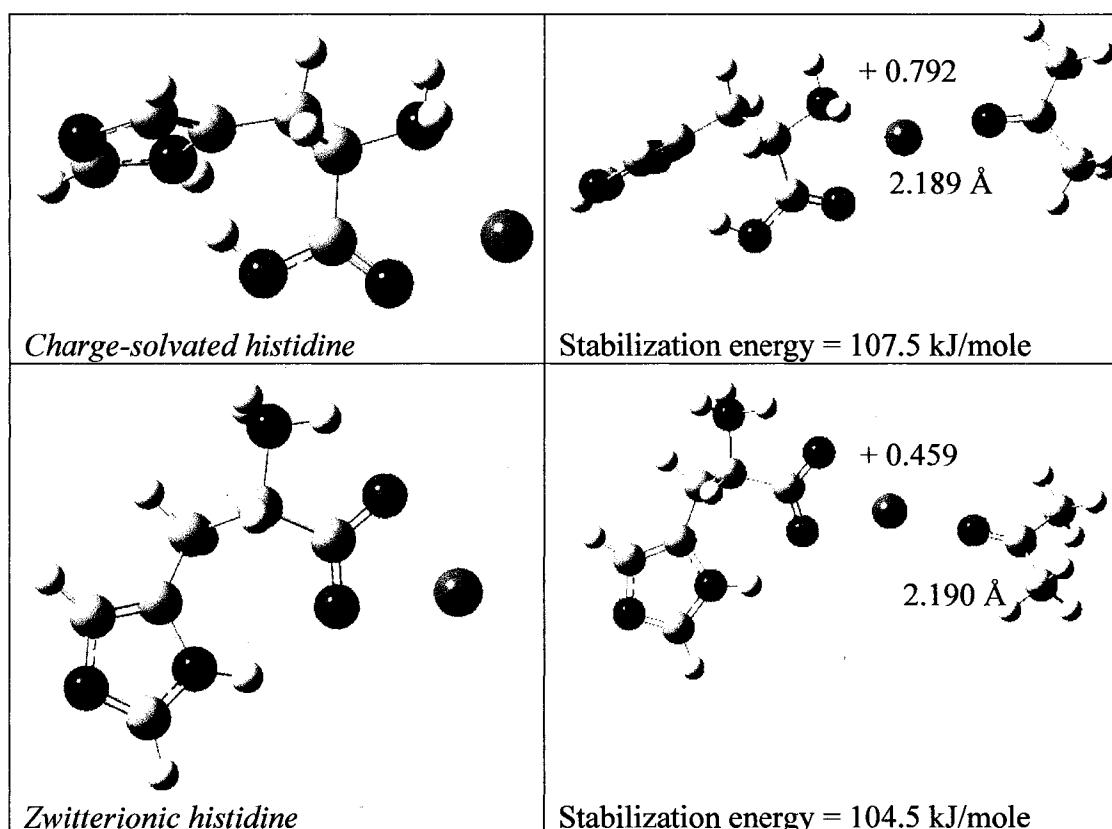


Figure 50. Theoretical calculations involving sodiated histidine. Both the distance from the Na^+ to the oxygen of the acetone and the stabilization energies are reported.

It is important to also note that there is more than one possible charge-solvated structure for histidine in the gas phase. The structure in Fig. 50 shows that the sodium cation is chelated by NO coordination. However, it is also possible that the aromatic side chain could also be used to chelate the ion. This additional

coordination would further stabilize the species. Nevertheless, the calculated stabilization energy for the species in Fig. 50 is consistent with the kinetic observation that histidine prefers the charge-solvated structure in the gas phase.

Lysine

Lysine is similar to arginine because it has a long carbon side chain capable of providing steric hindrance in the structure. It is expected that lysine and arginine should exhibit similar reaction trends, and indeed, this is the case. Figure 51 shows the kinetics data for the lithiated and sodiated amino acids. The fastest reacting species is $[\text{Bet}+\text{Li}^+]$. The remaining amino acids react more slowly, specifically, $[\text{LysME}+\text{Li}^+]$ and $[\text{Lys}+\text{Na}^+]$.

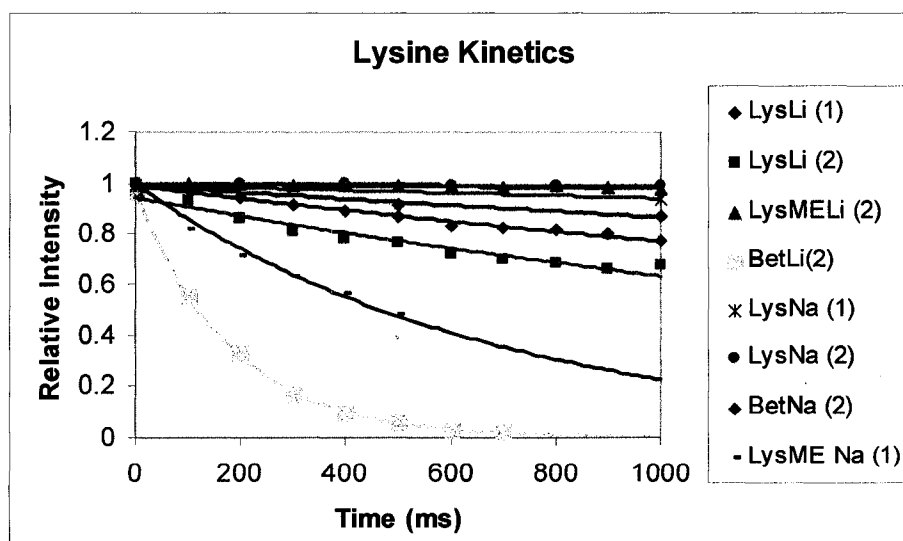


Figure 51. Lysine kinetics for reactions with acetone. Data acquired at estimated acetone pressures of 7×10^{-8} Torr (1) or 2×10^{-7} Torr (2).

Since the lysine reacts faster than the charge-solvated methyl ester, it is probable that lysine is zwitterionic in the gas phase. Slower reaction kinetics than the betaine zwitterion can be attributed to the shared hydrogen between the side chain nitrogen and the carboxyl oxygen. Therefore, it is likely that lysine is zwitterionic in the gas phase.

LysME species reacted much slower than most of the amino acids tested. The reaction kinetics for $[\text{LysME}+\text{K}^+]$ was slower than those observed for $[\text{LysME}+\text{Na}^+]$. Since there was no observable reaction between the potassiated LysME, there is no reaction data available. Data for reaction kinetics between acetone and $[\text{Lys}+\text{K}^+]$ and $[\text{Bet}+\text{K}^+]$ are shown in Fig. 52.

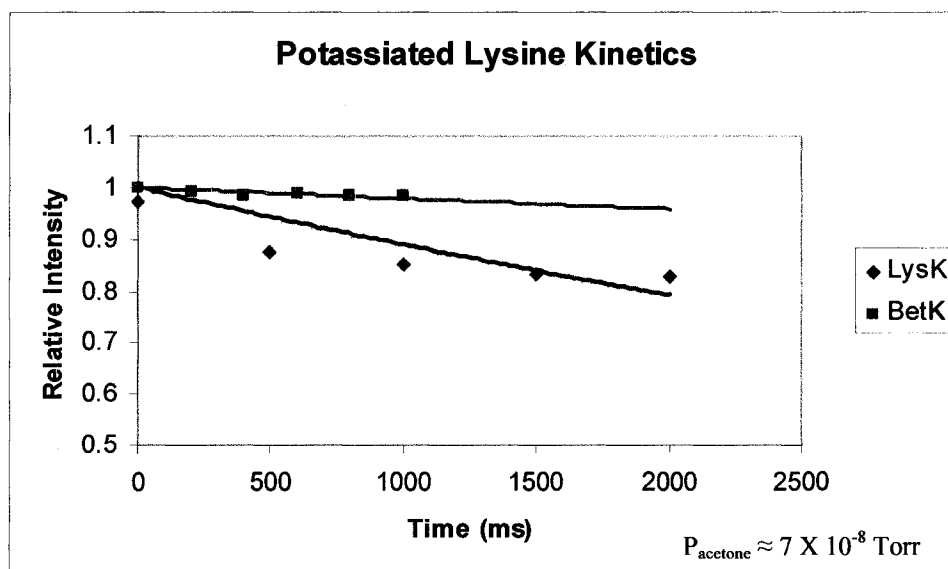


Figure 52. The rate kinetics of potassiated lysine for reactions with acetone.

The $[\text{Lys}+\text{K}^+]$ species reacts faster than $[\text{Bet}+\text{K}^+]$ and $[\text{LysME}+\text{K}^+]$. From this observation, it is possible to conclude that Lys displays reaction kinetics similar to those of gas-phase zwitterions. Since methyl esters tend to react slowly with acetone, charge-solvated amino acids would also be expected to react slowly. This is not the case with Lys, which is seen to react faster than Bet. This finding indicates that lysine is zwitterionic in the gas phase.

Theoretical calculations were performed on charge-solvated $[\text{Lys}+\text{Na}^+]$, zwitterionic $[\text{Lys}+\text{Na}^+]$, and $[\text{LysME}+\text{Na}^+]$. The distances and energies for all three species were very similar (Fig. 53). This indicates that there is little variation in the thermodynamic stabilization of the systems.

The structural optimization of the zwitterion shows that nitrogen and oxygen “share” a hydrogen atom. The sharing of this atom would slow down reaction kinetics of the zwitterion, which is what was experimentally observed. The charge-solvated structure shown in Fig. 53 displays a side chain N and carboxyl O coordination of the sodium ion. However, this is only one possible structure. As with Arg, another possible structure would be the chelation of the ion by NO and side chain N coordination. The chelation with three atoms would provide even greater stabilization to the system.

It was calculated that lysine is energetically more stable as a zwitterion in the gas phase. However, the stabilization energies of the charge-solvated and zwitterion complexes do not differ significantly. For data presented here, it can be concluded that alkali metal ion-stabilized lysine is zwitterionic in the gas phase.

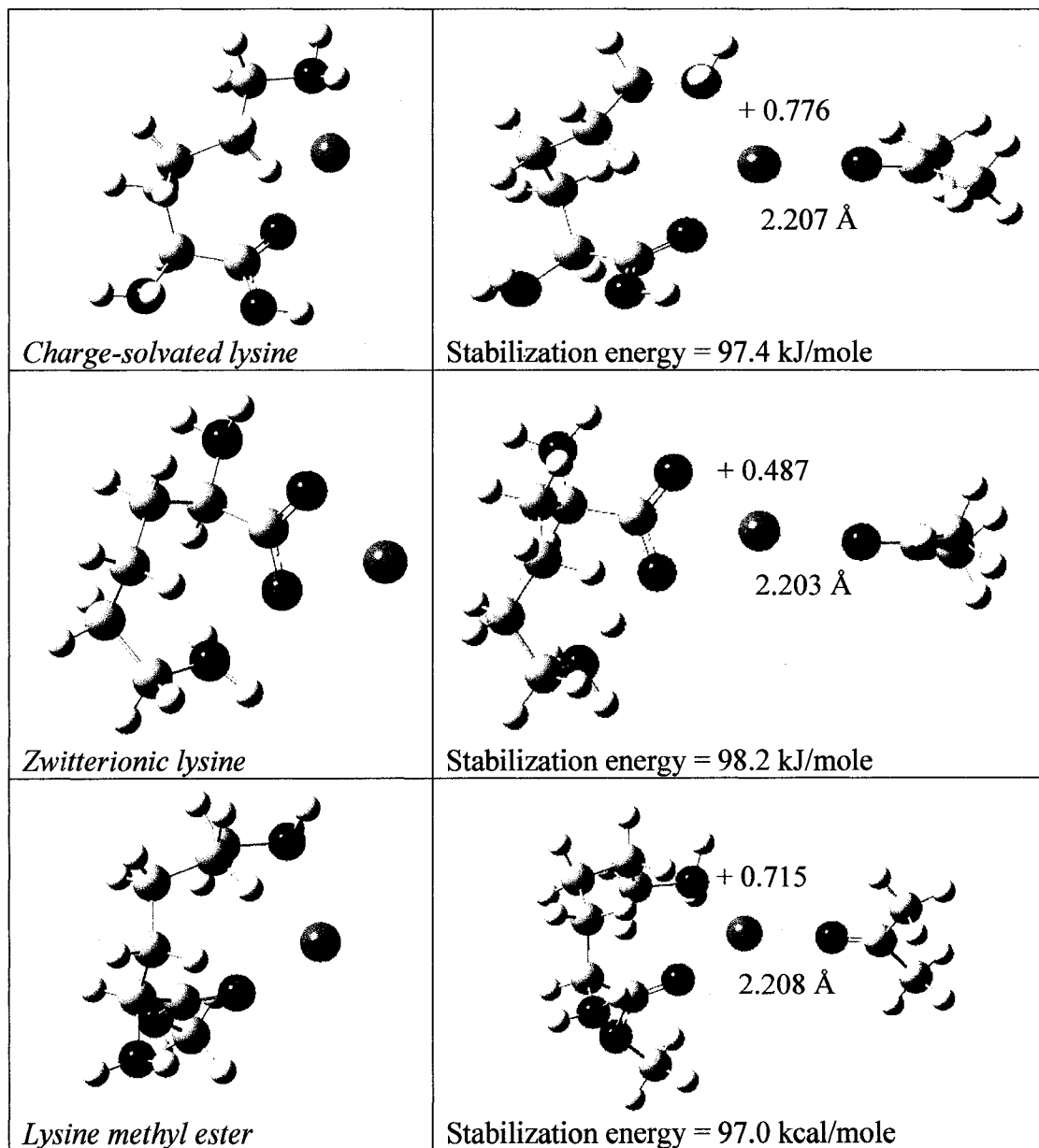


Figure 53. Computational results for sodiated Lys and LysME reacting with acetone.

Proline

As previously mentioned, proline is a known zwitterion in the gas phase. Both kinetic and thermodynamic experiments should confirm that proline is indeed zwitterionic. Lithiated proline kinetics show a variation in the expected trend (Fig. 54). It can be seen that both $[\text{ProME}+\text{Li}^+]$ and $[\text{Bet}+\text{Li}^+]$ react with almost identical kinetics, whereas $[\text{Pro}+\text{Li}^+]$ displays a slower reaction rate. Pro should react similarly to Bet since they are both known zwitterions. Additionally, ProME should react with kinetics different from a gas-phase zwitterion due to structural differences. The observation that $[\text{Pro}+\text{Li}^+]$ did not react similarly to Bet can be explained by the size and reactivity of Li^+ . Since Li^+ is small and very reactive, it is likely to interact quickly with acetone in any gas-phase structure.

When the same amino acid species are complexed to sodium, a different kinetics trend is observed (Fig. 55). These data show that the $[\text{Pro}+\text{Na}^+]$ and $[\text{Bet}+\text{Na}^+]$ species react much more similarly, as would be expected for gas-phase zwitterions. In this experiment, the sodiated ProME is the fastest reacting species. Given the kinetic trends demonstrated in Fig. 55, it is possible to state that $[\text{Pro}+\text{Na}^+]$ is a zwitterion in the gas phase.

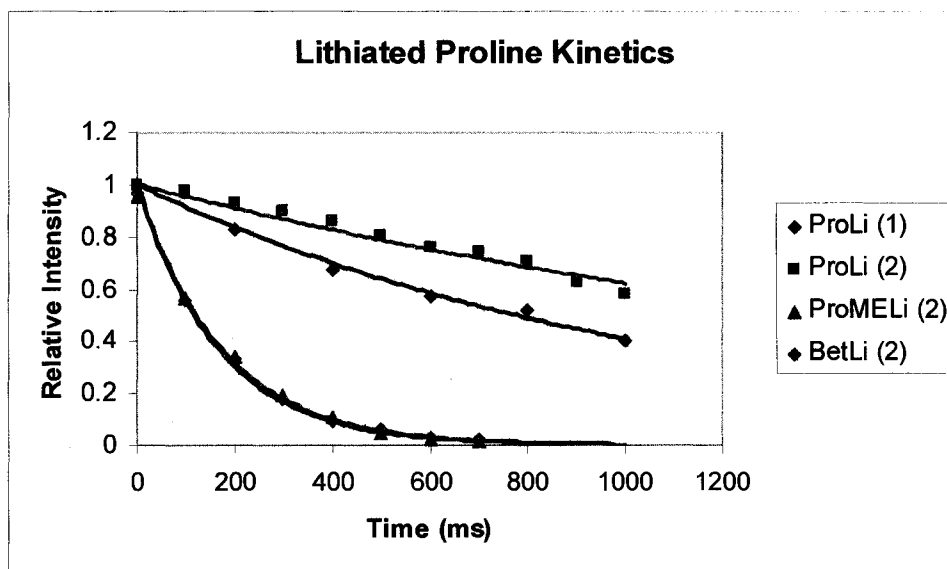


Figure 54. The reaction trends of the lithiated amino acids Pro, ProME, and Bet with acetone. Data acquired at estimated acetone pressures of 7×10^{-8} Torr (1) or 2×10^{-7} Torr (2).

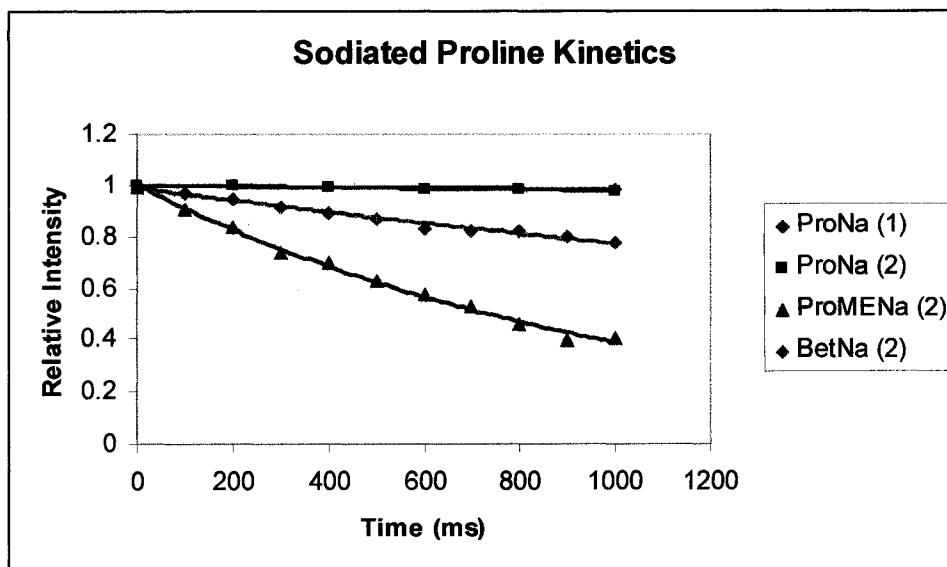


Figure 55. Sodiated proline kinetics for species reacting with acetone. Data acquired at estimated acetone pressures of 7×10^{-8} Torr (1) or 2×10^{-7} Torr (2).

A comparison of the kinetic trends of the alkali metal ion-complexed Pro species is shown in Fig. 56. This figure is helpful because it provides kinetic trend information for all of the Pro and Bet species. It can be seen that both $[\text{Pro}+\text{Na}^+]$ and $[\text{Pro}+\text{K}^+]$ react slowly compared to $[\text{Pro}+\text{Li}^+]$. A similar trend occurs with Bet. Since the Pro and Bet species react almost identically, these experiments confirm that proline is a zwitterion in the gas phase.

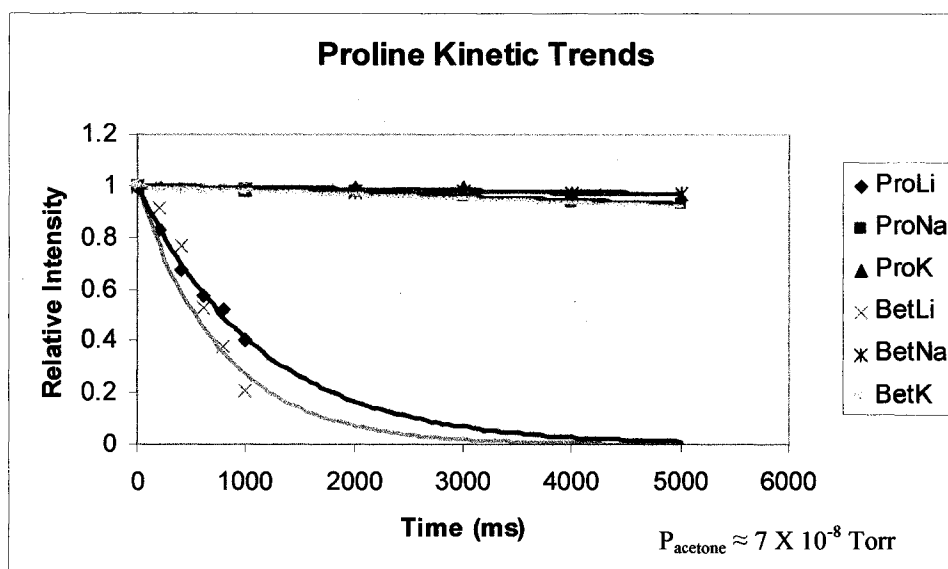


Figure 56. The kinetic trends of the $[\text{Pro}+\text{M}^+]$ species reacting with acetone. It is important to note that the lithiated species react similarly, whereas the sodiated and potassiated species react much more slowly.

Theoretical modeling calculations have shown that both $[\text{Pro}+\text{Na}^+\text{+acetone}]$ and $[\text{Bet}+\text{Na}^+\text{+acetone}]$ have similar stabilization energies and ion distances (Fig. 57). Calculations of sodiated ProME show that the distance between acetone and the metal cation is greater than for the distance between

acetone and the zwitterion-coordinated metal cation. In addition, the stabilization energy for proline methyl ester is less than for the zwitterion. These data corroborate the observation that the zwitterionic structure of proline is more stable in the gas phase.

Summary

A summary of kinetic and thermodynamic data acquired for the sodiated amino acid experiments is presented for Ala, Arg, Gly, His, Lys, and Pro (Table 15). Gaussian calculations were not performed for all methyl esters of these amino acids and were only performed on sodiated species. The reaction efficiency (Φ) was calculated using Eq. 2.2.

Other Amino Acids

The remaining amino acids were also analyzed via ion-molecule reactions. Methyl esters for these amino acids were not analyzed during the course of these experiments, and therefore structural identification for these species is not easily performed. It is possible to compare the reaction efficiency of all ion-molecule reactions to structurally distinguish these amino acids. This data is presented in Tables 16, 17, and 18. Gaussian computations can also be used to identify gas-phase structures of these species.

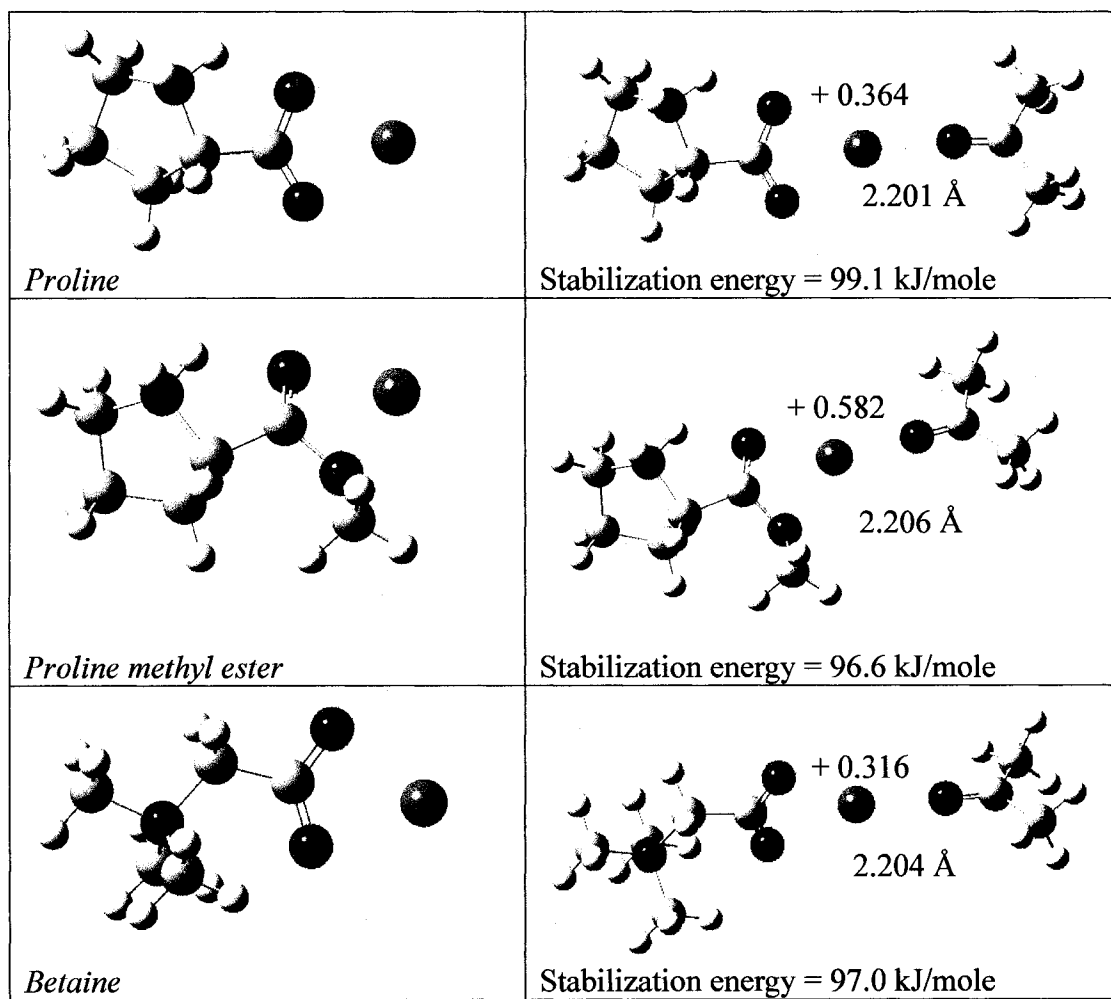


Figure 57. Computational results for sodiated Pro, ProME, and Bet reacting with acetone.

Table 15

Kinetic and Thermodynamic Data for Selected Sodiated Amino Acids and Model Compounds Reacting with Acetone.

Amino Acid		Φ^*	Bond Length [§] (Å)	Acetone Binding Energy [§] (kJ/mole)	Structural Determination
Alanine		$1.8 \times 10^{-1} \dagger$	--	--	Charge-solvated
Alanine methyl ester		5.7×10^{-2}	--	--	Charge-solvated
Arginine	Charge-solvated	$1.8 \times 10^{-2} \dagger$	2.204	97.4	Zwitterion
	Zwitterion		2.193	105.3	
Arginine methyl ester		2.6×10^{-2}	--	--	Charge-solvated
Betaine		$4.5 \times 10^{-2} \dagger$	2.204	97.0	Zwitterion
Glycine		$6.1 \times 10^{-2} \dagger$	2.186	107.8	Charge-solvated
Glycine methyl ester		5.6×10^{-2}	2.190	106.6	Charge-solvated
Histidine	Charge-solvated	$1.3 \times 10^{-3} \dagger$	2.189	107.4	Charge-solvated
	Zwitterion		2.190	104.5	
Histidine methyl ester		6.0×10^{-3}	--	--	Charge-solvated
Lysine	Charge-solvated	$3.1 \times 10^{-3} \dagger$	2.207	97.4	Zwitterion
	Zwitterion		2.203	98.2	
Lysine methyl ester		1.0×10^{-1}	2.208	97.0	Charge-solvated
Proline		$5.0 \times 10^{-3} \dagger$	2.200	99.1	Zwitterion
Proline methyl ester		2.91×10^{-1}	2.206	96.6	Charge-solvated

-- Data unavailable

*Experimental Kinetics

†Average value reported

§ Calculated by Gaussian

Lithiated Amino Acids

As previously observed, the lithiated amino acids are generally the faster reacting species in these experiments. It is often difficult to identify the structure of these amino acids. This is because both zwitterionic and charge-solvated species will react quickly. Since the error associated with rate determination is approximately thirty percent, these reactions do not differ significantly enough for valuable structural information to be obtained. Table 16 summarizes experimental data for lithiated species. Gaussian calculations were not performed for [A.A.+Li⁺] complexes.

Sodiated Amino Acids

Structural information can be obtained for sodiated amino acids due to the more variable kinetic trends that these species display. Unlike lithiated species, which all react fairly quickly and efficiently, sodiated species will show a variation in reactivity due to structural influence. Table 17 summarizes the data obtained for sodiated amino acids. In addition, structural identification as predicted by Gaussian calculations is also reported for modeled amino acids. Known structures of amino acids are identified as well as the proposed structures from the experimental and theoretical analyses.

Table 16

Experimental Results for Lithiated Amino Acids Reacting with Acetone.

Amino Acid	Φ	Known Structure
Alanine	1.0	--
Alanine methyl ester	5.0×10^{-1}	Charge-solvated
Arginine	$1.5 \times 10^{-3\dagger}$	--
Arginine methyl ester	1.3×10^{-2}	Charge-solvated
Asparagine	2.1×10^{-2}	--
Aspartic acid	5.1×10^{-1}	--
Betaine	1.1^\dagger	Zwitterion
Glutamine	2.2×10^{-2}	--
Glutamic acid	2.6×10^{-1}	--
Glycine	$6.0 \times 10^{-1\dagger}$	--
Glycine methyl ester	1.4×10^{-1}	Charge-solvated
Histidine	$4.3 \times 10^{-2\dagger}$	--
Histidine methyl ester	1.5×10^{-2}	Charge-solvated
Isoleucine	3.4×10^{-1}	--
Leucine	1.0	--
Lysine	$6.7 \times 10^{-2\dagger}$	--
Lysine methyl ester	2.2×10^{-1}	Charge-solvated
Methionine	2.6×10^{-1}	--
Phenylalanine	5.7×10^{-1}	--
Proline	$2.6 \times 10^{-1\dagger}$	Zwitterion
Proline methyl ester	1.8	Charge-solvated
Serine	8.2×10^{-2}	--
Threonine	8.4×10^{-2}	--
Tryptophan	3.1×10^{-1}	--
Tyrosine	3.1×10^{-1}	--
Valine	8.4×10^{-2}	--

† The average value is reported.

Table 17

Experimental Results for Sodiated Amino Acids Reacting with Acetone.

Amino Acid	Φ	Structure	
		Known	Proposed
Alanine	$1.7 \times 10^{-1\dagger}$	--	Zwitterion ^{a,b}
Alanine methyl ester	5.7×10^{-2}	Charge-solvated	--
Arginine	$1.8 \times 10^{-2\dagger}$	--	Zwitterion ^{a,b}
Arginine methyl ester	1.3×10^{-3}	Charge-solvated	--
Asparagine	3.9×10^{-4}	--	N/A
Aspartic acid	8.7×10^{-3}	--	N/A
Betaine	$4.5 \times 10^{-2\dagger}$	Zwitterion	--
Glutamine	1.3×10^{-3}	--	N/A
Glutamic acid	4.4×10^{-3}	--	N/A
Glycine	$6.1 \times 10^{-2\dagger}$	Charge-solvated	--
Glycine methyl ester	5.6×10^{-2}	Charge-solvated	--
Histidine	$1.3 \times 10^{-3\dagger}$	--	Charge-solvated ^{a,b}
Histidine methyl ester	6.0×10^{-3}	Charge-solvated	--
Isoleucine	8.6×10^{-2}	--	N/A
Leucine	4.8×10^{-1}	--	N/A
Lysine	$3.1 \times 10^{-3\dagger}$	--	Zwitterion ^{a,b}
Lysine methyl ester	2.6×10^{-3}	Charge-solvated	--
Methionine	1.8×10^{-2}	--	N/A
Phenylalanine	4.4×10^{-3}	--	N/A
Proline	$5.0 \times 10^{-3\dagger}$	Zwitterion	--
Proline methyl ester	2.9×10^{-1}	Charge-solvated	--
Serine	1.7×10^{-3}	--	N/A
Threonine	8.5×10^{-3}	--	N/A
Tryptophan	2.3×10^{-3}	--	N/A
Tyrosine	4.5×10^{-2}	--	N/A
Valine	1.7×10^{-1}	--	N/A

†Average value reported. a. Experimental b. Theoretical N/A not assigned

Although experiments with sodiated amino acids provide more information about structure than lithiated amino acid experiments, it is still difficult to determine the structure of some species. In cases for which the methyl ester of an amino acid was also analyzed, it was easier to determine structure. An amino acid that reacts with kinetics similar to its methyl ester is likely to be charge-solvated in the gas phase. If the amino acid differs in kinetics from the methyl ester, and is more similar to Bet, it is likely to be zwitterionic.

It is difficult to determine the structure of amino acids without using their complementary methyl esters because of the range of kinetics that the methyl esters display (see Fig. 35). Some methyl esters react exceptionally slowly (i.e., LysME and ArgME), whereas other methyl esters react much more quickly (i.e., ProME and AlaME). Since there is not a general reaction trend for all these methyl esters, it is difficult to compare amino acids to methyl esters that are not their own. For instance, the comparison of Asp to ArgME might not allow for an accurate structural determination.

Potassiated Amino Acids

It is also possible to use potassiated amino acid species for structural determination. Although some of the potassiated amino acids react too slowly for the experimental setup, it is possible to gather relevant kinetic data for those reactions which do occur during the time frame of the experiment. Table 18

summarizes the experimental and theoretical data obtained for potassiated amino acids. As with the analysis of potassiated species, it is hard to determine the structures of amino acids which do not have methyl ester counterparts. It can be seen that the proposed structures of amino acids for potassiated species are consistent with the proposed structures of sodiated amino acid species.

Conclusion

Ion-molecule reactions can be used to probe the structure of metal ion--amino acid complexes in the gas phase. Comparisons between known charge-solvated species, known zwitterion species, and the amino acid complexes in question can help to identify gas-phase structures. Theoretical calculations can be performed on these amino acids to aid in structure determination.

There were some instances in which the kinetic and/or thermodynamic results for the amino acids were similar enough to prevent certain structure identification. This is why it is essential to use both methods for structural identification. A more certain determination can be made when both kinetic and thermodynamic data are used in tandem.

Table 18

Experimental Results for Potassiated Amino Acids Reacting with Acetone.

Amino Acid	Φ	Structure	
		Known	Proposed
Alanine	$3.1 \times 10^{-3\dagger}$	--	Zwitterion ^{a,b}
Alanine methyl ester	‡	Charge-solvated	--
Arginine	‡	--	Zwitterion ^{a,b}
Arginine methyl ester	‡	Charge-solvated	--
Asparagine	8.8×10^{-4}	--	N/A
Aspartic acid	2.2×10^{-3}	--	N/A
Betaine	‡	Zwitterion	--
Glutamine	5.3×10^{-1}	--	N/A
Glutamic acid	4.0×10^{-4}	--	N/A
Glycine	$3.3 \times 10^{-3\dagger}$	Charge-solvated	--
Glycine methyl ester	‡	Charge-solvated	--
Histidine	‡	--	Charge-solvated ^{a,b}
Histidine methyl ester	‡	Charge-solvated	--
Isoleucine	3.5×10^{-2}	--	N/A
Leucine	8.7×10^{-3}	--	N/A
Lysine	3.1×10^{-2}	--	Zwitterion ^{a,b}
Lysine methyl ester	8.9×10^{-2}	Charge-solvated	--
Methionine	1.8×10^{-3}	--	N/A
Phenylalanine	1.8×10^{-2}	--	N/A
Proline	2.6×10^{-3}	Zwitterion	--
Proline methyl ester	‡	Charge-solvated	--
Serine	‡	--	N/A
Threonine	3.0×10^{-2}	--	N/A
Tryptophan	‡	--	N/A
Tyrosine	‡	--	N/A
Valine	‡	--	N/A

†Average value reported. ‡Rate unobtainable a. Experimental b. Theoretical N/A not assigned

Metal ion selection is also an important factor in the kinetics of the ion-molecule reactions. Lithiated amino acid species are exceptionally reactive. This is problematic because both charge-solvated and zwitterionic species will react in a similar fashion when complexed with Li^+ . This problem is alleviated with the use of larger cations, for instance sodium or potassium. Species with larger cations such as these will react in a more reasonable time frame.

Kinetic and thermodynamic results of these experiments indicate that both Ala and Pro are likely to form zwitterionic complexes with Na^+ and K^+ in the gas phase. $[\text{Pro}+\text{M}^+]$ is already known to be zwitterionic in the gas phase. Data for Arg and Lys indicate that both species form zwitterionic complexes with Na^+ and K^+ in the gas phase, although the large side chains of these amino acids interact with the metal ion so as to complicate this conclusion. Gly and His complexes with Na^+ and K^+ are both found to be charge-solvated in the gas phase. Glycine is known to be charge-solvated in the gas phase.

CHAPTER 4

USING ION-MOLECULE REACTIONS TO SIMULATE AROMATIC AMINO ACID INTERACTIONS WITH AMINO ACID--METAL ION COMPLEXES

Hydrogen bonds, salt bridges, and cation- π interactions are all responsible for the formation of secondary, tertiary, and quaternary structures of proteins. Proteins containing aromatic amino acids are often participants in cation- π interactions with metal species. It has been shown that many of these aromatic-metal interactions involve strong binding, especially with transition metals.¹⁶¹

To review, cation- π interactions are noncovalent interactions which occur between cations and neighboring π -systems (i.e., potassium and the face of benzene) (Fig. 58). These interactions are fairly common in proteins, occurring one time for every 77 amino acid residues. Approximately 26% of all Trp residues in a protein are thought to participate in significant cation- π interactions, most of them with the charged side chains of Arg and Lys.¹²⁵ Besides structural functions, cation- π interactions are also important for biomolecule function and selectivity.

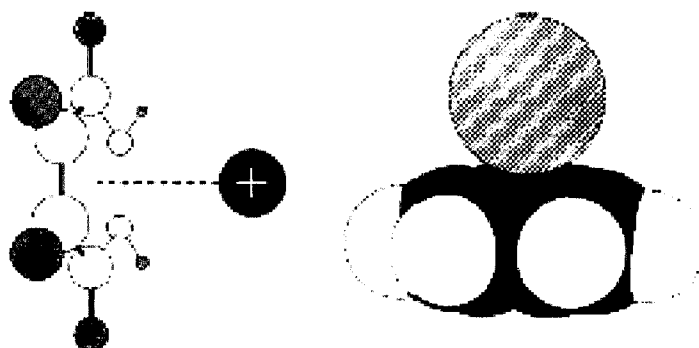


Figure 58. A visualization of a cation- π interaction (from Ma and Dougherty¹⁶¹). The figure on the left shows the positioning of the cation with respect to the π -system of benzene. The figure on the right is a space-filling model of a K^+ ...benzene complex.

The Relevance of Cation- π Interactions

Cation- π interactions play an important role in biomolecule structure and activity. Although some examples of these roles were highlighted in Chapter 1, there are many more instances in which cation- π interactions involving aromatic amino acids are prevalent: Protein structure;^{125, 126, 162, 163} ligand binding;^{121, 164-167} ion channel gating and formation;^{129, 168-170} metal cation--aromatic amino acid interactions;^{66, 98, 130, 135, 140, 148, 149, 156, 158} and RNA-,^{127, 171} DNA-,^{120, 128, 172} and protein-protein binding all involve cation- π interactions. Some additional examples of previously identified cation- π interactions are described here.

Protein Structure

Cation- π interactions are likely capable of stabilizing the secondary, tertiary, and/or quaternary structures of peptides and proteins. Gallivan and Dougherty found that proteins situate “cations at nonrandom positions relative to aromatics,” which allows for optimized cation- π interactions.¹²⁵ Helical peptides and proteins have been analyzed to investigate the stabilizing interactions between aromatic and basic side chains. It has been found that basic-aromatic interactions were favorable when the amino acid residues were in an $i, i + 4$ helix (Fig. 59).^{162, 163} This is likely due to cation- π interactions. Another example of cation- π interactions in a protein can be seen in the human growth hormone receptor extracellular domain (Fig. 59).¹⁶¹

Protein Regulation

Binding specificity is an important regulatory feature of many biomolecules. Tight control of ion channels, receptors, transporters, and other ligand-activated species is required for the successful function and survival of living systems. Many of these ligand-molecule interactions are controlled by specific molecular recognition which can be visualized as a lock-key system. Many studies have suggested that aromatic amino acids play an important role in molecular recognition via cation- π interactions.



Figure 59. Cation- π interactions in proteins. The figure on the left shows the α -helical $i, i + 4$ interaction of Phe and Lys in xylanase (adapted from Andrew et al.¹⁶³). The figure on the right shows the interaction of aromatic amino acids with Arg and Lys in the human growth hormone receptor extracellular domain (adapted from Ma and Dougherty¹⁶¹).

For example, cation- π interaction between an agonist and a tyrosine residue in the binding site of the neurotransmitter receptor protein GABA_c can alter protein function.¹⁷³ Both sugars galactose and glucose have been shown to interact with aromatic amino acids in the binding site of proteins.¹⁶⁷ Phenylalanine is essential for pyrethroid binding in insect sodium channels.¹⁷⁰ The mutation of a phenylalanine in the ion channel of the nucleotide-binding domain of cystic fibrosis transmembrane conductance regulator (CFTR) is the cause of most cases of cystic fibrosis. Studies have shown that the aromatic side chain of Phe is required for the appropriate function of CFTR.¹⁶⁹ Rotem et al.¹⁶⁶ have found that EmrE, an *E. coli* protein, requires the presence of tyrosine to function as an ion-coupled transporter.

Finally, the nicotinic acetylcholine receptor (nAChR) is a ligand-gated ion channel which is thought to participate in cation- π interactions. Acetylcholine binds the receptor, causing a conformational change to occur. This allows the ion channel to open. Figure 60 shows nAChR. The high aromatic amino acid content of the receptor provides an ideal situation for cation- π interactions.^{161, 165} As can be seen from these examples, there are a variety of biomolecules which are controlled by aromatic amino acid interactions.

Studying Aromatic Interactions with Metal Cations

It is important to study the interactions of metal cations with aromatic amino acids in order to better understand the function and control of many biomolecules.

Currently, there are three basic systems used to study aromatic-metal interactions (Fig. 61). The first system is used to study the interaction between a metal ion and an aromatic compound (Fig. 61A). The second system is used to study the interaction between a metal-containing species and an aromatic compound (Fig. 61B). The final system is used to study the interaction between a metal cation and an aromatic amino acid (Fig. 61C).

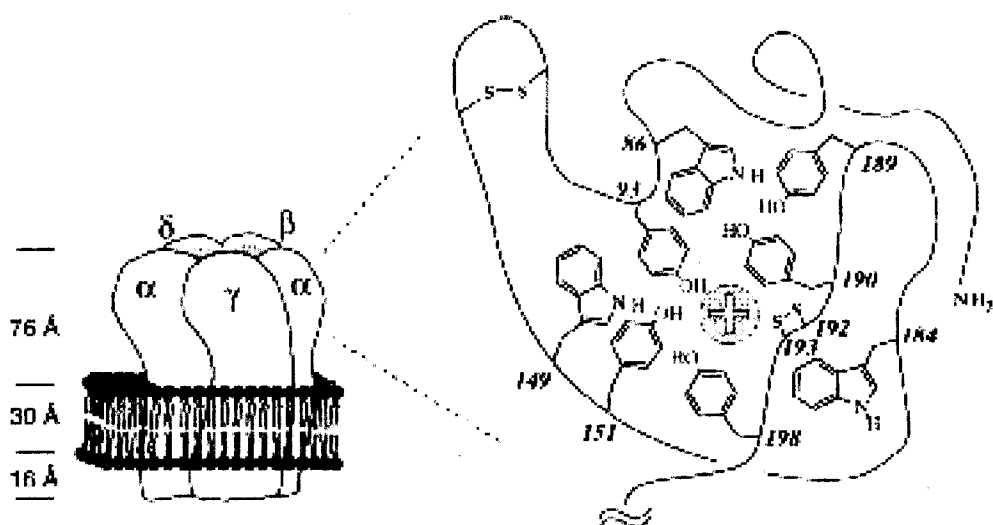


Figure 60. The nicotinic acetylcholine receptor. The figure on the left shows the overall receptor layout. The figure on the right shows the aromatic amino acids that could contribute to cation- π interactions in the α -subunit of the protein (from Ma and Dougherty¹⁶¹).

The cation- π interactions of metal cations and aromatics have been studied by a variety of groups (Fig. 61A). Using a theoretical approach, Ikuta and others have analyzed the interaction between selected alkali metal cations ($M^+ = Li^+, Na^+$, and K^+) with various aromatic molecules.^{174, 175} One study found that anthracene

and phenanthrene have a greater theoretical binding energy to sodium than is seen with benzene. It was also observed that potassium is less strongly bound, enabling movement of the cation along the aromatic molecule. It has been suggested that this observation could help to explain the selectivity and function of potassium channels.¹⁷⁴

It is also important to study the interaction of coordinated metal ions (XM^+) to aromatics (Fig. 61B). Also using theoretical methods, Cheng et al. studied the interaction of benzene to a variety of XM^+ species ($\text{X} = \text{H}^+, \text{F}^-, \text{Cl}^-, \text{OH}^-, \text{SH}^-, \text{CN}^-, \text{NH}_2^-, \text{and } \text{CH}_3^-$; $\text{M} = \text{Be}^{2+}, \text{Mg}^{2+}, \text{and } \text{Ca}^{2+}$).¹⁷⁶ The authors found that the interaction between the alkaline earth metals without counterions and benzene was stronger than the interaction between alkali metals with benzene. However, when a counterion was complexed to the cation in the form XM^+ , the interaction between the alkaline metals and benzene was similar to the interaction of alkali metals with benzene.¹⁷⁶

Of greatest relevance to this study is the analysis of the interaction between a metal ion and the aromatic side chain of an amino acid (Fig. 61C). A variety of experimental and theoretical experiments have been performed, mostly by the groups of Rodgers^{36-41, 46, 177} and Dunbar.^{63, 66, 130, 178} In a series of five studies, Amunugama and Rodgers analyzed the binding energies of alkali metals to aromatic molecules selected to model aromatic amino acid side chains; the aromatics toluene, fluorobenzene, aniline, phenol, and anisole were used (Fig. 62).^{36-38, 40} One observed trend with these threshold CID experiments of $[\text{M}^+ + \text{neutral}]$ complexes

showed that the size of the cation is directly related to the binding dissociation energy.

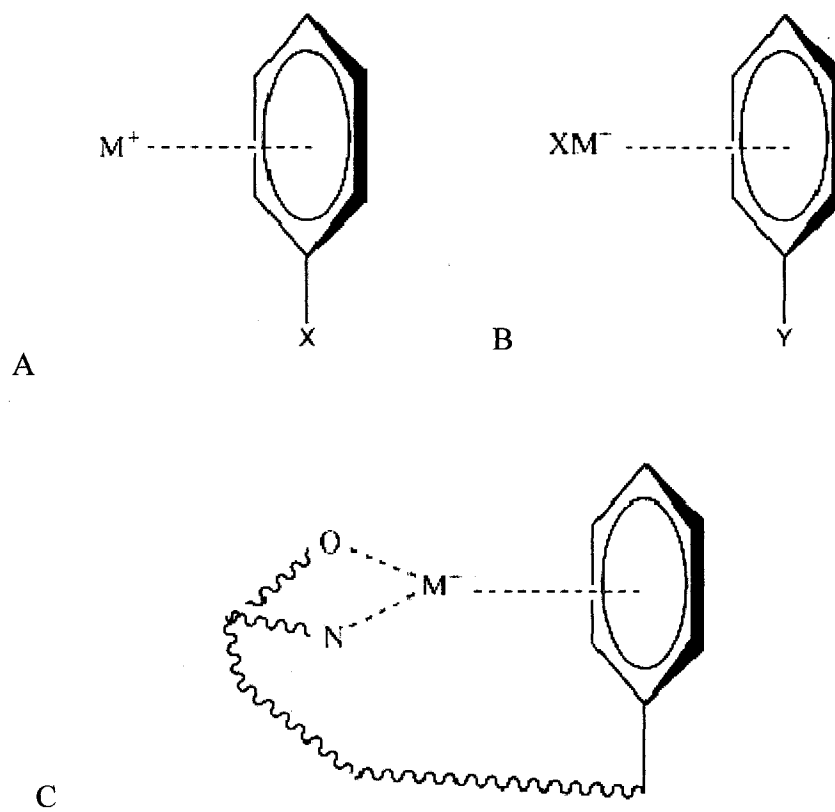


Figure 61. Aromatic interactions with metal cations. A. A metal cation interacting with an aromatic species. B. A metal complex interaction with an aromatic species. C. A metal cation interaction with the aromatic moiety of an amino acid.

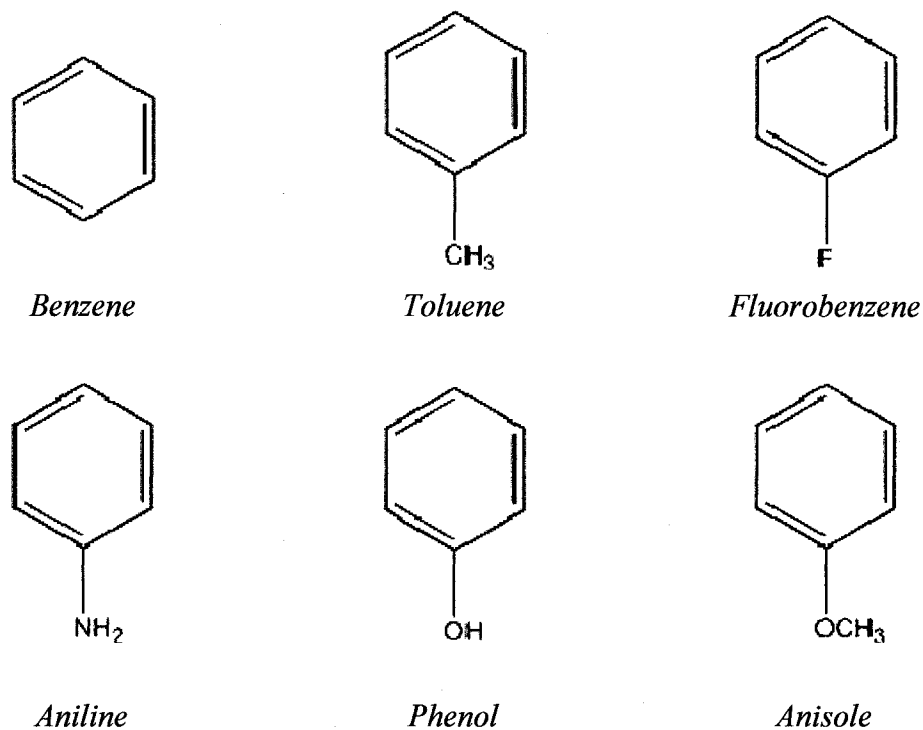
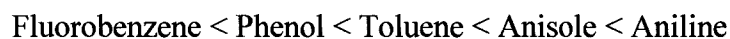


Figure 62. The substituted structures of the benzene molecule.

Additionally, Amunugama and Rodgers found the nature of the substituent group on the benzene ring directly affected the level of cation- π interaction observed for alkali metal-aromatic species. For instance, the presence of a methyl substituent increases the cation- π interaction between the cation and the ring. An increase in cation- π interactions was also observed for aniline, phenol, and anisole molecules.

On the other hand, the presence of a fluoro substituent on the benzene ring decreases the strength of the cation- π interaction. It has also been suggested that the strength of the cation- π interaction will continue to decrease as additional fluoro

substitutions are made to the benzene ring.^{36-38, 40} A comparison of the experimental ΔH_0 (kJ mol⁻¹) values for these neutrals bound to Li⁺ shows that the cation- π interactions increase in strength as follows:



This trend is also valid for complexes with the larger alkali cations.^{36-38, 40} This indicates that the “polarizability of the π ligand is a key factor in determining the strength of the binding in cation- π complexes.”³⁹

Threshold CID experiments were also performed on alkali metal complexes with the neutral molecule indole.³⁹ Indole is the aromatic side chain substituent of Trp (Fig. 63). It differs from the side chains of Phe and Tyr because there are two aromatic rings with available π -systems for binding. A comparison of the binding dissociation energies of the three aromatic amino acids shows that there is a preference for binding as $M^+\text{Phe} < M^+\text{Tyr} < M^+\text{Trp}$, where M^+ is sodium or potassium.³⁹

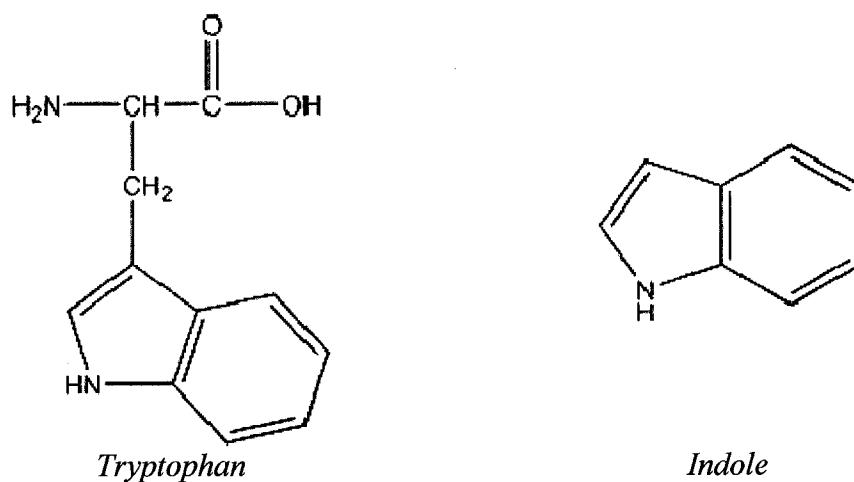


Figure 63. The indole side chain of tryptophan.

It was found that, as with the other threshold CID studies, the binding dissociation energies of these complexes decreased as the size of the alkali metal cation increased. Indole is also observed to have a stronger cation- π interaction than the other aromatics due to the extended π -system of the molecule. This finding helps to explain the large number of biological cation- π interactions that are observed.³⁹

The Dunbar group has also focused on these metal-aromatic amino acid interactions. Radiative association kinetics experiments coupled with theoretical modeling calculations were performed to analyze the interactions of metal ions with phenol (Tyr) and indole (Trp). It was found that nontransition metal binding to phenol had comparable energetics to benzene; however, transition metals such as Cr^+ and Fe^+ showed enhanced binding to phenol over benzene. As expected, indole was observed to bind more strongly to metal ions than phenol. Again, this is attributed to the expanded π -system of the indole molecule.⁶⁶

Further experiments using the kinetic method and theoretical calculations found that Trp binds Na^+ and K^+ more strongly than Phe and Tyr. In these experiments, both Phe and Tyr were shown to have similar binding energies for both sodium and potassium ions. In addition, a linear correlation between the proton affinity of an amino acid and the experimental binding energies of the amino acids was also demonstrated.⁶⁶

Reddy and Sastry also used a theoretical approach to analyze the interaction of a diverse group of cations with the aromatic groups of amino acids.¹⁴⁹ Their study focused on the interaction of Phe, Tyr, Trp, and His side chains with $\text{M} = \text{H}^+$,

Li^+ , Na^+ , K^+ , Ca^{2+} , Mg^{2+} , NH_4^+ , and NMe_4^+ . It was found that H^+ binds selectively to a carbon atom of the benzene ring. The metal and ammonium ions were found to be centrally positioned above the ring, participating in cation- π interactions. The theoretical energy of the metal interactions was ordered as follows:¹⁴⁹



Although many of these previous studies have provided much-needed information about the cation- π interactions of aromatic amino acids, information about these systems is not yet complete. Experiments using CID techniques are capable of investigating the energy required to break the metal-ring bond, as well as the NO coordination bonds from the amino acid to the metal (Fig. 64). CID experiments are limited in bond information. When the weakest bond (the cation- π interaction) is broken, the m/z ratio of the $[\text{A.A.}+\text{M}^+]$ complex is not altered. As subsequent bonds are broken, the NO coordination is lost and the complex fragments into an amino acid and a metal ion.

To investigate cation- π interactions, it is necessary to find a system that will allow for the specific analysis of only the metal-aromatic interactions. This analysis can be performed by allowing $[\text{A.A.}+\text{M}^{\text{X}+}]$ complexes to react with selected aromatic compounds (Fig. 64) through ion-molecule reactions. These aromatic compounds are chosen to model the aromatic side chains of the amino acids.

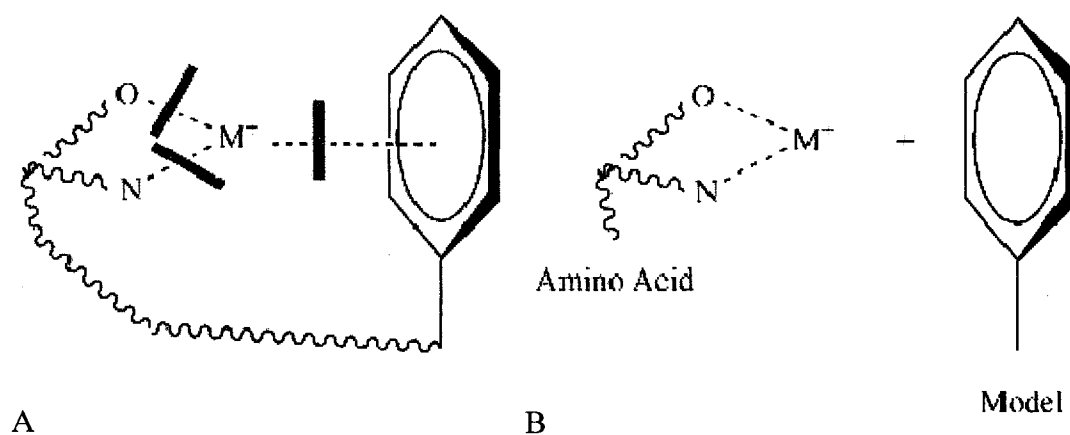


Figure 64. Modeling cation- π interactions. Red bars indicate the bonds broken in the experiment. A. A diagram of CID analysis, where all three amino acid- M^+ bonds are broken. B. A diagram of an association reaction in which only the cation- π interaction is analyzed.

The association/dissociation of the aromatic species to/from the $[A.A.+M^{X+}]$ complex alters the m/z ratio observed in the mass spectra; this is solely attributed to the cation- π interaction. The binding energy of the interaction can be calculated from the equilibrium of the association reaction. The simple equilibrium of these reactions is shown in Eq. 4.1:



where A^+ is the $[A.A.+M^+]$ species, B^+ is the $[A.A.+M^+ + \text{neutral}]$ species, and P_N is the pressure of the neutral in the ion trap. The equilibrium constant, K_{eq} , can then be calculated as follows (Eq. 4.2):

$$K_{eq} = \frac{B_{eq}}{A_{eq}} = \frac{k_1}{k_{-1}P_N} \quad (4.2)$$

where A_{eq} and B_{eq} are the concentrations of A^+ and B^+ at equilibrium.

Once K_{eq} has been determined, it can be used to calculate the Gibb's free energy, ΔG , of the reaction by rearranging Eq. 4.3:

$$K_{eq} = \exp\left(-\frac{\Delta G}{RT}\right) \quad (4.3)$$

Here, R is the ideal gas constant and $T = 300\text{K}$. Finally, ΔG can be used to calculate ΔH using Eq. 4.4:

$$\Delta G = \Delta H - T\Delta S \quad (4.4)$$

where $T = 300\text{K}$ and the entropy of the reaction, ΔS , was the average value for similar reactions which corresponds to the loss of three translational degrees of freedom for the neutral ($\sim 34 \pm 6 \text{ J mol}^{-1}\text{K}^{-1}$).¹⁷⁹ The uncertainty in ΔS is less of a factor in these calculations than the uncertainty in P_N . The ΔH is the bond energy for these ion-molecule reactions.

Model Neutrals

Previous studies have used benzene, phenol, indole, and pyrrole as model π -systems for the aromatic amino acids.³⁹ The selection of the model bases used for these particular experiments is accomplished by choosing model compounds closely structured to the amino acid side chain it is modeling while still being volatile enough to be introduced to the quadrupole ion trap through the helium line. The

neutral species used for these experiments are shown in Fig. 65.

Benzene is the basic structure for the aromatic side chains of amino acids (Fig. 65). Benzene is a simple aromatic with no attached substituents. In order to improve the modeling relevance of these experiments, aromatic molecules with appropriate substituents are required. Benzene was used experimentally to model aromatic amino acids and was also used for theoretical modeling calculations in the Gaussian program.

Toluene is similar in structure to the phenylalanine side chain, so it was chosen as an appropriate model for those experiments (Fig. 65). Toluene has been used to successfully model Phe by previous groups.^{37, 130} In these experiments, the aromatic moiety of the toluene molecule is used to model the aromatic side chain of phenylalanine.

The aromatic moiety of Tyr differs from Phe, having a hydroxide at the fourth position of the aromatic ring. The neutral closest in structure to the side chain of Tyr is 4-methyl-phenol (Fig. 66). Although this aromatic neutral is an identical match to the side chain of Tyr, it was not able to be used because it does not have a vapor pressure appropriate for these experiments.

Methyl anisole was chosen as a model for tyrosine. Methyl anisole is similar to the aromatic side chain of tyrosine because it contains an oxygen atom at the third position of the aromatic ring (Fig. 65). It is essential to maintain an oxygen bond at this position in order to ensure that the π -system of the aromatic ring model is consistent with that of the aromatic side chain.

Aromatic Amino Acid**Neutral Model**

All Aromatics

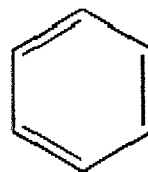
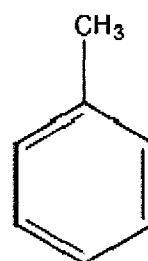
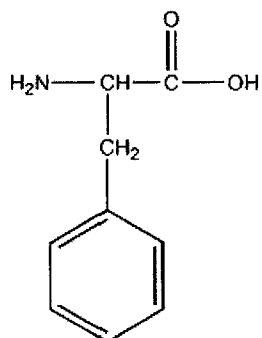
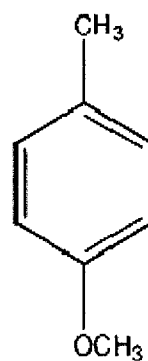
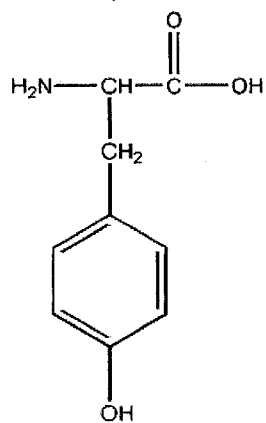
*Aromatic Amino Acids**Benzene**Phenylalanine**Toluene**Tyrosine**Methyl anisole*

Figure 65. The aromatic amino acids and their corresponding model neutrals used in this study.

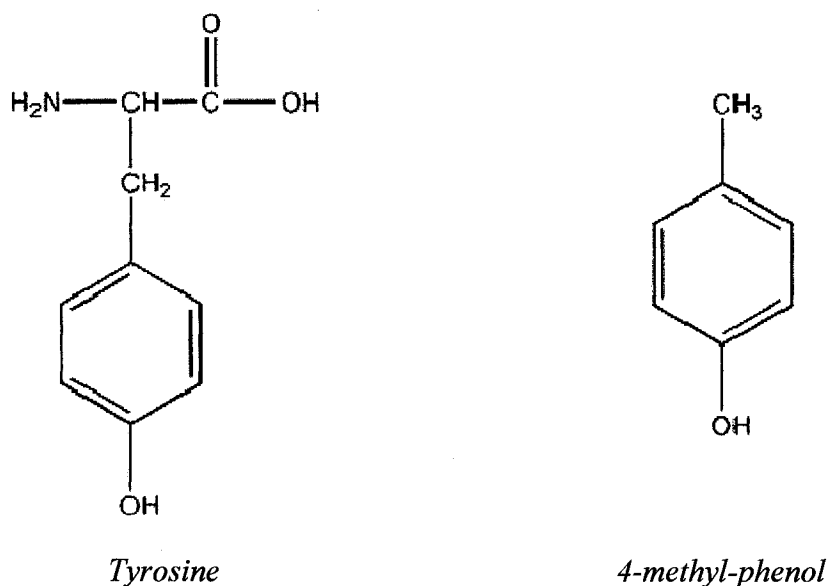


Figure 66. An identical neutral match to the side chain of Tyr.

Theoretical Studies with Benzene

Benzene is a simple six-carbon aromatic molecule and the basic structure of the neutrals used to model aromatic amino acids. A partial double bond is shared equally between the six carbons, which causes the π -system to be evenly distributed over the benzene ring. A Gaussian optimized benzene molecule is shown in Fig. 67.

Gaussian analysis of a variety of $[A.A.+M^+]$ complexes and benzene was performed in order to determine the binding energetics of the systems. The $[A.A.+M^++benzene]$ complexes were analyzed using the same method previously described in Chapter 2. Appendix C contains the images of all the

[A.A.+M⁺+benzene] systems studied as well as stabilization energy, metal-benzene distances, and metal charges.

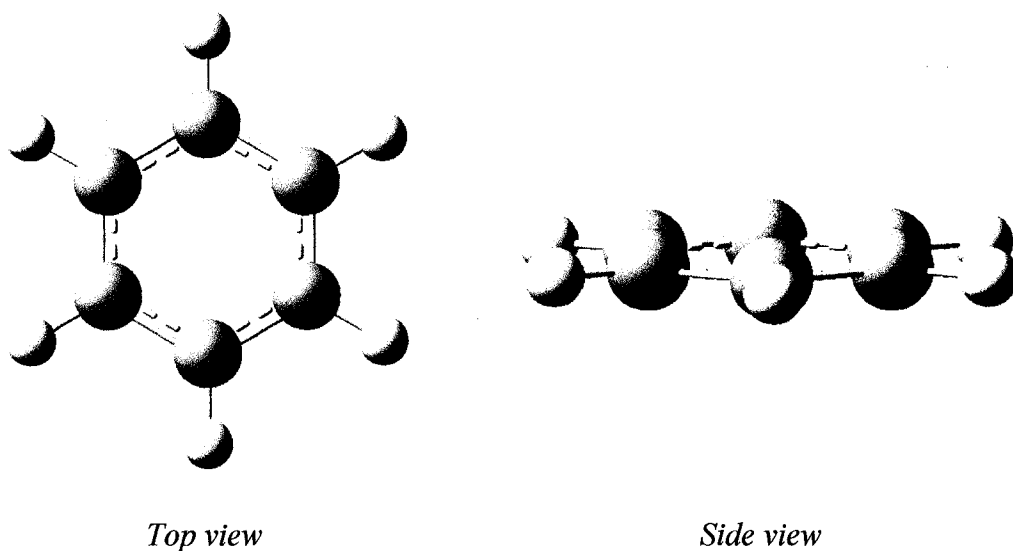


Figure 67. Benzene. The top view shows the even distribution of the double bonds to the six ring carbons. The side view shows that benzene is a planer molecule.

A common feature among the [A.A.+M⁺+benzene] reactions analyzed by Gaussian is that the center of the aromatic ring is positioned directly over the chelated metal ion (Fig. 68). This positioning indicates that the π -system of the benzene ring interacts with the metal ion in an evenly distributed fashion.

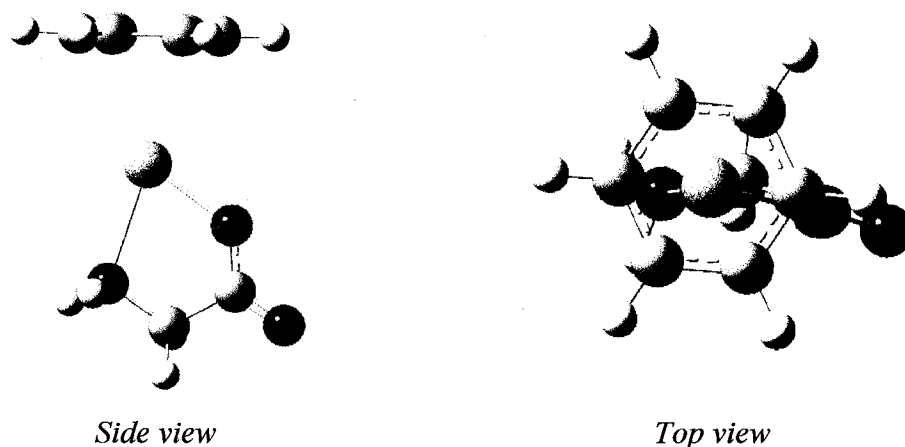


Figure 68. An example of the benzene-metal interaction (as depicted by Gaussian). The $[\text{Gly-H}+\text{Ca}^{2+}+\text{benzene}]^+$ system is shown here. The side view shows the face of the planer aromatic ring facing the metal cation. The top view clarifies that the benzene ring is centered over the metal ion.

Table 19 summarizes the data obtained through the *in silico* analysis. The stabilization energies of all the species are reported for all of the Gaussian optimized complexes. A larger stabilization energy indicates a stronger interaction between the benzene molecule and the $[\text{A.A.}-\text{H}+\text{Ca}^{2+}]^+$ complex. The species in Table 19 are listed in order of increasing stabilization energy.

When the data for the stabilization energies of the amino acids are viewed in order of increasing energy, a few trends appear. First, the amino acids with long side chains show the lowest calculated stabilization energy. Since the long side chains of Arg and Lys are capable of providing additional coordination sites to the metal cation, it is likely that the charge of the metal ion would be shielded from interaction with the aromatic ring.

Table 19

Theoretical Data for Benzene Reactions.

Amino Acid Complex [A.A.-H+Ca ²⁺] ⁺	Stabilization Energy (kJ/mole)	Distance* M ⁺ ...Benzene (Å)	M ⁺ Charge
Arginine	E = 101.4	2.613	1.050
Lysine	E = 108.7	2.616	1.043
Glutamic Acid	E = 111.6	2.592	1.022
Aspartic Acid	E = 116.6	2.594	1.016
Threonine	E = 120.4	2.583	0.980
Serine	E = 122.9	2.583	1.005
Glycine	E = 127.9	2.579	1.238

*Approximate distance to the center of the plane of the benzene ring.

The optimized structure of [Arg-H+Ca²⁺+benzene]⁺ shows that the calcium ion is coordinated by two oxygens and two nitrogens (Fig. 69). Similarly, Lys coordinates calcium with two oxygens and one nitrogen (Fig. 69). The additional side chain coordination is able to draw the positive charge away from the metal ion, creating a situation for weaker interaction between the [Arg-H+Ca²⁺]⁺ and [Lys-H+Ca²⁺]⁺ and benzene.

The next four amino acids in the table are shown to have higher stabilization energies. These amino acids all coordinate the metal ion with three oxygen atoms; two oxygens from the carboxyl terminus and an oxygen from the side chain. Glu has a longer side chain than Asp; therefore, it is capable of more easily shielding the calcium with its side chain. This causes the stabilization energy of Glu to be lower than Asp. The amino acids Ser and Thr have comparatively short side chains.

These short side chains prevent the calcium ion from being protected from the benzene interaction, allowing for greater stabilization energy.

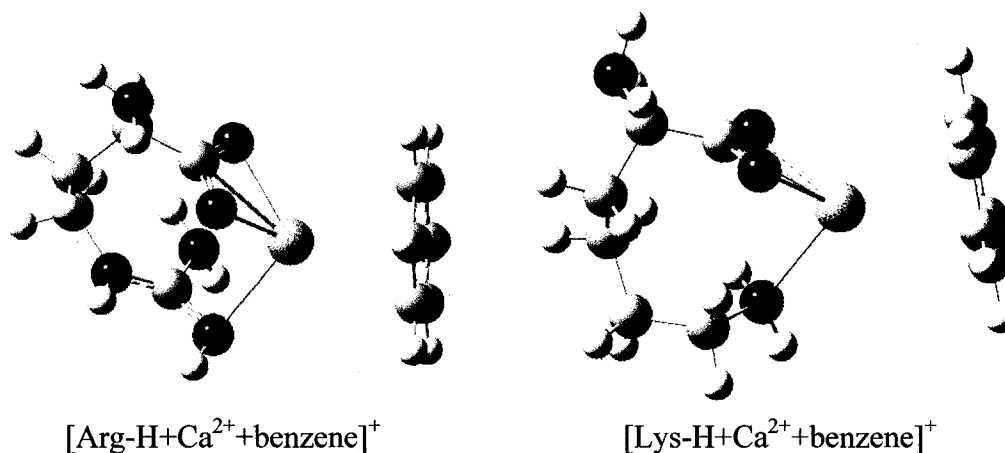


Figure 69. The side chain coordination of calcium by Arg and Lys.

Finally, [Gly-H+Ca²⁺]⁺ exhibited the greatest stabilization energy upon benzene binding. Of the seven amino acids studied, Gly is by far the simplest. With no side chain available for additional coordination and side chain hindrance, the complexed Ca²⁺ is fully capable of interaction with the benzene molecule (Fig. 68). With unrestricted access to calcium, the Gly complex would be expected to have the greatest calculated stabilization energy. This is confirmed by Gaussian, as shown in Table 18.

There is also a correlation between the calculated stabilization energy and the distance between the metal cation and the face of the benzene ring. As the stabilization energy increases, the distance between the metal ion and benzene

decreases. On the other hand, there does not appear to be a trend with regards to the charge of the metal ion.

A comparison of the proton affinities of the α -amino acids (from Wyttenbach et al.)¹⁰³ to the calculated stabilization energies of these complexes is shown in Fig. 70. It can be seen that there is a correspondence between the two values; as the proton affinity increases, the stabilization energy decreases. Both Asp and Glu differ slightly from this trend. This is likely because Asp and Glu are capable of binding Ca^{2+} more strongly than the other amino acids.

The calculated results from modeling reactions with the simple neutral benzene are found to be logically sound: The stabilization energy decreases as the amino acid side chain increases in chelating ability. Ion-molecule experiments for modeling the interaction of aromatic amino acids to $[\text{A.A.}+\text{M}^{n+}]$ species require the use of more complex neutral molecules. An increase in neutral complexity could limit the ability of experimental data to determine binding affinity.

For instance, bulky additions to the aromatic could prevent spatial alignment of the aromatic and the metal cation. Additionally, an increase of groups bound to the central ring could alter the π -system. Theoretical calculations can be used to supplement the findings of ion-molecule reactions. Since the calculations performed with benzene have successfully identified reaction trends, it is possible to use similar Gaussian analysis on more complex species.

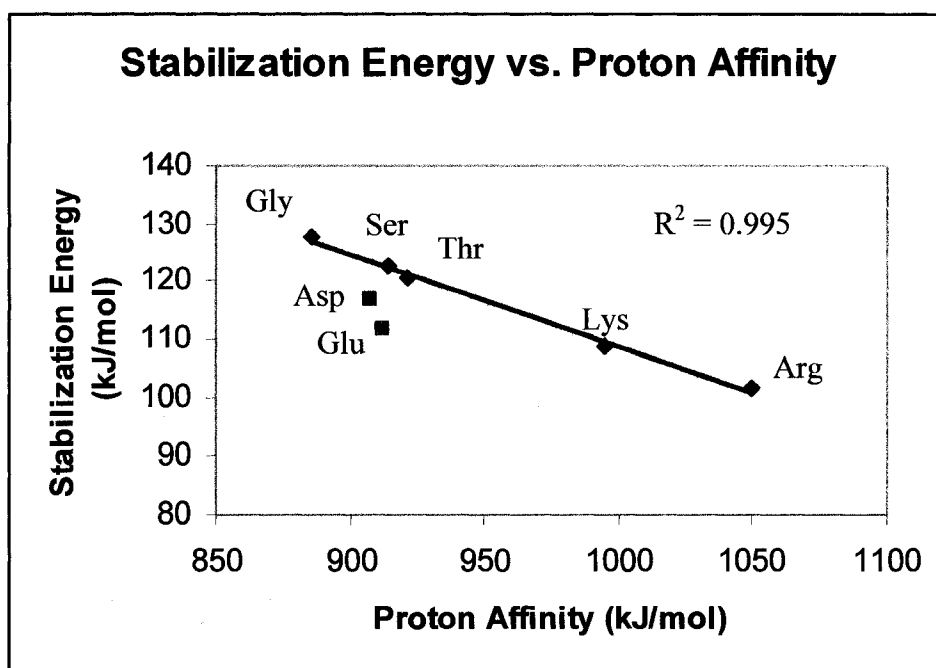


Figure 70. A comparison of the calculated stabilization energies and the proton affinities of the amino acids.

Phenylalanine Modeling

As previously mentioned, toluene was chosen to model the aromatic side chain of phenylalanine. The structure of toluene, as optimized by Gaussian, is shown in Fig. 71. Toluene is similar in structure to benzene; however, it contains a methyl group on the first position carbon. The addition of this methyl group disturbs the evenly distributed π -system of the aromatic ring. Toluene has a boiling point of 110-110 °C, a vapor pressure of 22 mmHg (at 20 °C), and a density of 0.865 g/mL (at 25 °C). It has a published polarizability of 12.25 \AA^3 .¹⁶⁰

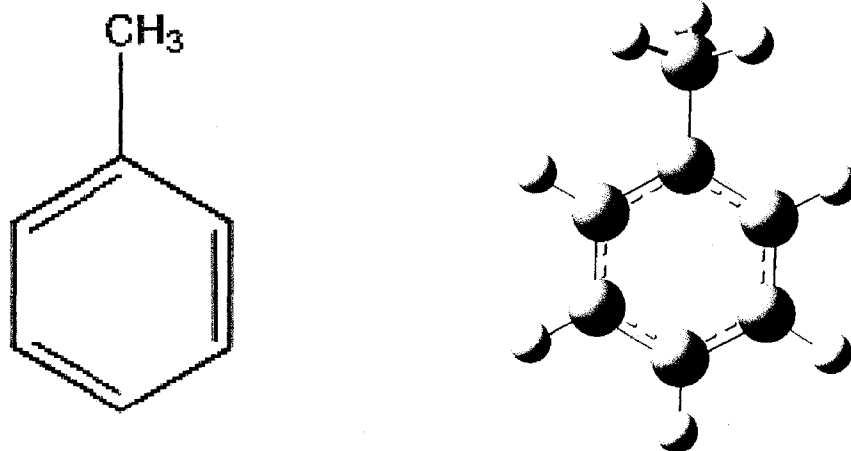


Figure 71. Toluene. The figure on the left is a simple drawing. The figure on the right is Gaussian optimized.

Method

Ion-molecule reactions, using toluene as the neutral species, were performed as detailed in Chapter 2. Both $[A.A.+M^+]$ species, where $M = Ag^+$ or Cu^+ , and $[A.A.-H+M^{2+}]^+$ species, where $M = Ca^+$, Co^+ , Fe^+ , Ni^+ or Zn^+ , were allowed to react with toluene until equilibrium was established. The KinFit analysis macro for Excel was then used to determine rate constants for the experiments.

Using Gronert's method, the estimated toluene pressure in the trap was calculated as 2.5×10^{-7} Torr by (Eq. 4.7):

$$P_{Toluene} (Torr) \approx (1 \times 10^{-3}) \left(\frac{30 \text{ uL Hr}^{-1} \cdot 0.865 \text{ gmL}^{-1}}{92 \text{ gmol}^{-1}} \right) \left(\frac{1}{2.00 \text{ L min}^{-1}} \right) \left(\frac{92 \text{ gmol}^{-1}}{4.003 \text{ gmol}^{-1}} \right)^{1/2} \quad (4.7)$$

In all of the reactions performed with toluene, $[\text{Ala-H}+\text{Cu}^{2+}]^+$ was the species with the largest k_2 , so it was used to estimate the pressure of toluene in the quadrupole ion trap. This was estimated to be 5.6×10^{-8} Torr by setting $k_2=k_f$, as in Chapter 3. The reaction efficiency (Φ) was calculated using Eq. 2.2.

Experimental Findings

Silver Studies

Although not typically considered a biologically relevant metal, silver is known to play important biological roles in a variety of species. Recently, it has been suggested that silver drug complexes could be targeted to DNA molecules providing a means of specific drug delivery.¹⁸⁰ Silver may also play a role in the regulation of genetic expression,¹⁸¹ as well as participating in peptide¹⁸² and protein binding.¹⁸³⁻¹⁸⁵ Silver is an important metal in these cases, so it is important to gather information regarding the interaction of amino acids with silver.

For the most part, $[\text{A.A.}+\text{Ag}^+]$ reactions were very efficient. Not all amino acids were experimentally observed. Among those that did, not all were found to have reached equilibrium with toluene. A sample spectrum for an observed reaction is shown in Fig. 72. The reaction for $[\text{Leu}+\text{Ag}^+]$ with toluene is shown in Fig. 73.

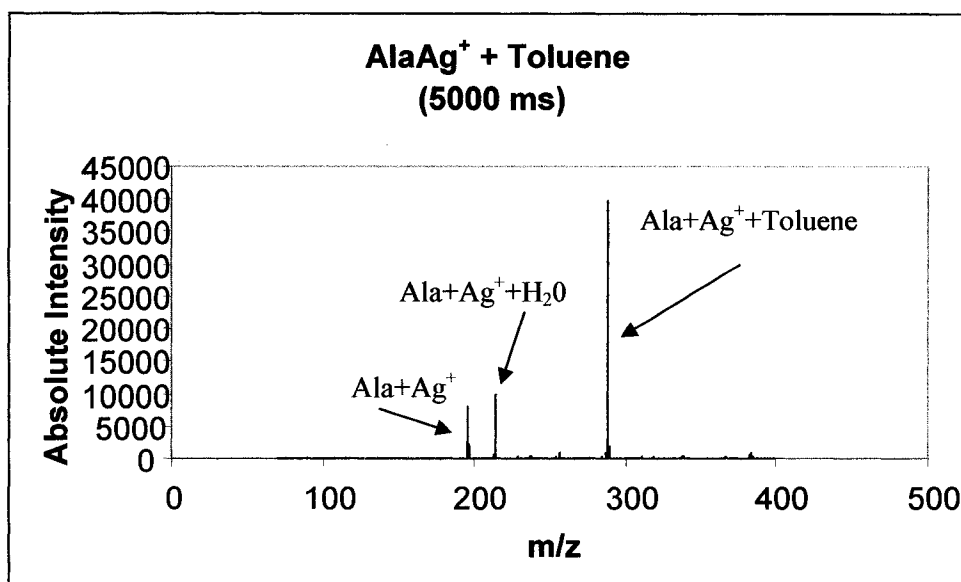


Figure 72. The reaction of [Ala+Ag⁺] with toluene with a 5000 ms scan delay. The addition of water is also observed.

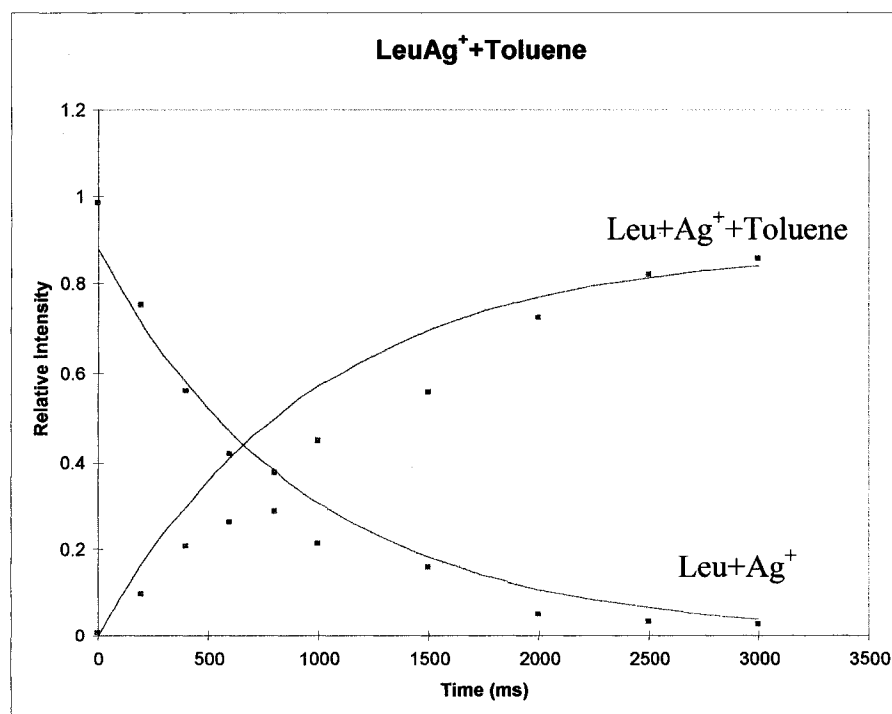


Figure 73. The reaction of [Leu+Ag⁺] with toluene. The trends lines are calculated and placed by the KinFit macro.

The KinFit program was used to determine the rate constant, k_1 , of reactions involving [A.A.+Ag⁺] complexes. The k_2 , k_f , and reaction efficiency (Φ) of these reactions are given in Table 20. The amino acids are listed in order of increasing efficiency.

Table 20

Reaction Data for Amino Acids Complexed to Silver Cations Reacting with Toluene.

Amino Acid	k_2	k_f	Φ
Met + Ag ⁺	4.8×10^{-11}	2.98×10^{-9}	1.6×10^{-2}
Ala + Ag ⁺	1.5×10^{-10}	3.10×10^{-9}	4.8×10^{-2}
Glu + Ag ⁺	1.5×10^{-10}	2.99×10^{-9}	5.0×10^{-2}
Gly + Ag ⁺	2.4×10^{-10}	3.14×10^{-9}	7.6×10^{-2}
Ser + Ag ⁺	2.7×10^{-10}	3.06×10^{-9}	9.0×10^{-2}
Thr + Ag ⁺	2.8×10^{-10}	3.04×10^{-9}	9.2×10^{-2}
Pro + Ag ⁺	3.1×10^{-10}	3.04×10^{-9}	1.0×10^{-1}
Val + Ag ⁺	3.5×10^{-10}	3.04×10^{-9}	1.2×10^{-1}
Ile + Ag ⁺	5.2×10^{-10}	3.01×10^{-9}	1.7×10^{-1}
Leu + Ag ⁺	5.3×10^{-10}	3.01×10^{-9}	1.8×10^{-1}

The data presented above is interesting because no apparent trends can be seen in the data. Although some amino acids with similar features are found to be grouped together, there is no widespread trend. For example, one would expect that amino acids with small side chains would exhibit similar reaction kinetics. It could be argued that Ala, Gly, and Val all have relatively small side chains. However, these three amino acids do not have similar reaction efficiencies and are separated in Table 19 by amino acids with larger side chains.

The lowest efficiency reaction occurred with the $[\text{Met}+\text{Ag}^+]$ species. Met has a relatively long side chain which contains a sulfur atom. Both Met and Ag^+ are considered to be soft species. This feature indicates that Met and Ag^+ are more likely to participate in covalent interactions. Since the interaction with toluene is largely noncovalent in nature, a slow reaction would likely be observed.

An interesting result of these reactions is that both Leu and Ile have nearly identical reaction kinetics and efficiencies. Both amino acids have similar R-groups, with a methyl group either on the first or second carbon of the side chain (Fig. 74). This methyl group may play an important role in binding the metal ion. The side chain of Val is one carbon shorter than that of Leu and Ile; however, it also contains a methyl group on the same carbon as Ile (Fig. 74). Val is also found to have a Φ slightly less than that of Ile.

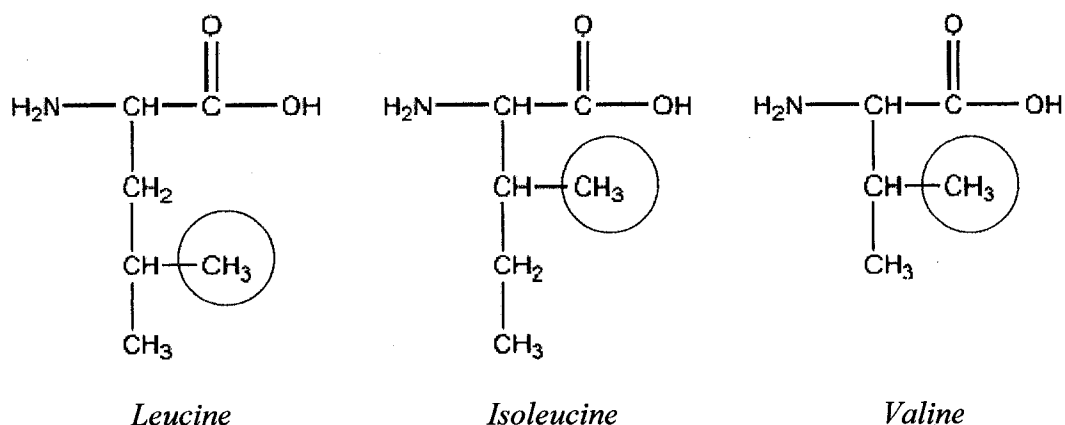


Figure 74. A structural comparison of Leu, Ile, and Val. The highlighted methyl group might be responsible for the similar reaction rate and efficiency of these amino acids when they are complexed to Ag^+ .

Additional features are contained by the remaining amino acids, which may explain their reaction efficiencies. It would be beneficial to have complementary Gaussian analysis of the [A.A.+Ag⁺+toluene] interactions to help explain the observed reaction kinetics. This information has not yet been acquired for these reactions.

Equilibrium data for these experiments were also used to calculate the binding energy of these complexes. The equilibrium constant, K_{eq} , was calculated for the reactions using Eq. 4.4. This value was then used to calculate the Gibb's free energy (ΔG) of the system (Eq. 4.5). The bond energy (ΔH) of the reaction was then calculated using Eq. 4.6. Table 21 contains these calculated values. The experimentally determined binding energies of the [A.A.+Ag⁺] complexes ranged from approximately 100-109 kJ mol⁻¹.

Table 21

Calculated Kinetic and Thermodynamic Values for Silver Reactions with Toluene.

Amino Acid	K_{eq} (atm ⁻¹)	ΔG (kJ mol ⁻¹)	ΔH (kJ mol ⁻¹)
Met + Ag ⁺	(2.50 X 10 ⁺¹⁰)	-59.7	-99.7
Ala + Ag ⁺	(6.84 X 10 ⁺¹¹)	-68.0	-108.0
Glu + Ag ⁺	(7.14 X 10 ⁺¹⁰)	-62.3	-102.3
Gly + Ag ⁺	(6.02 X 10 ⁺¹¹)	-67.7	-107.7
Ser + Ag ⁺	(4.28 X 10 ⁺¹¹)	-66.8	-106.8
Thr + Ag ⁺	(2.26 X 10 ⁺¹¹)	-65.2	-105.2
Pro + Ag ⁺	(8.34 X 10 ⁺¹¹)	-68.5	-108.5
Val + Ag ⁺	(7.30 X 10 ⁺¹¹)	-68.1	-108.1
Ile + Ag ⁺	(4.86 X 10 ⁺¹¹)	-67.1	-107.1
Leu + Ag ⁺	(4.92 X 10 ⁺¹¹)	-67.2	-107.2

Calcium Studies

Calcium plays an important biological role. Often obtained through diet, calcium is essential for the formation of strong bones and teeth, hormone control, and blood clotting, among many other things (see Table 4). A plethora of recent papers discuss the biological roles of calcium-binding proteins,¹⁸⁶⁻¹⁸⁹ including calbindin,¹⁹⁰⁻¹⁹² calmodulin,¹⁹³⁻¹⁹⁵ and parvalbumin.¹⁹⁶⁻¹⁹⁸ There is also a great interest in the function of voltage-gated calcium channels.¹⁹⁹⁻²⁰¹

A wide variety of medical disorders arise from the malfunction of calcium-protein interactions.²⁰² Unlike other disorders, these problems are often common and widespread; chronic kidney disease,²⁰³⁻²⁰⁵ hyperparathyroidism,²⁰⁶⁻²⁰⁸ osteoporosis,²⁰⁹⁻²¹¹ and rickets^{212, 213} are just a few examples. Given the vast biological importance of calcium, it is relevant to analyze the interaction of amino acids with calcium cations.

Unlike silver, calcium is a doubly charged cation. When it is complexed to the amino acid, a proton is lost, and the complex becomes singly charged. This occurs for all amino acid complexes with doubly charged cations. Reaction data was obtained for thirteen of the common amino acids. A sample mass spectrum is shown in Fig. 75, and a sample equilibrium plot is shown in Fig. 76.

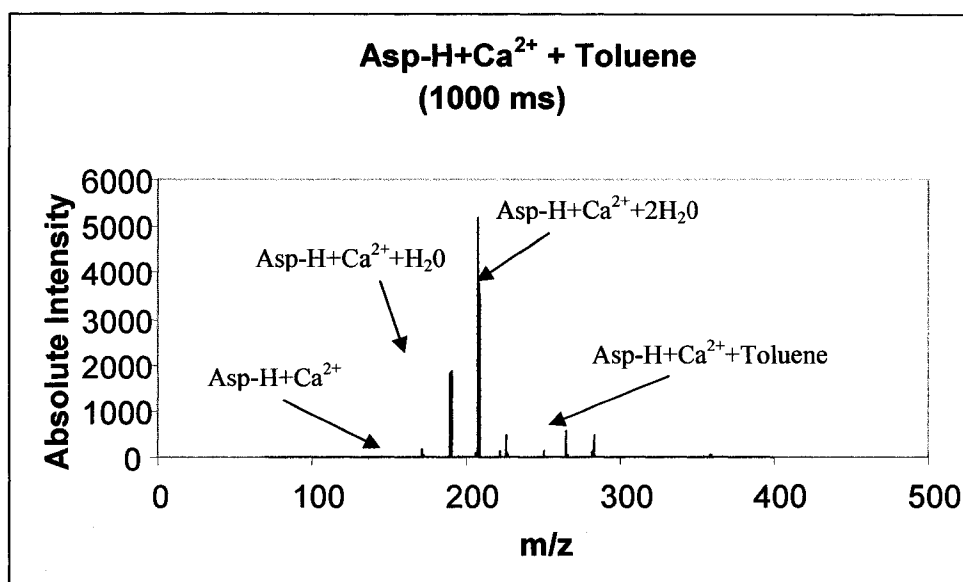


Figure 75. The reaction of $[\text{Asp-H+Ca}^{2+}]^+$ with toluene over a scan delay of 1000 ms. The addition of water molecules can be observed.

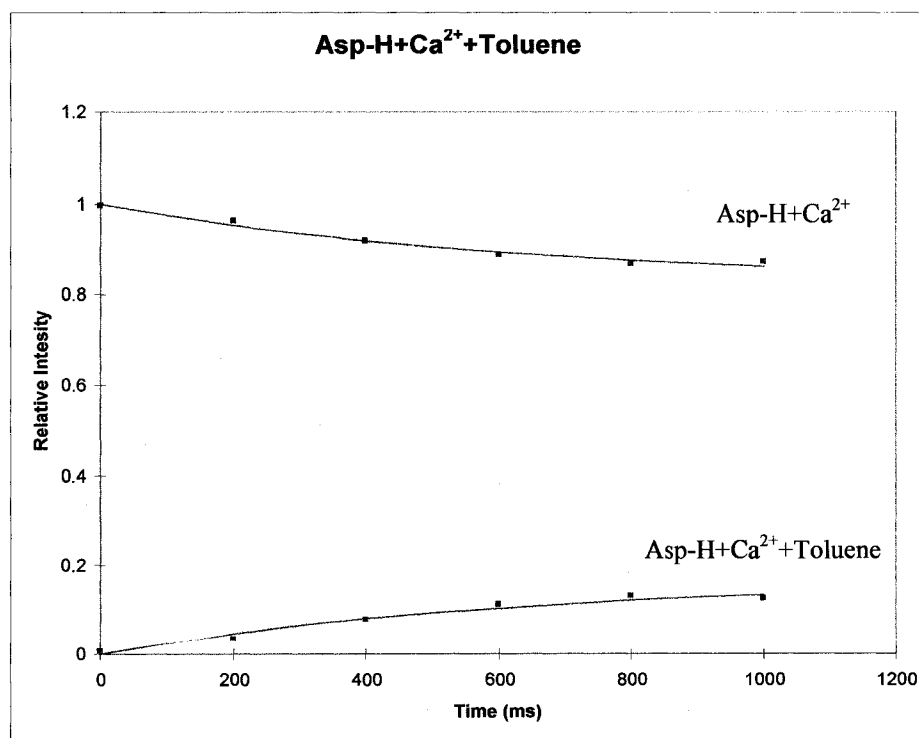


Figure 76. Reaction kinetics for $[\text{Asp-H+Ca}^{2+}]^+$ with toluene.

Table 22 provides both experimental data for $[A.A.-H+Ca^{2+}]^+$ species. The amino acids are listed in order of increasing Φ . As with the silver complexes, theoretical modeling calculations are unavailable for comparison. However, the experimental kinetics can still be analyzed for reaction trends.

Table 22

Data for Amino Acids Complexed to Calcium Reacting with Toluene.

Amino Acid	k_2	k_f	Φ
Gln-H + Ca ²⁺	1.7 X 10 ⁻¹¹	3.13 X 10 ⁻⁹	5.4 X 10 ⁻³
Asp-H + Ca ²⁺	1.9 X 10 ⁻¹¹	3.17 X 10 ⁻⁹	6.0 X 10 ⁻³
Ile-H + Ca ²⁺	7.0 X 10 ⁻¹¹	3.18 X 10 ⁻⁹	2.2 X 10 ⁻²
Thr-H + Ca ²⁺	8.0 X 10 ⁻¹¹	3.22 X 10 ⁻⁹	2.5 X 10 ⁻²
Glu-H + Ca ²⁺	8.0 X 10 ⁻¹¹	3.13 X 10 ⁻⁹	2.6 X 10 ⁻²
Val-H + Ca ²⁺	9.4 X 10 ⁻¹¹	3.22 X 10 ⁻⁹	2.9 X 10 ⁻²
Ser-H + Ca ²⁺	1.1 X 10 ⁻¹⁰	3.27 X 10 ⁻⁹	3.3 X 10 ⁻²
Gly-H + Ca ²⁺	1.2 X 10 ⁻¹⁰	3.44 X 10 ⁻⁹	3.4 X 10 ⁻²
Arg-H + Ca ²⁺	1.2 X 10 ⁻¹⁰	3.06 X 10 ⁻⁹	3.9 X 10 ⁻²
Met-H + Ca ²⁺	1.3 X 10 ⁻¹⁰	3.12 X 10 ⁻⁹	4.1 X 10 ⁻²
Lys-H + Ca ²⁺	1.3 X 10 ⁻¹⁰	3.13 X 10 ⁻⁹	4.3 X 10 ⁻²
Asn-H + Ca ²⁺	1.5 X 10 ⁻¹⁰	3.17 X 10 ⁻⁹	4.7 X 10 ⁻²
Leu-H + Ca ²⁺	3.1 X 10 ⁻¹⁰	3.18 X 10 ⁻⁹	9.7 X 10 ⁻²

The data presented in Table 22 is difficult to interpret. Both Glu and Asp were analyzed in this experiment, yet their exhibited reaction kinetics differs extremely. In fact, their reaction efficiency differs by a factor of ten. This is difficult to explain since the structure of the two differs only slightly (Fig. 77).

Since they are so similar, it would be expected that their kinetics would be similar as well.

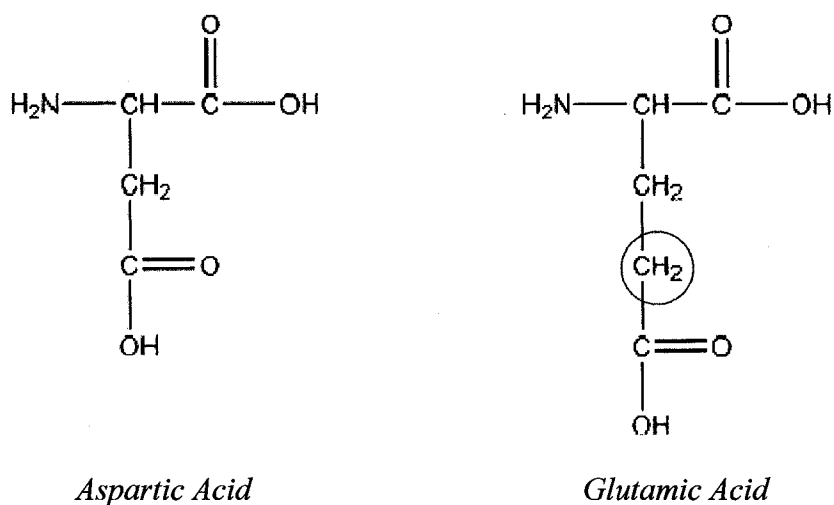


Figure 77. The structures of Asp and Glu. The only difference between the two species is highlighted.

Another interesting point is that Leu, Ile, and Val no longer exhibit similar reaction efficiencies. If their methyl group is involved in silver coordination and reactivity to toluene, it does not appear to be relevant for reactions with Ca^{2+} . It is also interesting that in these reactions, the Leu complex is again the fastest and most efficiently reacting species. Finally, it can be seen that amino acids with basic chain R-groups react with similar efficiency, as is observed for Arg and Lys. The Met complex displayed similar efficiency as well.

Thermodynamic and kinetic calculations were also performed on $[\text{A.A.}-\text{H}+\text{Ca}^{2+}]^+$ and toluene reactions. As before, K_{eq} , ΔG , and ΔH are reported in Table

23. It can be seen from these results that the experimentally determined binding energies for these reactions range from approximately 94-104 kJ mol⁻¹.

Table 23

Thermodynamic and Kinetic Data for [A.A.-H+Ca²⁺]⁺ Species Reacting with Toluene.

Amino Acid	K_{eq} (atm ⁻¹)	ΔG (kJ mol ⁻¹)	ΔH (kJ mol ⁻¹)
Gln-H + Ca ²⁺	5.14 X 10 ⁺⁹	-55.8	-96.8
Asp-H + Ca ²⁺	3.12 X 10 ⁺¹⁰	-60.3	-100.3
Ile-H + Ca ²⁺	2.28 X 10 ⁺¹⁰	-59.5	-99.5
Thr-H + Ca ²⁺	1.41 X 10 ⁺¹⁰	-58.3	-98.3
Glu-H + Ca ²⁺	2.37 X 10 ⁺¹⁰	-59.6	-99.6
Val-H + Ca ²⁺	1.22 X 10 ⁺¹⁰	-57.9	-97.9
Ser-H + Ca ²⁺	1.40 X 10 ⁺¹¹	-64.0	-104.0
Gly-H + Ca ²⁺	5.54 X 10 ⁺¹⁰	-61.7	-101.7
Arg-H + Ca ²⁺	(1.48 X 10 ⁺¹⁰)	-58.4	-98.4
Met-H + Ca ²⁺	3.25 X 10 ⁺¹⁰	-60.4	-100.4
Lys-H + Ca ²⁺	2.85 X 10 ⁺¹⁰	-60.0	-100.0
Asn-H + Ca ²⁺	3.98 X 10 ⁺¹⁰	-60.9	-100.9
Leu-H + Ca ²⁺	1.94 X 10 ⁺¹⁰	-59.1	-99.1

Cobalt Studies

Cobalt functions as an oxidase, participates in alkyl group transfer, and is contained in vitamin B₁₂. The binding of cobalt to enzymes and proteins is responsible for DNA cleavage,²¹⁴ enzyme deactivation and inhibition,^{215, 216} and other protein functions.²¹⁷⁻²¹⁹ Most often, medical disorders stemming from cobalt-metal malfunction is directly associated with vitamin B₁₂ deficiency.²²⁰⁻²²²

Experimental data was obtained for reactions of $[\text{A.A.}-\text{H}+\text{Co}^{2+}+\text{toluene}]^+$. A sample spectrum is given in Fig. 78, and a kinetics plot is shown in Fig. 79. As before, the data is summarized in Table 24.

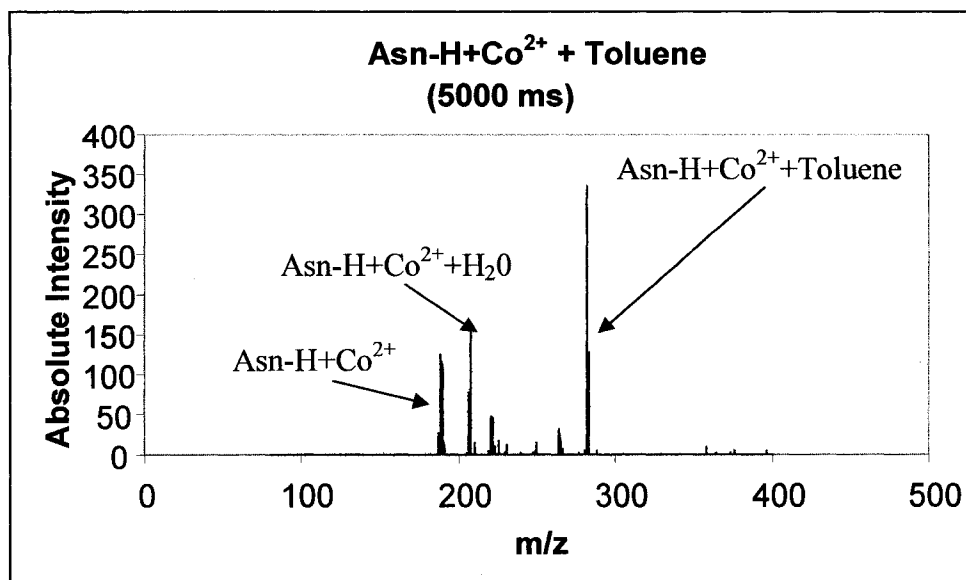


Figure 78. A sample spectrum of $[\text{Asn}-\text{H}+\text{Co}^{2+}]^+$ reacting with toluene over a 5000 ms scan delay.

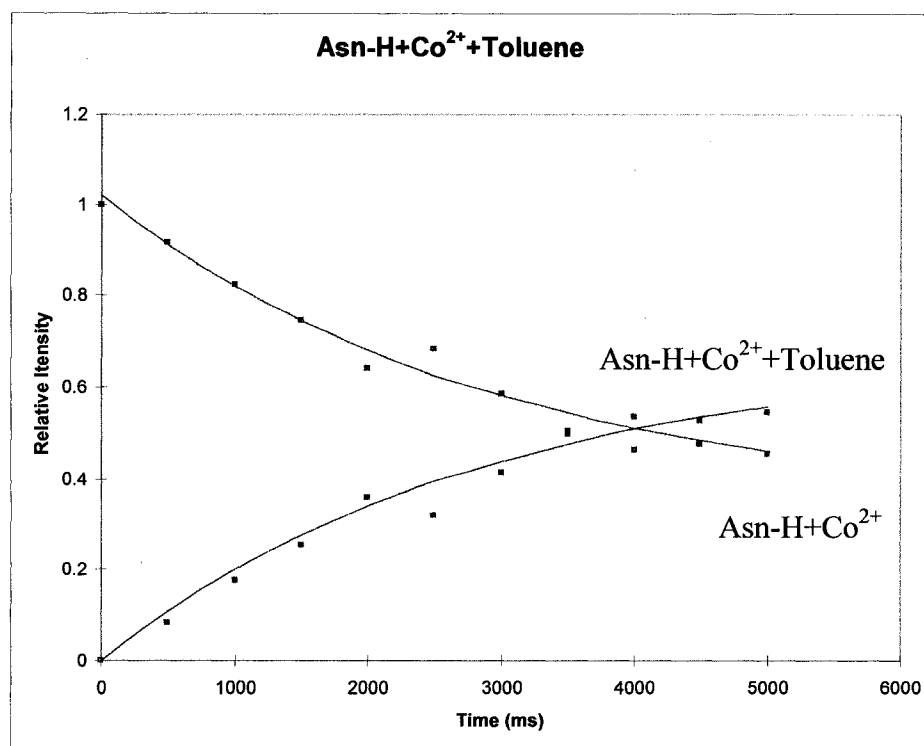


Figure 79. The kinetics plot of $[\text{Asn-H+Co}^{2+}]^+$ reacting with toluene.

Table 24

Data Obtained for Amino Acids Complexed to Cobalt Reacting with Toluene.

Amino Acid	k_2	k_f	Φ
Arg-H + Co ²⁺	1.9×10^{-11}	3.02×10^{-9}	6.2×10^{-3}
Lys-H + Co ²⁺	3.4×10^{-11}	3.08×10^{-9}	1.1×10^{-2}
Ile-H + Co ²⁺	5.8×10^{-11}	3.12×10^{-9}	1.9×10^{-2}
Thr-H + Co ²⁺	6.4×10^{-11}	3.15×10^{-9}	2.0×10^{-2}
Ser-H + Co ²⁺	7.0×10^{-11}	3.20×10^{-9}	2.2×10^{-2}
Gln-H + Co ²⁺	8.6×10^{-11}	3.08×10^{-9}	2.8×10^{-2}
Pro-H + Co ²⁺	1.0×10^{-10}	3.17×10^{-9}	3.2×10^{-2}
Cys-H + Co ²⁺	1.1×10^{-10}	3.14×10^{-9}	3.5×10^{-2}
Asn-H + Co ²⁺	1.2×10^{-10}	3.11×10^{-9}	3.7×10^{-2}
Ala-H + Co ²⁺	1.6×10^{-10}	3.26×10^{-9}	4.9×10^{-2}
Leu-H + Co ²⁺	1.9×10^{-10}	3.12×10^{-9}	6.1×10^{-2}

The most apparent trend that appears from this table is that the Leu complex is the fastest reacting species. In addition, both Arg and Lys complexes display similar results as would be expected for species with similar side chains. Both Thr and Ser have the same calculated reaction efficiency. This can be explained by the presence of a $-OH$ group on the primary carbon in their side chains (Fig. 80). Ile has similar reaction efficiency to Thr and Ser, which could also be explained by the presence of a methyl group on the primary carbon (Fig. 80). Again, theoretical results would help to explain the observed kinetics.

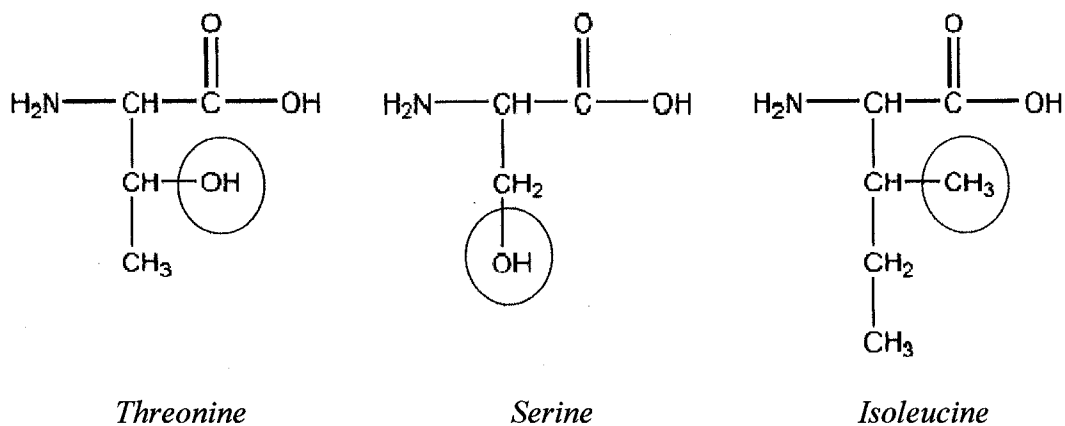


Figure 80. A comparison of Thr, Ser, and Ile. Each amino acid has a substituted group on its primary carbon. This could be responsible for their similar reaction kinetics and efficiencies.

Table 25 contains the calculated kinetic and thermodynamic data for cobalt reactions. The values were calculated as described previously. Here, the experimentally determined binding energies range from about 93-102 kJ mol^{-1} .

Table 25

Calculated Thermodynamic and Kinetic Results for Cobalt Complexes Reacting with Toluene.

Amino Acid	K_{eq} (atm^{-1})	ΔG (kJ mol^{-1})	ΔH (kJ mol^{-1})
Arg-H + Co^{2+}	$3.75 \times 10^{+9}$	-55.0	-95.0
Lys-H + Co^{2+}	$1.21 \times 10^{+10}$	-57.9	-97.9
Ile-H + Co^{2+}	$3.29 \times 10^{+9}$	-54.7	-94.7
Thr-H + Co^{2+}	$2.36 \times 10^{+10}$	-59.6	-99.6
Ser-H + Co^{2+}	$(6.99 \times 10^{+9})$	-56.5	-96.5
Gln-H + Co^{2+}	$1.61 \times 10^{+9}$	-52.9	-92.9
Pro-H + Co^{2+}	$4.81 \times 10^{+9}$	-55.6	-95.6
Cys-H + Co^{2+}	$(1.03 \times 10^{+10})$	-57.5	-97.5
Asn-H + Co^{2+}	$2.65 \times 10^{+10}$	-59.9	-99.9
Ala-H + Co^{2+}	$(6.65 \times 10^{+10})$	-62.2	-102.2
Leu-H + Co^{2+}	$1.49 \times 10^{+10}$	-58.4	-98.4

Copper Studies

Copper is a biologically relevant metal due to its role in electron transfer, dioxygen transport, and as an oxidase. Copper is coordinated by many proteins,²²³⁻²²⁷ including cytochrome oxidase,²²⁸⁻²³⁰ tyrosinase,²³¹⁻²³³ and metallothionein.²³⁴⁻²³⁶ Wilson's disease and Menke's disease are both well-known diseases caused by a malfunction in copper-protein interactions.^{4, 237-241}

For these Phe modeling experiments, the most information was obtained for reactions with $[\text{A.A.}+\text{Cu}^+]$ complexes. Both experimental and theoretical

information is available for a number of the amino acids studied. A sample spectrum and a kinetics plot are shown in Fig. 81 and Fig. 82, respectively.

Table 26 provides both the experimental and computational data. As with the previous studies, the amino acids are presented in order of increasing Φ . The stabilization energy is calculated through Gaussian, as previously described.

Appendix D shows the Gaussian structures and also contains energy and metal ion charge information.

Due to the availability of both experimental and theoretical data, it is possible to compare the reaction efficiency to the stabilization energy of the reactions. The species are listed in order of increasing reaction efficiency. It can be seen that as the reaction efficiency increases, so does the stabilization energy of the association reaction. This is expected since the most stable system (with the lowest energy and greatest stabilization energy) is more likely to form than higher energy species.

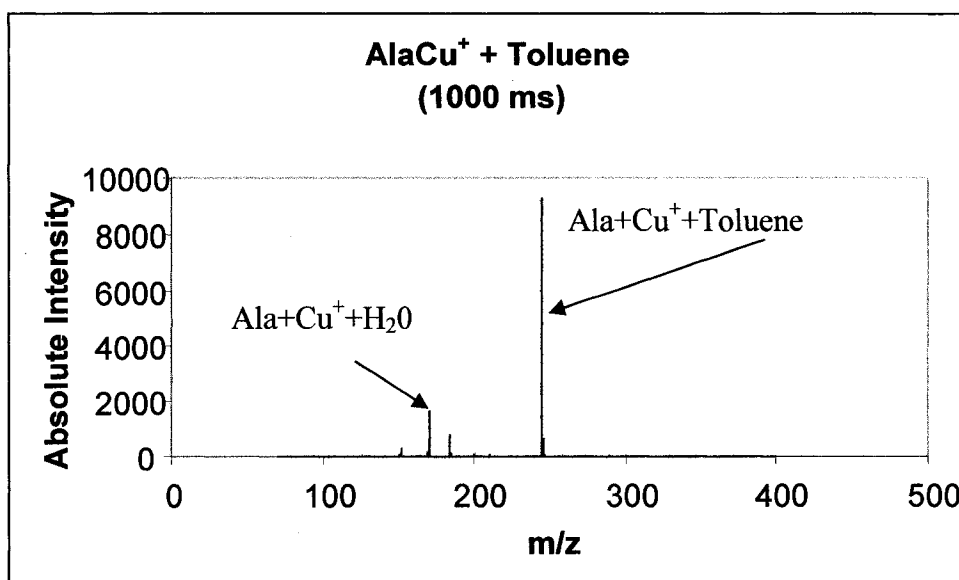


Figure 81. The reaction of [Ala+Cu⁺] with toluene over a 1000 ms scan delay. As before, an addition of water is observed.

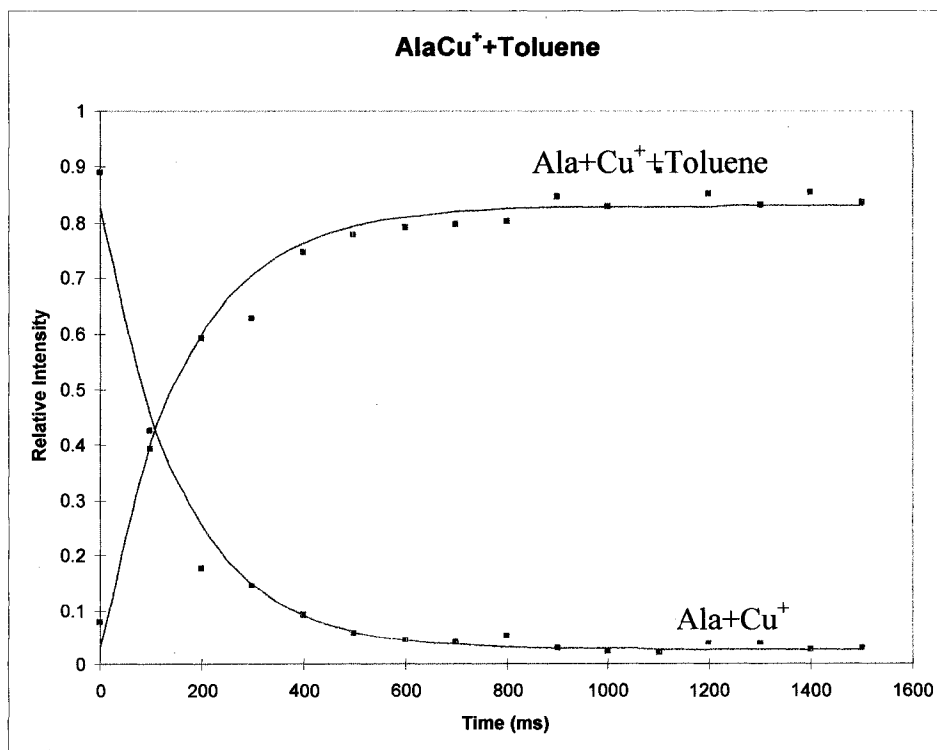


Figure 82. The kinetics of [Ala+Cu⁺] reacting with toluene.

Table 26

Experimental and Theoretical Results for Reactions of Amino Acids Complexed to Copper Reacting with Toluene.

Amino Acid	k_2	k_f	Φ	Stabilization Energy (kJ/mole)
Ser + Cu ⁺	6.1 X 10 ⁻¹¹	3.18 X 10 ⁻⁹	1.9 X 10 ⁻²	E = 150.1
Val + Cu ⁺	6.4 X 10 ⁻¹¹	3.14 X 10 ⁻⁹	2.0 X 10 ⁻²	--
Thr + Cu ⁺	7.6 X 10 ⁻¹¹	3.14 X 10 ⁻⁹	2.4 X 10 ⁻²	--
Met + Cu ⁺	8.4 X 10 ⁻¹¹	3.06 X 10 ⁻⁹	2.8 X 10 ⁻²	E = 157.2
Asn + Cu ⁺	2.1 X 10 ⁻¹⁰	3.10 X 10 ⁻⁹	6.8 X 10 ⁻²	--
Gly + Cu ⁺	2.5 X 10 ⁻¹⁰	3.30 X 10 ⁻⁹	7.5 X 10 ⁻²	E = 182.2
Asp + Cu ⁺	2.8 X 10 ⁻¹⁰	3.10 X 10 ⁻⁹	9.1 X 10 ⁻²	E = 191.0
Ala + Cu ⁺	3.0 X 10 ⁻⁹	3.04 X 10 ⁻⁹	1	--

-- indicates that Gaussian data is unavailable

In fact, there is a linear relationship between the experimental reaction efficiency and the theoretical stabilization energy. A plot of the two values is shown in Fig. 83. Although data is only available for four data sets, a linear regression analysis shows fairly good agreement, as indicated by the R² value of 0.9981. This is an important indication that these association reactions are providing reasonable and useful results.

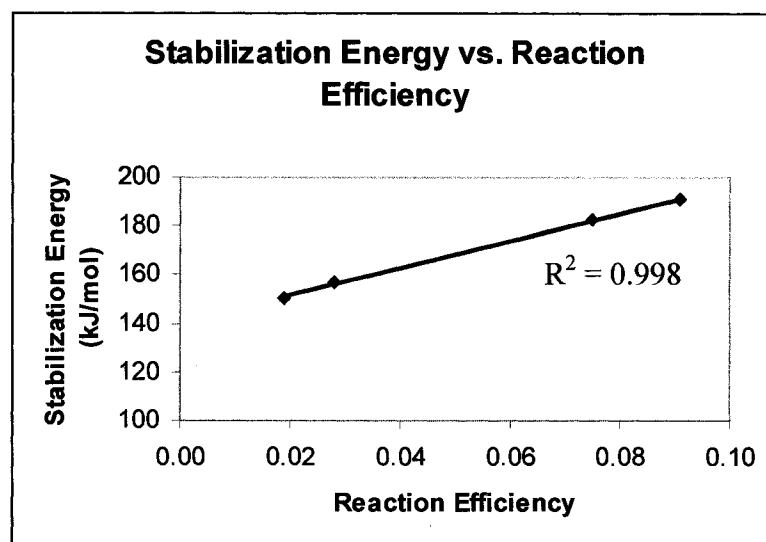


Figure 83. The linear correlation between stabilization energy and reaction efficiency. This data is shown for [A.A.+Cu⁺+toluene] complexes.

Experimental information was not obtained for [Pro+Cu⁺]; however, theoretical calculations indicate that the stabilization energy for the [Pro+Cu⁺+toluene] species is much less than the [Ser+Cu⁺+toluene] species. The stabilization energy for this complex was calculated to be 147.7 kJ mol⁻¹. [Pro+Cu⁺] was not observed to react with toluene during the course of these experiments. This indicates that the reaction efficiency was very low. Besides confirming observed trends, theoretical calculations may also be useful for predicting experimental kinetic observations.

As with the previous experiments, thermochemical and kinetic data were obtained from the experimental data. These values are shown in Table 27. For experiments with [A.A.+Cu⁺] complexes reacting with toluene, the experimentally

determine binding energy was determined to be between approximately 96 and 107 kJ mol⁻¹.

Table 27

Kinetic and Thermochemical Data for Copper Complexes Reacting with Toluene.

Amino Acid	K_{eq} (atm⁻¹)	ΔG (kJ mol⁻¹)	ΔH (kJ mol⁻¹)
Ser + Cu ⁺	(2.91 X10 ⁺¹⁰)	-60.1	-100.1
Val + Cu ⁺	(4.18 X10 ⁺¹⁰)	-61.0	-101.0
Thr + Cu ⁺	(2.89 X10 ⁺¹⁰)	-60.1	-100.1
Met + Cu ⁺	4.53 X10 ⁺¹¹	-66.9	-107.0
Asn + Cu ⁺	6.63 X10 ⁺⁹	-56.4	-96.4
Gly + Cu ⁺	2.18 X10 ⁺¹⁰	-59.3	-99.4
Asp + Cu ⁺	6.00 X10 ⁺¹⁰	-61.9	-101.9
Ala + Cu ⁺	4.31 X10 ⁺¹¹	-66.8	-106.8

Iron Studies

Iron is a well-known metal ion component of proteins. It has biological functions similar to copper. Iron has been found in a large number of proteins, including ferritin,²⁴²⁻²⁴⁴ nitrogenase,²⁴⁵⁻²⁴⁷ peroxidase,²⁴⁸ and hemoglobin.²⁴⁹⁻²⁵¹ Iron deficiency can cause anemia,²⁵²⁻²⁵⁴ excess iron can cause hemochromatosis.²⁵⁵⁻²⁵⁷ As before, iron was complexed with the amino acids, and experimental data was obtained via ion-molecule reactions. A sample spectrum is shown in Fig. 84 and a kinetics plot is shown in Fig. 85. The results are summarized in Table 27.

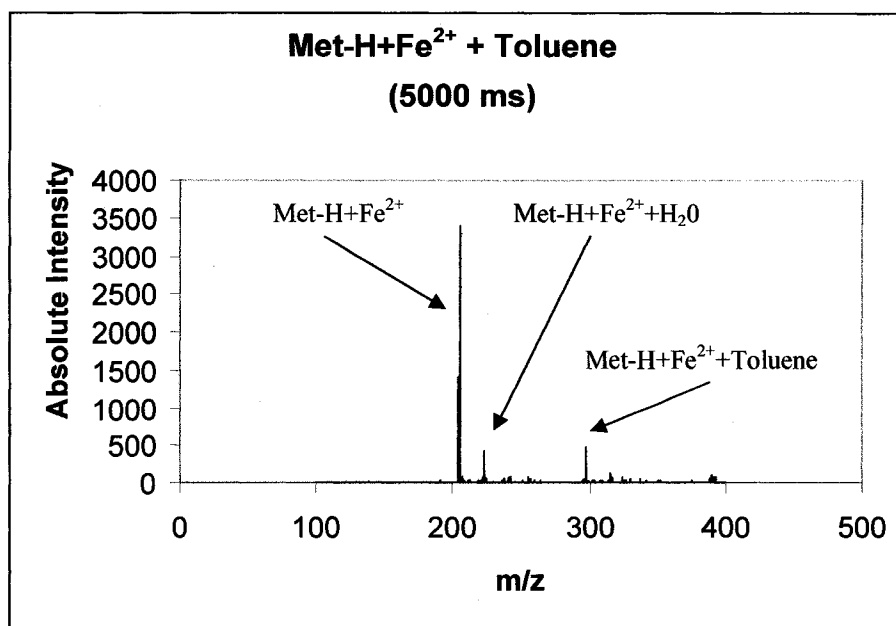


Figure 84. [Met-H+Fe²⁺]⁺ reacting with toluene over a 5000 ms scan delay.

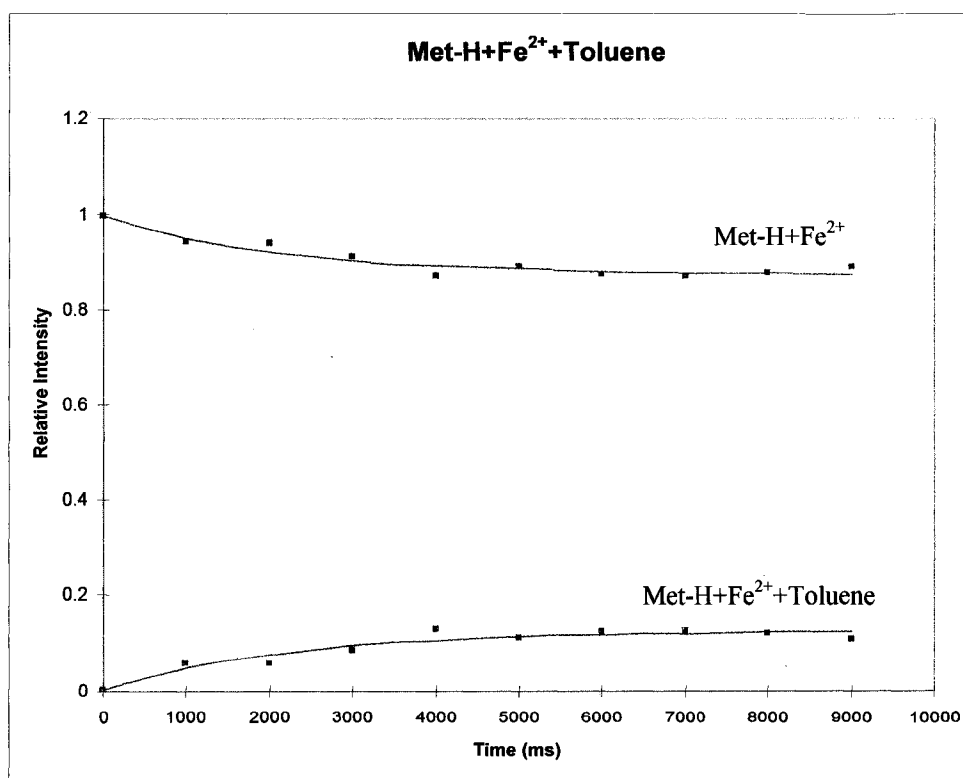


Figure 85. A kinetics plot for [Met-H+Fe²⁺]⁺ reacting with toluene.

The results in Table 28, as with the other experiments, have no readily apparent trends. As before, the amino acids with similar R-groups do not have similar reaction efficiencies. Thr is the fastest reacting species of the group. Both Ser and Pro have similar reactivities to Thr, so it appears that there is a favorable feature that all three amino acids contain.

Table 28

Experimental Results for Amino Acids Complexed with Iron Reacting with Toluene.

Amino Acid	k_2	k_f	Φ
Cys-H + Fe ²⁺	5.6 X 10 ⁻¹²	3.15 X 10 ⁻⁹	1.0 X 10 ⁻²
Lys-H + Fe ²⁺	1.7 X 10 ⁻¹¹	3.09 X 10 ⁻⁹	3.1 X 10 ⁻²
Leu-H + Fe ²⁺	2.4 X 10 ⁻¹¹	3.12 X 10 ⁻⁹	4.4 X 10 ⁻²
Met-H + Fe ²⁺	2.9 X 10 ⁻¹¹	3.08 X 10 ⁻⁹	5.4 X 10 ⁻²
Gln-H + Fe ²⁺	3.2 X 10 ⁻¹¹	3.09 X 10 ⁻⁹	5.9 X 10 ⁻²
Ile-H + Fe ²⁺	3.3 X 10 ⁻¹¹	3.12 X 10 ⁻⁹	6.1 X 10 ⁻²
Ala-H + Fe ²⁺	4.4 X 10 ⁻¹¹	3.27 X 10 ⁻⁹	7.6 X 10 ⁻²
Val-H + Fe ²⁺	6.4 X 10 ⁻¹¹	3.17 X 10 ⁻⁹	1.2 X 10 ⁻¹
Glu-H + Fe ²⁺	8.5 X 10 ⁻¹¹	3.08 X 10 ⁻⁹	1.6 X 10 ⁻¹
Ser-H + Fe ²⁺	1.4 X 10 ⁻¹⁰	3.21 X 10 ⁻⁹	2.5 X 10 ⁻¹
Pro-H + Fe ²⁺	1.4 X 10 ⁻¹⁰	3.17 X 10 ⁻⁹	2.5 X 10 ⁻¹
Thr-H + Fe ²⁺	1.5 X 10 ⁻¹⁰	3.16 X 10 ⁻⁹	2.7 X 10 ⁻¹

As previously detailed, Ser and Thr both have -OH groups attached to the primary carbon of the side chain. Pro differs from all amino acids because it does not have a typical side chain; the R-group of Pro is cyclic on the α -carbon. Pro may react with the same efficiency of Ser due to the positioning of the nitrogen atom of

the R-group. It is possible that the nitrogen is oriented toward iron in such a way that its interaction is similar to that of hydroxide group (Fig. 86).

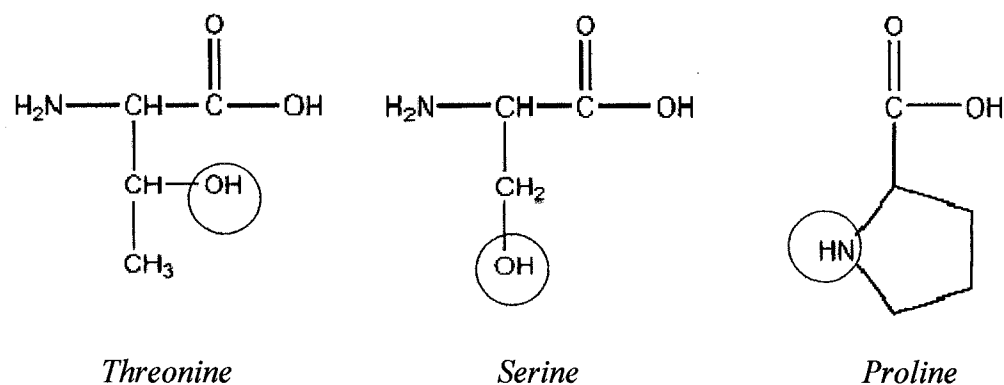


Figure 86. A comparison of Thr, Ser, and Pro.

Ile, Ala, and Val are also positioned near each other in the table. All three of these amino acids have side chain methyl groups available to complex the metal ion (Fig. 87). These methyl groups are all positioned on or near the α -carbon of the amino acid. The position of the methyl group on the side chain appears to be important since Leu also has a side chain methyl group, but it does not react with similar reaction efficiency.

Kinetic and thermodynamic data are presented in Table 29. These values were calculated using the same method as previously described. In these experiments, the binding energy generally ranged from approximately 89 to 100 kJ mol⁻¹. However, [Ser-H+Fe²⁺]⁺ differed from the eleven other amino acids. Its binding energy was calculated to be approximately 120 kJ mol⁻¹, which is substantially different for other observed binding energies.

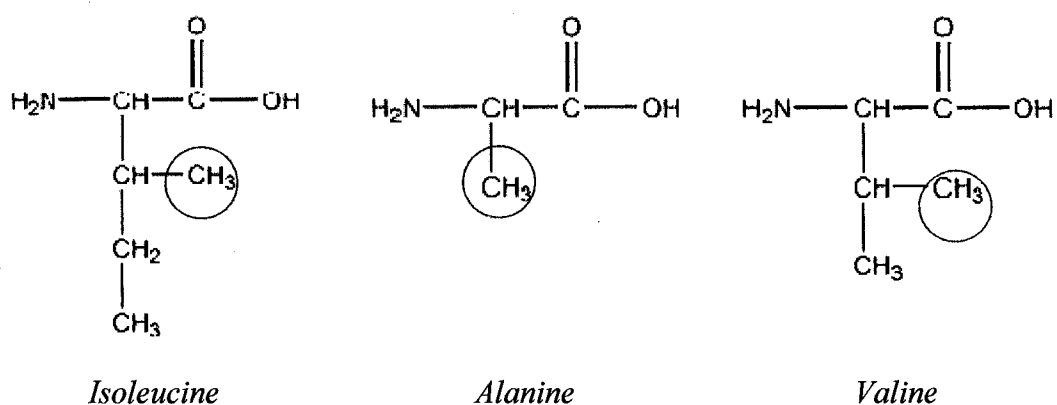


Figure 87. A comparison of Ile, Ala, and Val.

Table 29

Kinetic and Thermodynamic Data for Iron Complex Reactions with Toluene.

Amino Acid	K_{eq} (atm^{-1})	ΔG (kJ mol^{-1})	ΔH (kJ mol^{-1})
Cys-H + Fe^{2+}	$(2.98 \times 10^{+8})$	-48.7	-88.7
Lys-H + Fe^{2+}	$5.87 \times 10^{+8}$	-50.4	-90.4
Leu-H + Fe^{2+}	$2.05 \times 10^{+9}$	-53.5	-93.5
Met-H + Fe^{2+}	$1.94 \times 10^{+9}$	-53.3	-93.3
Gln-H + Fe^{2+}	$8.55 \times 10^{+8}$	-51.3	-91.3
Ile-H + Fe^{2+}	$1.68 \times 10^{+9}$	-53.0	-93.0
Ala-H + Fe^{2+}	$3.71 \times 10^{+9}$	-55.0	-95.0
Val-H + Fe^{2+}	$2.72 \times 10^{+10}$	-60.0	-99.9
Glu-H + Fe^{2+}	$2.05 \times 10^{+9}$	-53.5	-93.5
Ser-H + Fe^{2+}	$8.73 \times 10^{+13}$	-80.1	-120.1
Pro-H + Fe^{2+}	$1.80 \times 10^{+10}$	-58.9	-98.9
Thr-H + Fe^{2+}	$(1.71 \times 10^{+10})$	-58.8	-98.8

In situations like these, where trends do not readily appear, theoretical modeling calculations would be useful. Similar *in silico* modeling experiments

could be performed on iron complexes. Stabilization energies and reaction efficiencies could then be compared to identify kinetic and thermodynamic trends.

Nickel Studies

Nickel is thought to play a role in membrane conformation and is found in the protein urease.²⁵⁸⁻²⁶⁰ Nickel is often used as a therapeutic agent for certain medical treatments. Experimental data was obtained for twelve amino acids complexed to nickel. A sample spectrum and a kinetics plot are shown in Fig. 88 and Fig. 89, respectively. The results are presented in Table 30.

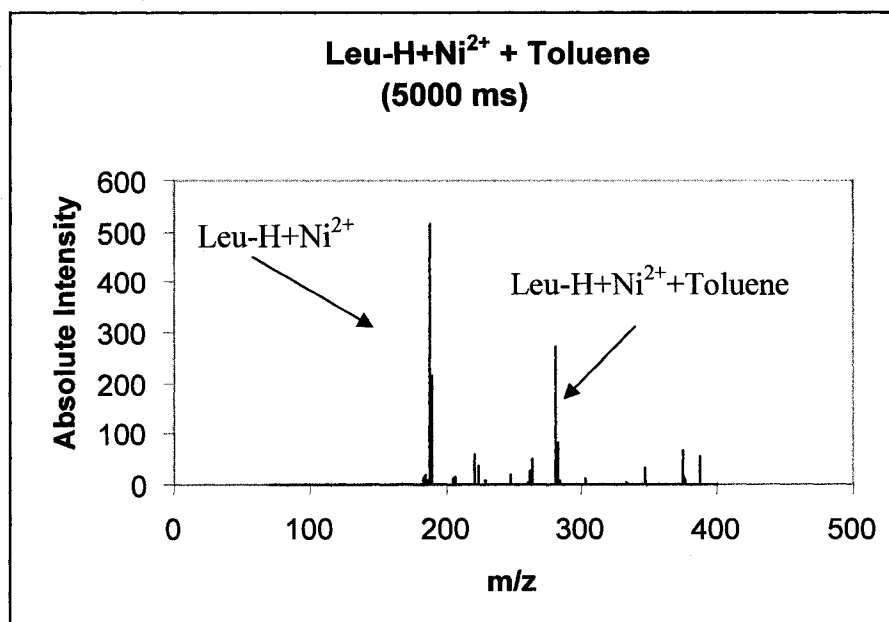


Figure 88. A spectrum of $[\text{Leu-H+Ni}^{2+}]^+$ reacting with toluene over a scan delay period of 5000 ms.

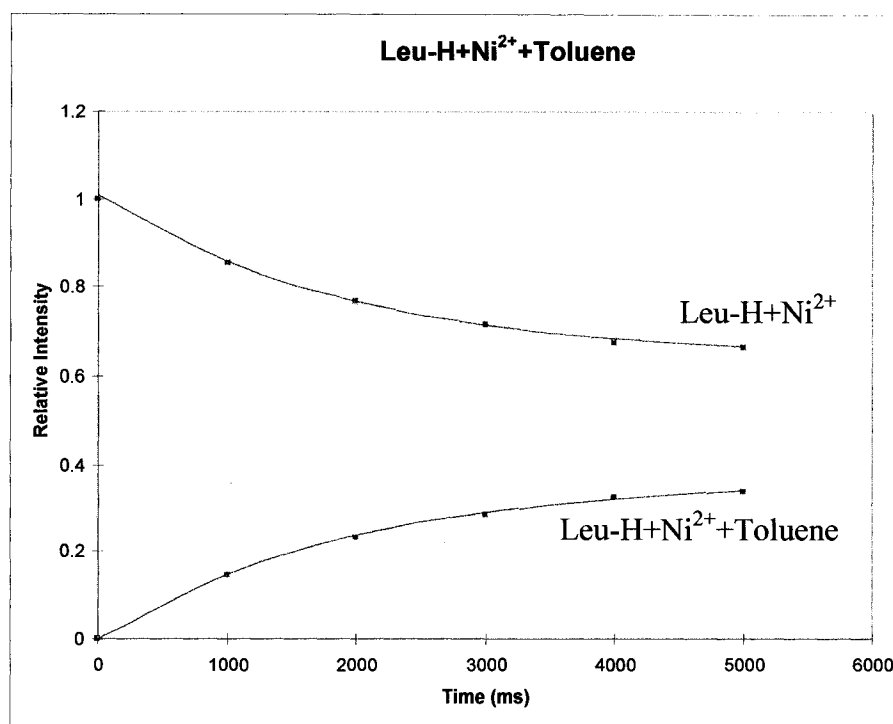


Figure 89. The kinetics of $[\text{Leu-H+Ni}^{2+}]^+$ reacting with toluene.

Table 30

Experimental Results for Amino Acids Complexed with Nickel Reacting with Toluene.

Amino Acid	k_2	k_f	Φ
Val-H+ Ni ²⁺	1.1×10^{-11}	3.16×10^{-9}	3.5×10^{-3}
Asn-H+ Ni ²⁺	1.6×10^{-11}	3.12×10^{-9}	5.2×10^{-3}
Pro-H+ Ni ²⁺	4.3×10^{-11}	3.17×10^{-9}	1.4×10^{-2}
Gln-H+ Ni ²⁺	5.4×10^{-11}	3.08×10^{-9}	1.7×10^{-2}
Leu-H+ Ni ²⁺	9.5×10^{-11}	3.12×10^{-9}	3.1×10^{-2}
Ser-H+ Ni ²⁺	1.2×10^{-10}	3.20×10^{-9}	3.8×10^{-2}
Thr-H+ Ni ²⁺	1.2×10^{-10}	3.15×10^{-9}	3.9×10^{-2}
Asp-H+ Ni ²⁺	1.6×10^{-10}	3.11×10^{-9}	5.2×10^{-2}
Glu-H+ Ni ²⁺	2.0×10^{-10}	3.08×10^{-9}	6.6×10^{-2}
Cys-H+ Ni ²⁺	2.2×10^{-10}	3.15×10^{-9}	6.9×10^{-2}
Ala-H+ Ni ²⁺	2.5×10^{-10}	3.26×10^{-9}	7.7×10^{-2}
Gly-H+ Ni ²⁺	3.7×10^{-10}	3.33×10^{-9}	1.1×10^{-1}

The two fastest reacting amino acids are the simplest amino acids: Gly and Ala. The R-groups for these amino acids are a hydrogen atom and a methyl group, respectively. A quick survey of the results in Table 30 shows that there are two sets of amino acids which behave similarly in these experiments: Ser and Thr and Glu and Cys. It has been previously observed that Ser and Thr have similar reaction rates and efficiencies. Again, this is likely due to similar features in their side chains.

The observation that Glu and Cys have very similar reaction efficiencies is interesting because the two amino acids do not have similar features. Cys has a relatively short side chain that contains a sulfur atom. Glu has a medium-length side chain with two oxygen atoms attached to the terminal carbon. Since Asp has a similar structure to Glu, it would be expected that the reaction efficiencies of Asp and Glu would be more similar. It can be seen, however, that the two amino acids are next to each other in order of increasing reaction efficiency. In addition, Cys and Ser have similar side chains, yet they are dissimilar in reaction efficiency.

Thermodynamic and kinetic data are presented for $[A.A.-H+Ni^{2+}]^+$ complexes reacting with toluene (Table 31). As with the other experiments, the calculated K_{eq} , ΔG , and ΔH for each species are reported. For these $[A.A.-H+Ni^{2+}]^+$ complexes, the experimental binding energy was determined to range from approximately 92-101 kJ mol⁻¹.

Table 31

Calculated Kinetic and Thermodynamic Values for [A.A.-H+Ni²⁺]⁺ Complexes Reacting with Toluene.

Amino Acid	K_{eq} (atm ⁻¹)	ΔG (kJ mol ⁻¹)	ΔH (kJ mol ⁻¹)
Val-H+ Ni ²⁺	1.32 X 10 ⁺⁹	-52.4	-92.4
Asn-H+ Ni ²⁺	2.91 X 10 ⁺⁹	-54.4	-94.4
Pro-H+ Ni ²⁺	6.58 X 10 ⁺⁹	-56.4	-96.4
Gln-H+ Ni ²⁺	1.38 X 10 ⁺⁹	-52.5	-92.5
Leu-H+ Ni ²⁺	7.86 X 10 ⁺⁹	-56.8	-96.8
Ser-H+ Ni ²⁺	(9.76 X 10 ⁺⁹)	-57.4	-97.4
Thr-H+ Ni ²⁺	(7.54 X 10 ⁺⁹)	-56.7	-96.7
Asp-H+ Ni ²⁺	2.72 X 10 ⁺⁹	-54.2	-94.2
Glu-H+ Ni ²⁺	1.52 X 10 ⁺⁹	-52.7	-92.7
Cys-H+ Ni ²⁺	2.62 X 10 ⁺¹⁰	-59.8	-99.8
Ala-H+ Ni ²⁺	3.46 X 10 ⁺¹⁰	-60.5	-100.5
Gly-H+ Ni ²⁺	(1.34 X 10 ⁺¹⁰)	-58.2	-98.2

Zinc Studies

Zinc was the final metal ion used in the study. As with the other metals in the study, zinc plays a large role in biochemical functions. Zinc is largely associated with the structural role it plays in proteins; the zinc finger domain is a common feature of many proteins (see Chapter 1). Some known zinc-containing proteins are carbonic anhydrase,²⁶¹⁻²⁶⁴ DNA polymerase,²⁶⁵⁻²⁶⁷ and alcohol dehydrogenase.²⁶⁸ A sample spectrum is shown in Fig. 90 and a sample kinetics plot is shown in Fig. 91. Data for ion-molecule reactions of [A.A.-H+Zn²⁺]⁺ with toluene is found in Table 32.

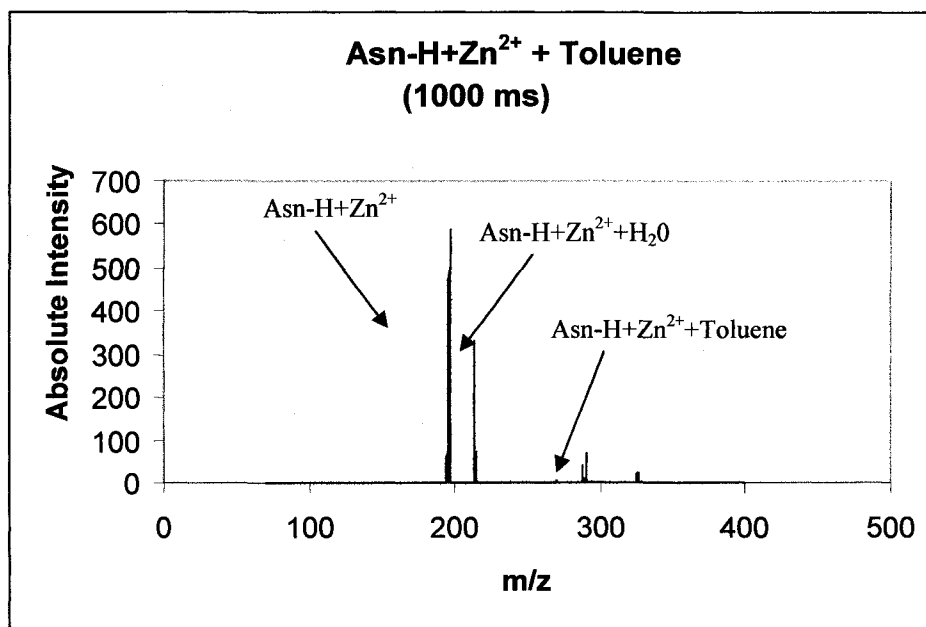


Figure 90. [Asn-H+Zn²⁺]⁺ reacting with toluene over a scan delay period of 1000 ms.

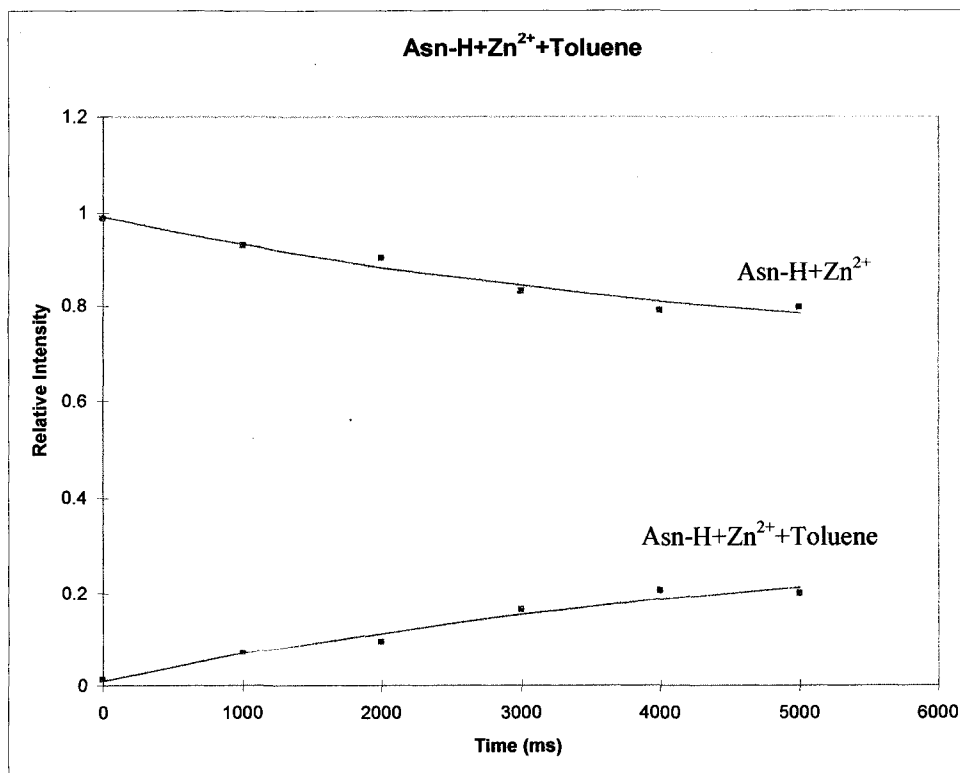


Figure 91. The kinetics of [Asn-H+Zn²⁺]⁺ reacting with toluene.

Table 32

Reaction Data for Amino Acid Complexes with Zinc Reacting with Toluene.

Amino Acid	k_2	k_f	Φ
Gly-H + Zn ²⁺	6.1 X 10 ⁻¹²	3.30 X 10 ⁻⁹	1.9 X 10 ⁻³
Glu-H + Zn ²⁺	9.0 X 10 ⁻¹²	3.06 X 10 ⁻⁹	2.9 X 10 ⁻³
Gln-H + Zn ²⁺	1.4 X 10 ⁻¹¹	3.07 X 10 ⁻⁹	4.7 X 10 ⁻³
Arg-H + Zn ²⁺	1.7 X 10 ⁻¹¹	3.01 X 10 ⁻⁹	5.7 X 10 ⁻³
Met-H + Zn ²⁺	2.9 X 10 ⁻¹¹	3.06 X 10 ⁻⁹	9.5 X 10 ⁻³
Asn-H + Zn ²⁺	3.4 X 10 ⁻¹¹	3.10 X 10 ⁻⁹	1.1 X 10 ⁻²
Thr-H + Zn ²⁺	3.7 X 10 ⁻¹¹	3.14 X 10 ⁻⁹	1.2 X 10 ⁻²
Pro-H + Zn ²⁺	3.9 X 10 ⁻¹¹	3.15 X 10 ⁻⁹	1.2 X 10 ⁻²
Leu-H + Zn ²⁺	5.5 X 10 ⁻¹¹	3.10 X 10 ⁻⁹	1.8 X 10 ⁻²
Cys-H + Zn ²⁺	7.4 X 10 ⁻¹¹	3.13 X 10 ⁻⁹	2.4 X 10 ⁻²
Asp-H + Zn ²⁺	2.1 X 10 ⁻¹⁰	3.10 X 10 ⁻⁹	6.7 X 10 ⁻²

The fastest reacting zinc species was Asp; the slowest reacting species was Gly. As with other reactions with different metals, structural aspects of the amino acids do not appear to be responsible for the observed kinetics. Again, theoretical calculations would help to identify factors that affect the reaction efficiency.

Table 33 contains the thermodynamic and kinetic data for these reactions. It was found that the experimental binding energies for these [A.A.-H+Zn²⁺]⁺ reactions were between 89 and 97 kJ mol⁻¹. These values are among the lowest binding energies observed in these toluene experiments.

Table 33

Thermodynamic and Kinetic Data for Reactions with Zinc and Toluene.

Amino Acid	K_{eq} (atm ⁻¹)	ΔG (kJ mol ⁻¹)	ΔH (kJ mol ⁻¹)
Gly-H + Zn ²⁺	(1.94 X 10 ⁺⁹)	-53.3	-93.3
Glu-H + Zn ²⁺	2.58 X 10 ⁺⁹	-54.1	-94.1
Gln-H + Zn ²⁺	1.96 X 10 ⁺⁹	-53.4	-93.4
Arg-H + Zn ²⁺	3.42 X 10 ⁺⁸	-49.0	-89.0
Met-H + Zn ²⁺	(6.20 X 10 ⁺⁹)	-56.2	-96.2
Asn-H + Zn ²⁺	6.57 X 10 ⁺⁹	-56.4	-96.4
Thr-H + Zn ²⁺	8.49 X 10 ⁺⁹	-57.0	-97.0
Pro-H + Zn ²⁺	1.40 X 10 ⁺⁹	-52.5	-92.5
Leu-H + Zn ²⁺	3.72 X 10 ⁺⁹	-55.0	-95.0
Cys-H + Zn ²⁺	(4.25 X 10 ⁺⁹)	-55.3	-95.3
Asp-H + Zn ²⁺	8.88 X 10 ⁺⁹	-57.1	-97.1

Summary

Figure 92 shows a graphical representation of the reaction efficiency data presented here. It can be readily seen that there is significant variation between the reaction efficiencies of the amino acids. None of the amino acids tested showed predictable trends. Amino acids with similar reaction efficiencies with one metal ion reacted with different reaction efficiencies when complexed to another metal ion. In addition, the choice of metal ion altered the reaction trend of individual amino acids. For instance, [Gly-H+Ni²⁺]⁺ was the fastest reacting species of the [Gly-H+Ni²⁺+toluene]⁺ species, yet the slowest reacting species of the zinc studies

was $[\text{Gly-H}+\text{Zn}^{2+}]^+$. Additionally, it can be seen that the fastest reacting species by far was $[\text{Ala}+\text{Cu}^+]$.

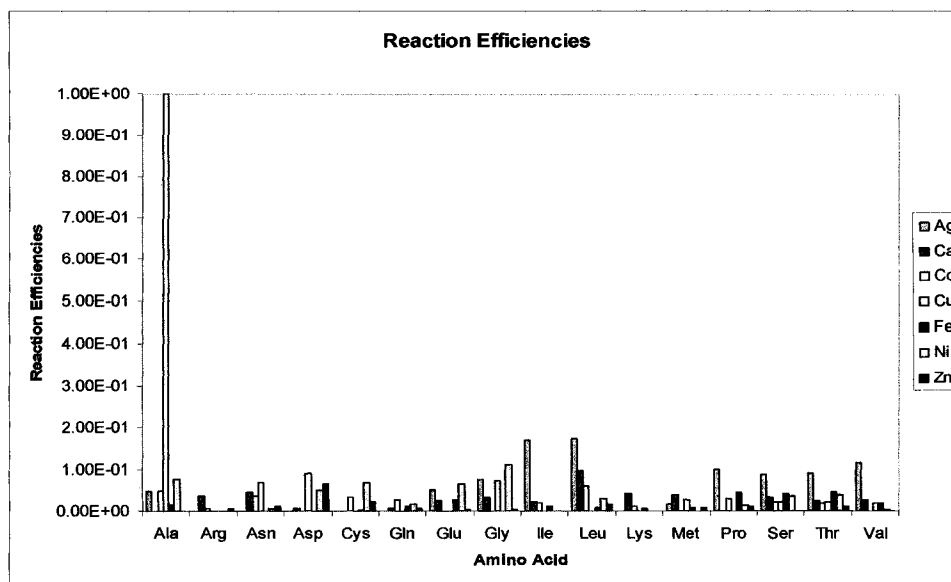


Figure 92. The reaction efficiencies of the amino acids.

Although these experiments are difficult to interpret, it is advantageous that theoretical modeling calculations can be correlated with experimental results.

Although experimental and theoretical data were only available for $[\text{A.A.}+\text{Cu}^++\text{toluene}]$ complexes, the linear correlation between the reaction efficiency and stabilization energy was obvious. Additional sets of data like that of Cu reactions will likely identify similar trends with other metal complexes.

Tyrosine Modeling

The aromatic side chain of Tyr can be modeled using methylanisole.

Methylanisole (MA) is a more complicated aromatic than benzene or toluene because it contains both a methyl group and a methyl phenyl ether group which are bonded in a paradistribution. The addition of these groups further disturbs the π -system of the benzene ring. MA has a boiling point of 174 °C, a vapor pressure of 5.25 mmHg (at 20 °C), and a density of 0.969g/mL (at 25 °C). It has an estimated polarizability of 14.10 \AA^3 .¹⁶⁰ The structure of methylanisole is shown in Fig. 93.

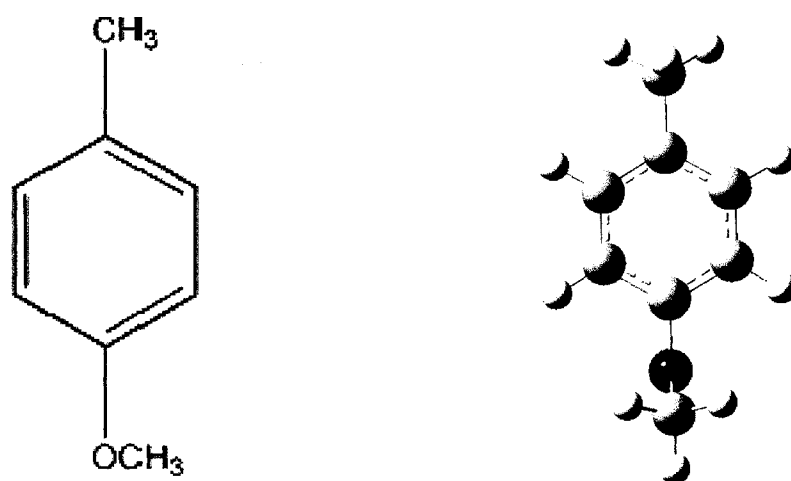


Figure 93. Methylanisole. The figure on the left is the structure. The figure on the right is Gaussian optimized.

Ion-Molecule Reactions

Tyrosine modeling reactions using MA as the neutral were performed as described previously in Chapter 2. As with toluene experiments, the KinFit macro for Excel was used to determine the experimental rate constant, k_I , for these reactions.

It was necessary to determine the pressure of MA in the quadrupole ion trap in order to calculate the reaction efficiencies of the various [A.A.+M⁺] species. The estimated pressure of MA in the quadrupole ion trap was calculated as 2.5×10^{-7} Torr using Gronert's method (Eq. 4.8):

$$P_{Toluene} (\text{Torr}) \approx (1 \times 10^{-3}) \left(\frac{30 \text{ uL Hr}^{-1} \cdot 0.969 \text{ gmL}^{-1}}{122 \text{ gmol}^{-1}} \right) \left(\frac{1}{2.00 \text{ L min}^{-1}} \right) \left(\frac{122 \text{ gmol}^{-1}}{4.003 \text{ gmol}^{-1}} \right)^{1/2} \quad (4.8)$$

As with the toluene experiments, the [A.A.+M⁺] species that reacted with the largest k_I was [Ala+Cu⁺]. Like before, k_2 was set equal to k_f , and the pressure of MA in the ion trap was then estimated to be approximately 8.8×10^{-8} Torr. [A.A.+Ag⁺] and [A.A.+Cu⁺] complexes were formed, and association reactions with MA were analyzed.

Silver Studies

Ion-molecule reactions of [A.A.+Ag⁺] with MA were performed. A sample spectrum is shown in Fig. 94, and a kinetics plots is shown in Fig. 95. The kinetic

rate constants and reaction efficiencies are reported in Table 34. As with previous experiments, the amino acids are listed in order of increasing Φ .

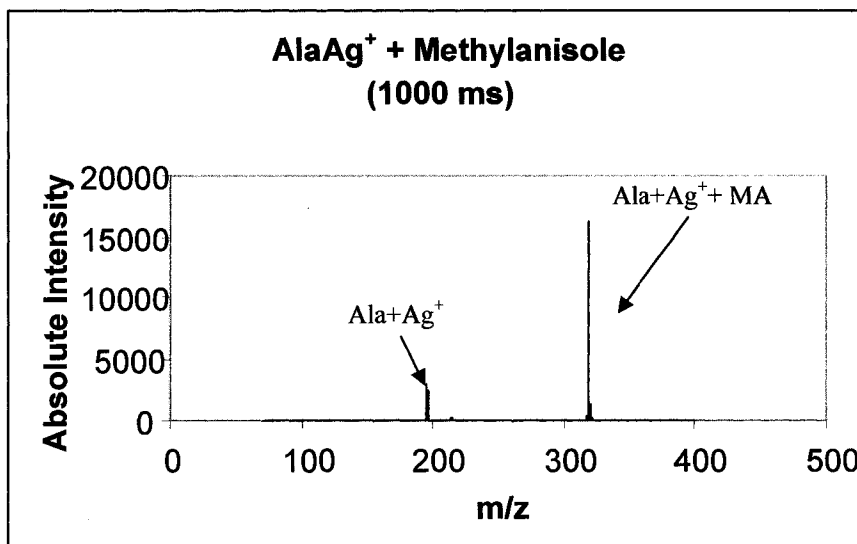


Figure 94. The reaction of [Ala+Ag⁺] with methylanisole over a scan delay period of 1000 ms.

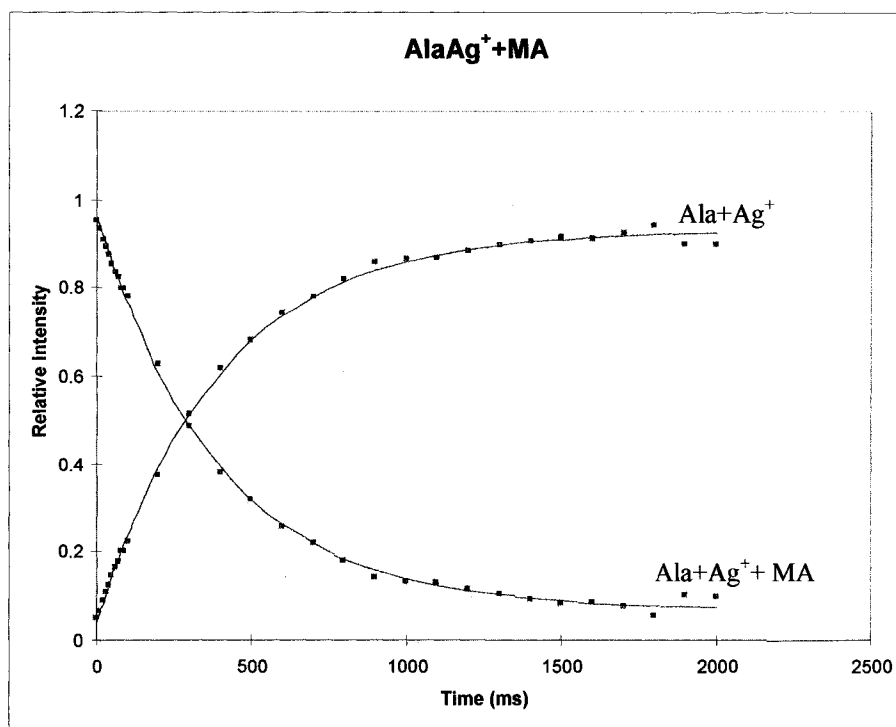


Figure 95. The reaction kinetics of $[Ala+Ag^+]$ with methylanisole.

Table 34

Reaction Data for Amino Acid Complexes with Silver Reacting with Methylanisole.

Amino Acid	k_2	k_f	Φ
Asn + Ag^+	2.1×10^{-10}	1.66×10^{-9}	1.3×10^{-1}
Gln + Ag^+	4.1×10^{-10}	1.64×10^{-9}	2.5×10^{-1}
Glu + Ag^+	4.3×10^{-10}	1.64×10^{-9}	2.6×10^{-1}
Ile + Ag^+	4.4×10^{-10}	1.66×10^{-9}	2.7×10^{-1}
Asp + Ag^+	5.3×10^{-10}	1.66×10^{-9}	3.2×10^{-1}
Gly + Ag^+	6.5×10^{-10}	1.75×10^{-9}	3.7×10^{-1}
Ala + Ag^+	7.6×10^{-10}	1.73×10^{-9}	4.4×10^{-1}

Of the amino acids complexed with silver, Ala was the fastest reacting and most efficient species. Unlike some of the toluene reactions, there are some apparent reaction trends presented in Table 34. First, Asn, Gln, and Glu are the slowest reacting and least efficient species of the study. All three of these amino acids contain a similarly positioned double-bonded oxygen atom on their side chain (Fig. 96). Asp also has a similarly bound oxygen atom on its side chain. Asp is separated in the table from the other amino acids by Ile. Nevertheless, it appears that the functional groups on the side chain directly affect the reaction efficiency; when amine groups are replaced by hydroxide groups, an increase in reaction efficiency is observed.

Gly and Ala complexes have the greatest reaction efficiency. These two amino acids have the simplest structure of the twenty common amino acids. It appears that a general feature of these reactions is that the species with the shorter side chains will react with the greatest efficiency.

Thermodynamic and kinetic calculations were also obtained for ion-molecule experiments of $[A.A.+Ag^+]$ complexes with methylanisole. Table 35 contains this data. For these experiments, it was found that the experimentally determined binding energy ranged from approximately 97 to 107 kJ mol⁻¹.

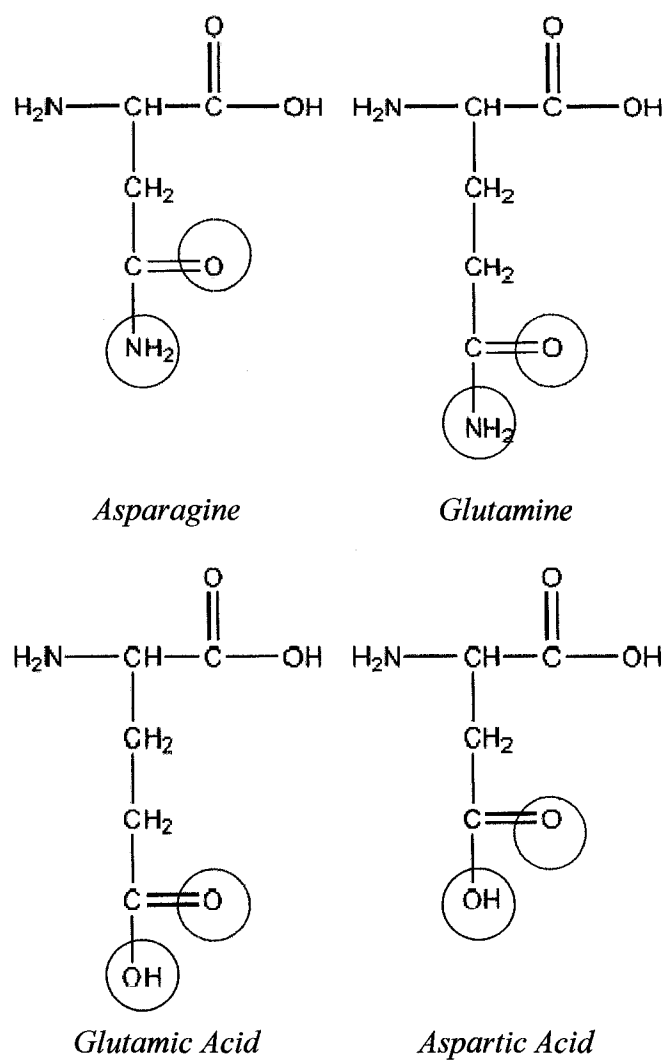


Figure 96. The structures of Asn, Gln, Glu, and Asp. Each of these amino acids has the common feature of a double-bonded oxygen on a side chain carbon (red). The lower efficiency species have amine groups (green), while the faster reacting species have hydroxide groups at the same position (blue).

Table 35

Thermodynamic and Kinetic Data for Reactions with Silver and Methylanisole.

Amino Acid	K_{eq} (atm^{-1})	ΔG (kJ mol^{-1})	ΔH (kJ mol^{-1})
Asn + Ag^+	$9.28 \times 10^{+9}$	-57.2	-97.2
Gln + Ag^+	$1.03 \times 10^{+10}$	-57.5	-97.5
Glu + Ag^+	$4.13 \times 10^{+11}$	-66.7	-106.7
Ile + Ag^+	($7.13 \times 10^{+10}$)	-62.3	-102.3
Asp + Ag^+	($2.42 \times 10^{+11}$)	-65.4	-105.4
Gly + Ag^+	$4.37 \times 10^{+11}$	-66.9	-106.9
Ala + Ag^+	$1.16 \times 10^{+11}$	-63.5	-103.5

Copper Studies

Copper complexes were successfully formed with twelve amino acids. A sample spectrum and kinetic plot are shown in Fig. 97 and Fig. 98. Kinetics data was obtained and is presented in Table 36.

As with [A.A.+ Ag^+ +MA] studies, the fastest reacting amino acid for copper studies was Ala. The reaction efficiencies of these reactions are much more diverse than with other studies, with Φ values ranging from 0.00048 to 1. [Arg+ Cu^+] is the least efficiently reacting species. This is likely due to the size of the Arg side chain. It is likely that Cu^+ is solvated by the chain, preventing interaction with the MA molecule. [Ile+ Cu^+] also exhibits a low reaction efficiency. This is likely due to a similar side chain interaction.

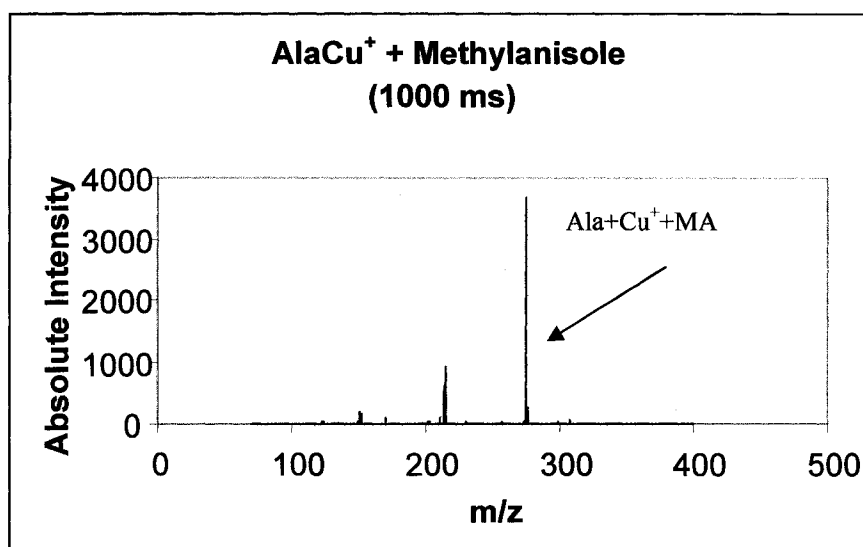


Figure 97. The reaction of [Ala+Cu⁺] with methylanisole after a 1000 ms scan delay.

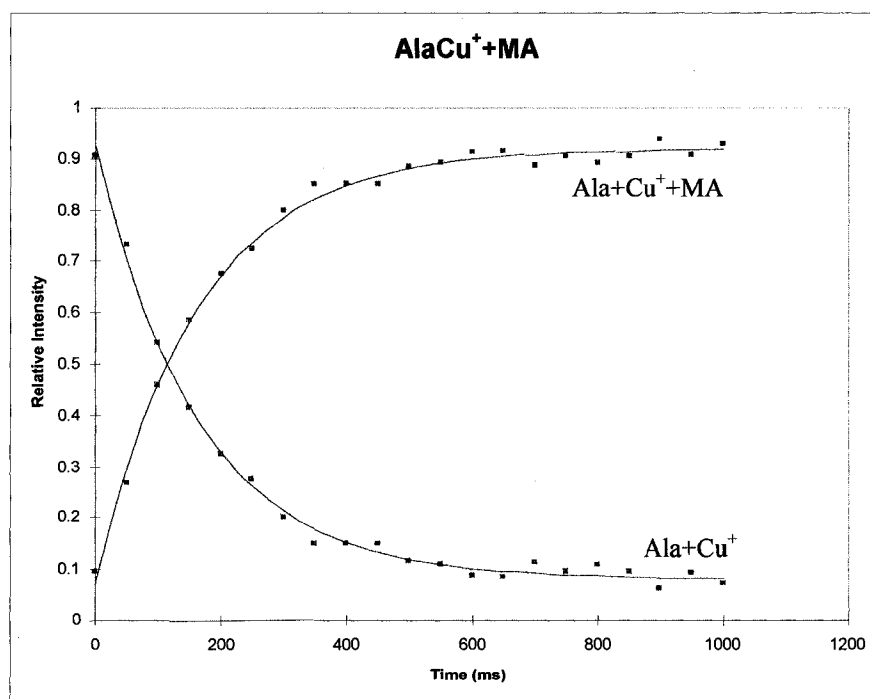


Figure 98. The reaction kinetics of [Ala+Cu⁺] with methylanisole.

Table 36

Reaction Data for Amino Acid Complexes with Copper and Methylanisole.

Amino Acid	k_2	k_f	Φ
Arg + Cu ⁺	9.7×10^{-13}	1.66×10^{-9}	5.8×10^{-4}
Ile + Cu ⁺	1.5×10^{-11}	1.72×10^{-9}	8.5×10^{-3}
Cys + Cu ⁺	(2.3×10^{-11})	1.74×10^{-9}	1.3×10^{-2}
Glu + Cu ⁺	(2.4×10^{-11})	1.70×10^{-9}	1.4×10^{-2}
Met + Cu ⁺	(4.2×10^{-10})	1.70×10^{-9}	2.5×10^{-1}
Asn + Cu ⁺	4.8×10^{-10}	1.72×10^{-9}	2.8×10^{-1}
Asp + Cu ⁺	5.6×10^{-10}	1.72×10^{-9}	3.3×10^{-1}
Thr + Cu ⁺	7.4×10^{-10}	1.75×10^{-9}	4.2×10^{-1}
Val + Cu ⁺	9.1×10^{-10}	1.75×10^{-9}	5.2×10^{-1}
Ser + Cu ⁺	(1.1×10^{-9})	1.77×10^{-9}	6.0×10^{-1}
Gly + Cu ⁺	1.4×10^{-9}	1.85×10^{-9}	7.3×10^{-1}
Ala + Cu ⁺	1.8×10^{-9}	1.81×10^{-9}	1

Both Cys and Glu react with similar efficiencies. There are no features in the structures of the amino acids that would indicate a functional group effect on these similar reaction efficiencies. However, Met and Cys both contain a sulfur atom in their side chains which could account for them being grouped in a similar position in Table 36. Asn and Asp are found to react with similar efficiencies. Similar to the [A.A.+Ag⁺+MA] study, the replacement of the amine group with a hydroxide group appears to play a factor in the increase in reaction rate and efficiency.

Finally, the amino acids with the shortest and simplest R-groups are found to react with the fastest kinetics and reaction efficiency. The similar reaction efficiencies of Thr, Val, and Ser were observed in previous experiments. Finally,

the two simplest amino acids, Gly and Ala, also react with similar efficiency as observed for the [A.A.+Ag⁺+MA] studies.

As with the previous experiments, the K_{eq} , ΔG , and ΔH values were determined for [A.A.+Cu⁺+MA] studies. These calculated values are presented in Table 37. It can be seen that the experimentally determined binding energies of these species ranged from approximately 85 to 108 kJ mol⁻¹.

Table 37

Kinetic and Thermodynamic Data for Reactions with Copper and Methylanisole.

Amino Acid	K_{eq} (atm ⁻¹)	ΔG (kJ mol ⁻¹)	ΔH (kJ mol ⁻¹)
Arg + Cu ⁺	7.88 X 10 ⁺⁷	-45.4	-85.4
Ile + Cu ⁺	1.97 X 10 ⁺⁹	-53.4	-93.4
Cys + Cu ⁺	7.95 X 10 ⁺⁸	-51.1	-91.1
Glu + Cu ⁺	2.37 X 10 ⁺⁹	-53.8	-93.8
Met + Cu ⁺	4.03 X 10 ⁺¹¹	-66.7	-106.7
Asn + Cu ⁺	7.45 X 10 ⁺⁹	-56.7	-96.7
Asp + Cu ⁺	8.65 X 10 ⁺⁹	-57.1	-97.1
Thr + Cu ⁺	1.83 X 10 ⁺¹⁰	-58.9	-98.9
Val + Cu ⁺	1.82 X 10 ⁺¹¹	-64.7	-104.7
Ser + Cu ⁺	2.31 X 10 ⁺¹¹	-65.3	-105.3
Gly + Cu ⁺	6.39 X 10 ⁺¹¹	-67.8	-107.8
Ala + Cu ⁺	9.90 X 10 ⁺¹⁰	-63.2	-103.2

Summary

Figure 99 compares the reaction efficiencies for [A.A.+Ag⁺] and [A.A.+Cu⁺] complexes with methylanisole. In general, the reactions with copper were more

efficient. This differs from ion-molecule reactions with toluene as the neutral, where silver complexes generally reacted with the greatest reaction efficiency.

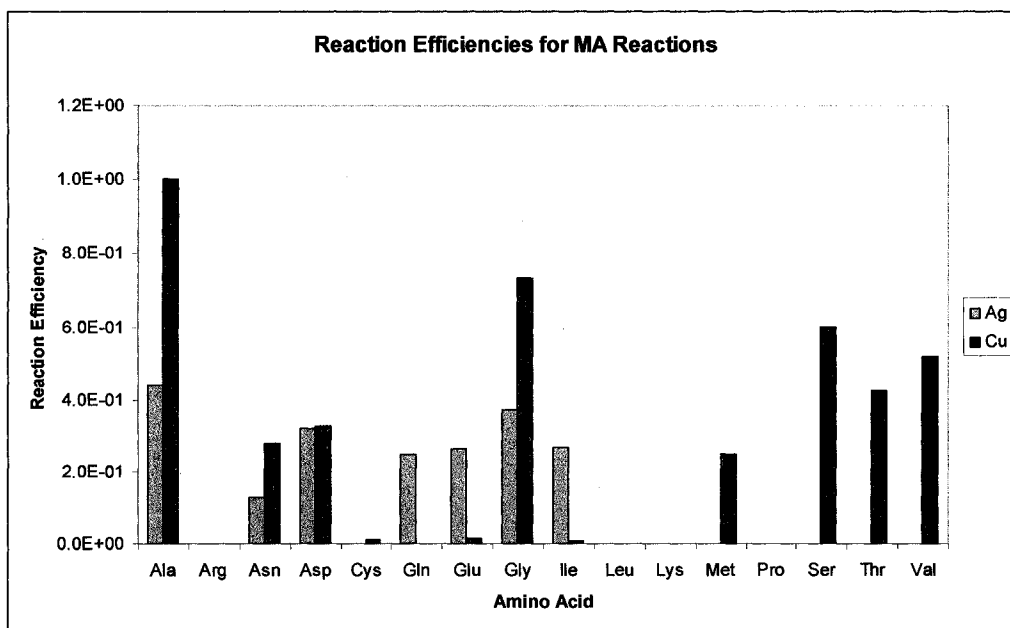


Figure 99. The reaction efficiencies of methylanisole reactions. Data presented for [A.A.+Ag⁺] and [A.A.+Cu⁺] complexes.

Results and Discussion

The cation- π interactions involving the aromatic groups of Phe and Tyr are often observed to occur with metal ions and positively charge amine groups in peptides and proteins. The aromatic groups of these amino acids have similar structures; however, the functional groups attached to the central benzene ring can alter the interaction of these aromatic amino acids with [A.A.+M⁺] complexes. Ion-

molecule reactions can be used to determine which [A.A.+M⁺+aromatic] interactions would be likely to occur in proteins.

It is apparent from the data presented for these aromatic modeling experiments that each non-aromatic amino acid reacts with different efficiencies depending on the metal ion species to which it is complexed. While it would be expected that kinetic trends would be easily correlated to amino acid structure, this is not the case. Experimental and theoretical results of [A.A.+Cu⁺] reactions with toluene demonstrate that kinetic observations have a linear correlation to stabilization energies of the species. The agreement between kinetic and thermodynamic data provides an indication that these ion-molecule reactions are capable of providing important reaction and binding information with regard to cation- π interactions.

The reaction efficiencies of [A.A.+Ag⁺] and [A.A.+Cu⁺] are compared in Fig. 100. In general, there are considerable differences between the interactions of toluene and methylanisole. For example, toluene is found to react with some amino acid complexes that were not observed to react with MA and vice versa. This provides important information regarding which aromatic interactions are likely to occur *in vivo*. In addition, some [A.A.+Ag⁺] complexes show an increased binding efficiency to one of the aromatic species. For example, there is a considerable increase in binding preference observed for toluene over MA with [Ile+Ag⁺]. Although less pronounced, [Ala+Ag⁺] demonstrates a distinct preference for interaction with MA over toluene.

There are a few instances in which the binding affinities of the $[A.A.+Ag^+]$ are not altered significantly by the neutral species. $[Glu+Ag^+]$ and $[Gly+Ag^+]$ react with the neutrals with similar reaction efficiencies. This indicates that Phe and Tyr are equally likely to participate in cation- π interactions.

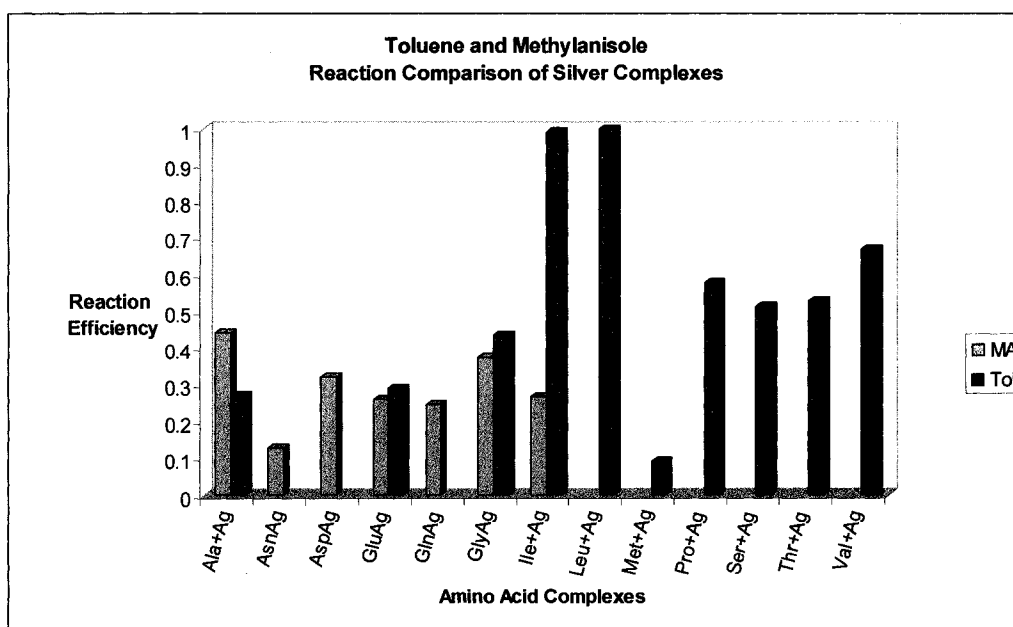


Figure 100. A comparison of reaction efficiencies for $[A.A.+Ag^+]$ complexes with toluene and methylanisole.

Similar side-by-side analysis can be performed for $[A.A.+Cu^+]$ reactions (Fig. 101). As with the silver studies, there are instances in which an amino acid will react with the neutral with a distinct preference. For example, Ala, Gly, Met, Ser, Thr, and Val complexes are observed to prefer to interact more strongly with

methylanisole than with toluene. However, Asn and Asp prefer to interact with toluene more than methylanisole.

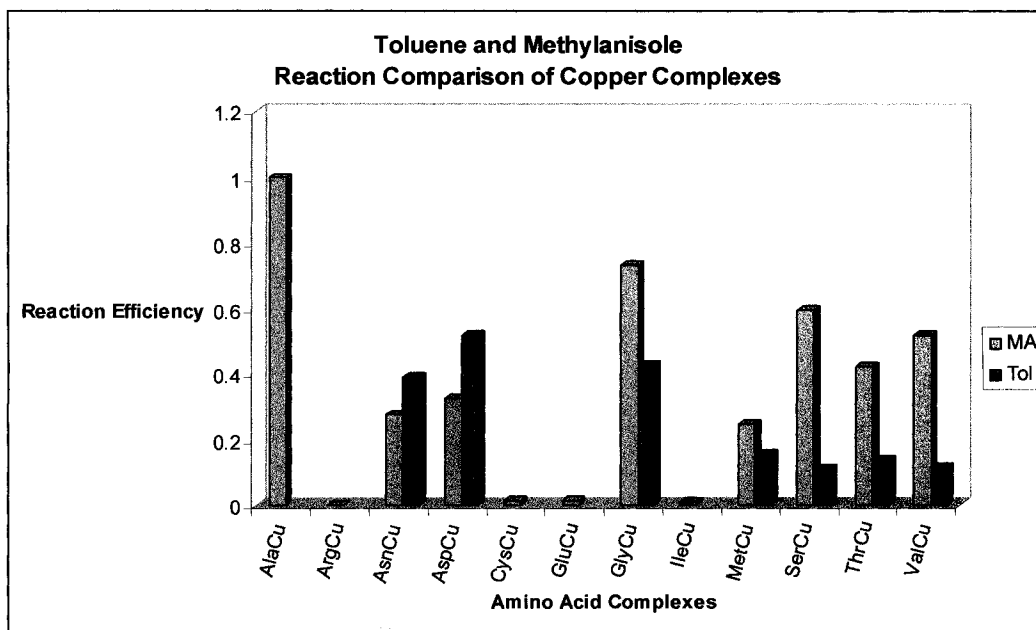


Figure 101. A comparison of reaction efficiencies for $[A.A.+Cu^+]$ complexes with toluene and methylanisole.

Unlike reactions with silver, there are no amino acids which demonstrate nearly identical reaction efficiencies. This is an important observation from a biochemical standpoint. There are many copper metalloproteins that exist in nature. These metalloproteins must show high levels of binding specificity and interactions in order to ensure proper functionality. The difference in binding preference even with similar molecules demonstrates the amazing selectivity of biomolecules.

Through these ion-molecule reactions, both observed and *in silico*, it has been shown that model aromatics prefer to bind with specific $[A.A.+M^+]$

complexes. It is assumed that the model aromatics will mimic the actual binding preferences of the amino acids in the gas phase. When this information is applied to the aromatic amino acids, association predictions can be made.

Theoretical calculations using the neutral benzene indicated that [A.A.-H+Ca²⁺] would show an increase in stabilization energy as follows:



This information can be used to predict that the reaction efficiency of the association will increase in the same order. Benzene is not an optimal neutral for experiments modeling aromatic amino acids since the R-groups of these species contain functional groups on the benzene ring. However, Gaussian calculations performed on the neutrals used to model these aromatic interactions can provide similar thermochemical results.

It was experimentally determined that Phe is most likely to show binding preference to [Leu+Ag⁺], [Leu-H+Ca²⁺], [Leu-H+Co²⁺], [Asp+Cu⁺], [Thr-H+Fe²⁺], [Gly-H+Ni²⁺], and [Asp-H+Zn²⁺]. Theoretical modeling calculations for [A.A.+Cu⁺] species were shown to follow a linear trend with reaction efficiency of these reactions. Although fewer studies were performed with methylanisole, it can be said that Tyr will likely show binding preference to [Ala+Ag⁺] and [Ala+Cu⁺].

Conclusions

It has been demonstrated here that the use of ion-molecule reactions to probe the kinetics of aromatic amino acid interactions is a viable means of predicting reactivity and binding. An in-depth look at the cation- π interactions can be achieved through kinetics experiments and theoretical computations. Information gathered from these experiments can be used to help determine protein structure, design target drugs, and advance protein engineering.

Aromatic amino acid ion-molecule reaction studies were undertaken for $[A.A.+M^+]$ species for a variety of metal ions. Data for association reactions with model neutrals can be obtained in a reasonable time frame, when compared with other analytical techniques. However, the time required to perform these experiments is not trivial.

Ion-molecule reactions were attempted for all non-aromatic amino acids complexed with seven different metal ions; for each modeling experiment, 119 $[A.A.+M^+]$ complexes were analyzed. The concentration of the $[A.A.+M^+]$ complexes needed to be optimized for the greatest signal intensity, and kinetics data needed to be obtained. Data acquisition time varied greatly depending on the stability of the $[A.A.+M^+]$ complex, reaction kinetics, and amount of scan delay increments used.

Theoretical calculations were necessary to complement experimental data. The data obtained from these calculations are significant for the scope of the

experiments; however, the computations come with a cost of time. The time required for Gaussian optimization and energy calculations increases drastically as the size of the species increase. With our lab's current computer power, the computational time can span from taking a few hours to a few weeks.

In general, the entire set of optimizations and calculations for the [A.A.+M⁺+neutral] could be obtained in approximately 2 weeks, which is a conservative estimate. This means that on average it would take approximately 34 weeks to complete theoretical calculations for only one set of metal complexes reacting with one neutral species. In addition, if theoretical calculations were performed for all 119 [A.A.+M⁺+toluene] reactions analyzed, assuming the same computational time, it would take ~ 4.5 years to complete these reactions. Unfortunately, this time frame is not optimal for a complete data analysis (experimental and theoretical) in a reasonable time frame.

Nevertheless, experimental and theoretical analysis of cation- π interactions has proved to be beneficial. It has been demonstrated that ion-molecule reactions can be effectively used to probe the reactivity of aromatic amino acids in the gas phase. Although much has been accomplished, the need for further investigation of these interactions remains.

CHAPTER 5

FUTURE DIRECTIONS

It has been demonstrated that the use of ion-molecule reactions is an effective and efficient means to probe the structure and reactivity of amino acids in the gas phase. The structure of amino acids in the gas phase has been a topic of interest for many years. It has been shown that the use of ion-molecule reactions is a relatively inexpensive and practical means to determine gas-phase amino acid structure. It has also been shown that the reactivity of amino acids in the gas phase can be probed when the neutral species is used to model aromatic amino acids. Although much information about amino acids has been gathered over the course of these experiments, the use of ion-molecule reactions to analyze amino acids has not yet been exhausted.

Simple modifications to the experiments can be performed in order to improve data collection and amino acid analysis. Additional neutral species can be chosen to provide data which can be compared to what has already been gathered. Different biologically relevant metals can be complexed to amino acids in the aromatic studies to study the interaction of a wider range of species. Interesting features of other amino acids can be exploited using ion-molecule reactions to probe the reactivity of those species. Finally, ion-molecule reactions could be used to identify species separated by high-performance liquid chromatography (HPLC) in a real-time analysis setup.

Structural Analysis

The current experimental setup for probing the structure of amino acids in the gas phase has allowed for data collection for many species. As has been previously shown, some of these amino acid species react significantly slower than other amino acids; these reactions are too slow to observe during the time frame of the experiments. Small modifications to the instrument would enable these slower reactions to be observed.

One possible adjustment that could be made is to alter the computer program that controls the scan delay of the instrument. The instrument has a scan delay limit of 9000 ms, which can be insufficient to observe slower reactions. If the scan delay limit could be increased, it is possible that ion-molecule reaction data could be obtained and used to identify the gas-phase structures of slower reacting species. Ideally, more data would be collected from software changes, but possible drawbacks to this change might render this option unfavorable.

The $[A.A.+M^+]$ and/or the $[A.A.+M^++neutral]$ species may not be stable at higher scan delays. Repetitive collisions with molecules in the trap would cause these molecules to fragment. This would affect data analysis because the decay curves of the $[A.A.+M^+]$ would no longer be dictated by kinetics. Both kinetic and collisional decay factors would be observed.

Another option is to alter the instrumental setup itself. One possibility is to introduce higher pressures of the neutral species into the ion trap. Another is to find

a neutral that is more reactive than the current neutral, acetone. The higher pressure of neutral would cause the kinetics to be observed for all amino acids in a much faster time frame. This would decrease the reaction time of already fast-reacting species but would also decrease the reaction time of the slower species. If the pressure was significantly different enough, it is theoretically possible to observe reactions for all amino acid species.

The pressure of neutral entering the quadrupole ion trap is governed by the flow rate of the syringe pump. Slower flow rates of neutral correspond to lower pressures of the neutral in the trap and vice versa. Increasing the flow rate of the neutral can be an effective way to increase the pressure of the neutral in the trap. However, there are limits to increasing the flow rate. The syringe pump has a maximum pump speed that it can operate at. Moreover, there is a point at which the helium gas will become “saturated” with the neutral species. Even if the flow rate is increased, a saturation limit will prevent higher pressures of the neutral from entering the trap. It is also possible that neutral species flowing into the helium line at too high a flow rate might block the line, where the liquid neutral might prevent the helium from flowing into the trap at optimal pressure.

One of the easiest modifications that can be made to these experiments is to alter the neutral species used for these experiments. Structural studies present in Chapter 3 used acetone as the neutral species, and for most of the amino acids, data could be obtained. It is possible that another neutral species would react faster with the $[A.A.+M^+]$ studied and would therefore provide information not yet obtained.

Future work should focus on probing the structure of amino acids in the gas phase while implementing one, if not all, of the previously suggested improvements. It will then be possible to collect data for the slow-reacting sodiated and potassiated species, as well as the $[A.A.+Cs^+]$ whose reactions were previously unobservable.

Reactivity of the Amino Acids

The reactivity of the aromatic amino acids was another focus of these ion-molecule reaction experiments. Neutral species were used to model interactions of $[A.A.+M^+]$ species with phenylalanine and tyrosine, where $M = Ag, Ca, Co, Cu, Fe, Ni,$ and Zn . Improvements to these experiments include the use of additional neutral models, the use of additional metal ions, the investigation of other amino acids with cyclic groups, and an increased production of corroborate theoretical computations.

For these ion-molecule reaction experiments, neutral species were selected that closely resemble the aromatic groups of Phe and Tyr. Although the neutrals used for these experiments provided relevant reactivity data, additional neutral species could be identified for future experiments. For example, the neutral species 4-methylindole could be used to model the aromatic side chain of Trp. It is also possible that other neutral species could be selected in an attempt to more specifically model the aromatic amino residues.

The aromatic reactivity studies here focused on amino acids complexed to a variety of transition metals and calcium. These metals are biologically significant

due to their contribution to protein function in the body. The scope of these experiments could be broadened by studying the interactions of model aromatic neutrals with amino acids complexed to different metal species. Other biologically relevant metal cations include magnesium, lithium, manganese, chromium, and molybdenum. Data from these studies would provide additional insight to these aromatic amino acid interactions.

Last, the reactivity of other amino acids can also be analyzed using ion-molecule reactions. A focus was placed on the aromatic amino acids Phe, Tyr, and Trp for these experiments. Future experiments could focus on amino acids with different features such as cyclic groups or sulfides. Both histidine and proline have cyclic groups on their side chains that would be capable of interacting with metal-complexed amino acids in interesting ways.

Neutral species could be selected to model these cyclic amino acids to investigate their reactivity. Examples of neutrals that could be used for ion-molecule reactions modeling cyclic amino acids are shown in Fig. 102. It is important to note that these examples are only suggestions and are not an exhaustive list of possible neutral species. Additionally, these neutrals are suggested as models due to their molecular similarity to the amino acid they are modeling and for their chemical characteristics.

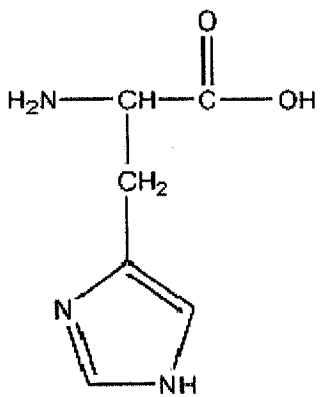
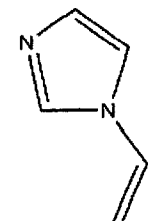
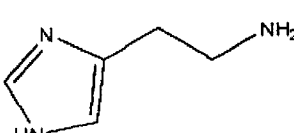
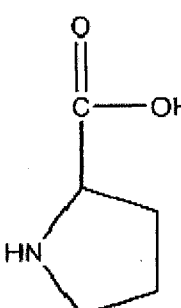
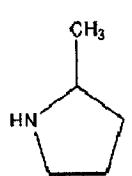
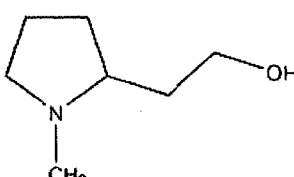
Amino Acid	Neutral Model
 <p data-bbox="503 829 617 873"><i>Histidine</i></p>	 <p data-bbox="1006 589 1218 655"><i>1-vinylimidazole</i> b.p. = 78-79 °C</p>  <p data-bbox="1023 895 1201 960"><i>Histamine</i> b.p. = 167 °C</p>
 <p data-bbox="503 1506 617 1550"><i>Proline</i></p>	 <p data-bbox="990 1223 1250 1288"><i>2-methylpyrrolidine</i> b.p. = 97-99 °C</p>  <p data-bbox="925 1594 1315 1659"><i>1-methyl-2-pyrrolidine ethanol</i> b.p. = 110-112 °C</p>

Figure 102. Cyclic amino acids and potential neutral models.

Cysteine and methionine are two amino acids which might also exhibit interesting interactions with $[A.A.+M^+]$ species. Both amino acids have sulfur-containing R-groups. As before, neutrals can be selected to model these amino acids to probe their reactivity in the gas phase. Fig. 103 shows these molecules.

Real-Time Analysis

Additionally, faster reactions in the quadrupole ion trap would facilitate real-time analysis of HPLC eluents. The current experimental setup is not capable of analyzing amino acid structure in a time frame suitable for LC-coupled analysis. In the event that reaction rates can be increased in the quadrupole ion trap, this method would be sufficient for real-time LC-coupled analysis.

This type of data acquisition is extremely important for high-throughput data analysis. With the ability of ion-molecule reactions to identify structural characteristics of amino acids in the gas phase comes an important advance in peptide and protein screening. Furthermore, this technique could be expanded to analyzing other biomolecules, including, but not limited to, carbohydrates, steroids, sugars, and DNA. Eventually, ion-molecule reactions could be developed for use as a molecular identifier in such areas as drug screening, histology, and genetic and disease testing.

Amino Acid	Neutral Model
$ \begin{array}{c} \text{O} \\ \parallel \\ \text{H}_2\text{N}-\text{CH}-\text{C}-\text{OH} \\ \\ \text{CH}_2 \\ \\ \text{SH} \end{array} $ <p style="text-align: center;"><i>Cysteine</i></p>	$ \begin{array}{c} \text{H}_3\text{C}-\text{CH}_2-\text{SH} \\ \\ \textit{Ethanethiol} \\ \text{b.p.} = 35\text{ }^\circ\text{C} \\ \\ \text{H}_2\text{C}=\text{CH}-\text{CH}_2-\text{SH} \\ \\ \textit{2-propene-1-thiol} \\ \text{b.p.} = 67-68\text{ }^\circ\text{C} \end{array} $
$ \begin{array}{c} \text{O} \\ \parallel \\ \text{H}_2\text{N}-\text{CH}-\text{C}-\text{OH} \\ \\ \text{CH}_2 \\ \\ \text{CH}_2 \\ \\ \text{S} \\ \\ \text{CH}_3 \end{array} $ <p style="text-align: center;"><i>Methionine</i></p>	$ \begin{array}{c} \text{H}_3\text{C}-\text{CH}_2-\text{S}-\text{CH}_3 \\ \\ \textit{Ethyl methyl sulfide} \\ \text{b.p.} = 66-67\text{ }^\circ\text{C} \\ \\ \text{H}_3\text{C}-\text{CH}_2-\text{CH}_2-\text{S}-\text{CH}_3 \\ \\ \textit{Methyl propyl sulfide} \\ \text{b.p.} = 95.5\text{ }^\circ\text{C} \end{array} $

Figure 103. Neutral models for sulfur-containing amino acids.

Conclusion

Significant advances have been made for the analysis of protein chemistry. The understanding of protein function and interaction is not trivial; the complex nature of peptides and proteins requires that a fundamental understanding of amino acids is achieved. As the structure and reactivity of these protein building blocks is better understood, the mystery of proteins will be better solved. Advances in protein chemistry are essential to the development of antibiotics, disease treatment, gene therapy, and a myriad of other medical advances. If nothing else, the increase in the understanding of proteins is proportional to an added appreciation of the nuances of these amazing biomolecules.

REFERENCES

1. Hart, H.; Craine, L. E.; Hart, D. J., *Organic chemistry: A Short Course*. Eleventh ed.; Houghton Mifflin Company: Boston, 2003.
2. McMurray, J., *Organic Chemistry*. Fifth ed.; Brooks/Cole: Pacific Grove, 2000.
3. Frisch, M. J.; Trucks, G. W.; Schlegel, H. B.; Scuseria, G. E.; Robb, M. A.; Cheeseman, J. R.; J.M. Montgomery, J.; Vreven, T.; Kudin, K. N.; Burant, J. C.; Millam, J. M.; Iyengar, S. S.; J. Tomasi; Barone, V.; Mennucci, B.; Cossi, M.; Scalmani, G.; Rega, N.; Petersson, G. A.; Nakatsuji, H.; Hada, M.; Ehara, M.; Toyota, K.; Fukuda, R.; Hasegawa, J.; Ishida, M.; Nakajima, T.; Honda, Y.; Kitao, O.; Nakai, H.; Klene, M.; Li, X.; Knox, J. E.; Hratchian, H. P.; Cross, J. B.; Adamo, C.; Jaramillo, J.; Gomperts, R.; Stratmann, R. E.; Yazyev, O.; Austin, A. J.; Cammi, R.; Pomelli, C.; Ochterski, J. W.; Ayala, P. Y.; Morokuma, K.; Voth, G. A.; Salvador, P.; Dannenberg, J. J.; Zakrzewski, V. G.; Dapprich, S.; Daniels, A. D.; Strain, M. C.; Farkas, O.; Malick, D. K.; Rabuck, A. D.; Raghavachari, K.; Foresman, J. B.; Ortiz, J. V.; Cui, Q.; Baboul, A. G.; Clifford, S.; Cioslowski, J.; Stefanov, B. B.; Liu, G.; Liashenko, A.; Piskorz, P.; Komaromi, I.; Martin, R. L.; Fox, D. J.; Keith, T.; Al-Laham, M. A.; Peng, C. Y.; Nanayakkara, A.; Challacombe, M.; Gill, P. M. W.; Johnson, B.; Chen, W.; Wong, M. W.; Gonzalez, C.; Pople, J. A. *Gaussian 03*, Revision C. 02; Gaussian, Inc.: Wallingford, CT, 2004.
4. Banci, L.; Bertini, I.; Cantini, F.; DellaMalva, N.; Herrmann, T.; Rosato, A.; Wuthrich, K., Solution structure and intermolecular interactions of the third metal-binding domain of ATP7A, the Menkes disease protein. *J. Biol. Chem.* **2006**, 281, 29141-29147.
5. Roat-Malone, R. M., *Bioinorganic Chemistry: A Short Course*. John Wiley & Sons, Inc.: Hoboken, 2002.
6. Garrett, R. H.; Grisham, C. M., *Biochemistry*. Second ed.; Saunders College Publishing: Fort Worth, 1999.
7. Davidson, M. W. Molecular Expressions: The Amino Acid Collection. <http://micro.magnet.fsu.edu/aminoacids/index.html> (October 15, 2006).

8. Sardesai, V. M., *Introduction to Clinical Nutrition*. Marcel Dekker, Inc.: New York, 1998.
9. Berdanier, C. D., *Advanced Nutrition: Micronutrients*. CRC Press LCC: Boca Raton, 1998.
10. Lippard, S. J.; Berg, J. M., *Principles of Bioinorganic Chemistry*. University Science Books: Mill Valley, 1994.
11. Cowan, J. A., *Inorganic Biochemistry: An Introduction*. Second Edition ed.; Wiley-VCH, Inc.: New York, 1997.
12. Masterton, W. L.; Hurley, C. N., *Chemistry: Principles & Reactions*. Third ed.; Saunders College Publishing: Fort Worth, 1997.
13. Emsley, J., *The Elements*. Oxford University Press, Inc.: New York, 1998.
14. Garcia, J. S.; de Magalhaes, C. S.; Arruda, M. A. Z., Trends in metal-binding and metalloprotein analysis. *Talanta* **2006**, 69, 1-15.
15. Ho, T.-L., The hard soft acids bases (HSAB) principle and organic chemistry. *Chem. Rev.* **1975**, 75, 1-20.
16. Datta, D., On Pearson's HSAB principle. *Inorg. Chem.* **1992**, 31, 2797-2800.
17. Shoeib, T.; Gorelsky, S. I.; Lever, A. B. P.; Siu, K. W. M.; Hopkinson, A. C., When does the hard and soft acid base principle apply in the gas phase? *Inorg. Chim. Acta* **2001**, 315, 236-239.
18. Chattaraj, P. K.; Schleyer, P. v. R., An ab initio study resulting in a greater understanding of the HSAB principle. *J. Am. Chem. Soc.* **1994**, 116, 1067-1071.
19. Shoeib, T.; Aribi, H. E.; Siu, K. W. M.; Hopkinson, A. C., A study of silver (I) ion-organonitrile complexes: Ion structures, binding energies, and substituent effects. *J. Phys. Chem. A* **2001**, 105, 710-719.
20. Molecular Biology Web Book. <http://www.web-books.com/MoBio/Free/CH4F2.htm#4F1> (September 3, 2006).
21. Dass, C., *Principles and Practice of Biological Mass Spectrometry*. John Wiley & Sons, Inc.: New York, 2001.

22. March, R. E.; Todd, J. F. J., *Practical Aspects of Ion Trap Mass Spectrometry: Fundamentals of Ion Trap Mass Spectrometry*. CRC Press: Boca Raton, 1995; Vol. I.
23. Sleno, L.; Volmer, D. A., Ion activation methods for tandem mass spectrometry. *J. Mass Spectrom.* **2004**, 39, 1091-1112.
24. Ho, Y.; Kebarle, P., Studies of the dissociation mechanisms of deprotonated mononucleotides by energy resolved collision-induced dissociation. *Int. J. Mass Spectrom. Ion Processes* **1997**, 165/166, 433-455.
25. Anderson, S. G.; Blades, A. T.; Klassen, J.; Kebarle, P., Determination of ion-ligand bond energies and ion fragmentation energies of electrospray-produced ions by collision-induced dissociation threshold measurements. *Int. J. Mass Spectrom. Ion Processes* **1995**, 141, 217-228.
26. Valina, A. B.; Amunugama, R.; Huang, H.; Rodgers, M. T., Collision-induced dissociation and theoretical studies of Na⁺-Acetonitrile complexes. *J. Phys. Chem. A* **2001**, 105, 11057-11068.
27. Armentrout, P. B.; Rodgers, M. T., An absolute sodium cation affinity scale: threshold collision-induced dissociation experiments and ab initio theory. *J. Phys. Chem. A* **2000**, 104, 2238-2247.
28. Krouse, I. H.; Lardin, H. A.; Wenthold, P. G., Gas-phase ion chemistry and ion thermochemistry of phenyltrifluorosilane. *Int. J. Mass Spectrom.* **2003**, 227, 303-314.
29. Amicangelo, J. C.; Armentrout, P. B., Absolute binding energies of alkali-metal cation complexes with benzene determined by threshold collision-induced dissociation experiments with ab initio theory. *J. Phys. Chem. A* **2000**, 104, 11420-11432.
30. Vitale, G.; Valina, A. B.; Huang, H.; Amunugama, R.; Rodgers, M. T., Solvation of copper ions by acetonitrile. Structures and sequential binding energies of Cu⁺(CH₃CN)_x, X=1-5, from collision-induced dissociation and theoretical studies. *J. Phys. Chem. A* **2001**, 105, 11351-11364.
31. Julian, R. R.; Akin, M.; May, J. A.; Stoltz, B. M.; Beauchamp, J. L., Molecular recognition of arginine in small peptides by supramolecular complexation with dibenzo-30-crown-10 ether. *Int. J. Mass Spectrom.* **2002**, 220, 87-96.

32. Rogalewicz, F.; Hoppilliard, Y.; Ohanessian, G., Structures and fragmentations of zinc (II) complexes of amino acids in the gas phase IV. Solvent effect on the structure of electrosprayed ions. *Int. J. Mass Spectrom.* **2003**, 227, 439-451.
33. Hayes, L. A.; Chappell, A. M.; Jellen, E. E.; Ryzhov, V., Binding of metalloporphorins to model nitrogen bases: collision-induced dissociation and ion-molecule reaction studies. *Int. J. Mass Spectrom.* **2003**, 227, 111-120.
34. Schafer, M.; Schmuck, C.; Geiger, L.; Chalmers, M. J.; Hendrickson, C. L.; Marshall, A. G., Structurally related non-covalent complexes examined by quadrupole ion trap (QIT) MS2 and infrared multiphoton dissociation Fourier transform ion cyclotron resonance mass spectrometry IRMPD-FT-ICR MS: evidence for salt-bridge structures in the gas phase. *Int. J. Mass Spectrom.* **2004**, 237, 33-45.
35. Borisov, O. V.; Goshe, M. B.; Conrads, T. P.; Rakov, V. S.; Veenstra, T. D.; Smith, R. D., Low-energy collision-induced dissociation fragmentation analysis of cysteinyl-modified peptides. *Anal. Chem.* **2002**, 74, 2284-2292.
36. Amunugama, R.; Rodgers, M. T., Influence of substituents on cation-pi interactions 5. Absolute binding energies of alkali metal cation-anisole complexes determined by threshold collision-induced dissociation and theoretical studies. *Int. J. Mass Spectrom.* **2003**, 222, 431-450.
37. Amunugama, R.; Rodgers, M. T., Influence of substituents on cation-pi interactions. 1. Absolute binding energies of alkali metal cation-toluene complexes determined by threshold collision-induced dissociation and theoretical studies. *J. Phys. Chem. A* **2002**, 106, 5529-5539.
38. Amunugama, R.; Rodgers, M. T., Influence of substituents of cation-pi interactions. 3. Absolute binding energies of alkali metal cation-aniline complexes determined by threshold collisional-induced dissociation and theoretical studies. *Int. J. Mass Spectrom.* **2003**, 227, 339-360.
39. Ruan, C.; Yang, Z.; Hallowita, N.; Rodgers, M. T., Cation-pi interactions with a model for the side chain of tryptophan: Structures and absolute binding energies of alkali metal cation-indole complexes. *J. Phys. Chem. A* **2005**, 109, 11539-11550.
40. Amunugama, R.; Rodgers, M. T., The influence of substituents on cation-pi interactions. 4. Absolute binding energies of alkali metal cation-phenol complexes determined by threshold collision-induced dissociation and theoretical studies. *J. Phys. Chem. A* **2002**, 106, 9718-9728.

41. Amunugama, R.; Rodgers, M. T., Influence of substituents on cation- π interactions. 2. Absolute binding energies of alkali metal cation-fluorobenzene complexes determined by threshold collision-induced dissociation and theoretical studies. *J. Phys. Chem. A* **2002**, 106, 9092-9103.
42. Chu, Y.; Yang, Z.; Rodgers, M. T., Solvation of copper ions by acetone. Structures and sequential binding energies of Cu^+ (acetone) $_x$, $x=1-4$ from collision-induced dissociation and theoretical studies. *J. Am. Soc. Mass. Spectrom.* **2002**, 13, (453-468).
43. Yang, Z.; Rodgers, M. T., Influence of halogenation on the properties of uracil and its noncovalent interactions with alkali metal ions. Threshold collision-induced dissociation and theoretical studies. *J. Am. Chem. Soc.* **2004**, 126, 16217-16226.
44. Rodgers, M. T.; Armentrout, P. B., Noncovalent interactions of nucleic acid bases (uracil, thymine, and adenine) with alkali metal ions. Threshold collision-induced dissociation and theoretical studies. *J. Am. Chem. Soc.* **2000**, 122, 8548-8558.
45. Rodgers, M. T.; Armentrout, P. B., A thermodynamic "vocabulary" for metal ion interactions in biological systems. *Acc. Chem. Res.* **2004**, 37, 989-998.
46. Amunugama, R.; Rodgers, M. T., Absolute alkali metal ion binding affinities of several azines determined by threshold collision-induced dissociation and ab initio theory. *Int. J. Mass Spectrom.* **2000**, 195/196, 439-457.
47. Rodgers, M. T.; Armentrout, P. B., Absolute alkali metal ion binding affinities of several azoles determined by threshold collision-induced dissociation. *Int. J. Mass Spectrom.* **1999**, 185/186/187, 359-380.
48. Reyzer, M. L.; Brodbelt, J. S.; Kerwin, S. M.; Kumar, D., Evaluation of complexation of metal-mediated DNA-binding drugs to oligonucleotides via electrospray ionization mass spectrometry. *Nucleic Acids Res.* **2001**, 29, e103.
49. Jockusch, R. A.; Schnier, P. D.; Price, W. D.; Strittmatter, E. F.; Demirev, P. A.; Williams, E. R., Effects of charge state on fragmentation pathways, dynamics, and activation energies of ubiquitin ions measured by blackbody infrared radiative dissociation. *Anal. Chem.* **1997**, 69, 1119-1126.
50. Price, W. D.; Williams, E. R., Activation of peptide ions by blackbody radiation: factors that lead to dissociation kinetics in the rapid energy exchange limit. *J. Phys. Chem. A* **1997**, 101, 8844-8852.

51. Price, W. D.; Schnier, P. D.; Williams, E. R., Tandem mass spectrometry of large biomolecule ions by blackbody infrared radiative dissociation. *Anal. Chem.* **1996**, *68*, 859-866.
52. Lemoff, A. S.; Bush, M. F.; O'Brien, J. T.; Williams, E. R., Structures of lithiated lysine and structural analogues in the gas phase: effects of water and proton affinity on zwitterionic stability. *J. Phys. Chem. A* **2006**, *110*, 8433-8442.
53. Schnier, P. D.; Williams, E. R., Analysis of isomeric mixtures using blackbody infrared radiative dissociation: determining isomeric purity and obtaining individual tandem mass spectra simultaneously. *Anal. Chem.* **1998**, *70*, 3033-3041.
54. Jockusch, R. A.; Williams, E. R., Binding energies of proton-bound dimers of imidazole and n-acetylalanine methyl ester obtained by blackbody infrared radiative dissociation. *J. Phys. Chem. A* **1998**, *102*, 4543-4550.
55. Stevens, J., S.M.; Dunbar, R. C.; Price, W. D.; Sena, M.; Watson, C. H.; Nichols, L. S.; Riveros, J. M.; Richardson, D. E.; Eyler, J. R., Blackbody infrared radiative dissociation of partially solvated mixed ligand Ru(II) complex ions. *J. Phys. Chem. A* **2004**, *108*, 9892-9900.
56. Jockusch, R. A.; Lemoff, A. S.; Williams, E. R., Effect of metal ion and water coordination on the structure of a gas-phase amino acid. *J. Am. Chem. Soc.* **2001**, *123*, 12255-12265.
57. Jockusch, R. A.; Price, W. D.; Williams, E. R., Structure of cationized arginine (Arg-M⁺, M=H, Li, Na, K, Rb, and Cs) in the gas phase: Further evidence for zwitterionic arginine. *J. Phys. Chem. A* **1999**, *103*, 9266-9274.
58. Price, W. D.; Jockusch, R. A.; Williams, E. R., Is arginine a zwitterion in the gas phase? *J. Am. Chem. Soc.* **1997**, *119*, 11988-11989.
59. Strittmatter, E. F.; Wong, R. L.; Williams, E. R., Gas-phase basicity of (CH₃)₃N⁺-C₆H₄-COO⁻ zwitterions: a new class of organic super bases. *J. Am. Chem. Soc.* **2000**, *122*, 1247-1248.
60. Kamariotis, A.; Boyarkin, O. V.; Mercier, S. R.; Beck, R. D.; Bush, M. F.; Williams, E. R.; Rizzo, T. R., Infrared spectroscopy of hydrated amino acids in the gas phase: protonated and lithiated valine. *J. Am. Chem. Soc.* **2006**, *128*, 905-916.
61. Polfer, N. C.; Oomens, J.; Moore, D. T.; von Helden, G.; Meijer, G.; Dunbar, R. C., Infrared spectroscopy of phenylalanine Ag(I) and Zn(II) complexes in the gas phase. *J. Am. Chem. Soc.* **2006**, *128*, 517-525.

62. Kapota, C.; Lemaire, J.; Maitre, P.; Ohanessian, G., Vibrational structure of charge solvation vs. salt bridge isomers of sodiated amino acids in the gas phase. *J. Am. Chem. Soc.* **2004**, 126, 1836-1842.
63. Ryzhov, V.; Klippenstein, S. J.; Dunbar, R. C., Radiative association of NO⁺ with 3-pentanone: rate, binding energy, and temperature dependence. *J. Am. Chem. Soc.* **1996**, 118, 5462-5468.
64. Grimm, R. L.; Mangrum, J. B.; Dunbar, R. C., Complexation of gas-phase metal ions with furan: experimental and quantum chemical binding energies. *J. Phys. Chem. A* **2004**, 108, 10897-10905.
65. Gapeev, A.; Yang, C.-N.; Klippenstein, S. J.; Dunbar, R. C., Binding energies of gas-phase metal ions with pyrrole: experimental and quantum, chemical results. *J. Phys. Chem. A* **2000**, 104, 3246-3256.
66. Ryzhov, V.; Dunbar, R. C., Interactions of phenol and indole with metal ions in the gas phase: models for Tyr and Trp side-chain binding. *J. Am. Chem. Soc.* **1999**, 121, 2259-2268.
67. Lin, C.-Y.; Dunbar, R. C., Radiative association kinetics and binding energies of chromium ions with benzene and benzene derivatives. *Organometallics* **1997**, (16), 2691-2697.
68. Sudha, R.; Kohtani, M.; Jarrold, M. F., Non-covalent interactions between unsolvated peptides: helical complexes based on acid-base interactions. *J. Phys. Chem. B* **2005**, 109, 6442-6447.
69. Taraszka, J. A.; Li, J.; Clemmer, D. E., Metal-mediated peptide ion conformations in the gas phase. *J. Phys. Chem. B* **2000**, 104, (4545-4551).
70. Kinnear, B. S.; Kaleta, D. T.; Kohtani, M.; Hudgins, R. R.; Jarrold, M. F., Conformations of unsolvated valine-based peptides. *J. Am. Chem. Soc.* **2000**, 122, 9243-9256.
71. Ruotolo, B. T.; Tate, C. C.; Russell, D. H., Ion mobility-mass spectrometry applied to cyclic peptide analysis: conformational preferences of gramicidin S and linear analogues in the gas phase. *J. Am. Soc. Mass. Spectrom.* **2004**, 15, 870-878.
72. Hudgins, R. R.; Woenckhaus, J.; Jarrold, M. F., High resolution ion mobility measurements for gas phase proteins: correlation between solution phase and gas phase conformations. *Int. J. Mass Spectrom. Ion Processes* **1997**, 165/166, 497-507.

73. Koeniger, S. L.; Merenbloom, S. I.; Sevugarajan, S.; Clemmer, D. E., Transfer of structural elements from compact to extended states in unsolvated ubiquitin. *J. Am. Chem. Soc.* **2006**, 128, 11713-11719.
74. Koeniger, S. L.; Merenbloom, S. I.; Clemmer, D. E., Evidence for many resolvable structures within conformation types of electrosprayed ubiquitin ions. *J. Phys. Chem. B* **2006**, 110, 7017-7021.
75. Myung, S.; Wiseman, J. M.; Valentine, S. J.; Takats, Z.; Cooks, R. G.; Clemmer, D. E., Coupling desorption electrospray ionization with ion mobility/mass spectrometry for analysis of protein structure: evidence for desorption of folded and denatured states. *J. Phys. Chem. B* **2006**, 110, 5045-5051.
76. Baker, E. S.; Bushnell, J. E.; Wecksler, S. R.; Lim, M. D.; Manard, M. J.; Dupuis, N. F.; Ford, P. C.; Bowers, M. T., Probing shapes of bichromophoric metal-organic complexes using ion mobility mass spectrometry. *J. Am. Chem. Soc.* **2005**, 127, 18222-18228.
77. Baker, E. S.; Manard, M. J.; Gidden, J.; Bowers, M. T., Structural analysis of metal interactions with the dinucleotide duplex, dCG*dCG, using ion mobility mass spectrometry. *J. Phys. Chem. B* **2005**, 109, 4808-4810.
78. Gidden, J.; Bowers, M. T., Gas-phase conformations of deprotonated and protonated mononucleotides determined by ion mobility and theoretical modeling. *J. Phys. Chem. B* **2003**, 107, 12829-12837.
79. Gidden, J.; Bushnell, J. E.; Bowers, M. T., Gas-phase conformations and folding energetics of oligonucleotides: dTG- and dGT-. *J. Am. Chem. Soc.* **2001**, 123, 5610-5611.
80. Myung, S.; Fioroni, M.; Julian, R. R.; Koeniger, S. L.; Baik, M.-H.; Clemmer, D. E., Chirally directed formation of nanometer-scale proline clusters. *J. Am. Chem. Soc.* **2006**, 128, 10833-10839.
81. Wytenbach, T.; Witt, M.; Bowers, M. T., On the question of salt bridges of cationized amino acids in the gas phase: Glycine and arginine. *Int. J. Mass Spectrom.* **1999**, 182/183, 243-252.
82. Cooks, R. G.; Patrick, J. S.; Kotiaho, T.; McLuckey, S. A., Thermokinetic determination by kinetic method. *Mass Spectrom. Rev.* **1994**, 13, 287-339.
83. Cooks, R. G.; Wong, P. S. H., Kinetic method of making thermochemical determinations: advances and applications. *Acc. Chem. Res.* **1998**, 31, 379-386.

84. Cerda, B. A.; Wesdemiotis, C., Li⁺, Na⁺, and K⁺ binding to the DNA and RNA nucleobases. Bond energies and attachment sites from the dissociation of metal ion-bound heterodimers. *J. Am. Chem. Soc.* **1996**, 118, 11884-11892.
85. Cerda, B. A.; Hoyau, S.; Ohanessian, G.; Wesdemiotis, C., Na⁺ binding to cyclic and linear dipeptides. Bond energies, entropies of Na⁺ complexation, and attachment sites from the dissociation of Na⁺-bound heterodimers and ab initio calculations. *J. Am. Chem. Soc.* **1998**, 120, 2437-2448.
86. Cerda, B. A.; Wesdemiotis, C., Zwitterionic vs. charge-solvated structures in the binding of arginine to alkali metal ions in the gas phase. *Analyst* **2000**, 125, 657-660.
87. Cerda, B. A.; Wesdemiotis, C., The relative copper (I) ion affinities of amino acids in the gas phase. *J. Am. Chem. Soc.* **1995**, 117, 9734-9739.
88. Brodbelt, J. S., Analytical applications of ion-molecule reactions. *Mass Spec. Rev.* **1997**, 16, 91-110.
89. Vachet, R. W.; Callahan, J. H., Quadrupole ion trap studies of the structure and reactivity of transition metal ion pair complexes. *J. Mass Spectrom.* **2000**, 35, 311-320.
90. Vachet, R. W.; Hartman, J. A. R.; Callahan, J. H., Ion-molecule reactions in a quadrupole ion trap as a probe of the gas-phase structure of metal complexes. *J. Mass Spectrom.* **1998**, 33, 1209-1225.
91. Vachet, R. W.; Hartman, J. A. R.; Gertner, J. W.; Callahan, J. H., Investigation of metal complex coordination structure using collision-induced dissociation and ion-molecule reactions in a quadrupole ion trap mass spectrometer. *Int. J. Mass Spectrom.* **2001**, 204, 101-112.
92. O'Hair, R. A. J.; Vrkic, A. K.; James, P. F., Gas-phase synthesis and reactivity of the organomagnesates [CH₃MgL₂]⁻ (L=Cl and O₂CCH₃): from ligand effects to catalysis. *J. Am. Chem. Soc.* **2004**, 126, 12173-12183.
93. Gronert, S., Mass spectrometric studies of organic ion/molecule reactions. *Chem. Rev.* **2001**, 101, 329-360.
94. Combariza, M. Y.; Vachet, R. W., The utility of ion-molecule reactions in a quadrupole ion trap mass spectrometer for analyzing metal complex coordination structure. *Analytica Chimica Acta* **2003**, 496, 233-248.

95. Gronert, S.; Huang, R., A strong preference for a salt-bridge structure in the gas phase: reactions of deprotonated amino acids with borane. *J. Am. Chem. Soc.* **2001**, *123*, 8606-8607.
96. Julian, R. R.; Hodyss, R.; Beauchamp, J. L., Salt bridge stabilization of charged zwitterionic arginine aggregates in the gas phase. *J. Am. Chem. Soc.* **2001**, *123*, 3577-3583.
97. Petzold, C. J.; Leavell, M. D.; Leary, J. A., Screening and identification of acidic carbohydrates in bovine colostrum by using ion/molecule reactions and Fourier transform ion cyclotron resonance mass spectrometry: specificity toward phosphorylated complexes. *Anal. Chem.* **2004**, *76*, 203-210.
98. Gapeev, A.; Dunbar, R. C., Cation-pi interactions and the gas-phase thermochemistry of the Na⁺/phenylalanine complex. *J. Am. Chem. Soc.* **2001**, *123*, 8360-8365.
99. Gapeev, A.; Dunbar, R. C., Na⁺ affinities of gas-phase amino acids by ligand exchange equilibrium. *Int. J. Mass Spectrom.* **2003**, *228*, 825-839.
100. Amicangelo, J. C.; Armentrout, P. B., Ligand exchange reactions of sodium cation complexes examined using guided ion beam mass spectrometry: relative and absolute dissociation free energies and entropies. *J. Phys. Chem. A* **2004**, *108*, 10698-10713.
101. Veenstra, T. D., Electrospray ionization mass spectrometry in the study of biomolecular non-covalent interactions. *Biophys. Chem.* **1999**, *79*, 63-79.
102. Lemoff, A. S. B., M.F.; Williams, E.R., Binding energies of water to sodiated valine and structural isomers in the gas phase: The effect of proton affinity on zwitterion stability. *J. Am. Chem. Soc.* **2003**, *125*, 13576-13584.
103. Wytenbach, T.; Witt, M.; Bowers, M. T., On the stability of amino acid zwitterions in the gas phase: The influence of derivatization, protein affinity, and alkali ion addition. *J. Am. Chem. Soc.* **2000**, *122*, 3458-3464.
104. Strittmatter, E. F.; Lemoff, A. S.; Williams, E. R., Structure of cationized glycine, Gly-M₂⁺ (M=Be, Mg, Ca, Sr, Ba), in the gas phase: Intrinsic effect on cation size on zwitterion stability. *J. Phys. Chem. A* **2000**, *104*, 9793-9796.
105. Ramek, M.; Nagy, P. I., Theoretical investigation of the neutral/zwitterionic equilibrium of γ -aminobutyric acid (GABA) conformers in aqueous solution. *J. Phys. Chem. A* **2000**, *104*, 6844-6854.

106. Nagy, P. I.; Noszal, B., Theoretical study of the tautomeric/conformational equilibrium of aspartic acid zwitterions in aqueous solution. *J. Phys. Chem. A* **2000**, *104*, 6834-6843.
107. Ahn, D.-S.; Park, S.-W.; Jeon, I.-S.; Lee, M.-K.; Kim, N.-H.; Han, Y.-H.; Lee, S., Effects of microsolvation on the structures and reactions of neutral and zwitterion alanine: Computational study. *J. Phys. Chem. B* **2003**, *107*, 14109-14118.
108. Julian, R. R.; Beauchamp, J. L.; Goddard, W. A., Cooperative salt bridge stabilization of gas-phase zwitterions in neutral arginine clusters. *J. Phys. Chem. A* **2002**, *106*, 32-34.
109. Feng, W. Y.; Gronert, S.; Lebrilla, C., The lithium cation binding energies of gaseous amino acids. *J. Phys. Chem. A* **2003**, *107*, 405-410.
110. Marino, T.; Russo, N.; Toscano, M., Interaction of Li⁺, Na⁺, and K⁺ with the proline amino acid. Complexation modes, potential energy profiles, and metal ion affinities. *J. Phys. Chem. B* **2003**, *107*, 2588-2594.
111. Kish, M. M.; Ohanessian, G.; Wesdemiotis, C., The Na⁺ affinities of α -amino acids: Side-chain substituent effects. *Int. J. Mass Spectrom.* **2003**, *227*, 509-524.
112. Bertran, J.; Rodriguez-Santiago, L.; Sodupe, M., The different nature of bonding in Cu⁺-glycine and Cu²⁺-glycine. *J. Phys. Chem. B* **1999**, *103*, 2310-2317.
113. Marino, T.; Russo, N.; Toscano, M., Gas-phase metal ion (Li⁺, Na⁺, Cu⁺) affinities of glycine and alanine. *J. Inorg. Biochem.* **2000**, *79*, 179-185.
114. Wyttenbach, T.; Kemper, P. R.; Bowers, M. T., Design of a new electrospray ion mobility mass spectrometer. *Int. J. Mass Spectrom.* **2001**, *212*, 13-23.
115. Lee, S.; Wyttenbach, T.; Bowers, M. T., Gas phase structures of sodiated oligosaccharides by ion mobility/ion chromatography methods. *Int. J. Mass Spectrom.* **1997**, *167/168*, 605-614.
116. Baker, E. S.; Manard, M. J.; Gidden, J.; Bowers, M. T., Structural analysis of metal interactions with the dinucleotide duplex, dCG*dCG, using ion mobility mass spectrometry. *J. Phys. Chem. B* **2005**, *109*, 4808-4810.
117. Lemoff, A. S.; Bush, M. F.; Wu, C.-C.; Williams, E. R., Structures and hydration enthalpies of cationized glutamine and structural analogues in the gas phase. *J. Am. Chem. Soc.* **2005**, *127*, 10276-10286.

118. Lemoff, A. S.; Williams, E. R., Binding energies of water to lithiated valine: Formation of solution-phase structure in vacuo. *J. Am. Soc. Mass. Spectrom.* **2004**, *15*, 1014-1024.
119. Mohajeri, A.; Karimi, E., AIM and NBO analysis of cation- π interaction. *J. Mol. Struct. (Theochem)* **2006**, *774*, 71-76.
120. Rooman, M.; Lievin, J.; Buisine, E.; Wintjens, R., Cation- π /H-bond stair motifs at protein-DNA interfaces. *J. Mol. Biol.* **2002**, *319*, 67-76.
121. Anderson, M. A.; Ogbay, B.; Arimoto, R.; Sha, W.; Kisselev, O. G.; Cistola, D. P.; Marshall, G. R., Relative strength of cation- π vs. salt-bridge interactions: The Gta(340-360) peptide/rhodopsin system. *J. Am. Chem. Soc.* **2006**, *128*, 7531-7541.
122. Minoux, H.; Chipot, C., Cation- π interactions in proteins: can simple models provide an accurate description? *J. Am. Chem. Soc.* **1999**, *121*, 10366-10372.
123. Mecozzi, S.; West, J., A.P.; Dougherty, D. A., Cation- π interactions in aromatics of biological and medicinal interest: Electrostatic potential surfaces as a useful qualitative guide. *Proc. Natl. Acad. Sci. USA* **1996**, *93*, 10566-10571.
124. Meadows, E. S.; De Wall, S. L.; Barbour, L. J.; Gokel, G. W., Alkali metal cation- π interactions observed by using a lariat ether model system. *J. Am. Chem. Soc.* **2001**, *123*, 3092-3107.
125. Gallivan, J. P.; Dougherty, D. A., Cation- π interactions in structural biology. *Proc. Natl. Acad. Sci. USA* **1999**, *96*, 9459-9464.
126. Gromiha, M. M., Influence on cation- π interactions in different folding types of membrane proteins. *Biophys. Chem.* **2003**, *103*, 251-258.
127. DiNitto, J. P.; Huber, P. W., A role for aromatic amino acids in the binding of *Xenopus* ribosomal protein L5 to 5S rRNA. *Biochemistry* **2001**, *40*, 12645-12653.
128. Wintjens, R.; Lievin, J.; Rooman, M.; Buisine, E., Contribution of cation- π interactions to the stability of protein-DNA complexes. *J. Mol. Biol.* **2000**, *302*, 395-410.
129. Williams, K.; Pahk, A. J.; Kashiwagi, K.; Masuko, T.; Nguyen, N. D.; Igarashi, K., The selectivity filter of the N-Methyl-D-Aspartate receptor: A tryptophan residue controls block and permeation of Mg^{2+} . *Mol. Pharmacol.* **1998**, *53*, 933-941.

130. Ryzhov, V.; Dunbar, R. C.; Cerda, B.; Wesdemiotis, C., Cation- π effects in the complexation of Na^+ and K^+ with Phe, Tyr, and Trp in the gas phase. *J. Am. Soc. Mass. Spectrom.* **2000**, 11, 1037-1046.
131. Gokel, G. W.; Barbour, L. J.; De Wall, S. L.; Meadows, E. S., Macrocyclic polyethers as probes to assess and understand alkali metal cation- π interactions. *Coord. Chem. Rev.* **2001**, 222, 127-154.
132. Burley, S. K.; Petsko, G. A., Amino-aromatic interactions in proteins. *FEBS* **1986**, 203, 139-143.
133. Gronert, S., Estimation of effective ion temperatures in a quadrupole ion trap. *J. Am. Soc. Mass. Spectrom.* **1998**, 8, 845-848.
134. Dunbar, R. C.; Petrie, S., Magnesium monocationic complexes: A theoretical study of metal ion binding energies and gas-phase association kinetics. *J. Phys. Chem. A* **2005**, 109, 1411-1419.
135. Siu, F. M.; Ma, N. L.; Tsang, C. W., Cation- π interactions in sodiated phenylalanine complexes: Is phenylalanine in the charge-solvated or zwitterionic form? *J. Am. Chem. Soc.* **2001**, 123, (3397-3398).
136. Remko, M.; Rode, B. M., Effect of metal ions (Li^+ , Na^+ , K^+ , Mg^{2+} , Ca^{2+} , Ni^{2+} , Cu^{2+} , and Zn^{2+}) and water coordination on the structure of glycine and zwitterionic glycine. *J. Phys. Chem. A* **2006**, 110, 1960-1967.
137. Rulisek, L.; Havlas, Z., Theoretical studies of metal ion selectivity. 1. DFT calculations of interaction energies of amino acid side chains with selected transition metal ions (Co^{2+} , Ni^{2+} , Cu^{2+} , Zn^{2+} , Cd^{2+} , and Hg^{2+}). *J. Am. Chem. Soc.* **2000**, 122, 10428-10439.
138. Rulisek, L.; Havlas, Z., Theoretical studies of metal ion selectivity. 3. A theoretical design of the most specific combinations of functional groups representing amino acid side chains for the selected metal ions (Co^{2+} , Ni^{2+} , Cu^{2+} , Zn^{2+} , Cd^{2+} , and Hg^{2+}). *J. Phys. Chem. B* **2003**, 107, 2376-2385.
139. Julian, R. R.; Jarrold, M. F., Gas-phase zwitterions in the absence of a net charge. *J. Phys. Chem. A* **2004**, 108, 10861-10864.
140. Zhang, S.-L.; Liu, L.; Fu, Y.; Guo, Q.-X., Cation- π interactions of Cu^+ . *Theochem* **2005**, 757, 37-46.
141. Foresman, J. B.; Frisch, A., *Exploring Chemistry with Electronic Structure Methods*. Second ed.; Gaussian, Inc.: Pittsburgh, 1996.

142. Gutowski, M.; Skurski, P.; Simons, J., Dipole-bound anions of glycine based on the zwitterion and neutral structures. *J. Am. Chem. Soc.* **2000**, 122, (10159-10162).
143. Jockusch, R. A.; Lemoff, A. S.; Williams, E. R., Hydration of valine-cation complexes in the gas phase: On the number of water molecules necessary to form a zwitterion. *J. Phys. Chem. A* **2001**, 105, 10929-10942.
144. Gronert, S., Gas phase studies of the competition between substitution and elimination reactions. *Acc. Chem. Res.* **2003**, 36, 848-857.
145. Antoine, R.; Broyer, M.; Dugourd, P.; Breaux, G.; Hagemester, F. C.; Pippen, D.; Hudgins, R. R.; Jarrold, M. F., Direct probing of zwitterion formation in unsolvated peptides. *J. Am. Chem. Soc.* **2003**, 125, 8996-8997.
146. Talley, J. M.; Cerda, B. A.; Ohanessian, G.; Wesdemiotis, C., Alkali metal ion binding to amino acids vs. their methyl esters. Affinity trends and structural changes. *Chem. Eur. J.* **2002**, 8, 1377-1388.
147. Pletneva, E. V.; Laederach, A. T.; Fulton, D. B.; Kostic, N. M., The role of cation- π interactions in biomolecular association. Design of peptides favoring interactions between cationic and aromatic amino acid side chains. *J. Am. Chem. Soc.* **2001**, 123, 6232-6245.
148. Rimola, A.; Sodupe, M.; Tortajada, J.; Rodriguez-Santiago, L., Gas phase reactivity of Cu^+ -aromatic amino acids. An experimental and theoretical study. *Int. J. Mass Spectrom.* **2006**, 257, 60-69.
149. Reddy, A. S.; Sastry, G. N., Cation [$\text{M} = \text{H}^+$, Li^+ , Na^+ , K^+ , Ca^{2+} , Mg^{2+} , NH_4^+ , and NMe_4^+] interactions with the aromatic motifs of naturally occurring amino acids: a theoretical study. *J. Phys. Chem. A* **2005**, 109, 8893-8903.
150. Gallivan, J. P.; Dougherty, D. A., A computational study of cation- π interactions vs. salt bridges in aqueous media: implications for protein engineering. *J. Am. Chem. Soc.* **2000**, 122, 870-874.
151. Olson, C. A.; Shi, Z.; Kallenbach, N. R., Polar interactions with aromatic side chains in alpha-helical peptides: $\text{CH}\cdots\text{OH}$ bonding and cation- π interactions. *J. Am. Chem. Soc.* **2001**, 123, 6451-6452.
152. Aliste, M. P.; MacCallum, J. L.; Tieleman, D. P., Molecular dynamics simulations of pentapeptides at interfaces: salt bridge and cation- π interactions. *Biochemistry* **2003**, 42, 8976-8987.

153. Sulpizi, M.; Carloni, P., Cation- π versus OH- π interactions in proteins: a density functional study. *J. Phys. Chem. B* **2000**, 104, 10087-10091.
154. Gromiha, M. M.; Parry, D. A. D., Characteristic features of amino acid residues in coiled-coil protein structures. *Biophys. Chem.* **2004**, 111, 95-103.
155. Moision, R. M.; Armentrout, P. B., The special five-membered ring of proline: An experimental and theoretical investigation of alkali metal cation interactions with proline and its four- and six-membered ring analogues. *J. Phys. Chem. A* **2006**, 110, 3933-3946.
156. De Wall, S. L.; Meadows, E. S.; Barbour, L. J.; Gokel, G. W., Solution- and solid-state evidence for alkali metal cation- π interactions with indole, the side chain of tryptophan. *J. Am. Chem. Soc.* **1999**, 121, 5613-5614.
157. Singha, A.; Dasgupta, S.; Roy, A., Comparison of metal-amino acid interaction in Phe-Ag and Tyr-Ag complexes by spectroscopic measurements. *Biophys. Chem.* **2006**, 120, 215-224.
158. Shoeib, T.; Cunje, A.; Hopkinson, A. C.; Siu, K. W. M., Gas-phase fragmentation of the Ag⁺-Phenylalanine complex: Cation- π interactions and radical cation formation. *J. Am. Soc. Mass. Spectrom.* **2002**, 13, 408-416.
159. Gronert, S., Determine the gas-phase properties and reactivities of multiply charged ions. *J. Mass Spectrom.* **1999**, 34, 787-796.
160. Miller, K. J.; Savchik, J. A., A new empirical method to calculate average molecular polarizabilities. *J. Am. Chem. Soc.* **1979**, 101, 7206-7213.
161. Ma, J. C.; Dougherty, D. A., The cation- π interaction. *Chem. Rev.* **1997**, 97, 1303-1324.
162. Butterfield, S. M.; Patel, P. R.; Waters, M. L., Contribution of aromatic interactions to α -helix stability. *J. Am. Chem. Soc.* **2002**, 124, 9751-9755.
163. Andrew, C. D.; Bhattacharjee, S.; Kokkoni, N.; Hirst, J. D.; Jones, G. R.; Doig, A. J., Stabilizing interactions between aromatic and basic side chains in α -helical peptides and proteins. Tyrosine effects on helix circular dichroism. *J. Am. Chem. Soc.* **2002**, 124, 12706-12714.
164. Watanabe, T.; Ariga, Y.; Sato, U.; Toratani, T.; Hashimoto, M.; Nikaidou, N.; Kezuka, Y.; Nonaka, T.; Sugiyama, J., Aromatic residues within the substrate-binding cleft of *Bacillus circulans* chitinase A1 are essential for hydrolysis of crystalline chitin. *Biochem. J.* **2003**, 376, 237-244.

165. Schmitt, J. D.; Sharples, C. G. V.; Caldwell, W. S., Molecular recognition in nicotinic acetylcholine receptors: The importance of pi-cation interactions. *J. Med. Chem.* **1999**, 42, 3066-3074.
166. Rotem, D.; Steiner-Murdoch, S.; Schuldiner, S., Identification of tyrosine residues critical for the function of an ion-coupled multidrug transporter. *J. Biol. Chem.* **2006**, 281, 18715-18722.
167. Sujatha, M. S.; Sasidhar, Y. U.; Balaji, P. V., Energetics of galactose- and glucose-aromatic amino acid interactions: Implications for binding in galactose-specific proteins. *Protein Sci.* **2004**, 13, 2502-2514.
168. Koeppe, I., R.E.; Hatchett, J.; Jude, A. R.; Providence, L. L.; Andersen, O. S.; Greathouse, D. V., Neighboring aliphatic/aromatic side chain interactions between residues 9 and 10 in gramicidin channels. *Biochemistry* **2000**, 39, 2235-2242.
169. Cui, L.; Aleksandrov, L.; Hou, Y.-X.; Gentzsch, M.; Chen, J.-H.; Riordan, J. R.; Aleksandrov, A. A., The role of cystic fibrosis transmembrane conductance regulator phenylalanine 508 side chain in ion channel gating. *J. Physiol.* **2006**, 572, 347-358.
170. Tan, J.; Liu, Z.; Wang, R.; Huang, Z. Y.; Chen, A. C.; Gurevitz, M.; Dong, K., Identification of amino acid residues in the insect sodium channel critical for pyrethroid binding. *Mol. Pharmacol.* **2005**, 67, 513-522.
171. Elton, D.; Medcalf, L.; Bishop, K.; Harrison, D.; Digard, P., Identification of amino acid residues of influenza virus nucleoprotein essential for RNA binding. *J. Virol.* **1999**, 73, 7357-7367.
172. Deng, Z.; Chen, C.-J.; Zerby, D.; Delecluse, H.-J.; Lieberman, P. M., Identification of acidic and aromatic residues in the Zta activation domain essential for Epstein-Barr virus reactivation. *J. Virol.* **2001**, 75, 10334-10347.
173. Lummis, S. C. R.; Beene, D. L.; Harrison, N. J.; Lester, H. A.; Dougherty, D. A., A cation-pi binding interaction with a tyrosine in the binding site of the GABA_A receptor. *Chem. Biol.* **2005**, 12, 993-997.
174. Ikuta, S., A theoretical study on the conformations and energetics on the cation-pi interaction between monovalent ions ($M^+=Li^+, Na^+, \text{ and } K^+$) and anthracene and phenanthrene molecules. *J. Mol. Struct. (Theochem)* **2000**, 530, 201-207.

175. Hashimoto, S.; Ikuta, S., A theoretical study on the conformations, energetics, and solvation effects on the cation- π interaction between monovalent ions Li^+ , Na^+ , and K^+ and naphthalene molecules. *J. Mol. Struct. (Theochem)* **1999**, 468, 85-94.
176. Cheng, Y.-H.; Liu, L.; Fu, Y.; Chen, R.; Li, X.-S.; Guo, Q.-Y., Counterion effects on the cation- π interaction between alkaline earth cations and benzene. *J. Phys. Chem. A* **2002**, 106, 11215-11220.
177. Ruan, C.; Rodgers, M. T., Cation- π interactions: structures and energetics of complexation of Na^+ and K^+ with the aromatic amino acids, phenylalanine, tyrosine, and tryptophan. *J. Am. Chem. Soc.* **2004**, 126, 14600-14610.
178. Dunbar, R. C., Complexation of Na^+ and K^+ to aromatic amino acids: A density functional computational study of cation- π interactions. *J. Phys. Chem. A* **2000**, 104, (8067-8074).
179. Keesee, R. G.; Castleman, A. W., Jr., Thermochemical Data on the Formation of Ion Clusters. *J. Phys. Chem. Ref. Data* **1986**, 15, 1012-1070.
180. Navarro, M.; Cisneros-Fajardo, E. J.; Marchan, E., New silver polypyridyl complexes: synthesis, characterization and biological activity on *Lershmania mexicana*. *Arzneimittelforschung* **2006**, 56, 600-604.
181. Liu, T.; Nakashima, S.; Hirose, K.; Shibasaka, M.; Katsuhara, M.; Ezaki, B.; Giedroc, D. P.; Kasamo, K., A novel cyanobacterial SmtB/ArsR family repressor regulates the expression of a CPx-ATPase and a metallothionein in response to both Cu(I)/Ag(I) and Zn (II)/Cd(II) . *J. Biol. Chem.* **2004**, 279, 17810-17818.
182. Mehra, R. K.; Tran, K.; Scott, G. W.; Mulchandari, P.; Saini, S. S., Ag(I) -binding to phytocheletins. *J. Inorg. Biochem.* **1996**, 61, 125-142.
183. Shen, X. C.; Liang, H.; Guo, J. H.; Song, C.; He, X. W.; Yuan, Y. Z., Studies on the interaction between Ag(+) and human serum albumin. *J. Inorg. Biochem.* **2003**, 95, 124-130.
184. Li, H.; Otvos, J. D., ^{111}Cd NMR studies of the domain specificity of Ag^+ and Cd^+ binding to metallothionein. *Biochemistry* **1996**, 35, 13929-13936.
185. Li, H.; Otvos, J. D., HPLC characterization of Ag^+ and Cu^+ metal exchange reactions with Zn- and Cd- metallothioneins. *Biochemistry* **1996**, 35, 13937-13945.

186. Lee, H. S.; Nam, Y. S., Immunohistochemical location of calcium binding proteins and some neurotransmitters in myenteric plexus of goat stomach. *J. Vet. Sci.* **2006**, *7*, 315-319.
187. Rajkowska, G.; O'dwyer, G.; Teleki, Z.; Stockmeier, C. A.; Miguel-Hidalgo, J. J., GABAergic neurons immunonegative for calcium binding proteins are reduced in prefrontal cortex in major depression. *Neuropsychopharmacology* **2006**, [Epub ahead of print].
188. Lee, O. J.; Hong, S. M.; Razui, M. H.; Peng, D.; Powell, S. M.; Smoklin, M.; Moskaluk, C. A.; El-Rifai, W., Expression of calcium-binding proteins S100A2 and S100A4 in Barrett's adenocarcinomas. *Neoplasia*. **2006**, *8*, 843-850.
189. Sturchler, E.; Cox, J. A.; Durussel, I.; Weibel, M.; Heizmann, C. W., S100A16, a novel calcium-binding protein of the EF-hand superfamily. *J. Biol. Chem.* **2006**, [Epub ahead of print].
190. Yoshida, T.; Matsuda, H.; Yamamoto, Y.; Hayashida, Y.; Tsiukuda, M.; Kusakabe, T., Chronic hypoxia alters calbindin D-28k immunoreactivity in lingual and laryngeal taste buds in the rat. *Histol Histopathol.* **2006**, *21*, 1271-1276.
191. Selke, K.; Muller, A.; Kukley, M.; Schramm, J.; Dietrich, D., Firing pattern and calbindin-D(28k) content of human epileptic granule cells. *Brain Res.* **2006**, *1120*, 191-210.
192. Lambers, T. T.; Mahieu, F.; Oancia, E.; Hoofd, L.; de Lange, F.; Mensenkamp, A. R.; Voets, T.; Nilius, B.; Clapham, D. E.; Hoenderop, J. G.; Bindels, R. J., Calbindin-D28k dynamically controls TRPV5-mediated Ca²⁺ transport. *EMBO J.* **2006**, *25*, 2978-2988.
193. Ohashi, K.; Yamazaki, T.; Kitamura, S.; Ohta, S.; Izumi, S.; Koninami, S., Allosteric inhibition of rat neuronal nitric-oxide synthase caused by interference with the binding of calmodulin to the enzyme. *Biochem. Biophys. Acta* **2006**, [Epub ahead of print].
194. Friedberg, F., Centrin isoforms in mammals. Relation to calmodulin. *Mol. Biol. Rep.* **2006**, *33*, 243-252.
195. Shen, W. G.; Peng, W. X.; Dai, G.; Xu, J. F.; Zhang, Y.; Li, C. J., Calmodulin is essential for angiogenesis in response to hypoxic stress in endothelial cells. *Cell Biol. Int.* **2006**, [Epub ahead of print].

196. Vongvatcharanon, U.; Imsunpang, S.; Promwikorn, W.; Vongvatcharanon, S., Up-regulation of parvalbumin expression in newborn and adult rat heart. *Acta Histochem.* **2006**, 108, 447-454.
197. Zhao, J.; Nelson, D. J.; Huo, S., Potential influence of Asp in the Ca(2+) coordination position 5 of parvalbumin on the calcium-binding affinity: A computational study. *J. Inorg. Biochem.* **2006**, 100, 1879-1887.
198. Pantazopoulos, H.; Lange, N.; Baldessarini, R. J.; Berretta, S., Parvalbumin neurons in the entorhinal cortex of subjects diagnosed with bipolar disorder or schizophrenia. *Biol. Psychiatry* **2006**, [Epub ahead of print].
199. McDonough, S. I., Gating modifier toxins of voltage-gated calcium channels. *Toxicon.* **2006**, [Epub ahead of print].
200. Field, M. J.; Cox, P. J.; Stott, E.; Melrose, H.; Offord, J.; Su, T. Z.; Bromwell, S.; Corradini, L.; England, S.; Winks, J.; Kinloch, R. A.; Hendrich, J.; Dolphin, A. C.; Webb, T.; Williams, D., Identification of the $\alpha_2\text{-}\delta_1$ subunit of voltage-dependent calcium channels as a molecular target for pain mediating the analgesic actions of pregabalin. *Proc. Natl. Acad. Sci. USA* **2006**, 103, 17537-17542.
201. Seu, L.; Pitt, G. S., Dose-dependent and isoform-specific modulation of Ca²⁺ channels by RGK GTPases. *J. Gen. Physiol.* **2006**, 128, 605-613.
202. Murphey, E.; Bassett, J. H.; Williams, G. R., Disorders of calcium metabolism. *Practitioner* **2006**, 250, 4-6,8.
203. Gal-Moscovici, A.; Sprague, S. M., The role of calcimimetics in chronic kidney disease. *Kidney Int.* **2006**, 70, 568-572.
204. Ersay, F. F., Osteoporosis in the elderly with chronic kidney disease. *Int. Urol. Nephrol.* **2006**, [Epub ahead of print].
205. Moe, S. M., Vascular calcification and renal osteodystrophy relationship in chronic kidney disease. *Eur. J. Clin. Invest.* **2006**, 36, Suppl 2: 51-62.
206. Corbetta, S.; Eller-Vainicher, C.; Filopanti, M.; Sueli, P.; Vezzoli, G.; Arcidiacono, T.; Loli, P.; Syren, M. L.; Soldati, L.; Beck-Peccoz, P.; Spada, A., R990G polymorphism of the calcium-sensing receptor and renal calcium excretion in patients with hyperparathyroidism. *Eur. J. Endocrinol.* **2006**, 155, 687-692.

207. Erbil, Y.; Ademoglu, E.; Ozbey, N.; Issever, H., Reply-correlations between vitamin D status and biochemical/clinical and pathological parameters in primary hyperparathyroidism. *World J. Surg.* **2006**, [Epub ahead of print].
208. Scillitani, A.; Guarnieri, V.; Battista, C.; De Geronimo, S.; Moscarella, L. A.; Chiadini, I.; Cignarelli, M.; Minisola, S.; Bertoldo, F.; Francucci, C. M.; Malavolta, N.; Piovesan, A.; Lucia Mascia, M.; Muscarella, S.; Hendy, G. N.; D'Agruma, L.; Cole, D. E., Primary hyperparathyroidism and the presence of kidney stones are associated with different haplotypes of the calcium-sensing receptor. *J. Clin. Endocrinol. Metab.* **2006**, [Epub ahead of print].
209. Cheskis, B. J.; Freedman, L. P.; Nagpal, S., Vitamin D receptor ligands for osteoporosis. *Curr. Opin. Investig. Drugs* **2006**, *7*, 906-911.
210. Ralston, S. H.; de Crombrughe, B., Genetic regulation of bone mass and susceptibility to osteoporosis. *Genes Dev.* **2006**, *20*, 2492-2506.
211. Holick, M. F., The role of vitamin D for bone health and fracture prevention. *Curr. Osteoporos. Rep.* **2006**, *4*, 96-102.
212. Nicolaidou, P.; Papadopoulou, A.; Matsinos, Y. G.; Georgouli, H.; Fretzayas, A.; Papadimitriou, A.; Priftis, K.; Douros, K.; Chrousos, G. P., Vitamin D receptor polymorphisms in hypocalcemic vitamin D-resistant rickets carriers. *Horm. Res.* **2006**, *67*, 179-183.
213. Holick, M. E., Resurrection of vitamin D deficiency and rickets. *J. Clin. Invest.* **2006**, *116*, 2062-2072.
214. Yellappa, S.; Seetharamappa, J.; Rogers, L. M.; Chitta, R.; Singhal, R. P.; D'Souza, F., Binding, electrochemical activation, and cleavage of DNA by cobalt (II) tetrakis-N-methyl pyridyl porphyrin and its beta-pyrrole brominated derivative. *Bioconjug. Chem.* **2006**, *17*, 1418-1425.
215. Badarou, A.; Page, M. I., Enzyme deactivation due to metal-ion dissociation during turnover of the cobalt-beta-lactamase hydrolysis of beta-lactams. *Biochemistry* **2006**, *12*, 11012-11020.
216. Scampellini, M.; Wu, A. J.; Kampf, J. W.; Pecoraro, V. L., Corroborative models of the cobalt (II) inhibited Fe/Mn superoxide dismutases. *Inorg. Chem.* **2005**, *44*, 5001-5010.
217. Angelini, N.; Micali, N.; Mineo, P.; Scamporrino, E.; Villari, V.; Vitalini, D., Uncharged water-soluble Co(II)-porphyrin: A receptor for aromatic alpha-amino acids. *J. Phys. Chem. B* **2005**, *109*, 18645-18651.

218. Scholten, U.; Merchan, A. C.; Bernaver, K., Electron-transfer-mediated binding of optically active cobalt (III) complexes to horse heart cytochrome C. *J. R. Soc. Interface.* **2005**, *2*, 109-112.
219. Liao, M. S.; Watts, J. D.; Huang, M. J., Effects of peripheral substituents and axial ligands on the electronic structure and properties of cobalt porphyrins. *J. Phys. Chem. A* **2005**, *109*, 11996-12005.
220. Frank, A.; McPartlin, J.; Danielsson, R., Nova Scotia moose mystery -- a mouse sickness related to cobalt- and vitamin B12 deficiency. *Sci. Total Environ.* **2004**, *318*, 89-100.
221. Kapadia, C. R., Vitamin B12 in health and disease: part I --inherited disorders of function, adsorption, and transport *Gastroenterologist* **1995**, *3*, 329-344.
222. Flippo, T. S.; Holder, W. D., Jr., Neurologic degeneration associated with nitrous oxide on anesthesia in patients with vitamin B12 deficiency. *Arch. Surg.* **1993**, *128*, 1351-1355.
223. Cubine, P. A.; Pierrel, F.; Winge, D. R., Copper trafficking to the mitochondrion and assembly of copper metalloenzymes. *Biochem. Biophys. Acta* **2006**, *1763*, 759-772.
224. Abajian, C.; Yatsunyk, L. A.; Ramirez, B. E.; Rosenzweig, A. C., Yeast cox17 solution structure and copper (I) binding. *J. Biol. Chem.* **2004**, *279*, 53584-53592.
225. Rosenzweig, A. C.; Sazinsky, M. H., Structural insights into dioxxygen-activating copper enzymes. *Curr. Opin. Struct. Biol.* **2006**, [Epub ahead of print].
226. Shleev, S.; Tkac, J.; Christenson, A.; Ruzgas, T.; Yaropolov, A. I.; Whittaker, J. W.; Gorton, L., Direct electron transfer between copper-containing proteins and electrodes. *Biosens. Bioelectron.* **2005**, *20*, 2517-2554.
227. Bianke, G.; Chaurin, V.; Egorov, M.; Lebreton, J.; Constable, E. C.; Housecroft, C. E.; Haner, R., Copper complex-assisted DNA hybridization. *Bioconjug. Chem.* **2006**, *17*, 1441-1446.
228. Cobine, P. A.; Pierrel, F.; Bestwick, M. L.; Winge, D. R., Mitochondrial matrix copper complex used in metallation of cytochrome oxidase and superoxide dismutase. *J. Biol. Chem.* **2006**, [Epub ahead of print].

229. Banci, L.; Bertini, I.; Ciofi-Baffoni, S.; Katsari, E.; Katsaros, N.; Kubicek, K.; Mangani, S., A copper (I) protein possibly involved in the assembly of CuA center of bacterial cytochrome c oxidase. *Proc. Natl. Acad. Sci. USA* **2005**, 102, 3994-3999.
230. Wilson, M. T.; Torres, J., Reactions of nitric oxide with copper containing oxidases; cytochrome c oxidase and laccase. *IUBMB Life* **2004**, 56, 7-11.
231. Matoba, Y.; Kumagai, T.; Yamamoto, A.; Yoshitsu, H.; Sugiyama, M., Crystallographic evidence that the dinuclear copper center of tyrosinase is flexible during catalysis. *J. Biol. Chem.* **2006**, 281, 8981-8990.
232. Park, K. H.; Park, Y. D.; Lee, J. R.; Hahn, H. S.; Lee, S. J.; Bae, C. D.; Yang, J. M.; Kim, D. E.; Hahn, M. J., Inhibition kinetics of mushroom tyrosinase by copper-chelating ammonium tetrathiomolybdate. *Biochem. Biophys. Acta* **2005**, 1726, 115-120.
233. Tepper, A. W.; Bubacco, L.; Canters, G. W., Interaction between the type-3 copper protein tyrosinase and the substrate analogue p-nitrophenol studied by NMR. *J. Am. Chem. Soc.* **2005**, 127, 567-575.
234. Ogra, Y.; Aoyama, M.; Suzuki, K. T., Protective role of metallothionein against copper depletion. *Arch. Biochem. Biophys.* **2006**, 451, 112-118.
235. Suntres, Z. E.; Liu, E. M., Prooxidative effect of copper-metallothionein in the acute cytotoxicity of hydrogen peroxide in Ehrlich ascites tumor cells. *Toxicology* **2006**, 217, 155-168.
236. Linde, A. R.; Klein, D.; Summer, K. H., Phenomenon of hepatic overload of copper in Mugil cephalus: role of metallothionein and patterns of copper cellular distribution. *Basic Clin. Pharmacol. Toxicol.* **2005**, 97, 230-235.
237. Hayashi, H.; Yano, M.; Fujita, Y.; Wakusawa, S., Compound overload of copper and iron in patients with Wilson's disease. *Med. Mol. Morphol.* **2006**, 39, 121-126.
238. Das, S. K.; Ray, K., Wilson's disease: An update. *Nat. Clin. Pract. Neurol.* **2006**, 2, 482-493.
239. Mufti, A. R.; Burstein, E.; Csomos, R. A.; Graf, P. C.; Wilkinson, J. C.; Dick, R. D.; Challar, M.; Son, J. K.; Bratton, S. B.; Su, G. L.; Brewer, G. J.; Jakob, U.; Duckett, C. S., XIAP is a copper binding protein deregulated in Wilson's disease and other copper toxicosis disorders. *Mol. Cell* **2006**, 21, 775-785.

240. Schlieff, M. L.; West, T.; Craig, A. M.; Holtzmann, D. M.; Gitlin, J. D., Role of Menkes copper-transporting ATPase in NMDA receptor-mediated neuronal toxicity. *Proc. Natl. Acad. Sci. USA* **2006**, 103, 14919-14924.
241. Lim, C. M.; Cater, M. A.; Mercer, J. F.; La Fontaine, S., Copper-dependent interaction of glutaredoxin with the N termini of the copper-ATPases (ATP7A and ATP7B) defective in Menkes and Wilsons diseases. *Biochem. Biophys. Res. Commun.* **2006**, 348, 428-436.
242. De Domenico, I.; Vaughn, M. B.; Li, L.; Bagley, D.; Musci, G.; Ward, D. M.; Kaplan, J., Ferroportin-mediated mobilization of ferritin iron precedes ferritin degradation by the proteasome. *EMBO J.* **2006**, 25, 5396-5404.
243. Thiel, E. C.; Matzapetakis, M.; Liu, X., Ferritins: iron/oxygen biominerals in protein nanocages. *J. Biol. Inorg. Chem.* **2006**, 11, 803-810.
244. Sakurai, K.; Nabeyama, A.; Fujimoto, Y., Ascorbate-mediated iron release from ferritin in the presence of alloxan. *Biomaterials* **2006**, 19, 323-33.
245. Curatti, L.; Ludden, P. W.; Rubio, L. M., NifB-dependent in vitro synthesis of the iron-molybdenum cofactor of nitrogenase. *Proc. Natl. Acad. Sci. USA* **2006**, 103, 5297-5301.
246. Peters, J. W.; Szilagyi, R. K., Exploring new frontiers of nitrogenase structure and mechanism. *Curr. Opin. Chem. Biol.* **2006**, 10, 101-108.
247. Sen, S.; Peters, J. W., The thermal adaptation of the nitrogenase Fe protein from the thermophilic *Methanobacter thermoautotrophicus*. *Proteins* **2006**, 62, 450-460.
248. Baltistuzzi, G.; Bellei, M.; De Rienzo, F.; Sola, M., Redox properties of the Fe³⁺/Fe²⁺ couple in *Arthromyces ramosus* class II peroxidase and its cyanide adduct. *J. Biol. Inorg. Chem.* **2006**, 11, 586-592.
249. Zhou, S.; Olson, J. S.; Fabian, M. W., M.J.; Gow, A. J., Biochemical rates of alpha hemoglobin bound to alpha hemoglobin-stabilizing protein AHSP. *J. Biol. Chem.* **2006**, 281, 32611-32618.
250. Smagghe, B. J.; Kundu, S.; Hoy, J. A.; Halder, P.; Wieland, T. R.; Savage, A.; Venugopal, A.; Goodman, M.; Premer, S.; Hargrove, M. S., Role of phenylalanine B10 in plant nonsymbiotic hemoglobins. *Biochemistry* **2006**, 15, 513-521.

251. Ajioka, R. S.; Phillips, J. D.; Kushner, J. P., Biosynthesis of heme in mammals. *Biochem. Biophys. Acta* **2006**, 1763, 723-736.
252. Mackenzie, B.; Takanaga, H.; Hubert, N.; Rolfs, A.; Hediger, M. A., Functional properties of multiple isoforms of the human divalent metal-ion transporter DMT1. *Biochem. J.* **2006**, [Epub ahead of print].
253. Antanasiu, V.; Manolescu, B.; Stoian, I., Hepcidin-central regulator of iron metabolism. *Eur. J. Haematol.* **2006**, [Epub ahead of print].
254. Ganz, T., Hepcidin -- a peptide hormone at the interface of innate immunity and iron metabolism. *Curr. Top. Microbiol. Immunol.* **2006**, 306, 183-198.
255. Nair, M.; Weiss, G., Molecular and clinical aspects of iron homeostasis: From anemia to hemochromatosis. *Wien. Klin. Wochenschr.* **2006**, 118, 442-462.
256. Liuzzi, J. P.; Aydemir, F.; Nam, H.; Knutson, M. D.; Cousins, R. J., Zip14 (slc39a14) mediates non-transferrin-bound iron uptake into cells. *Proc. Natl. Acad. Sci. USA* **2006**, 103, 13612-13617.
257. Goswami, T.; Andrews, N. C., Hereditary hemochromatosis protein, HFE, interaction with transferrin receptor 2 suggest a molecule mechanism for mammalian iron sensing. *J. Biol. Chem.* **2006**, 281, 28494-28498.
258. Stola, M.; Musiani, F.; Mangani, S.; Turano, P.; Safarov, N.; Zambelli, B.; Ciurli, S., The nickel site of *Bacillus pasteurii* UreE, a urease metallo-chaperone, as revealed by metal-binding studies and X-ray absorption spectroscopy. *Biochemistry* **2006**, 45, 6495-6509.
259. Belzer, C.; Stoof, J.; Beckwith, C. S.; Kuipers, E. J.; Kusters, J. G.; van Vlies, A. H., Differential regulation of urease activity in *Helicobacter hepaticus* and *Helicobacter pylori*. *Microbiology* **2005**, 151, 3989-3995.
260. Won, H. S.; Lee, B. J., Nickel-binding properties of the c-terminal tail peptide of *Bacillus pasteurii* UreE. *J. Biochem.* **2004**, 136, 635-641.
261. Bhatt, D.; Tu, C.; Fisher, S. Z.; Hernandez Prada, J. A.; McKenna, R.; Silverman, D. N., Proton transfer in a Thr200His mutant of human carbonic anhydrase II. *Proteins* **2005**, 61, 239-245.
262. Duda, D. M.; Tu, C.; Fisher, S. Z.; An, H.; Yoshioka, C.; Govindasany, L.; Laipis, P. J.; Agbandje-McKenna, M.; Silverman, D. N.; McKenna, R., Human carbonic anhydrase III: Structural and kinetic study of catalysis and proton transfer. *Biochemistry* **2005**, 44, 10046-10053.

263. Marino, T.; Russo, N.; Toscano, M., A comparative study of the catalytic mechanisms of the zinc and cadmium containing carbonic anhydrase. *J. Am. Chem. Soc.* **2005**, *127*, 4242-4253.
264. Gudiksen, K. L.; Urback, A. R.; Gitlin, I.; Yang, J. M.; Vazques, J. A.; Costello, C. E.; Whitesides, G. M., Influence of the Zn (II) cofactor on the refolding of bovine carbonic anhydrase after denaturation with sodium dodecyl sulfate. *Anal. Chem.* **2004**, *76*, 7151-7161.
265. Sanchez Garcia, J.; Ciufu, L. F.; Yang, X.; Kearsey, S. E.; MacNeill, S. A., The c-terminal zinc finger of the catalytic subunit of DNA polymerase delta is responsible for direct interaction with the b-subunit *Nucleic Acids Res.* **2004**, *32*, 3005-3016.
266. Frick, D. N.; Richardson, C. C., DNA primases. *Annu. Rev. Biochem.* **2001**, *70*, 39-80.
267. Barnes, M. H.; Leo, C. J.; Brown, N. C., DNA polymerase III of Gram-positive eubacteria is a zinc metalloprotein conserving an essential finger-like domain. *Biochemistry* **1998**, *37*, 15254-15260.
268. Leskovac, V.; Trivic, S.; Pericri, D., The three zinc-containing alcohol dehydrogenases from baker's yeast, *Saccharomyces cerevisiae*. *FEMS Yeast Res.* **2002**, *2*, 481-494.

APPENDIX A
THE AMINO ACIDS

Amino Acid	Abbreviation	Structure
Alanine	Ala	$ \begin{array}{c} \text{O} \\ \parallel \\ \text{H}_2\text{N}-\text{CH}-\text{C}-\text{OH} \\ \\ \text{CH}_3 \end{array} $
Arginine	Arg	$ \begin{array}{c} \text{O} \\ \parallel \\ \text{H}_2\text{N}-\text{CH}-\text{C}-\text{OH} \\ \\ \text{CH}_2 \\ \\ \text{CH}_2 \\ \\ \text{CH}_2 \\ \\ \text{NH} \\ \\ \text{C}=\text{NH} \\ \\ \text{NH}_2 \end{array} $
Asparagine	Asn	$ \begin{array}{c} \text{O} \\ \parallel \\ \text{H}_2\text{N}-\text{CH}-\text{C}-\text{OH} \\ \\ \text{CH}_2 \\ \\ \text{C}=\text{O} \\ \\ \text{NH}_2 \end{array} $
Aspartic Acid	Asp	$ \begin{array}{c} \text{O} \\ \parallel \\ \text{H}_2\text{N}-\text{CH}-\text{C}-\text{OH} \\ \\ \text{CH}_2 \\ \\ \text{C}=\text{O} \\ \\ \text{OH} \end{array} $

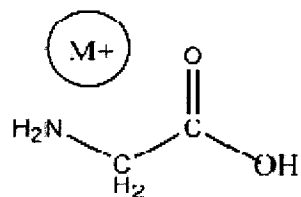
Cysteine	Cys	$\begin{array}{c} \text{O} \\ \parallel \\ \text{H}_2\text{N}-\text{CH}-\text{C}-\text{OH} \\ \\ \text{CH}_2 \\ \\ \text{SH} \end{array}$
Glutamine	Gln	$\begin{array}{c} \text{O} \\ \parallel \\ \text{H}_2\text{N}-\text{CH}-\text{C}-\text{OH} \\ \\ \text{CH}_2 \\ \\ \text{CH}_2 \\ \\ \text{C}=\text{O} \\ \\ \text{NH}_2 \end{array}$
Glutamic Acid	Glu	$\begin{array}{c} \text{O} \\ \parallel \\ \text{H}_2\text{N}-\text{CH}-\text{C}-\text{OH} \\ \\ \text{CH}_2 \\ \\ \text{CH}_2 \\ \\ \text{C}=\text{O} \\ \\ \text{OH} \end{array}$
Glycine	Gly	$\begin{array}{c} \text{O} \\ \parallel \\ \text{H}_2\text{N}-\text{CH}-\text{C}-\text{OH} \\ \\ \text{H} \end{array}$

Histidine	His	$\begin{array}{c} \text{O} \\ \parallel \\ \text{H}_2\text{N}-\text{CH}-\text{C}-\text{OH} \\ \\ \text{CH}_2 \\ \\ \text{N} \\ \diagup \quad \diagdown \\ \text{C} \quad \text{C} \\ \diagdown \quad \diagup \\ \text{NH} \end{array}$
Isoleucine	Ile	$\begin{array}{c} \text{O} \\ \parallel \\ \text{H}_2\text{N}-\text{CH}-\text{C}-\text{OH} \\ \\ \text{CH}-\text{CH}_3 \\ \\ \text{CH}_2 \\ \\ \text{CH}_3 \end{array}$
Leucine	Leu	$\begin{array}{c} \text{O} \\ \parallel \\ \text{H}_2\text{N}-\text{CH}-\text{C}-\text{OH} \\ \\ \text{CH}_2 \\ \\ \text{CH}-\text{CH}_3 \\ \\ \text{CH}_3 \end{array}$
Lysine	Lys	$\begin{array}{c} \text{O} \\ \parallel \\ \text{H}_2\text{N}-\text{CH}-\text{C}-\text{OH} \\ \\ \text{CH}_2 \\ \\ \text{CH}_2 \\ \\ \text{CH}_2 \\ \\ \text{CH}_2 \\ \\ \text{NH}_2 \end{array}$

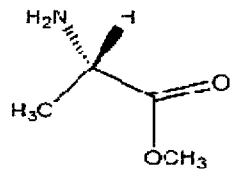
Methionine	Met	$\begin{array}{c} \text{O} \\ \parallel \\ \text{H}_2\text{N}-\text{CH}-\text{C}-\text{OH} \\ \\ \text{CH}_2 \\ \\ \text{CH}_2 \\ \\ \text{S} \\ \\ \text{CH}_3 \end{array}$
Phenylalanine	Phe	$\begin{array}{c} \text{O} \\ \parallel \\ \text{H}_2\text{N}-\text{CH}-\text{C}-\text{OH} \\ \\ \text{CH}_2 \\ \\ \text{C}_6\text{H}_5 \end{array}$
Proline	Pro	$\begin{array}{c} \text{O} \\ \parallel \\ \text{C}-\text{OH} \\ \\ \text{C}_5\text{H}_9\text{N} \end{array}$
Serine	Ser	$\begin{array}{c} \text{O} \\ \parallel \\ \text{H}_2\text{N}-\text{CH}-\text{C}-\text{OH} \\ \\ \text{CH}_2 \\ \\ \text{OH} \end{array}$

Threonine	Thr	$\begin{array}{c} \text{O} \\ \parallel \\ \text{H}_2\text{N}-\text{CH}-\text{C}-\text{OH} \\ \\ \text{CH}-\text{OH} \\ \\ \text{CH}_3 \end{array}$
Tryptophan	Trp	$\begin{array}{c} \text{O} \\ \parallel \\ \text{H}_2\text{N}-\text{CH}-\text{C}-\text{OH} \\ \\ \text{CH}_2 \\ \\ \text{Indole ring} \end{array}$
Tyrosine	Tyr	$\begin{array}{c} \text{O} \\ \parallel \\ \text{H}_2\text{N}-\text{CH}-\text{C}-\text{OH} \\ \\ \text{CH}_2 \\ \\ \text{Benzene ring} \\ \\ \text{OH} \end{array}$
Valine	Val	$\begin{array}{c} \text{O} \\ \parallel \\ \text{H}_2\text{N}-\text{CH}-\text{C}-\text{OH} \\ \\ \text{CH}-\text{CH}_3 \\ \\ \text{CH}_3 \end{array}$

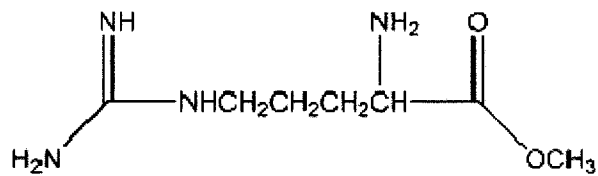
APPENDIX B
STRUCTURES OF THE STANDARD
CHARGE-SOLVATED SPECIES



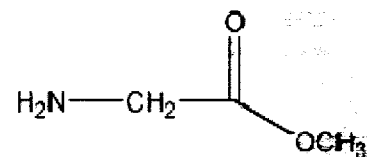
Charge-solvated



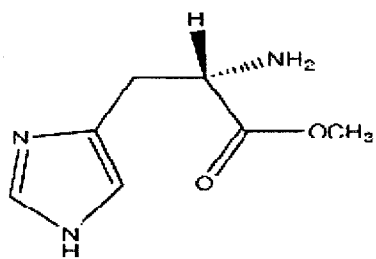
Alanine Methyl Ester



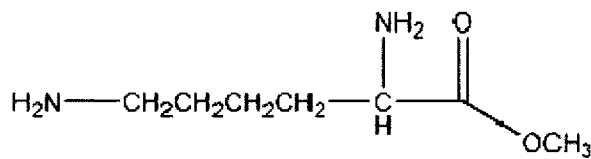
Arginine Methyl Ester



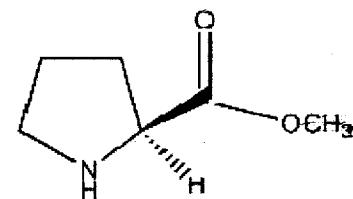
Glycine Methyl Ester



Histidine Methyl Ester



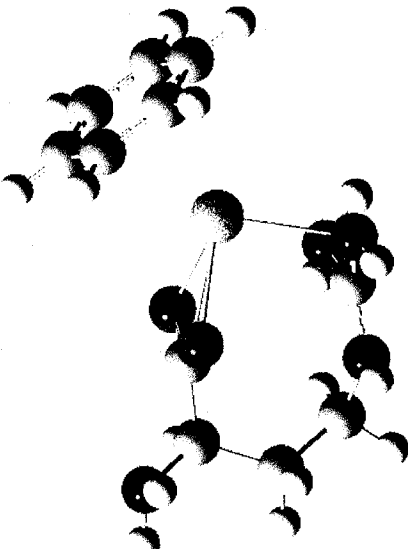
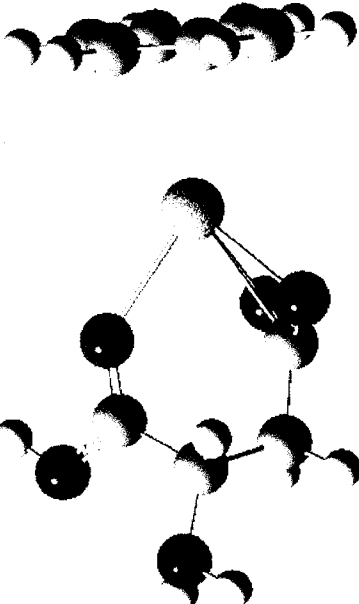
Lysine Methyl Ester

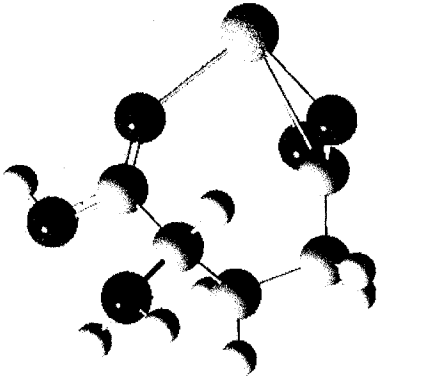
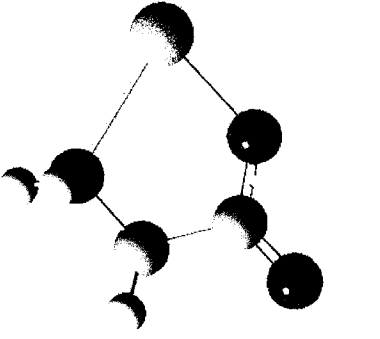


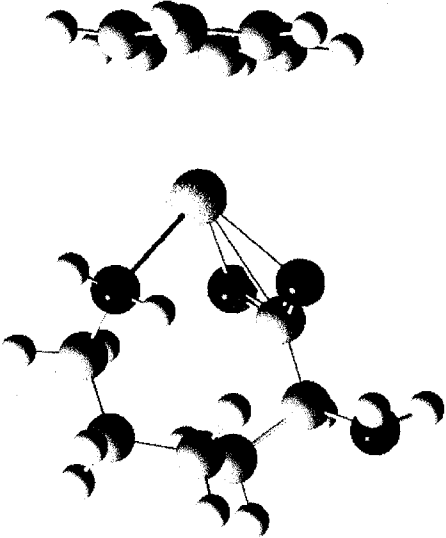
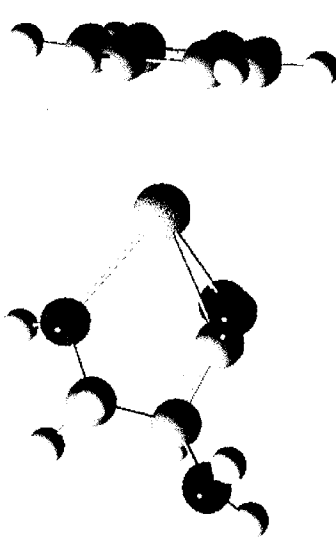
Proline Methyl Ester

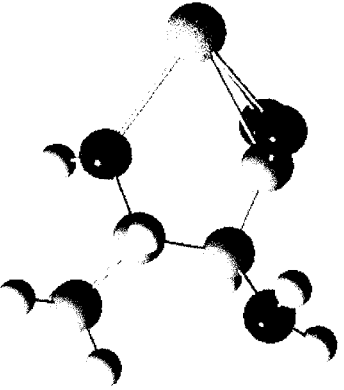

APPENDIX C

THEORETICAL MODELING RESULTS FOR
AMINO ACID--METAL ION COMPLEXES
WITH BENZENE

Amino Acid	[A.A.+M ⁺ +benzene]	Benzene Binding Energy (kcal/mole)	Distance* M ⁺ ...Benzene (Å)	M ⁺ Charge [†]
Arginine-H+Ca ²⁺		24.3	2.613	1.050
Aspartic Acid-H+Ca ²⁺		27.9	2.594	1.016

Glutamic Acid- $\text{H}+\text{Ca}^{2+}$		26.7	2.592	1.022
Glycine- $\text{H}+\text{Ca}^{2+}$		30.6	2.579	1.238

Lysine- H+Ca ²⁺	 <p>A ball-and-stick model showing the interaction between a lysine molecule and a calcium ion (Ca²⁺). The lysine molecule is represented by a central carbon atom (grey) bonded to a hydrogen atom (white), an amino group (two black atoms), and a side chain consisting of a methylene group (grey) and a terminal amino group (two black atoms). The calcium ion (grey) is coordinated to the two oxygen atoms of the terminal amino group. Dotted lines indicate the coordination bonds between the calcium ion and the oxygen atoms.</p>	26.0	2.616	1.043
Serine- H+Ca ²⁺	 <p>A ball-and-stick model showing the interaction between a serine molecule and a calcium ion (Ca²⁺). The serine molecule is represented by a central carbon atom (grey) bonded to a hydrogen atom (white), an amino group (two black atoms), and a hydroxyl group (grey and black). The calcium ion (grey) is coordinated to the oxygen atoms of both the amino group and the hydroxyl group. Dotted lines indicate the coordination bonds between the calcium ion and the oxygen atoms.</p>	29.4	2.583	1.005

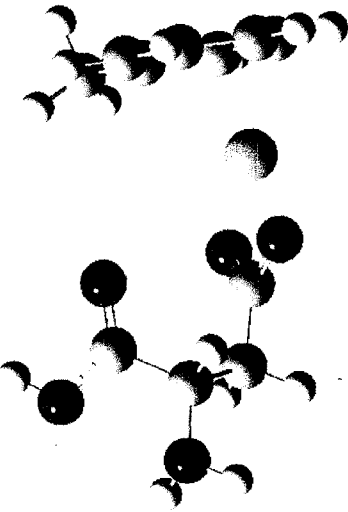
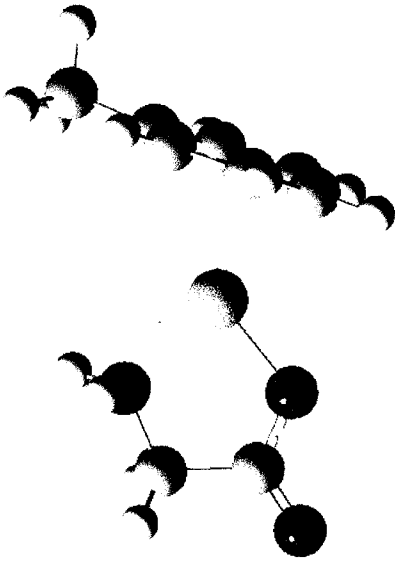
Threonine- H+Ca ²⁺	 	E = 28.8	2.583	0.980
----------------------------------	--	----------	-------	-------

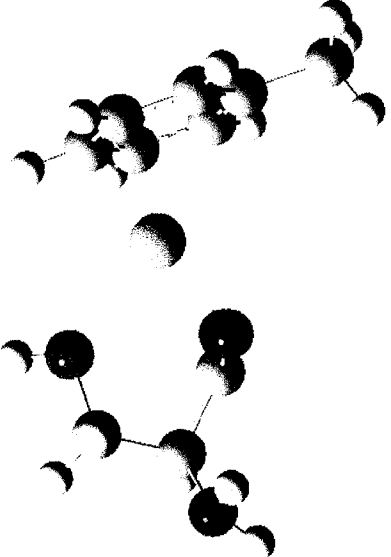
* From the center of the benzene ring to the metal ion † As reported by Gaussian

* From the center of the benzene ring to the metal ion † As reported by Gaussian

APPENDIX D

THEORETICAL MODELING OF
PHENYLALANINE INTERACTIONS
USING TOLUENE

Amino Acid	[A.A.+M ⁺ Toluene]	Toluene Binding Energy (kcal mol ⁻¹)	M ⁺ Charge
Aspartic Acid+ Cu ⁺		45.7	1.114
Glycine-H+ Cu ²⁺		43.6	0.418

Serine-H ⁺ Cu ²⁺	 A diagram illustrating the interaction between the benzene ring and the metal ion. On the left, a benzene ring is shown with its p-orbitals. On the right, a copper ion (Cu ²⁺) is shown with its d-orbitals. The interaction between the benzene ring and the metal ion is depicted as a series of overlapping lobes, representing the formation of a pi-complex. The diagram shows the benzene ring on the left, a central sphere representing the metal ion, and the copper ion on the right. The interaction is shown as a series of overlapping lobes between the benzene ring and the metal ion, and between the metal ion and the copper ion.	35.9	0.484
---	---	------	-------

* From the center of the benzene ring to the metal ion

† As reported by Gaussian

APPENDIX E
ABBREVIATIONS

A.A.	amino acid	CFTR	cystic fibrosis transmembrane conductance regulator
[A.A.+M ⁺]	amino acid+ metal complex		
AlaME	alanine methyl ester	CI	chemical ionization
		CID	collision-induced dissociation
APCI	atmospheric pressure chemical ionization	DFT	density functional theory
		DNA	deoxyribonucleic acid
ArgME	arginine methyl ester	EA	ethyl acetate
a.u.	arbitrary units	EI	electron ionization
B3LYP	Becke-style 3- parameter density functional theory with Lee-Yang- Parr correlation	EPR	electron paramagnetic resonance
		ESI	electrospray ionization
Bet	betaine	FAB	fast atom bombardment
		FT-ICR	Fourier transform-ion cyclotron resonance
BIRD	blackbody infrared radiative dissociation	GABA	gamma-aminobutyric acid
bp	boiling point	GC	gas chromatography
But	butylamine	GlyME	glycine methyl ester
CAD	collision-activated dissociation	HisME	histidine methyl ester
		HPLC	high performance liquid chromatography
CAPTURE	Cation- π Trends Using Realistic Electrostatics	HSAB	hard-soft acid-base
CE	capillary Electrophoresis	IM	ion-molecule
		IR	infrared

IRMPD	infrared multiphoton dissociation	RAK	radiative association kinetics
LC	liquid chromatography	RI	relative intensity
LysME	lysine methyl ester	RNA	ribonucleic acid
MALDI	matrix-assisted laser desorption/ionization	rRNA	ribosomal ribonucleic acid
MA	methylanisole	STO	Slater-type orbitals
MS	mass spectrometry	TEA	triethylamine
N/A	not available/ not assigned	THF	tetrahydrofuran
nAChR	nicotinic acetylcholine receptor	TMH	transmembrane helix
NBO	natural bond order	TMS	transmembrane strand
NMDA	<i>N</i> -methyl-D-aspartate	TOF	time-of-flight
NMR	nuclear magnetic resonance	χ	dipole correction factor
PA	proton affinity		
PDB	protein database		
ProME	proline methyl ester		
QIT	quadrupole ion trap		